Investigating high circulating IGF-1 as a risk factor for development of prostate cancer



Ashwin Menon Nandakumar

Linacre College
Department of Oncology
University of Oxford

Thesis submitted for the degree of

Doctor of Philosophy in Oncology

Hilary Term 2022

ABSTRACT

Prostate cancer is the commonest cancer in UK men. Prostate cancers upregulate type 1 insulin-like growth factor receptor (IGF-1R), and men with high serum IGF-1 have an increased risk of prostate cancer and of dying from prostate cancer. Subjects with low circulating IGF-1 are strongly protected from cancer; together with preclinical and bioinformatic data this supports a causative association. Unpublished Macaulay lab immunohistochemistry (IHC) data found association of high serum IGF-1 with IGF-1R upregulation in malignant prostatic epithelium, and a trend to association with nuclear IGF-1R, which has a transcriptional role. IGFs are also reported to be immunosuppressive, and could therefore influence anti-tumour immune responses. The main aim of this project was to investigate changes in the tumour epithelium and tumour microenvironment (TME) through which high IGF-1 promotes prostate cancer risk and progression. Firstly, IHC in 6 prostate biopsies showed a trend to increased IGF-1R and significant increase in internalised IGF-1R, suggesting receptor activation, in malignant vs benign prostate epithelium. Chromogenic *in situ* hybridisation in 17 prostatectomies showed *IGF1R* mRNA upregulation in malignant areas indicating transcriptional regulation. In prostate cancer cell lines, I found that short (24 hrs) and long term (8-12 weeks, to mimic lifelong high IGF supply) culture in IGF-1 downregulated IGF-1R. This may result from feedback of pathway activation and is inconsistent with tissue level findings. IGF-1 did cause persistent increase in nuclear IGF-1R, which has been associated with advanced prostate cancer stage. Secondly, I tested effects of IGF-1 on the immune mediators in prostate cancer cell cultures. IGF-1 upregulated immune associated genes *CXCL8, CXCL10*, *CCL5*, *IFNB1* and *ARG2*,

reported to be upregulated by the NF-κB and cytosolic DNA sensing cGAS-STING pathways. In DU145 prostate cancer cells IGF-1 caused phosphorylation of cGAS-STING pathway proteins IRF3 and TBK1, however the mechanism of this effect is not yet clear. IGF-1 also resulted in the transcriptional upregulation of *CD274*, encoding PD-L1, in prostate cancer and colorectal cancer cells. Analysis of TCGA data suggested that prostate cancers with high endogenous *IGF1* mRNA had higher expression of *CD274*, consistent with my cell line data, and of *S1P*, *CXCL12*, *CCL5* and *CCL4*, which are associated with increased tumour infiltration of CD4+ T regulatory (Tregs) and immunosuppressive M2 macrophages. Finally, association of IGF axis components with the TME was characterised using multiplex immunofluorescence (M-IF) and RNA sequencing (RNA-seq). In prostatectomies of men with known serum IGF-1, M-IF and RNA-seq were conducted on 32 Formalin-Fixed Paraffin-Embedded tissues. Patients with high circulating IGF-1 had increased tumour infiltration of CD4+ T cells, a trend to increased PD-L1 positivity but no association with CD4+ or FOXP3+ Treg positivity. RNA-seq analysis on tumour areas was challenging due to poor quality of extracted RNAs, and no differentially expressed genes were identified in tumours of patients with high circulating IGF-1. However, dividing cases by high vs low endogenous *IGF1* indicated deregulation of focal adhesion, leukocyte transendothelial migration and macrophage associated pathways. In high *IGF1* tumours, upregulated genes included IGF pathway genes *FOXO1*, *BCL2*, *ZEB1*, *IGFBP5* (a marker of IGF axis activation), and chemokine *CXCL12* that promotes chemotaxis of lymphocytes including Tregs. Downregulated genes included *TAP1*, required for antigen transport and presentation, *SOX4* and NF-κB regulator *TRAF4.* In 9 fresh frozen prostate tumour samples, single cell RNA-seq showed infiltration of M2 macrophages and MDSCs, with enrichment of *IGF1* in tumour infiltrating fibroblasts and of IGF-2 scavenger *IGF2R* in myeloid cells

and proliferating CD8 and NK cells. In summary, IGF-1 promoted sustained nuclear IGF-1R translocation and upregulated PD-L1 and cytokine expression in prostate cancer cells, and endogenous *IGF1* associated with *CXCL12* upregulation and *TAP1* downregulation, supporting an immunosuppressive role for IGF-1 in localised prostate tumours. These findings have potential relevance to prostate cancer risk, immunotherapy and risk of lethal disease.

Acknowledgement

First and foremost, I am incredibly grateful to my supervisor Dr Valentine Macaulay. I am thankful for the opportunity she gave me to undertake a DPhil in her lab and her constant support and guidance during the past four years. She has taught me perseverance, encouraged me to take risks and helped me grow as a scientist.

I would not be in this position if it weren't for my mum, dad, brother and family who have supported me and allowed me to pursue my passion. Thank you for constantly dealing with my complaining when an experiment didn't work. Special mention to all my six dogs who made my thesis writing tolerable.

I am incredibly grateful for my lab mates for their support during the past four years. Thank you, Dr Guillaume Rieunier, Dr Eliot Osher, Dr Nick Coupe, Dr Jack Mills, Dr Xiaoning Wu, Jenetta Soo, Dr Matthew Ellis, Jinseon Kim, Zhi Wong, Dr Avigail Taylor, Dr Monica Mantri and Cameron Lang. You have made lab work bearable.

I am also grateful for the constant support and guidance from my co-supervisor Prof Ian Mills and collaborators Prof Freddie Hamdy, Prof Clare Verrill, Mr Alastair Lamb, Jane Niederer, Dr Richard Colling, Dr Gill Pelvender, Prof Len Seymour, Dr Hena Khalique, Dr Sally Frost, Dr Sarah Larkin, Dr Tim James, Dr Alistair Easton, Leticia Campo, Molly Browne, Mari-lenna Issaias, Dr Shivan Sivakumar, Dr Neil Ashley, Dr Craig Waug, Dr

Kevin Clark, Dr Sally-Ann Clark, Dr Philip Charlton, Dr Nasullah Khalid Alham,m Ashwin Jainarayanan, David Maldonado-Perez and Miriam O'Hanlon.

I would also like to thank my all my friends who have made my oxford experience memorable and have helped me keep my mental wellbeing in check. Thank you Dr Florian Groelly, Eboni Bucknor, Gerardo Montalvo Zurbia Flores, Dr Luana Campos Soares, Charlotte Oxley, Kishan Gosai, Indervir Ranauta, Dr Sovan Sarkar, Dr Egon Jacobus Ambuludi, Tiffiany Ma, Dr Sam Bader, Dr Asmita Thapa, Dr Annamaria Ruggiano, Dr Shudong Li, Dr Ignacio Torrecilla, Dr Susan Kilgas, Kay Shigemori, Dr Maryam Alkadhimi, Dr Samuel Hume, Dr Giovanna Granata and Dr Angela Diana.

I am also grateful for the financial support from the Human Immune Discovery Initiative (HIDI) fund, UCARE, Rosetrees Trust and my scholarship from Linacre College.

I declare that the work presented in this thesis is my own research work, except for the following experiments and analyses which were performed with the help of others:

- RNAScope quantification shown in Chapter 3, Figure 3-5 and Table 3-1 were performed by Dr Nasullah Khalid Alham, Department of Engineering Science, University of Oxford.
- Multiplex immunofluorescence imaging shown in Chapter 5, Figures 5-1-3 were performed by Leticia Campo with supervision of Dr Alistair Easton in the Translational Histopathology Laboratory, University of Oxford.
- Fresh prostate tissues were collected thanks to surgeons Professor Freddie Hamdy and Dr Alastair Lamb. Samples were collected by David Maldonado-Perez and Miriam O'Hanlon, Oxford Centre for Histopathology Research (OCHRe). Malignant and tumour punches were sampled by pathologists by Professor Clare Verrill, Dr Richard Colling or Dr Gill Pelvender.
- Samples for single-cell sequencing were sorted (Figure 5-13b) by Craig Waug, Kevin Clark or Sally-Ann Clark at. The MRC Weatherall Institute of Molecular Medicine (WIMM) Flow Cytometry facility. Single-cell sequencing was performed by WIMM Single Cell facility by Facility Manager Dr Neil Ashley and Research Assistant Shayla Venkaya.
- Single-cell sequencing analysis shown in Chapter 5, Figures 5-14-21 were conducted by Ashwin Jainarayanan, The Kennedy Institute of Rheumatology.

This thesis is dedicated to the loving memory of Devadas Payyakkal and Arjun Satheesh who motived me to undertake a DPhil in Oncology.

Table of Contents

ABSTRACT **2**

ACKNOWLEDGEMENT **5**

TABLE OF CONTENTS **9**

LIST OF FIGURES **12**

LIST OF TABLES **15**

LIST OF ABBREVIATIONS **15**

1 CHAPTER I: INTRODUCTION **24**

1.1 PROSTATE CANCER 24
1.2 INSULIN-LIKE GROWTH FACTOR AXIS 31
1.2.1 Ligands of the IGF axis *32*
1.2.2 Receptors of the IGF axis *33*
1.2.3 IGF- binding proteins and proteases/ Regulation of IGF bioactivity *35*
1.3 IGF-1R SIGNALLING 36
1.3.1 PI3K/AKT pathway *37*
1.3.2 MAPK pathway *38*
1.3.3 NF-κB pathway *39*
1.3.4 JAK/STAT pathway *40*
1.4 IGF-1 AXIS AND TUMORIGENESIS 42
1.4.1 IGF axis expression and activation in cancers *43*
1.4.2 IGF-1R as a therapeutic target in cancer *45*
1.4.3 IGF axis and cancer risk *46*
1.5 RELEVANCE OF CIRCULATING IGF-1 AND TISSUE IGF-1R EXPRESSION IN INFLUENCING PROSTATE CANCER RISK 48
1.6 IGF AXIS AND ANTI-TUMOUR IMMUNITY 51
1.6.1 Anti-tumour immunity *51*
1.6.2 The immune microenvironment of prostate cancer *58*
1.6.3 Immunosuppressive role of IGFs *59*
1.6.4 Effects of the IGF axis on the lymphoid lineage *59*
1.6.5 Effects of IGFs on the myeloid lineage *61*
1.6.6 Immunosuppressive effects of IGFs on the tumour epithelium *62*
1.7 AIMS OF THE PROJECT 65

2 CHAPTER 2: MATERIALS AND METHODS **67**

2.1 CELL LINES 67
2.2 CELL TREATMENTS 69
2.2.1 IGF-1 treatment *69*
2.2.2 IGF1R siRNA treatment *70*
2.2.3 Small molecule inhibitors *71*
2.3 IMMUNOFLUORESCENCE 71
2.4 QUANTITATIVE REAL-TIME POLYMERASE CHAIN REACTION (QRT-PCR) 72
2.4.1 Ribonucleic acid (RNA) extraction *72*
2.4.2 Complementary DNA (cDNA) synthesis *73*
2.4.3 Primer design and validation *74*
2.4.4 qRT-PCR *76*
2.4.5 Relative quantification *76*
2.5 WESTERN BLOT 77
2.6 FLOW CYTOMETRY 80

2.7 Clinical samples 81
2.7.1 Fixed tissues 81
2.7.2 Fresh tissues 81
2.8 Immunohistochemistry 82
2.9 Colorimetric *In Situ* Hybridisation using RNAScope 84
2.10 Multiplex Immunofluorescence 86
2.11 HALO Image analysis 87
2.12 RNA Extraction from FFPE tissue sections 88
2.13 RNA library preparation and sequencing 90
2.14 RNA-sequencing data processing and analysis 90
2.15 Fresh tissue processing for single-cell sequencing 91
2.16 Single-cell sequencing with 10X genomics 93
2.17 Single-cell sequencing analysis 93
2.18 Statistical Analysis 94

3 CHAPTER III: INVESTIGATING THE ASSOCIATION BETWEEN CIRCULATING LEVELS OF IGF-1 AND IGF-1 RECEPTOR EXPRESSION IN PROSTATE CANCER. 95

3.1 Introduction 95
3.2 Results 96
3.2.1 Testing IGF-I Receptor β antibody in IHC 96
3.2.2 Investigating IGF-1R localisation in prostate cancer. 97
3.2.3 Investigating whether IGF1R mRNA parallels IGF-1R protein detected by IHC in prostate cancer 101
3.2.4 Testing in vitro association between IGF-1 and IGF-1R in prostate cancer cell line models . 107
3.2.5 Effect of IGF-1 concentration on IGF-1R subcellular localisation. 117
3.3 Discussion 120

4 CHAPTER IV: INVESTIGATING THE ASSOCIATION OF IGF-1 AND IMMUNOSUPPRESSION IN PROSTATE CANCER EPITHELIUM 125

4.1 Introduction 125
4.2 Results 126
4.2.1 Effects of IGF-1 on the expression of immune-modulatory cytokines in prostate cancer cell lines 126
4.2.2 Investigating effect of IGF-1 on cGAS-STING pathway 128
4.2.3 Investigating effects of IGF-1 on the expression of immune checkpoint ligand PD-L1 in vitro 131
4.2.4 Investigating the association between tumour endogenous IGF1R, IGF1 and the expression of cytokines and CD274 (PD-L1) from publicly available data. 143
4.3 Discussion 150

5 CHAPTER V: INVESTIGATING THE ASSOCIATION OF IGF AXIS COMPONENTS WITH PROSTATE CANCER IMMUNE INFILTRATION. 155

5.1 Characterising the T lymphocyte population in primary prostate cancer 156
5.2 Analysing the transcriptomic profile of tumours from patients with high vs low circulating IGF-1. 165
5.3 Investigating associations of tumour endogenous *IGF1* with T cell infiltration and PD-L1 positivity in M-IF. 177
5.4 Single-cell sequencing of fresh prostate cancers to characterise the tumour microenvironment 179
5.5 Expression of IGF axis associated genes in prostate cancer infiltrating cells 185
5.6 Characterising the myeloid infiltrating population in prostate cancer. 187
5.7 Characterising the lymphoid infiltrating population in prostate cancer. 191
5.8 Expression of IGF axis ligands and receptors across the lymphocyte population. 196
5.9 Discussion 198

6 CHAPTER VI: DISCUSSION & FUTURE WORK 207

7 CHAPTER VII: APPENDIX 218

7.1 T CELL INFILTRATION AND PD-L1 EXPRESSION IN CANCER VS BENIGN PROSTATE SECTIONS 218
7.2 T CELL INFILTRATION AND PD-L1 EXPRESSION IN HIGH VS LOW IGF-1R TUMOUR AREAS 219
7.3 ANALYSIS OF T CELL INFILTRATION AND PD-L1 EXPRESSION WITH GLEASON GRADE GROUP AND PSA. 220
7.4 LIST OF DIFFERENTIALLY UPREGULATED GENES IN PATIENTS WITH HIGH ENDOGENOUS *IGF1* 221
7.5 LIST OF DIFFERENTIALLY DOWNREGULATED GENES IN PATIENTS WITH HIGH ENDOGENOUS *IGF1* 232

REFERENCES 239

List of Figures

Figure 1-1 IGF-1R Signalling pathway 41
Figure 1-2 Association of high circulating IGF-1 and IGF-1R expression 50
Figure 1-3 Common Mechanisms of CD8+ T cell activation and inactivation in cancer ... 57
Figure 1-4 Hypothesised role of the IGF axis in tumour immune suppression 64
Figure 3-1 Testing IGF-1R antibody specificity 96
Figure 3-2 IGF-1R IHC performed on EPIC TMA. 100
Figure 3-3 Sample output from Visiopharm 102
Figure 3-4 IGF1R mRNA detected by RNA Scope 103
Figure 3-5 Analysis of IGF1R mRNA expression in ProMPT cohort using RNA Scope 106
Figure 3-6 IGF-1R protein expression after short term treatment of prostate cancer cells with 30 nM IGF-1. 108
Figure 3-7 IGF1R expression after short term IGF-1 treatment of prostate cancer cells with 30 nM IGF-1 109
Figure 3-8 Expression and activation of signalling proteins in DU145 & VCaP cells after 8-12 weeks culture in 30 nM IGF-1. 111
Figure 3-9 IGF-1R expression after co-stimulation with 30 nM IGF-1 and 28 nM DHT 113
Figure 3-10 Effect of increasing concentration of IGF-1 on IGF-1R expression in the presence or absence of DHT 115
Figure 3-11 Prostate cancer TCGA analysis investigating association of endogenous IGF1 and IGF1R mRNA expression 117
Figure 3-12 IGF-1R Immunofluorescent staining of VCaP cultures treated for 8-12 weeks with 30 nM IGF-1 or solvent 119
Figure 4-1 Effect of IGF-1 on expression of cytokines and immunomodulatory targets .. 128
Figure 4-2 IGF-1 induced activation of the cGAS-STING pathway measured using western blot 130
Figure 4-3 Identifying cell lines to test for IGF-1 induced PD-L1 expression 132
Figure 4-4 Effects of short-term serum starvation on PD-L1 surface expression 134
Figure 4-5 Effect of IGF-1 on PD-L1 surface expression 136

Figure 4-6 Effect of transcriptional inhibition on IGF-stimulated increase in PD-L1 surface expression 138
Figure 4-7 Effects of IGF-1 stimulation on PD-L1 expression in prostate cancer cell lines. 140
Figure 4-8 Investigating the mechanism of IGF-1 induced upregulation of PD-L1 expression 142
Figure 4-9 Gene expression of immune-modulatory cytokines in high vs low *IGF1* prostate cancer tumours from TCGA. 145
Figure 4-10 CD274 (PD-L1) expression in prostate and colorectal tumours with high or low IGF1R and IGF1 expression 147
Figure 4-12 Effect of MYC inhibition with IGF-1 stimulation on PD-L1 surface expression. 149
Figure 5-1 Initial optimisation of multiplex immunofluorescence for immune markers. . 157
Figure 5-2 Multiplex immunofluorescence workflow on HALO 158
Figure 5-3 Multiplex imaging of radical prostatectomy 160
Figure 5-4 T cell infiltration and PD-L1 expression in benign and malignant compartments of prostate cancer 162
Figure 5-5 Testing associations of circulating IGF-1 with T cells and PD-L1 positivity in prostate cancer 163
Figure 5-6 FFPE RNA Sequencing filtering threshold 167
Figure 5-7 IGF1 normalised count obtained from RNA sequencing analysis. 170
Figure 5-8 RNA Sequencing analysis of prostate cancers with high vs low endogenous IGF1 mRNA 171
Figure 5-9 Over Representation Analysis using KEGG pathways 173
Figure 5-10 Functional enrichment analyses of genes deregulated in high IGF1 mRNA tumours using Biocarta and Wikipathway functional enrichment analyses and GSEA with the KEGG database 175
Figure 5-11 Testing association between tumour endogenous IGFBP5, CD274, STAT5A and IFIT1 with tumour IGF1 mRNA expression 177
Figure 5-12 M-IF analysis of tumours with high vs low tumour endogenous IGF1 178
Figure 5-13 Prostate cancer single-cell sequencing workflow 180

Figure 5-14 Single-cell sequencing analysis characterising prostate cancer microenvironment. 183
Figure 5-15 Heatmap of single-cell sequencing cell population clusters 184
Figure 5-16 IGF axis expression across cell types 186
Figure 5-17 Characterisation of the tumour infiltrating myeloid subpopulation 190
Figure 5-18 Characterising the tumour infiltrating lymphocytes in prostate cancer 193
Figure 5-19 Expression of cytotoxic markers in the tumour infiltrating lymphocyte population 194
Figure 5-20 Expression of immune checkpoints across the lymphocyte populations 195
Figure 5-21 Expression of IGF axis markers across the lymphocyte population. 197
Figure 7-1 Immune infiltration and PD-L1 expression in prostate cancer 218
Figure 7-2 Association between IGF-1R expression, T cell infiltration and PD-L1 expression 219
Figure 7-3 Associations between Gleason grade group and PSA levels on T cell infiltration and PD-L1 expression. 220

List of Tables

Table 2-1 List of cell lines 69

Table 2-2 List of primers 75

Table 2-3 List of western blot primary antibodies 79

Table 2-4 Antibodies used for M-IF 87

Table 3-1 Tumour IGF-1R immunoreactive score, Tumour IGF1R mRNA intensity and circulating IGF-1 levels from ProMPT subjects 105

Table 5-1 T cell and PD-L1 expression in benign and malignant compartments of prostate cancer stroma and epithelium. 162

Table 5-2 Testing associations between tumour IGF-1R, Gleason score and PSA vs T cell and PD-L1 positivity in prostate cancer 165

Table 5-3 Top 10 differentially expressed genes in high IGF-1 tumours 172

Table 7-1 List of differentially upregulated genes in high IGF1 patients 231

Table 7-2 List of differentially downregulated genes in high IGF1 patients. 238

List of Abbreviations

4EBP1	Eukaryotic translation initiation factor 4E-binding protein 1
ActD	Actinomycin D
ADCC	Antibody-dependent cell cytotoxicity
ADCP	Antibody-dependent cellular phagocytosis
ADT	Androgen-depravation therapy
AKT	Protein kinase B
ALS	Acid labile subunit
ANOVA	Analysis of variance
APC	Antigen presenting cell
AR	Androgen receptor
Arg2	Arginase 2
BCL2	B-cell lymphoma 2
BCR	B cell receptor
BRAF	V-raf murine sarcoma viral oncogene homolog B1
BSA	Bovine serum albumin
CCL21	Chemokine C-C motif ligand 21
CCL4	Chemokine C-C motif ligand 4
CCL5	Chemokine C-C motif ligand 5
CD	Cluster of differentiation
CDK	Cyclin dependent kinase
cDNA	Complementary DNA

cGAS	Cyclic GMP-AMP Synthase
CK5	Cytokeratin 5
CREB	cAMP response element binding protein
CSF-R	Colony-stimulating factor-1 receptor
CTLA-4	Cluster of differentiation 152
CXCL10	Chemokine C-X-C motif ligands 10
CXCL12	Chemokine C-X-C motif ligand 12
CXCL8	Chemokine C-X-C motif ligands 8
DAB	3,3'-Diaminobenzidine
DC	Dendritic cells
dH_2O	Distilled water
DHT	Dihydrotestosterone
DMEM	Dulbecco's Modified Eagle Medium
dMMR	Deficient MMR
DMSO	Dimethyl sulphoxide
DNA	Deoxyribonucleic acid
DRE	Digital rectal examination
DTT	Dithiothreitol
E2F	E2 factor
EDTA	Ethylenediaminetetraacetic acid
eIF4E	Eukaryotic translation initiation factor 4E
Elk-1	Erythroblastosis virus E26 oncogene homolog 1-like gene 1
EPIC	European Prospective Investigation into Cancer and Nutrition

ERK	Extracellular signal-regulated kinases
EZH1	Enhancer Of Zeste 1 Polycomb Repressive Complex 2 Subunit
FBS	Fetal Bovine Serum
FDR	False discovery rate
FFPE	Formalin-fixed paraffin-embedded
FGFR2	Fibroblast growth factor receptor 2
FMD	Fasting-mimicking diets
FOXO	Forkhead box O
FOXO1	Forkhead box protein O1
FOXP3	Forkhead box P3
GBM	Glioblastoma multiforme
GDP	Guanosine diphosphate
GFR	Growth Factor Reduced
GH	Growth hormone
GRB2	Growth factor protein 2
GSEA	Gene set enrichment analysis
GSK3	Glycogen synthase kinase 3
GTP	Guanosine-5'-triphosphate
GZMB	Granzyme
H_2O_2	Hydrogen peroxide
HSPC	Hematopoietic stem and progenitor cells
IF	Immunofluorescence
IFIT1	Interferon Induced Protein With Tetratricopeptide Repeats 1

IFN-γ	Interferon gamma γ
IFNB1	Interferon β 1
IGF	Insulin-like growth factor
IGF-1	Insulin-like growth factor 1
IGF-1R	Insulin-like growth factor receptor 1
IGF-2	Insulin-like growth factor 2
IGF-2R	Insulin-like growth factor receptor 2
IGFBP	IGF binding protein
IKK	IkappaB kinase
IL-x	Interleukin-x
INSR	Insulin receptor
IRF3	Interferon regulatory factor 3
IRS	Immunoreactive scores
IRS1	insulin receptor substrate 1
IRS2	insulin receptor substrate 2
ISH	In situ hybridization
IκBα	nuclear factor of kappa light polypeptide gene enhancer in B-cells inhibitor, α
JAK	Janus kinase
JNK	Jun N-terminal kinases
KEGG	Kyoto Encyclopedia of Genes and Genomes
LAG3	Lymphocyte Activating 3
LHRH	Luteinizing hormone-releasing hormone
M-IF	Multiplex Immunofluorescence

MAIT	Mucosal-associated invariant T
MAPK	Mitogen-activated protein kinase
MDSC	Myeloid derived suppressor cells
MEK	MAPK/ERK kinase
MFI	Median Fluorescence Intensity
MHC class I	Major histocompatibility complex I
MHC class II	Major histocompatibility complex II
MPEC	Mouse Prostate Epithelial Cells
MRC1	Mannose Receptor C-Type 1
mTOR	Mammalian target of rapamycin
mTORC1	Mammalian target of rapamycin complex 1
mTORC2	Mammalian target of rapamycin complex 2
Myc	Master Regulator of Cell Cycle Entry and Proliferative Metabolism
NBF	Neutral buffered formalin
NCBI	National Centre for Biotechnology Information
NF-κB	Nuclear Factor Kappa-light-chain-enhancer of activated B cells
NK cells	Natural killer cells
NKT	Immunohistochemistry
NKT	Natural Killer T cells
NTC	No-template control
OCHRe	Oxford Centre for Histopathology Research
ORA	Over-Representation Analysis

ORB	Oxford Radcliffe Biobank
PAP	Prostatic acid phosphatase
PBS	Phosphate buffered Saline
PCA	Principal component analysis
PCK	Pan-cytokeratin
PD-1	Programmed cell death protein 1
PD-L1	Programmed death-ligand 1
PDK1	Phosphoinositide-dependent kinase 1
PE	Phycoerythrin
PI3K-AKT	Phosphoinositide 3-kinase-Protein kinase B
PIP2	Phosphatidylinositol-4, 5-bisphosphate
PIP3	Phosphatidylinositol-3, 4, 5-triphosphate
PPIB	Peptidylprolyl Isomerase B
ProMPT	Prostate Cancer Mechanisms of Progression and Treatment
PSA	Prostate-specific antigen
PSCA	Prostate Stem Cell Antigen
PSMA	Prostate-specific membrane antigen
PTEN	Phosphatase and tensin homolog
RAF	Rapidly accelerated fibrosarcoma
RAS	Rat sarcoma virus
RIN	RNA integrity number
RNA	Ribonucleic acid
RNA-Seq	RNA Sequencing
RPMI	Roswell Park Memorial Institute Medium

RT	Room temperature
RTK	Tyrosine kinase receptor
S100A8	S100 calcium-binding protein A8
S100A9	S100 calcium-binding protein A9
S1P	Sphingosine-1-phosphate
S6K	S6 kinase beta-1
SDS	Sodium dodecyl sulfate
SEM	Standard error of the mean
Sh2	Src homology 2
Shc	Src homology and collagen
SOS	Son of sevenless
SOX4	SRY-Box Transcription Factor 4
STAT	Signal transducer and activator of transcription
STAT5A	Signal Transducer And Activator Of Transcription 5A
STING	Stimulator of interferon genes
STS	Short-term starvation
T helper 1	T helper 1
T helper 17	T helper 17
T helper 2	T helper 2
TAA	Tumour associated antigen
TAP1	Transporter associated with antigen processing 1
TAP2	Transporter associated with antigen processing 2
TBK1	TANK Binding Kinase 1
TCGA	The Cancer Genome Atlas

TCM	Central memory T cells
TCR	T cell receptor
TEM	effector memory T cell
TGF-β	Transforming growth factor β
TKI	Tyrosine kinase inhibitors
TMA	Tissue microarray
TMB	Tumour mutational burden
TNF- α	Tumor necrosis factor α
TRAF4	TNF receptor-associated factor 4
Tregs	T regulatory cells
TRUS	Transrectal ultrasound
TSA	Tumour specific antigen
UMAP	Uniform Manifold Approximation and Projection
VEGF	Vascular endothelial growth factor
WFDC1	WAP Four-Disulfide Core Domain 1
WIMM	Weatherall Institute of Molecular Medicine
ZEB1	Zinc finger E-box-binding homeobox 1

1 Chapter I: Introduction

1.1 Prostate cancer

Prostate cancer is the most common cancer in men in the UK and second most common cause of cancer deaths amongst them (www.cancerresearchuk.org). Epidemiological reports from 2018 confirm that prostate cancer has replaced breast cancer to become the third most common cause of cancer deaths in the UK. One in 6 men in the UK are at a risk of developing prostate cancer in their lifetime. Its incidence rates have increased by 41% in the UK in the last two decades (1993-2017) and is predicted to increase by another 12% in the next two (2014-2035) (Smittenaar et al., 2016). Risk factors associated with prostate cancer include age, ethnicity, genetic history, diet, obesity and high circulating levels of insulin-like growth factor-1 (IGF-1) (Perez-Cornago et al., 2017; Travis et al., 2016). Amongst these risk factors, the only parameters that can be controlled are diet, obesity and IGF-1 levels.

Most prostate cancers are adenocarcinomas, and are thought to arise from prostatic intraepithelial neoplasia (PIN), a pre-malignant condition characterised by atypical cells in the ducts and/or glands of the prostate, without evidence of invasion (De Marzo et al., 2016). Prostate cancer can be curable if detected at an early stage. Currently, the two common methods of detection are prostate-specific antigen (PSA) testing and a digital rectal examination (DRE) (www.nhs.uk/conditions/prostate-cancer/diagnosis/). A DRE involves an internal examination of the prostate to check for asymmetry, nodule/induration and prostatic volume. PSA testing involves measuring the serum levels of PSA. PSA, encoded

by the *KLK3* gene, is a glycoprotein produced by the epithelial cells of the prostate. It helps to liquefy semen by lysing proteins in the seminal coagulum and plays an important role in the male reproductive system (Balk et al., 2003; Nicotera et al., 2009). Elevated serum levels (higher than 3ng/ml) of PSA could be a sign of prostate cancer. However, it could also be an indicator for non-malignant conditions such as benign prostatic hyperplasia, prostatitis or a urinary infection (www.nhs.uk/conditions/prostate-cancer). Even though PSA has been regarded as the current gold standard for prostate cancer detection, PSA testing has not been adopted as routine screening although can be tested if requested, and abnormal levels do not confirm the presence of cancer nor vice versa. Recent advancements have identified multiple serum and urine based tests that could replace the PSA test or be used in combination with it (Tan et al., 2019; Stovsky et al., 2019). The Prostate Health Index (PHI) blood test measures levels of -2proPSA (precursor of PSA), total and percent free PSA and has shown better results in diagnosing prostate cancer and predicting aggressive disease compared to total/percent free PSA test (Loeb et al., 2015; Lazzeri et al., 2013; Filella and Giménez, 2013; Jansen et al., 2010; Nicotera et al., 2009). Similarly, the prostate cancer urine test detects the mRNA expression of *PCA3* (prostate cancer gene 3) which is overexpressed in prostate cancer tissues and results from this assay can determine if a prostate biopsy is necessary (Duffy, 2020). Nevertheless, their effectiveness and benefits are yet to be evaluated in long term cancer survival data and until then, PSA tests remain to be the forefront of prostate cancer screening.

An abnormal result from the PSA test or the DRE could be a sign of a malignancy. Diagnosis of prostate cancer is performed by magnetic resonance imaging (MRI) of the pelvis (Stabile et al., 2020) followed by histopathological analysis of the prostate biopsy usually obtained

by a transrectal ultrasound (TRUS) guided approach. Prostate tissues are commonly graded using the Gleason scoring system (Gleason, 1992). A score of 1 indicates well differentiated non-cancerous tissue whereas a score of 5 would indicate a poorly differentiated anaplastic tissue. Since prostate cancers are made up of areas of different grades, the Gleason system takes into account the two most prominent areas that make up the cancer and two grades are given to each patient, stating the score of the most abundant grade first and the second most abundant second. These are added together to form the Gleason sum score. Recently, Gleason scores have been reported as cancer grade groups, where a Gleason score of 6 is grade group 1, Gleason score 3+4 = 7 is grade group 2, Gleason score 4+3 = 7 is grade group 3, Gleason score 4+4 = 8 is grade group 4 and Gleason score 9-10 falls under grade group 5 (Pierorazio et al., 2013; Humphrey, 2017). MRI and CT scans are used to stage patients by checking the extent of involvement of the prostate, pelvic lymph nodes and any distant metastatic spread.

Once diagnosed, there are several treatment options for patients with prostate cancer and these are dependent on the patient age, health status and stage and grade of the tumour. It is recognised that some prostate cancers behave very aggressively, while others are much more indolent, with little understanding of the causes of these different behaviours (Sandhu et al., 2021). Common treatment options include radical prostatectomy, radiotherapy, chemotherapy, androgen-deprivation therapy (ADT) or active monitoring. Localised prostate cancers are potentially curable by radical prostatectomy or radiotherapy. Patients with a small amount of cancers of grade group 1-2 may be assigned to active surveillance (Hamdy et al., 2016). Men with locally advanced or metastatic prostate cancer that is not curable are treated with ADT initially in the form of luteinising hormone-releasing hormone

(LHRH) agonists or LHRH antagonists (Moul, 2014; Parmar et al., 1987). The dependence of androgen stimulation for the growth and progression of prostate cancer makes ADT a commonly used therapeutic strategy (Teo et al., 2019; Huggins, 1941). Large trials such as Systemic Therapy in Advancing or Metastatic Prostate Cancer: Evaluation of Drug Efficacy (STAMPEDE) have also shown survival benefit from adding chemotherapy and/or newer endocrine agents upfront, soon after starting ADT (Damodaran et al., 2019; Attard et al., 2022; Purshouse and Protheroe, 2019; Ali et al., 2021). However, cancer progression is often seen despite androgen blockade and this leads into a castrate-resistant state. This progression is fuelled by changes in the tumour cells such as increased intra-tumoral synthesis of androgen, amplification and gain of function mutations of the androgen receptor (AR) gene (*AR*) increased expression of AR splice variants (AR-V7) that can activate the signalling pathway independent of ligand activation and increased expression of AR coactivators, that help stimulate AR transcriptional (Montgomery et al., 2008; Visakorpi et al., 1995; Taylor et al., 2015; Guo et al., 2009; Chan et al., 2012; Fujimoto et al., 2007; Agoulnik et al., 2006).

Castrate resistant metastatic prostate cancers are treated with addition of newer forms of ADT since AR signalling is still activated in them. Residual androgen biosynthesis in castrate resistant patients can be targeted with Abiraterone, which inhibits 17 α-hydroxylase /C17,20-lyase (CYP17), required for androgen biosynthesis, and response monitored by changes in PSA levels (de Bono et al., 2011; Hotte and Saad, 2010). The use of second-generation AR antagonist, Enzalutamide, a more potent receptor inhibitor has also shown promising results when compared to its first-generation counterpart, Bicalutamide (Fizazi et al., 2014). Enzalutamide binds to the AR with greater affinity, prevents its nuclear translocation and recruitment of coactivators, and also supresses the function of androgen

response elements (Tran et al., 2009). Additionally, combination of endocrine therapy with the chemotherapy agent docetaxel, a microtubule inhibitor, has been attributed with improved progression free-survival (Tannock et al., 2004; James et al., 2016). Patients whose cancers are resistant to abiraterone, enzalutamide and/or docetaxel have been shown to have better overall survival when treated with cabazitaxel, a tubulin binding taxane, although the toxicity is considerable (De Bono et al., 2010). Patients with prostate tumours that harbour mutations in *BRCA1/2*, *ATM* and/or *PALB2* are also eligible for treatment with Poly(ADP-ribose) polymerase (PARP) inhibitors (Cattrini et al., 2021; de Bono et al., 2021).

Prostate cancers display high levels of hypoxia and recent work have indicated that increased hypoxia is predictive of prostate cancer metastasis (Xia et al., 2021). The increased proliferation of tumour cells surpassing the speed of neovasculature development initiates hypoxic environments in prostate cancer (Xia et al., 2021; Bharti et al., 2019). Hypoxia is associated with castration resistance, biochemical relapse after radiotherapy and a higher Gleason grade (Hompland et al., 2018; Fraga et al., 2015; Fernandez et al., 2015; Milosevic et al., 2012). Prostate cancers also show gain and increased expression of *RRM2B*, which permit cancers to sustain DNA replication in hypoxic conditions to promote tumour progression. (Ng et al., 2018; Foskolou et al., 2017).

Over the last decade there have been numerous immunotherapy trials for treatment of solid tumours, targeting immune checkpoints. Trials in melanoma, lung, bladder and kidney cancer have been successful but immunotherapy in prostate cancer has had limited benefits (Kwon et al., 2014a; Vitkin et al., 2019; Lu et al., 2017). Phase III clinical trials with ipilimumab (anti-CTLA-4) on metastatic castration-resistant prostate cancer (mCRPC)

patients pre-chemotherapy (Beer et al., 2017) and post-chemotherapy (Kwon et al., 2014b) failed to achieve the primary endpoint of improved overall survival. Anti-PD-1 monotherapy trials in mCRPC also showed no benefit (Topalian et al., 2012; Hansen et al., 2016; Antonarakis et al., 2020). Inhibition of immune checkpoints CTLA-4 in mCRPC resulted in upregulation of PD-1 and PD-L1 with increased tumour infiltrating T cells (Gao et al., 2017). This led to a Phase II clinical trial (NCT02985957) using the combination of anti-PD-1 and anti-CTLA-4 inhibitors in mCRPC. Preliminary results of this trial after recruitment of 90 patients reported objective response rates of 25% and 10% in pre- and post-chemotherapy patients and the trial is currently expanding to include additional patents (Sharma et al., 2020). Other check-point options include targeting B7-H3 (NCT02923180, NCT02381314), LAG-3 (NCT03607890) and TIGIT (NCT02794571) (Runcie and Dallos, 2021). Increased expression of B7-H3 is seen in prostate cancer and is associated with adverse outcomes and cancer progression (Runcie and Dallos, 2021; Rodrigues et al., 2018; Powderly et al., 2020). Anti-B7-H3 antibodies have demonstrated manageable safety profile and early evidence of anti-tumour results with reduction of PSA in phase I/II clinical trials in mCRPC (Powderly et al., 2020). Immunotherapy options also include prostate cancer vaccines targeting tumour associated antigens. Sipuleucel-T was the earliest approved cancer vaccine where antigen presenting cells including dendritic cells are activated and primed towards the prostatic acid phosphatase (PAP) protein ex vivo and administered (Bansal et al., 2021; Sandhu et al., 2021). Though early results showed an improvement in overall survival in mCRPC, there were no differences in PSA levels or disease progression (Kantoff et al., 2010). Similarly, prostate cancer vaccines targeting PSA, prostate-specific membrane antigen (PSMA) and prostate stem cell antigen (PSCA) are also undergoing clinical trials (Runcie and Dallos, 2021).

The lack of benefits from immunotherapy in prostate cancer may be attributed to the composition of the infiltrating immune cells, which are unable to recognise the tumour cells as foreign (Schumacher and Schreiber, 2015; Erlandsson et al., 2019; Vitkin et al., 2019; Bilusic et al., 2017; Chen et al., 2021; Tuong et al., 2021). In malignant cells, intracellular antigenic proteins are cleaved in proteasome to short peptides (typically 8-9 residues). These antigenic peptides can be divided into tumour associated antigens (TAA) or tumour specific antigens (TSA). TSA arise from proteins that are expressed by unmutated genes, that are overexpressed in cancer cells in comparison to the normal. TSA originate from cancer specific somatic mutations and are not expressed in normal cells (Zhang et al., 2021b). Antigenic peptides are transported from cytosol into ER by transporter associated with antigen processing (TAP1/2) complexes (Cerundolo et al., 1990; Williams et al., 2002). In the ER the peptides are loaded onto MHC Class I molecules with β_2 microglobulin, trafficked through Golgi apparatus to cell surface for presentation to CD8+ cytotoxic T cells via binding to T cell receptor (Townsend et al., 1986, 1989). This process is important in eliciting an anti-tumour immune response (Han et al., 2020).

Most peptides presented by tumour cells are from highly expressed but unmutated genes and are rarely recognised as foreign, whereas neoantigens result from somatic mutations, are expressed only in tumour cells and are good targets for immunotherapy (Zhang et al., 2021b). Primary prostate cancer has been reported to contain lower numbers of somatic mutations and therefore a reduced neoantigen repertoire, when compared to cancers with high mutations/neoantigens such as lung cancer and melanoma (Alexandrov et al., 2013). Reduced neoantigen expression results in lower T cell:MHC Class I associated interactions,

reducing antigen presentation and immune mediated tumour elimination. (Schreiber et al., 2011). Conversely, advanced prostate cancer tumours with DNA damage repair defects including defective mismatch repair (dMMR) and microsatellite instability (MSI) displayed increased T cell infiltration and PD-L1 expression. These tumours also presented increased expression of transcripts associated with T cell and NK cell recruitment and function (Rodrigues et al., 2018). Therefore, using DNA damage repair status as a biomarker could yield better results to immunotherapy in prostate cancers. The immune microenvironment of prostate cancer is discussed in more detail in section 1.6.2 below. New treatment advancements are being made to manage prostate cancer (Sandhu et al., 2021) but concurrently, efforts also need to be made to reduce its increasing incidence.

1.2 Insulin-like growth factor axis

The Insulin like growth factor (IGF) axis plays a prominent role in human growth and development by signalling proliferation, inhibiting apoptosis and inducing differentiation (Jones and Clemmons, 1995). The axis is comprised of proteins that includes ligands Insulin like growth factor type 1 and 2 (IGF-1, IGF-2), insulin like growth factor receptors type 1 and 2 (IGF-1R, IGF-2R), a family of high affinity ligand binding proteins (IGFBPs) that regulate IGF bioactivity, IGFBP proteases and IGF-1R hybrid receptors formed with the insulin receptor (INSR) (Baserga et al., 2003; Cohen et al., 1994). Aberrant expression of components of the IGF axis can be seen in various cancers, including prostate cancer (Chitnis et al., 2008; Kasprzak et al., 2017).

1.2.1 Ligands of the IGF axis

The IGF axis is predominantly activated by the ligands IGF-1 and IGF-2. IGF-1 is a single polypeptide of 70 amino acid residues that share a structural homology similar to IGF-2 and insulin (Rinderknecht and Humbel, 1978; Kasprzak et al., 2017). It is secreted by the liver upon stimulation by growth hormone (GH) to have actions at distant sites (endocrine secretion), and also produced in tissues by stromal fibroblasts and immune cells (paracrine secretion) and as a pro-survival factor by tumour cells (autocrine secretion) (Laron, 2001; Bhowmick et al., 2004; Bowers et al., 2015; Huang et al., 2015). Similarly, IGF-2 is a 67-amino acid long single chain polypeptide which shares a 65% structural homology with IGF-1 (Brzozowski et al., 2002). Unlike IGF-1, IGF-2 production is not tightly regulated by the GH (Pollak, 2008). It is secreted mainly as an endocrine factor by the liver but also produced in tissues via paracrine and autocrine secretion (Xu et al., 2017; Unger et al., 2017). IGF-2 expression is subject to genomic imprinting, being expressed only from the paternal allele (Giannoukakis et al., 1993).

Ligand induced activation of the IGF axis occurs primarily by activating IGF-1R (De Meyts and Whittaker, 2002). IGF-1R binds to IGF-1 with the highest affinity (1-5 nM), followed by IGF-2 (4-5-fold lower). IGF-1 and -2 have 45-52% sequence identity with insulin, and whereas IGFs are single chain proteins, the C-peptide of insulin is cleaved off leaving disulphide-bonded A and B chains. Insulin can also binds to IGF-1R, but with over 100 fold lower binding affinity than IGF-1 (Brzozowski et al., 2002; Belfiore et al., 2009b; Denley et al., 2004; Forbes et al., 2002; Adams et al., 2000).

1.2.2 Receptors of the IGF axis

The IGF axis is commonly activated through IGF-1R. IGF-1R is a heterotetrameric transmembrane tyrosine kinase receptor (RTK) that is encoded on chromosome 15 (Adams et al., 2000; Moschos and Mantzoros, 2002). It is expressed on most types of cells in the body including immune cells (Moschos and Mantzoros, 2002). Mature IGF-1R is composed of two extracellular alpha (α) and two transmembrane beta (β) subunits which are linked by disulphide bonds (Adams et al., 2000; Ullrich et al., 1986). The *IGF1R* gene codes for a 1367 amino acid precursor (pre-pro receptor) which includes a 30-reside signal peptide at the N-terminus. The signal peptide is then cleaved to generate the pro receptor (220 kDa) and is then transported into the endoplasmic reticulum where it undergoes glycosylation and dimerisation. IGF-1R is further cleaved in the Golgi apparatus to form the mature receptor containing two alpha (~135 kDa) and two beta (~98 kDa) subunits (Adams et al., 2000; Ullrich et al., 1986; De Meyts and Whittaker, 2002). The mature receptor is then trafficked to the plasma membrane via the trans-Golgi network (Li et al., 2019). At the plasma membrane, the two alpha subunits together form the extracellular ligand binding site and the two beta transmembrane subunits contain the intracellular tyrosine kinase domains (Xu et al., 2018; De Meyts and Whittaker, 2002). Ligand binding to IGF-1R induces a conformational change that activates the kinase domain in the beta subunit, causing autophosphorylation of tyrosine residues 1131, 1135 and 1136 (Adams et al., 2000; Kavran et al., 2014). Autophosphorylation results in the recruitment and phosphorylation of docking proteins including insulin receptor substrate-1 (IRS-1), IRS-2 and Src homology and collagen (Shc), leading to activation of downstream pathways of which the most studied are the Phosphoinositide 3-kinase-Protein kinase B (PI3K-AKT) and RAS-Mitogen-activated

protein kinase (MAPK) pathway (Chitnis et al., 2008). Activated IGF-1R undergoes internalisation and is then degraded, recycled back to the plasma membrane or translocated into the nucleus (Aleksic et al., 2010; Sehat et al., 2010; Aleksic et al., 2018; Mills et al., 2021).

IGF-1R shares the exon structure, domain structure and 70% sequence homology with the INSR (Baserga et al., 2003; Denley et al., 2004; Ullrich et al., 1986). In cells that express both receptors, the close homology between IGF-1R and INSR results in assembly of hybrid receptors formed by association of half IGF-1R and half INSR (Slaaby et al., 2006; Belfiore et al., 2009b). INSR is activated by insulin and IGF-2, and plays a major role in glucose homeostasis (Andersen et al., 2017). Upon activation, INSR signals mainly via the PI3K/AKT pathway and regulates both metabolic and mitogenic processes (Rajapaksha and Forbes, 2015). INSR has two isoforms INSR-A and INSR-B generated by alternative splicing of exon 11 (Vella et al., 2018). INSR-A lacks exon 11, binds both insulin and IGF-2 with high affinity and is involved in foetal development and apoptosis protection. INSR-B contains exon 11, which encodes the carboxy-terminus of the alpha subunit, and regulates glucose uptake by facilitating glucose transport into the cell after insulin binding to the receptor (Meyts, 2016). INSR-B binds insulin with the highest affinity over IGFs and is expressed commonly in the liver, skeletal muscle and adipose tissue (Meyts, 2016; Sciacca et al., 2003). The hybrid receptor IGF-1R/INSR-A can bind IGF-1, 2 and insulin, and has both metabolic and mitogenic effects (Belfiore et al., 2009a; Pandini et al., 2002; Sciacca et al., 2012). Hybrid receptors formed between IGF-1R and INSR-B can only bind IGF-1 and is reported to have mitogenic effects (Pandini et al., 2002; Sciacca et al., 2012). Finally, IGF-2R (also known as the mannose-6-phosphate receptor, M6PR) is a monomeric protein

that lacks a kinase domain (El-Shewy and Luttrell, 2009). IGF-2R is responsible for binding, internalising and lysosomal degradation of IGF-2 to negatively regulate IGF signalling, and also mediates intracellular trafficking of lysosomal enzymes, and activation of TGF-β (Braulke, 1999; Baserga et al., 2003; Williams et al., 2007; Kasprzak et al., 2017).

1.2.3 IGF- binding proteins and proteases/ Regulation of IGF bioactivity

IGF bioactivity in the body is regulated by several mechanisms. Firstly, there is a family of 6 IGF binding proteins (IGFBPs) which share highly conserved N- and C- termini, that enable them to bind IGFs with high affinity (Bach, 2018; Clemmons et al., 1991; Duan and Allard, 2018). IGFBPs protect IGFs from proteolytic degradation and aid in IGF transport from the liver and tissue distribution (Kasprzak et al., 2017; Bach, 2018; Duan and Allard, 2018). These binding proteins selectively bind IGF-1 and IGF-2 and do not bind to insulin. Binding affinity of IGFBPs to IGFs vary with subtype (Duan and Allard, 2018; Bach, 2018). While IGFBP-1, -3, -4 can bind IGF-1 and -2 with a similar affinity, IGFBP-2, -5 and -6 bind IGF-2 with an increased affinity (Baxter, 2014). At the tissue level, IGFBPs bind to IGFs with a higher affinity than IGF-1R and other receptors, and so generally antagonise ligand induced activation of the IGF axis (Duan and Allard, 2018). IGFBPs 1, 3 and 5 have been shown in some models to potentiate IGF actions by releasing IGFs to interact with IGF-1R, and several IGFs including IGFBP3 have IGF-independent actions (Bach, 2018; de Silva et al., 2019; Firth and Baxter, 2002).

IGFBP-3 is the most abundant binding protein in serum (100 nM/L), and it bind 75-80% of circulating IGF-1 (Duan and Allard, 2018). IGF and IGFBP3 in circulation form a ternary

complex (~150 kDa) with a glycoprotein, acid labile subunit (ALS) (Baxter, 2014; Duan and Allard, 2018). Formation of this ternary complex increases the half-life of IGF-1 and addition of the ALS subunit prevents bound IGF-1 from diffusing out of the circulation via the capillaries (Duan and Allard, 2018; Jones and Clemmons, 1995; Rajaram et al., 1997). IGFBP activity is regulated by its proteolytic cleavage, which reduces its binding affinity to IGFs and allows free IGFs to bind to and activate the IGF axis (Baxter, 2014; Bunn and Fowlkes, 2003). The three main characterised classes of IGFBP proteinases are serine proteinases, metalloproteinases and cathepsins (Bunn and Fowlkes, 2003).

1.3 IGF-1R signalling

Binding of IGF-1 or IGF-2 to IGF-1R or hybrid receptors leads to autophosphorylation of the tyrosine residues 1131, 1135 and 1136 in the kinase domain which activates downstream signalling pathways, of which the two main characterised are the Phosphoinositide 3-kinase/Protein kinase B (PI3K/AKT) and the mitogen-activated protein kinase (MAPK) pathway (Baserga et al., 2003; Adams et al., 2000) (*Figure 1-1*). Phosphorylation of tyrosine residues creates binding sites for docking proteins IRS 1-2 and Shc (Simpson et al., 2017). The recruitment of IRS proteins initiates signalling via the PI3K/AKT pathway, while recruitment of Shc directs signalling through the MAPK pathway. Activation of these pathways contribute to mitogenic signalling by regulating proliferation, cell survival, migration, and metabolism (Pollak, 2012, 2008).

1.3.1 PI3K/AKT pathway

Signalling via the PI3K/AKT pathway starts with recruitment of docking protein IRS-1 to the phosphorylated IGF-1R (Kasprzak et al., 2017). Class I heterodimeric PI3Ks which consists of a regulatory (p85) and a catalytic (p110) subunit are responsible for IGF activated signal transduction via the PI3K/AKT pathway (Alzahrani, 2019; Chitnis et al., 2008). Tyrosine phosphorylation of IRS-1 by IGF-1R leads to recruitment and binding of regulatory p85 to Src homology 2 (SH2) domain, relieving p85's inhibitory action on the catalytic subunit p110 (Burgering and Coffer, 1995). PI3K then catalyses the conversion of phosphatidylinositol-4, 5-bisphosphate (PIP2) to phosphatidylinositol-3, 4, 5-triphosphate (PIP3) by phosphorylation of PIP2 (Czech, 2000). Activated PIP3 is anchored to the plasma membrane and recruits both phosphoinositide-dependent kinase 1 (PDK1) and protein kinase B (AKT) (Vanhaesebroeck and Alessi, 2000). The action of PI3K is tightly regulated by tumour suppressor Phosphatase and tensin homolog (PTEN). PTEN is responsible for dephosphorylating PIP3 to PIP2 and prevent over activation of the AKT axis (Alzahrani, 2019). Translocation of 3-Phosphoinositide-dependent kinase 1 (PDK1) and AKT to the membrane by PIP3 results in phosphorylation of AKT by PDK1 at Thr 308 (Vivanco and Sawyers, 2002). Complete activation of AKT occurs after phosphorylation of its Ser473 residue by mammalian target of rapamycin (mTOR) complex 2 (mTORC2), which is known to be activated by IGF-1R (Sarbassov et al., 2005).

Activated AKT localises into the cytosol and nucleus and can regulate cellular process such as proliferation, cell survival and migration by phosphorylating multiple targets (Manning and Cantley, 2007; Jean and Kiger, 2014). AKT can indirectly activate mammalian target of

rapamycin complex 1 (mTORC1), which phosphorylates downstream targets ribosomal protein S6 kinase beta-1 (S6K) and eukaryotic translation initiation factor 4E-binding protein 1 (4EBP1) (Khaleghpour et al., 1999). The inhibitory phosphorylation of 4EBP1 dissociates it from the complex with eukaryotic translation initiation factor 4E (eIF4E), and promotes protein translation of mRNAs encoding proteins that increase proliferation such as MYC and Cyclin D1 (Chang et al., 2003). PI3K/AKT pathway also promotes proliferation by inhibitory phosphorylation of targets such as Glycogen synthase kinase 3 (GSK3), forkhead box O (FOXO) and cyclin dependent kinase (CDK) inhibitors p21 and p27 (Alao, 2007; Carracedo and Pandolfi, 2008). This pathway also promotes survival by inhibiting apoptosis via increased expression of antiapoptotic proteins Bcl-2 and Bcl-xL, and inhibitory phosphorylation of Bad, caspase 9 and FOXOs (Chitnis et al., 2008; Baserga et al., 2003; Hay and Sonenberg, 2004; Nicholson and Anderson, 2002). AKT also has the ability to interact with cytoskeletal proteins to promote cell migration and can reduce glucose release and increase synthesis of glycogen via GSK-3β inhibition(Chin and Toker, 2009; Lochhead et al., 2001; Denduluri et al., 2015a).

1.3.2 MAPK pathway

Ligand binding induces IGF-1R tyrosine kinase activity and recruits docking protein Shc, growth factor protein 2 (GRB2) and the exchange factor mammalian homolog of son of sevenless (SOS) (Guo et al., 2020). Formation of the GRB2-SOS complex with the receptor leads to the increase in membrane concentration of SOS that is within close proximity of RAS (Bandaru et al., 2019). Activated GRB2-SOS complex removes GDP from the RAS family of proteins which allows RAS to bind to GTP and activate the RAS pathway

(Simanshu et al., 2017). This is followed by a phosphorylation cascade, where GTP bound RAS recruits serine/threonine kinase, RAF. RAF then phosphorylates mitogen activated protein kinase 1/2 (MEK1/2), and MEK1/2 phosphorylates extracellular signal-regulated kinases 1/2 (ERK 1/2) (Dhillon et al., 2007). Activated ERKs can phosphorylate multiple transcription regulators such as FOS, MYC, JUN, erythroblastosis virus E26 oncogene homolog 1-like gene 1 (ELK-1) cAMP response element binding protein (CREB) and JNK (Denduluri et al., 2015b; Chitnis et al., 2008; Farabaugh et al., 2015; Murphy et al., 2002, 2004). Phosphorylation of these downstream targets enhances their transcriptional activity and upregulate genes that induce cellular proliferation and cell cycle progression (Pulverer et al., 1991; Cao et al., 2011). Aberrant mutations and expression in proteins of the downstream ERK cascade are known to be tumorigenic (Dhillon et al., 2007).

1.3.3 NF-κB pathway

The IGF axis can activate the canonical Nuclear Factor Kappa-light-chain-enhancer of activated B cells (NF-κB) pathway through activation of PI3K/AKT signalling (Wang et al., 2020a; Chetty et al., 2006a; Zhao et al., 2011; Salminen and Kaarniranta, 2010; Che et al., 2002; Balaram, 1999). The NF-κB heterodimer consists of subunits RelA (p65) and p50 that exists in a complex with its inhibitor, nuclear factor of Kappa light polypeptide gene enhancer in B-cells inhibitor, alpha (IκBα) in the cytoplasm. (Lawrence, 2009). Binding of IκBα to NF-κB sequesters NF-κB (p65/p50) in the cytoplasm and prevents its activity as a transcription factor by preventing nuclear translocation (Liu et al., 2017b). IGF signalling phosphorylates AKT to activate IκB kinase (IKK), which in turn phosphorylates IκBα

(Salminen and Kaarniranta, 2010). This inhibitory phosphorylation tags IκBα for ubiquitination and proteasome mediated degradation, allowing NF-κB to translocate into the nucleus (Liu et al., 2017b). This pathway is known to regulate transcription, cell survival, cytokine production and trigger immune related inflammatory response (Lawrence, 2009). Reports have also suggested that PDK1, upstream of AKT can also activate NF-κB pathway by phosphorylation of IκBα (Liu et al., 2017a; Salminen and Kaarniranta, 2010).

1.3.4 JAK/STAT pathway

The IGF axis can also activate the Janus kinase (JAK)/ signal transducer and activator of transcription (STAT) pathway (Himpe and Kooijman, 2009; Takahashi et al., 1999; Su et al., 2018). IGF-1 induced activation of IGF-1R can lead to phosphorylation of both JAK1 and JAK2 (Gual et al., 1998; Himpe and Kooijman, 2009; Su et al., 2018). Activated JAKs create binding sites on the receptor for proteins which contain an SH2 domain like STAT1-6. Once STATs are recruited and bind to the receptor, they are phosphorylated by JAKs at their tyrosine residues. This phosphorylation allows STATs to dissociate from the receptor and translocate into the nucleus, where they functions as a transcription factor (Kisseleva et al., 2002). IGF-1R has also been reported to phosphorylate STAT1/3 directly or via AKT and activate this signalling cascade (Salminen et al., 2021; Su et al., 2018; Yadav et al., 2005; Takahashi et al., 1999; Ebong et al., 2004; Zong et al., 2000). Activation of the JAK/STAT pathway can initiate cytokine signalling and is involved in regulating both innate and adaptive immunity (Kisseleva et al., 2002). Activated JAKs can also signal via both the

PI3K/AKT and MAPK pathways as its phosphorylation creates binding sites for adapter proteins with an SH2 domain (Rawlings et al., 2004).

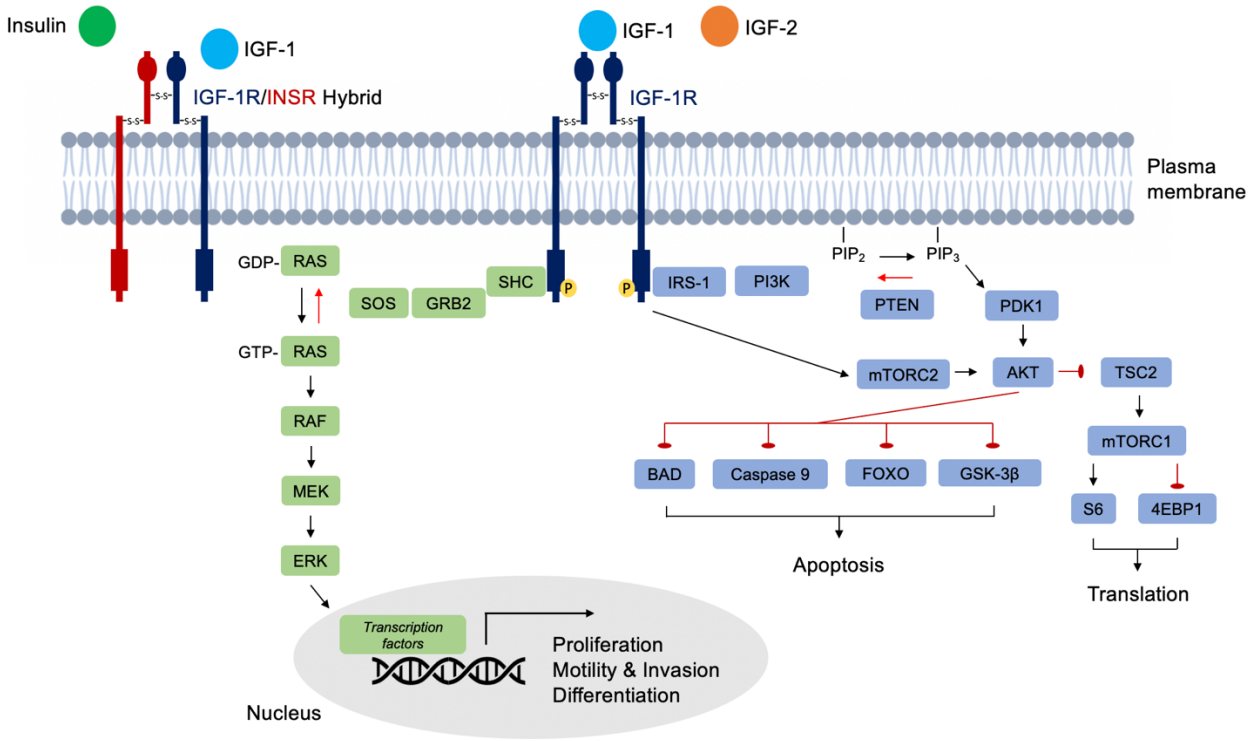


Figure 1-1 IGF-1R Signalling pathway. Figure shows the two most characterised signalling pathways downstream of IGF-1R. IGF-1 induced IGF-1R activation promotes signalling via the PI3K-AKT and MAPK pathways. Pathway activation leads to cancer cell proliferation, survival, differentiation and metastasis. Figure assembled using Biorender from references cited in the text.

1.4 IGF-1 axis and tumorigenesis

Aberrant activation of the IGF axis has been implicated in various diseases such as cancers, acromegaly, diabetes, thyroid eye disease and skin diseases (Pollak, 2008; Fernando et al., 2021). In the context of cancer, dysregulation of the IGF pathway can be seen in cancers of the prostate, lung, breast, ovarian, liver, pancreas, colon, rectum, and bone (Denduluri et al., 2015b; Sachdev and Yee, 2007; Kasprzak et al., 2017). IGF axis through its signalling via the PI3K-AKT, MAPK, NF-κB and JAK/STAT pathways can induce multiple hallmarks of cancer such as sustaining cellular proliferation and cell survival, deregulating cellular metabolism, promoting metastasis, angiogenesis and preventing immune destruction (Hanahan, 2022; Pollak, 2008; Kasprzak et al., 2017). IGFs are particularly important in maintaining cell survival by preventing apoptosis, mainly acting on the intrinsic pathway by regulating anti-and pro-apoptotic proteins (section 1.3.1 above). In the absence of pro-survival signals, pro-apoptotic proteins form mitochondrial membrane pores, releasing cytochrome C from mitochondia and activating caspase 9 and 3, leading to degradation of proteins and DNA (Elmore, 2007). IGF-1 can also protect from apoptosis triggered by the extrinsic pathway, which is activated by Fas ligand and TNF-α binding to their respective receptors to activate caspases 8 and 3 (Guo et al., 2017; Xu et al., 2013; Wang et al., 2006). Similarly, IGFs can promote angiogenesis by regulating the expression of vascular endothelial growth factor (VEGF) (Fukuda et al., 2002). VEGF is also induced by hypoxia and hypoxic conditions have been reported to upregulate the expression of IGF-1 (Shweiki et al., 1992; Joung et al., 2007). Activation of the IGF axis can prevent hypoxia induced apoptosis and transcriptionally upregulate the expression of HIF-1α (Fukuda et al., 2002).

1.4.1 IGF axis expression and activation in cancers

Genetic alterations leading to deregulation of IGF pathway components and overexpression of proteins involved in the IGF axis can lead to increased IGF-1R signalling and can be seen in many cancers (Kasprzak et al., 2017). IGF axis activation can occur due to loss of *IGF2* imprinting in multiple tumour types including prostate cancer (Damaschke et al., 2017; Cui et al., 2003). Inactivation of *IGF2R*, the scavenger receptor for free IGF-2 has been reported in prostate, breast and lung cancers, and is also detectable in high-grade PIN, suggesting that it is an early event in the development of the disease (Hu et al., 2005; Cui et al., 2003; Damaschke et al., 2017). Amplification of *IGF1R* has been reported in breast cancer, gastrointestinal stromal tumours, non-small cell lung cancers, thymic epithelial tumours and osteosarcoma (Wu et al., 2019; Farabaugh et al., 2015; Badzio et al., 2010; Mimae et al., 2012; Al-Saad et al., 2017; Behjati et al., 2017; Tarn et al., 2008). Increased IGF-1R protein expression without gene amplification has been reported in laryngeal, cervical, pancreatic, gastric and renal cancers and associates with adverse survival (Mountzios et al., 2013; Huang et al., 2008; Hirakawa et al., 2013; Numata et al., 2016; Sichani et al., 2010; Humar et al., 2017). Our group has reported that primary prostate cancers overexpress IGF-1R, and the receptor is upregulated on progression to androgen independent metastatic prostate cancer, and detectable in bone metastases (Hellawell et al., 2002; Massoner et al., 2011; Turney et al., 2011). Increased IGF-1R expression in primary prostate cancer is also associated with a higher risk of post-radiotherapy recurrence (Aleksic et al., 2017). Recent work from the Macaulay lab also links IGF-1R overexpression to radioresistance and association with adverse outcome in paediatric/young adult high-grade glioma (Simpson et al., 2020). Similarly, IGF-1R overexpression is also associated with radioresistance in rectal,

cervical and breast tumours (Turner et al., 1997; Lloret et al., 2007; Peiró et al., 2009; Wu et al., 2014). Consistent with these reports, our group showed that IGF-1R inhibition enhances sensitivity to ionising radiation by delaying double-strand break repair (Chitnis et al., 2014).

Activation of IGF-1R by IGF-1 leads to receptor internalisation, followed by degradation, recycling back to the cell surface or translocation into the nucleus (Aleksic et al., 2010). IGF-1R nuclear translocation has also been reported to require SUMOylation of three lysine residues of the β-subunit together with co-localisation with nuclear transport receptor importin-β and nucleoporin RanBP2 (Sehat et al., 2010; Packham et al., 2014). Recent work from the lab has also shown that upon IGF-1 stimulation, both α- and β-subunits of IGF-1R undergo nuclear transport (Mills et al., 2021). To test clinical associations of nuclear IGF-1R in prostate cancer, Dr Tamara Aleksic in our laboratory performed immunohistochemical staining for IGF-1R using an immunohistochemistry technique she had validated (Aleksic et al., 2016). She stained 147 formalin-fixed paraffin-embedded (FFPE) radical prostatectomies of patients recruited in Oxford to the Prostate Cancer Mechanisms of Progression and Treatment (ProMPT) study (https://gtr.ukri.org/project/F3045258-1D21-4189-BD51-B1D15232AF6D). IGF-1R signal was scored by Professor Clare Verrill, Consultant Uro-Pathologist to generate IGF-1R immunoreactive scores (IRS) in the membrane, cytoplasm and nucleus (maximum score 12 in each subcellular compartment). Total IGF-1R IRS (0-36) was calculated by summing the scores of the membrane, cytoplasm and nucleus, and an internalised score (0-24) was calculated by summing the scores of cytoplasmic and nuclear IRS. IGF-1R nuclear translocation was seen in ~30% of cases in the malignant prostatic epithelium in comparison to ~8% in benign epithelium, and nuclear

IGF-1R was significantly associated with an advanced tumour stage in prostate cancer (Aleksic et al., 2018). Overexpression of IGF-1R and its internalisation into the nucleus was also reported to increase chemotherapy resistance (Yuan et al., 2018; Codony-Servat et al., 2017). Furthermore, presence of nuclear IGF-1R staining was associated with a better progression free survival and overall survival in sarcoma patients treated with IGF-1R antibody (Asmane et al., 2012), suggesting that nuclear IGF-1R might indicate dependence on IGF signaling. Upon localisation into the nucleus, IGF-1R-β was found to bind to the DNA, interacting with RNAPol2 to upregulate the expression of *JUN* and *FAM21* (Aleksic et al., 2018). Others have also reported that nuclear IGF-1R can interact with nucleolar protein NOM1, transcription factor LEF1 and proliferating cell nuclear antigen (PCNA) (Warsito et al., 2012; Waraky et al., 2017; Solomon-Zemler et al., 2019).

1.4.2 IGF-1R as a therapeutic target in cancer

The increased expression and function of IGF-1R in established cancers (Pollak, 2008; Sell et al., 1994; O'Connor, 2003) make it an attractive cancer therapeutic target using tyrosine kinase inhibitors (TKIs), antibodies against IGF-1R or the IGF ligands. Though preclinical studies have been promising, clinical trials have been disappointing (Simpson et al., 2017; Baserga, 2013; Guha, 2013; Yee, 2012). IGF-1R TKIs cause dose-limiting hyperglycaemia due to the co-inhibition of INSR due to the high sequence homology between the INSR and IGF-1R kinase domains (De Meyts and Whittaker, 2002; Favelyukis et al., 2001). Anti-IGF-1R monoclonal antibodies can also induce downregulation of INSR in hybrid receptors, and do not inhibit potentially compensatory IGF-2 activation of INSR-A (Malaguarnera and Belfiore, 2011). Targeting IGF-1 and IGF-2 directly has shown promise by avoiding the

potential for hyperglycaemia seen when using anti-IGF-1R antibodies and TKIs; these IGF neutralising antibodies Xentuzumab and Dusigitumab are currently in clinical trials (de Bono et al., 2020; Schmid et al., 2021).

1.4.3 IGF axis and cancer risk

Subjects with low circulating IGF-1 are strongly protected from cancer (Melnik et al., 2011; Guevara-Aguirre et al., 2011). Early work from Dr Zvi Laron reported a new syndrome, termed Laron Dwarfism, of congenital IGF-1 deficiency due mutations in the GH receptor (GHR) leading to lack of IGF-1 production. The lack of IGF-1 in these subjects termed Laron dwarfs resulted in their reduced height and obesity (Laron et al., 1968, 2006). These subjects or those with deletions in the *GHR* or *IGF1* genes did not develop cancer between the ages of 3 - 75 years (Steuerman et al., 2011; Shevah and Laron, 2007). Similarly, epidemiological studies in Ecuadorian Laron dwarfs showed only one subject out of 99 was diagnosed with cancer, and she was disease free at the time of reporting three years later (Guevara-Aguirre et al., 2011).

Conversely, high circulating levels of IGF-1 are known to associate with an increased risk of cancers including breast, colorectal and prostate cancer (Chan et al., 1998; Key et al., 2010; Rinaldi et al., 2010; Hankinson et al., 1998; Ma et al., 1999; Knuppel et al., 2020). Men with high serum levels of IGF-1 have a 1.3-.1.4 fold increased risk of developing prostate cancer when comparing the highest vs lowest fifths (Roddam et al., 2008; Travis et al., 2016). Investigating effects of IGF-1 in cancers with a lower incidence, a UK Biobank study has recently reported that high IGF-1 circulating levels were associated with an

increased risk of thyroid cancer, malignant melanoma, and multiple myeloma (Knuppel et al., 2020). Analysis of the association between height and adiposity in the European Prospective Investigation into Cancer and Nutrition (EPIC) cohort has revealed that taller and obese men have an elevated risk for high grade prostate cancer and prostate cancer death (Perez-Cornago et al., 2017). This association is likely to involve the IGF axis as it is implicated in pre- and post-natal development and height (Liu et al., 1993; Baker et al., 1993). Furthermore, results from Mendelian Randomisation studies suggest that the association between circulating IGF-1 levels and risk of prostate, breast and colorectal cancer could be causal (Murphy et al., 2020a; b; Watts et al., 2021).

With majority of circulating IGF-1 being bound to IGFBP-3, which is also secreted by the liver in response to growth hormone, there may also be an association between serum IGFBP-3 and prostate cancer risk, although some studies reported increased prostate cancer risk and some decreased risk with increasing IGFBP-3 levels (Borugian et al., 2008). Higher concentrations of IGFBP-3 were associated with increased colorectal cancer risk (Murphy et al., 2020a), while studies of IGF-2 have generally been small and shown no association with cancer risk. In a meta-analysis of ~24,000 men from 21 studies, Travis and colleagues reported that IGF-1, IGF-2 and IGFBP-3 were positively associated with prostate cancer risk, although there was little information on IGF-2. After mutual adjustment of IGF-1 and IGFBP-3, only IGF-1 remained significantly associated with risk of prostate cancer (Travis et al., 2016).

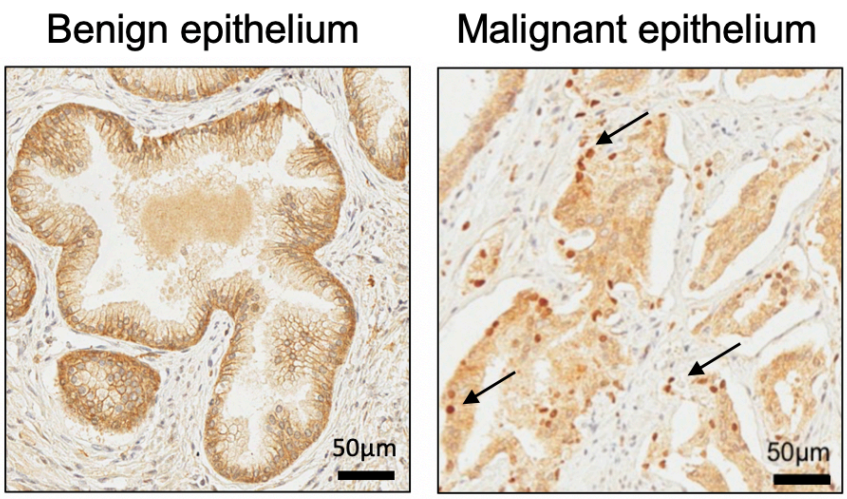
1.5 Relevance of circulating IGF-1 and tissue IGF-1R expression in influencing prostate cancer risk

Following the assessment of IGF-1R expression and subcellular localisation in FFPE radical prostatectomies of patients recruited to the ProMPT study (Aleksic et al., 2018), the same cases were used in the Macaulay lab to test for association between circulating levels of IGF-1 and expression and localisation of IGF-1R in benign and malignant prostatic epithelium. Out of the 147 ProMPT patients selected for study 139 had frozen aliquots of serum available for IGF-1 assay. Circulating IGF-1 levels were measured from the patient sera using the IDS-iSYS Insulin like Growth Factor-I (IGF-I) assay (IDS Immunodiagnosticsystems, Boldon Colliery UK) in the Biochemistry Laboratory at the John Radcliffe Hospital (Oxford), supervised by Professor Tim James.

Results from the analysis suggested a significant association between high circulating levels of IGF-1 and increased IGF-1R expression in malignant but not benign prostatic epithelium (Figure 1-2). There was also a non-significant trend ($p = 0.095$) to association of high serum IGF-1 and nuclear IGF-1R (Aleksic et al, unpublished). Parallel to these results, IGF-1 has been reported to upregulate *IGF1R* gene transcription *in vitro* (Sarfstein et al., 2012; deMoura et al., 2000), although several studies have also implicated IGF-1 in downregulating IGF-1R (Schillaci et al., 1998; Girnita et al., 2005). The association of circulating IGF-1 and IGF-1R expression in the malignant epithelium and not benign epithelium could suggest that IGFs are promoters rather than drivers of the disease. Supporting a role for IGF-1R expression, a study investigating the preventative effects of pregnancy on risk of breast cancer found significant hypermethylation of *Igf1r* resulting in

reduced *Igf1r* mRNA expression in post-partum mammary epithelium (Katz et al., 2015). Understanding the relationship between IGF-1 and IGF-1R expression may help us uncover how increased IGF-1 levels contribute to a higher prostate cancer risk.

a.



b.

Benign	n	Median IGF-1 nmol/l	p value
IGF-1R ≤10	77	16.54	p=0.871
IGF-1R >10	60	16.68	
Malignant			
IGF-1R ≤14	79	15.58	p=0.038
IGF-1R >14	60	17.07	

Figure 1-2 Association of high circulating IGF-1 and IGF-1R expression. (a) IGF-1R IHC conducted on radical prostatectomies from men recruited to ProMPT study by Dr Tamara Aleksic. Tissues showed increased IGF-1R expression together with increased nuclear IGF-1R (black arrows) in the malignant epithelium than the benign epithelium. (b) Table shows the association between serum circulating IGF-1 and IGF-1R expression. Radical prostatectomy tissues (n=139) obtained from men recruited to the ProMPT study were stained for IGF-1R by Dr Tamara Aleksic. Tissues were scored based on their IGF-1R expression and localisation by Prof Clare Verrill and total IGF-1R immunoreactive score given (sum of: membrane + cytoplasm + nuclear). Table shows total IGF-1R scores in benign and malignant prostate epithelium, divided by median score, and median serum IGF-1 values.

1.6 IGF axis and anti-tumour immunity

The role of IGFs in regulating immune responses have been discussed in literature for over 30 years. IGFs can drive erythropoiesis, granulopoiesis, and lymphopoiesis, and are reported regulate both innate and adaptive responses with both pro- and anit- tumourigenic consequences (Miyagawa et al., 2000, Merchav et al., 1988, Clark et al., 1993; Kecha et al., 2000; Kooijman et al., 1997; 1995; Landreth et al., 1992). Before discussing the literature on this subject I will briefly summarise the components of the immune response.

1.6.1 Anti-tumour immunity

A prominent hallmark of cancer is its ability to avoid immune destruction (Hanahan and Weinberg, 2000, 2011; Hanahan, 2022). Cells and tissues in the body are under constant immune surveillance. Cancers have the ability to grow by 1) avoiding immune detection 2) stimulating immunosuppressive cells and 3) disarming the tumour-targeting immune cells (Dunn et al., 2004; Chen and Mellman, 2017). The immune contexture in the tumour microenvironment is important for mediating an anti-tumour immune response (Fridman et al., 2017).

Tumour surveillance is carried out by both innate and adaptive immune responses. The innate response is fast acting and non-specific, while the adaptive response is memory mediated (Gajewski et al., 2013; Vesely et al., 2011). Immune cell signalling, cell-cell communication and recruitment to areas of infection or malignant growth are mediated by secreted proteins termed cytokines and chemokines (Zlotnik and Yoshie, 2012). Cytokines

play a major role in inflammation and immunity and are commonly produced my macrophages, lymphocytes, B cells, fibroblasts and epithelial cells (Ozga et al., 2021). Cytokines can be classified based on the immune response they generate, into proinflammatory or anti-inflammatory/immunosuppressive. Proinflammatory cytokines include Interleukin -1 (IL-1), IL-6, IL-8, Tumour necrosis factor α (TNFα) and type I-III interferons including IFNγ (Mantovani et al., 2019; Borish and Steinke, 2003). Immunosuppressive cytokines include IL-10 and IL-12 (Opal and DePalo, 2000). Cytokines such as IL-2 and IL-15 can also regulate of the adaptive immunity by stimulating the proliferation of CD8+ T cells and natural killer (NK) cells (Turner et al., 2014). Unlike IL-2, IL-15 does not promote proliferation of immunosuppressive regulatory T cells (Tregs), and secretion of IL-15 was recently shown to be enhanced by co-culture with prostate cancer cells (Sakellariou et al., 2020; Watkinson et al., 2020). Finally, chemokines are a family of cytokines that are secreted by immune cells. Chemokines stimulate immune cells to migrate towards the chemokine source, which is usually a site of infection, malignant growth or would healing (Vilgelm and Richmond, 2019).

The components of innate immunity include cells of common myeloid lineage such as neutrophils, monocytes, macrophages, dendritic cells (DC), eosinophils, basophils, mast cells, myeloid derived suppressor cells (MDSC) and lymphoid lineage NK cells. Monocytes population can be classified into classical and non-classical monocytes. Classical monocytes form the major monocytic population and commonly differentiate into tissue resident macrophages (Kapellos et al., 2019). They also secrete pro-inflammatory cytokines such as TNFα and IL-6 (Zimmermann et al., 2010). Non-classical monocytes are patrolling monocytes and are reported to involved in maintaining vascular homeostasis by clearing

dying and apoptotic cells in the luminal side of the vascular endothelium (Quintar et al., 2017; Carlin et al., 2013). Most tissue macrophages arise from monocytes and can be classified into M1 and M2 subtypes based on their polarisation. The classification into M1 and M2 subtypes were based on the work from Mills et al, who described M1 macrophages to be similar to pro-inflammatory IFNγ secreting T helper 1 (Th1) lymphocytes and M2 macrophages to be similar to immune suppressive IL-10 secreting T helper 2 (Th2) lymphocyte (Mills et al., 2000).

The innate system is responsible for initiating the adaptive response, while mediating its own effector responses including phagocytosis by macrophages and polymorphonuclear cells, and cytotoxic killing by granulocytes and NK cells (Vesely et al., 2011). Phagocytosis involves the phagocytic cell recognising foreign pathogens/cells via their non-self-antigens, engulfing them and killing by lysosomal degradation (Feng et al., 2019). NK cell mediated cytotoxicity targets cancer cells and virus infected cells that downregulate MHC Class 1, which cannot be otherwise cleared by cytotoxic lymphocytes (Topham and Hewitt, 2009). If target cells fail to display MHC class I, this leads to the secretion of cytotoxic molecules such as perforin and granzyme by NK cells and death of target cells via apoptosis (Demaria et al., 2019). Conversely, recognition of MHC Class I receptors by NK cells prevent their activation (Moretta et al., 2002; Waldhauer and Steinle, 2008). Eosinophils, basophils and mast cells are also able to secrete inflammation inducing cytokines such as leukotrienes, to attract more immune cells (Pandya et al., 2016).

The myeloid lineage includes cells such as MDSCs and the M2 polarised macrophages that can negatively regulate components of both the innate and adaptive immune system (Biswas

and Mantovani, 2010; Cheng et al., 2008). These cells can suppress the body's ability to mount an immune response against tumours and have been recently targeted in therapy (Murray, 2017; Sinha et al., 2008)

The adaptive response is an antigen specific immune response and is slower in onset in comparison to innate immunity (Pandya et al., 2016). It consists of B and T lymphocytes with a common lymphoid progenitor. T and B cells are named after the organ in which they develop, namely the thymus and the bone marrow (Alberts et al., 2002). T cells arise from haematopoietic stem cells from the bone marrow that migrate to the thymus, where they mature and are exported to the periphery (Mildner and Jung, 2014). B cells develop in the bone marrow and mature in the spleen (Shahaf et al., 2016). T cells can be further divided into two sub-groups based on their ability to identify pathogens/cells via MHC class 1 presentation (Chien et al., 2003). T cells that recognise non-self-antigens without MHC presentation are referred to $\gamma\delta$T cells. The majority of the T cell population are $\alpha\beta$ T cells which require antigens to be presented in MHC complexes (Hennecke and Wiley, 2001). The $\alpha\beta$ T cells can be further divided into two subgroups, CD4+ T cells and CD8+ T cells (Koretzky, 2010). The naïve CD4+ T cells become effector T cells after they bind to MHC class II molecules which are present on antigen presenting cells (APCs) such as B cells, macrophages and DCs (Swain et al., 2012). The CD4+ T cells can differentiate into subtypes Th1 cells, Th2 cells, T helper 17 (Th17) cells, or Tregs (Gajewski et al., 2013). IL-12 promotes the differentiation of CD4+ T cells into Th1 cells that secrete proinflammatory cytokines such as IFNγ and TNF-β that augment immune response against intracellular pathogens (Paul and Seder, 1994; Seder et al., 1993; Hsieh et al., 1993). IL-4 promotes the differentiation of CD4+ T cells into Th2 cells that secrete cytokines such as IL-10, IL-5 and

IL-13 and are involved in protection against extracellular pathogens and enhance B cell antibody production (Dong and Flavell, 2000; Gros et al., 1990). Development of Th17 cells are induced by IL-6 and transforming growth factor-β (TGF-β) (Qin et al., 2009; Kimura and Kishimoto, 2010). Th17 cells are named after ability to produce pro-inflammatory cytokine IL-17 which stimulates stromal cells to produce inflammatory cytokines to recruit neutrophils to the site of infection. They are also important for defence against extracellular pathogens, especially in the mucosal and. epithelial barriers (Tesmer et al., 2008). Similar to Th17 cells, Tregs are also induced by TGF-β and IL-2, but without the presence of pro-inflammatory cytokines like IL-6 (Veldhoen et al., 2006; Mangan et al., 2006; Bettelli et al., 2006). Tregs secrete immunosuppressive cytokine IL-10 and are known to inhibit immune function (Littman and Rudensky, 2010). The balance between pro-inflammatory Th17 cells and anti-inflammatory Tregs are crucial for regulating autoimmunity, and deregulation of Th17/Treg balance has been reported in inflammatory bowel disease, rheumatoid arthritis and multiple sclerosis (Lee, 2018).

The cytotoxic CD8+ T cells bind to pathogens/abnormal self-antigens via interaction between the T cell receptor (TCR) and antigen/MHC class 1 complex (Figure 1-3). T cells also expresses co-stimulatory CD28 receptor that binds to CD80 (B7.1) and CD86 (B7.2) on antigen presenting cells (Bromley et al., 2001). Binding of CD28 to CD80/86 results in signalling via PI3K/AKT pathway (Garçon et al., 2008) and is crucial for complete activation, survival and proliferation of T cells (Rudd et al., 2009). A major mechanism through which activated CD8+ T cells kill cancer cells and virus infected cells is through apoptosis. This is triggered via the extrinsic pathway and also by the exocytosis of perforin which makes pores in target cells allowing entry of cytotoxic enzymes called granzymes

that cause cell death by DNA cleavage (granzyme A) and activation of caspase 3 (granzyme B) (Lieberman, 2003; Elmore, 2007). T cells also express inhibitory receptors such as cytotoxic T-lymphocyte-associated protein 4 (CTLA-4) and programmed cell death protein 1 (PD-1) (Fuertes Marraco et al., 2015). T cell activation results in surface upregulation of CTLA-4, which can bind CD80/86 with a higher affinity than CD28, preventing activation (Leach et al., 1996). Inhibitory PD-1 signalling is important in peripheral tolerance of T cells, to prevent activation of self-reactive T cells (Ishida et al., 1992). PD-1 binds to Programmed death-ligand 1 (PD-L1), expressed by antigen presenting cells and tumour cells (Patsoukis et al., 2020). PD-1: PD-L1 binding inhibits CD28/TCR co-stimulation, blocks proliferation of T cells by halting them in G1 cell cycle phase (Patsoukis et al., 2012). Ligand binding to PD-1 also inhibits the PI3K/AKT pathway activation and upregulates apoptotic factors such as Bim (Gibbons et al., 2012). PD-1 is not only expressed by CD8+ T cells, they are also expressed in CD4+ cells, Tregs, NK cells, B cells and monocytes (Konkel et al., 2010; Kumagai et al., 2020). Binding of PD-L1 on Tregs to PD-1 results in their upregulation of FOXP3 and enhances their survival ad suppressive capabilities (Francisco et al., 2009).

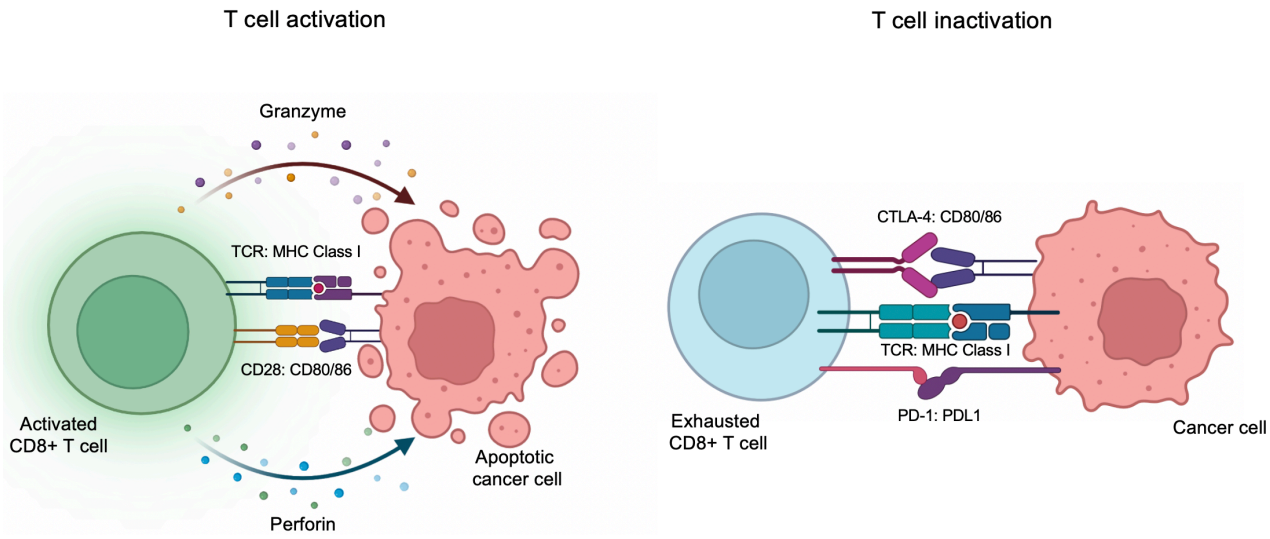


Figure 1-3 Common Mechanisms of CD8+ T cell activation and inactivation in cancer. T cells are activated upon binding of their TCR with peptide containing MHC Class I presented by antigen presenting tumour cells or APCs. T cell activation is completed after binding of co-stimulatory CD28 receptor with CD80 or CD86 on the antigen presenting cells, leading to PI3K/AKT signalling, T cell proliferation and survival. T cell activation induces expression of immune checkpoint CTLA-4, which binds CD80/CD86 with a higher affinity, preventing TCR activation. Similarly cancer cells express PD-L1, which bind to PD-1 on T cells inhibiting their activation, proliferation and inducing apoptosis. Figure assembled using Biorender from references cited in the text.

Finally, B cells migrate to the secondary lymphoid organs after maturation in the bone marrow and here they are activated upon binding to antigens via their B cell receptor (BCR) (Pieper et al., 2013). B cells produce antibody molecules that are inserted into the plasma membrane to form part of the B-cell receptor (Von Behring and Kitasato, 2015). After activation by an antigen, B cells proliferate and differentiate into plasma cells that secrete antibodies (immunoglobulins) and cytokines which can regulate inflammation (Hoffman et al., 2016). Professional APCs including B cells, DCs and macrophages also take up extracellular antigenic peptides which are digested in lysosomes and presented on cell surface in context of MHC Class II to prime Th2 helper cells (Maddur and Bayry, 2015).

Binding of Th2 TCR to MHC Class II leads to the release cytokines such as IL-4, IL-5, IL-9 and IL-13, which promotes B cell proliferation and antibody producing plasma cells (Nutt et al., 2015; Walker and McKenzie, 2017). Efficient tumour clearance makes use of both innate and adaptive immune responses and deregulation of both types of response can often be seen in patients with cancer (Vesely et al., 2011).

1.6.2 The immune microenvironment of prostate cancer

The immune contexture of prostate cancer has been reported to be infiltrated with immunosuppressive cells such as Tregs, M2 macrophages and Myeloid-derived suppressor cells (MDSC) (Calcinotto et al., 2018; Davidsson et al., 2018, 2012; Erlandsson et al., 2019; Chen et al., 2021; Song et al., 2022). Studies have found an increased percentage of Tregs in the prostate cancer infiltrating lymphocyte population (Kiniwa et al., 2007). Tregs from the peripheral blood of prostate cancer patients display increased suppressive abilities when compared to the healthy donors, tested using co-culture proliferation assays with CD4+ T cells (Yokokawa et al., 2008). Men with prostate cancers that show increased infiltration of Tregs have an increased risk of death from the disease (Davidsson et al., 2012). Prostate cancer is also infiltrated with immunosuppressive M2 associated macrophages and higher M2 infiltration is also associated with increased prostate cancer lethality (Erlandsson et al., 2019). Finally, immunosuppressive MDSCs have also been shown to infiltrate prostate tumours and drive castration resistance in prostate cancers via IL-23 secretion, activating AR signalling (Gabrilovich and Nagaraj, 2009; Calcinotto et al., 2018). The reduced neoantigen load and presence of immunosuppressive cells such as Tregs, M2 macrophages and MDSCs make prostate cancer an immunologically "cold" tumour.

1.6.3 Immunosuppressive role of IGFs

There is increasing evidence linking the IGF axis with regulation of the ability to mount an anti-tumour immune response. IGFs have been reported to regulate aspects of both the epithelial and stromal immune components in cancer (Trojan et al., 1993; Resnicoff et al., 1994; Liu et al., 1998; Schillaci et al., 1998; Nordstrand et al., 2017a). The principal receptor of the IGF axis, IGF-1R is also expressed by lymphoid cells such as T and B cells as well as myeloid cells such as dendritic cells, NK cells and macrophages (Kooijman et al., 1992; Badolato et al., 1994; Spadaro et al., 2017).

1.6.4 Effects of the IGF axis on the lymphoid lineage

Almost 30 years ago it was reported that downregulating IGF-1 expression using antisense in rat glioblastoma cells made them non-tumorigenic, with upregulated MHC Class I and B7 molecules. Injection of these modified cells prevented establishment of subcutaneous and brain tumours formed by unmodified tumour cells, and induced regression of established unmodified brain tumours which showed CD8+ cytotoxic lymphocyte infiltration. (Trojan et al., 1996, 1993). Similar results were shown using antisense IGF-1R in rat glioblastoma and mouse breast cancer and neuroblastoma models (Resnicoff et al., 1994; Liu et al., 1998; Schillaci et al., 2006). Supporting an inhibitory effect of IGFs on CD8+ cells, IGF-1R overexpression in lung cancer cell lines resulted in the inhibition of CD8+ cytotoxic T cells *in vitro*, mediated by increasing the expression of immune checkpoint B7-H4 through MAPK signalling (Zhao et al., 2020). IGFs have also been reported to induce the proliferation and function of immunosuppressive Tregs, which are known to infiltrate immune-cold prostate cancer and associate with cancer progression (Flammiger et al., 2013;

Davidsson et al., 2018; Rao et al., 2020; Fridman et al., 2017). IGFs are reported to increase proliferation and activation of Tregs by upregulation of transcription factors FOXP3 and E2F, CD71, activation marker CD33 and downstream genes activated via TCR and IL-2 stimulation (Bilbao et al., 2014b; Miyagawa et al., 2017; Johannesson et al., 2014; Farabaugh et al., 2015; Lu et al., 2014). IGF-1 stimulation was reported to stimulate the proliferation of Tregs, suppressing autoimmune diseases such as type 1 diabetes and multiple sclerosis (Bilbao et al., 2014b) and allergic contact dermatitis (Johannesson et al., 2014) in murine models. IGFs also contribute to secretion of immunosuppressive cytokine IL-10, which has been implicated in stimulating Tregs (Chaudhry et al., 2011; Ng et al., 2013; Warzecha et al., 2003; Kooijman and Coppens, 2004). Supporting the clinical relevance of these findings in prostate cancer, IGF-1R immunohistochemistry and transcriptomic profiling of prostate cancer bone metastases showed an inverse relationship between IGF-1R expression and immune-relevant pathways including phagocytosis, leucocyte chemotaxis, lymphocyte proliferation and cell adhesion (Nordstrand et al., 2017b).

IGF-1 administration has been reported to enhance B cell proliferation and induce B cell lymphopoiesis in the bone marrow (Dowery et al., 2021; Douglas et al., 2008; Baudler et al., 2005). Components of the IGF axis especially *Irs1* and *Igf1r* have been found to be downregulated via epigenetic regulation in bone marrow B cell precursors. Given that *Irs1* null mice have increased life- and health -span like *Igf1r* heterozygous mice, and that *Irs1* null mice have an aged T cell profile that is comparable to young mice (Holzenberger et al., 2003; Selman et al., 2008, 2011), it is possible that the precursor B cells persisting in aged mice may have adapted best to altered stress conditions in aging. Finally, paracrine secretion

of IGF-1 by B cells has been implicated in inducing acquired resistance of melanoma to BRAF and MEK inhibitors (Somasundaram et al., 2017).

1.6.5 Effects of IGFs on the myeloid lineage

IGFs can also influence cells of the myeloid compartment including DCs and macrophages. IGFs can supress DC function, its antigen presentation and priming of CD8+ T cells by regulating PI3K-AKT and MAPK pathways downstream of IGF-1R (Somri-Gannam et al., 2020; Xuan et al., 2017; Huang et al., 2015). Igf-1 stimulation can also induce bone marrow derived DC secretion of immunosuppressive IL-10 and IGF-1R inhibition can restore DC mediated anti-tumour function (Huang et al., 2015). Downregulation of *Igf1r* expression in a murine breast cancer cell line showed a decrease in proliferation and upregulation of the pro inflammatory cytokines TNF- α and IFN-γ. Murine syngeneic models with Igf1r depleted breast cancer cells displayed delayed tumour growth and increased infiltration of lymphocytes and polymorphonuclear neutrophils (Durfort et al., 2012). Additionally, liver specific deletion of Igf1 in a murine model of colon cancer liver metastasis increased the accumulation of hepatic stellate cells and neutrophils with a pro-inflammatory/anti-tumour phenotype and Igf-1r downregulation, together with tumour cell apoptosis and reduced liver metastases (Rayes et al., 2018; Fernandez et al., 2017). IL-4 differentiated M2-like macrophages are capable of secreting Igf-1 and ablation of *igf1r* in these cells resulted in a reduction in genes associated with the M2 phenotype activation (Spadaro et al., 2017). IGFs effect on M2 polarisation was attributed to its signalling via the PI3K-AKT and JAK/STAT pathway and disruption of this signalling prevented the induction of M2 phenotype (Barrett et al., 2015). Furthermore, monocytes and macrophages are a potential source of tumour

endogenous IGF-1 production (Spadaro et al., 2017; Tonkin et al., 2015; Nackiewicz et al., 2020; Wu et al., 2020). Tissue endogenous secretion of IGF-1 and IGF-2 by tumour-associated macrophages and myofibroblasts results in induction of chemoresistance in pancreatic cancer cells (Ireland et al., 2016). By activating IGF-1R on glioblastoma multiforme (GBM) cells, macrophage-derived IGF-1 has been reported to promote resistance to colony-stimulating factor-1 receptor (CSF-R) inhibition, and the combination of IGF-1R inhibition with CSF-1R inhibition was able to prevent this resistance and significantly prolong survival in a murine GBM model (Quail et al., 2016). IGF-1 and IGF-2 are both involved in the metabolic transition of macrophages from glycolysis to oxidative phosphorylation, resulting in maturation into an anti-inflammatory M2 phenotype (Du et al., 2019). IGF-2 secreted by mesenchymal stem and/or stromal cells in a low oxygen environment also upregulates the expression of immune inhibitory PD-L1 in these macrophages. Expression of PD-L1 by these cells could also enhance the immunosuppressive potential of Tregs via PD-L1:PD-1 interactions (Du et al., 2019; Francisco et al., 2009). IGF-1 primed monocytes are also immunosuppressive in nature and secrete IL-10 (Ge et al., 2015).

1.6.6 Immunosuppressive effects of IGFs on the tumour epithelium

Signaling pathways regulated by IGF-1R and other receptor tyrosine kinases may affect tumour immune responses influencing the tumour cells themselves. Patients with oesophageal squamous cell carcinoma and clear cell renal cell carcinoma who had hyper progressive disease after anti-PD-1 treatment had tumours that transcriptionally upregulated the IGF-1, MAPK and PI3K/AKT pathways, had a mutation in *IGFBP2*, encoding IGFBP2

that negatively regulates IGF-1 bioactivity (Xiong et al., 2018). PD-L1 expression is also known to be regulated by both the PI3K/AKT and ERK/MAPK pathways. Drugs targeting PI3K/AKT reduced PD-L1 transcription and expression, while activation of the MAPK pathway was reported to upregulate PD-L1 via AP-1(Mittendorf et al., 2014; Chen et al., 2015). Conversely, inhibition of MEK using trametinib upregulated MHC class 1 and PD-L1 expression in head and neck squamous cell carcinoma, making the tumour cells more sensitive to anti-PD-L1 inhibitors (Kang et al., 2019). These data suggest that IGFs could regulate PD-L1 expression, and this could be via AKT and MAPK pathways.

The ability of the IGF axis to influence immune responses through its effects on both the epithelial and stromal immune components could contribute to the role of IGFs in promoting prostate cancer risk as well as progression of established tumours and resistance to immunotherapy. From the published literature, the hypothesised roles of IGFs in immune suppression are illustrated in Figure 1-4. IGFs may aid in maturation of immunosuppressive cells and downregulate the activation of cytotoxic cells, reshaping the tumour microenvironment to become immunosuppressive. Given the known involvement of IGFs in prostate cancer biology and risk (Turney et al., 2011; Hellawell et al., 2002; Aleksic et al., 2017, 2010; Travis et al., 2016; Perez-Cornago et al., 2017; Watts et al., 2021; Siech et al., 2022; Holly et al., 2020) it will be important to understand whether effects of IGF-1 on the immune microenvironment contribute to its role in prostate cancer risk and progression.

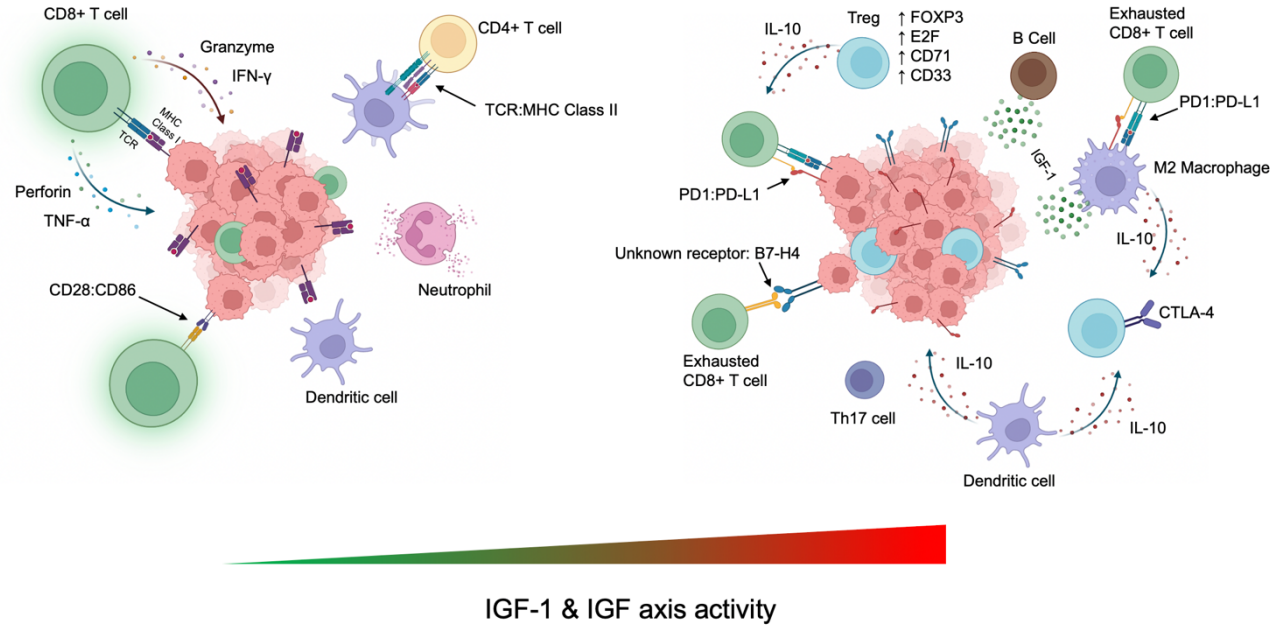


Figure 1-4 Hypothesised role of the IGF axis in tumour immune suppression. Low IGF axis activity is associated with reduced tumorigenicity and in some models with an increased anti-tumour immune response with increased infiltration of cytotoxic neutrophils and CD8+ cells, secretion of cytokines such as TNFα and IFNγ, activation, infiltration and antigen presentation of dendritic cells and increased MHC Class I expression and CD86 expression in tumour cells. On the other hand, increased IGF axis activity may contribute to infiltration and proliferation of Tregs and M2 macrophages, secretion of immunosuppressive IL-10 cytokine, paracrine secretion of IGF-1 and CD8+ exhaustion by PD-L1 and B7-H4 expression. These effects could result in an immunosuppressive tumour environment, promoting tumour growth and treatment resistance in prostate cancer. Figure assembled using Biorender from references cited in the text.

1.7 Aims of the project

As stated in the introduction, aberrant activation of the IGF axis has been linked to tumour growth and spread (Denduluri et al., 2015b; Sachdev and Yee, 2007; Kasprzak et al., 2017; Hellawell et al., 2002; Massoner et al., 2011; Turney et al., 2011). High circulating IGF-1 has been associated with increased cancer risk for prostate, breast and colon cancer (Chan et al., 1998; Key et al., 2010; Rinaldi et al., 2010; Hankinson et al., 1998; Ma et al., 1999; Knuppel et al., 2020; Roddam et al., 2008; Travis et al., 2016), and is very likely causative (Murphy et al., 2020a; b; Watts et al., 2021). However, the underlying mechanisms through which IGF-1 increases risk of prostate cancer remain uncertain. The overarching aim of this project is to **understand the biological mechanisms through which high circulating IGF-1 levels contribute to an increased risk of prostate cancer.** To understand the mechanisms associated with cancer risk, the role of IGFs in both the prostatic epithelium and the tumour stroma will be investigated.

The association between high circulating IGF-1 levels and IGF-1R expression in malignant but not benign prostatic epithelium may suggest that IGFs are promoters, rather than drivers of tumorigenesis. Based on the current literature, it can be hypothesised that high serum IGF-1 upregulates IGF-1R in cancers, promoting the growth of occult tumours to become clinically significant. To understand the role of IGFs in the prostatic epithelium, I will interrogate the following aim:

Aim 1: To investigate whether expression of *IGF1R* mRNA parallels IGF-1R protein levels detected by IHC in primary prostate cancer, and to develop an *in vitro* model to test for

effects of IGF-1 on IGF-1R expression and subcellular localisation in prostate cancer cells. To mimic chronic exposure to high serum IGF-1, I will use acute vs long term IGF-1 stimulation in prostate cancer cell lines.

There is strong evidence in literature to suggest that IGFs can influence the ability to mount an anti-tumour immune response. Based on this, it can by hypothesised that the pro-tumorigenic effects of high IGF-1 is partly mediated by its immunosuppressive effects on the tumour microenvironment. To understand the role of IGFs in immunosuppression, I will investigate the following aims:

Aim 2: Test for immunosuppressive effects of IGF-1 on the tumour epithelium using prostate cancer cell line models, and assess associations between IGF supply and selected immune markers in publicly available transcriptional data.

Aim 3: To investigate associations of high circulating IGF-1 with the number and phenotype of tumour infiltrating immune cells in primary prostate cancers using bulk RNA sequencing, single-cell RNA sequencing and multiplexed immunofluorescence imaging.

The long-term aims of this project are to understand how high serum IGF-1 associates with risk of prostate cancer, in order to develop new approaches to risk reduction. Understanding how IGFs influence the immune response may also aid in better treatment of immune-cold prostate cancer, especially in patients with advanced prostate cancer, where immunotherapy has not been successful.

2 Chapter 2: Materials and Methods

2.1 Cell lines

All cell lines used for the experiments below are listen in . Cells were cultured as monolayers at 37°C in the specified medium and CO_2 percentage as listed in . Human prostate cancer cell line DU145, Mouse Prostate Epithelial Cells (MPEC) (Barclay and Cramer, 2005), and human colorectal cancer cell line H747 (NCI-H747) cells were cultured in RPMI 1640 Medium (Gibco, #21875034) supplemented with 10% Fetal Bovine Serum (FBS, Gibco, #10500064) and 1% Penicillin-Streptomycin (Gibco, #15140122). Additionally, MPEC cells were also supplemented with 100nM of Dihydrotestosterone (DHT, Sigma, #D-073). Murine prostate cancer cells derived from primary tumours in high Myc-mouse: MyC-CaP (Watson et al., 2005a), and human prostate cancer VCaP cells were cultured in Dulbecco's Modified Eagle Medium (DMEM, Gibco, #41966029) supplemented with 10% FBS, and 1% Penicillin-Streptomycin. MPEC cells were received from Prof Ian Mills.

DU145, MPEC, H747 and MyC-CaP cells were passaged when they were over 80% confluent. Cells were disaggregated using Trypsin/EDTA 10x (Lonza, #LZBE02-007E), diluted to a 5x working solution with sterile phosphate buffered saline (PBS) and incubated for 3 mins at 37°C. Trypsin was then neutralised with 10% FBS containing medium and cells reseeded. Non-adherent VCaP cells were cultured on Matrigel Growth Factor Reduced (GFR) Basement Membrane Matrix (Corning, #356230) coated flasks and passaged when they were 90% confluent. Pipette tips were chilled in the fridge at 4°C for 15 mins prior to

being used to coat flasks with Matrigel. Matrigel was diluted with chilled DMEM (10% FBS, and 1% Penicillin-Streptomycin) to prepare a 300 µg/ml solution. The diluted solution was added to the flasks (2 ml for T175 flasks, 1 ml for T75 flasks) and spread evenly across their surface. The flasks were then incubated at room temperature for an hour for the Matrigel to solidify, after which any excess Matrigel was removed. To passage the VCaP cells, the culture medium was first collected from the flask to save any floating cells and 1 ml conditioned medium set aside to add to the new flasks. Cells were disaggregated with the above-mentioned diluted Trypsin solution at 37°C for 3 mins and neutralised with old culture medium. This was then spun down at 300 x g for 5 mins and the cell pellet resuspended in fresh DMEM medium (10% FBS, and 1% Penicillin-Streptomycin). Cells were reseeded at 30-40% confluence and the 1 ml of conditioned medium was added back to the flasks.

Early passage cells were routinely banked in cryopreservation solution (5% dimethyl sulphoxide (DMSO) and 95% FBS) and frozen slowly in a 'Mr Frosty' at -80 °C. Cryopreserved cells were unbanked by thawing the vials in the 37°C water bath and transferring the cell suspension to a culture flask containing warm culture medium. The culture medium was changed after 24 hours to remove DMSO and dead cell debris. All cultures were also routinely monitored for mycoplasma infection using the MycoAlert kit (Promega, #LT07-703).

Cell line	Origin	Species	Medium	CO_2 requirement
DU145	Prostate cancer	Human	RPMI 1640	5%
VCaP	Prostate cancer	Human	DMEM	10%
MyC-CaP	Prostate cancer	Mouse	DMEM	5%
MPEC	Benign prostate epithelium	Mouse	RPMI	5%
H747	Colorectal cancer	Human	RPMI	5%

Table 2-1 List of cell lines. Tables indicates cell lines used in this project, their origin, species, medium cultured in and their CO_2 requirements.

2.2 Cell treatments

2.2.1 IGF-1 treatment

For short-term (4 hrs or 24 hrs) IGF-1 stimulation assays, cells were serum starved by replacing 10% FBS culture media with 0% FBS culture media for 24 hrs. This was followed by 30 nM IGF-1 stimulation for the indicated times. Solvent control of 10nM HCl was used for control treatments. For long-term IGF-1 treatments, DU145 cells were adapted in low serum culture (0.2% FBS) for four weeks and then treated with solvent control (10 nM HCl) or 30 nM IGF-1 for 8-12 weeks. VCaP cells were grown in 10% FBS cultures and then treated with control or 30 nM IGF-1 for 8-12 weeks. Culture medium was replaced with fresh IGF-1 supplemented medium every 3 days as IGF-1 had a half-life of ~3 days. Long term cultures were tested for endogenous production of IGF-1 using conditioned medium collected from confluent cultures. Media was centrifuged to remove any cells and stored at -80°C until ready for analysis. IGF-1 assays were performed in the Biochemistry

Laboratory, John Radcliffe Hospital using the IDS-iSYS Insulin like Growth Factor-I (IGF-I) assay (IDS Immunodiagnosticsystems, Boldon Colliery UK) supervised by Professor Tim James.

2.2.2 *IGF1R* siRNA treatment

Cells were seeded at 4 x 10^5 cells per 6 cm dish to become 30-40% confluent the following day. They were then transfected with 50 nM IGF1R (Hs_IGF1R_1, Qiagen) or All Stars negative control (Qiagen) siRNAs using Oligofectamine transfection reagent (Invitrogen, #12252011). Briefly, 2.5 µl of 20 µM siRNA stock was mixed with 558 µl Optimem (Gibco, #31985070) and incubated for 10 mins at room temperature. In another tube, 4.5 µl Oligofectamine was mixed with 150 µl Optimem and incubated concurrently at room temperature for 10 mins. After the first incubation, both the mixes were combined and incubated for 25 mins at room temperature. Cells were washed twice with Optimem and 285 µl Optimem was added to each dish. Following this, 715 µl of the siRNA mixture was added to each plate and the cells were incubated at 37°C for 4 hrs. After the incubation, dishes were topped up with 100 µl FCS and 4ml RPMI supplemented with 10% FBS. After transfection, cells were grown for 48 hrs and then used for downstream applications. Quality of the siRNA knockdown was assessed using western blot.

2.2.3 Small molecule inhibitors

IGF-1R tyrosine kinase activity was inhibited using the small molecule inhibitor BMS-754807 (Bristol Myers Squibb, #S1124). AKT pathway was inhibited using the allosteric inhibitor (Astrazeneca, #S8019). MEK1/2 pathway was inhibited using trametinib (GlaxoSmithKline, #S2673).

2.3 Immunofluorescence

Coverslips were sterilised by washing in 75% ethanol and placed in a 6-well plate. Any remaining ethanol on the coverslip was removed by washing the wells with sterile PBS. For immunofluorescence (IF) of loosely-adherent VCaP cells, coverslips were coated with Poly-L-lysine (Sigma, #P8920) for cell attachment. This process involved adding 1 ml of neat Poly-L-lysine onto sterilised coverslips for 5 mins. After incubation, all the Poly-L-lysine was aspirated and the coverslips were washed with sterile PBS 3 times. They were then left to airdry (~3 hrs) at room temperature until ready to be used for IF.

To perform the assay, 300,000 cells were seeded onto the prepared coverslips and cultured overnight. Cells were serum starved the next day for 24 hours and then treated with 30 nM of IGF-1 for 24 hours. After treatments, cells were fixed for 20 mins at room temperature (RT) by aspirating medium and replacing with 1 ml fixation solution (4% paraformaldehyde, 0.1% Triton X-100 in PBS). Fixation solution was then aspirated and replaced with 1 ml permeabilisation solution (0.5% Triton X-100 in PBS) and incubated for an additional 3 mins at RT with rocking. After aspirating permeabilisation solution, wells were washed with

PBS (2 times, 3 mins each) and incubated with blocking solution (5% BSA, 0.3% Triton X-100 in PBS) at RT for 1 hr with rocking to reduce non-specific binding of antibodies. Then 800 µL of IGF-1R-β antibody (Cell Signaling Technology, CST; #9750) diluted (1:500) with blocking buffer was added to the relevant wells and the 6 well plate was incubated at 4°C with rocking for ~18 hours.

Next day, cells were washed in PBS (3 times, 3 mins each), incubated with Alexa fluor-488 conjugated anti-rabbit secondary antibody (CST, 1:2000 dilution in blocking buffer) for 1 hour at RT in the dark. This was followed by 3 washes with PBS and incubation in 3 drops of actin-phalloidin stain neat (Alexa Fluor 568 Phalloidin, Invitrogen, #A12380) for 10 mins. After staining, wells were washed with PBS (3 times, 3 mins each), and coverslips were mounted with Vectashield mounting medium containing 4′,6-diamidino-2-phenylindole (DAPI,Vector Laboratories, #H-1200-10). Edges of the coverslips were sealed with nail varnish and slides were stored in the dark at 4°C. IGF-1R-β staining was visualised on Zeiss LSM780, confocal microscope system and scanned images were quantified for nuclear staining using Fiji Image J (version 2.0).

2.4 Quantitative real-time Polymerase Chain Reaction (qRT-PCR)

2.4.1 Ribonucleic acid (RNA) extraction

Before RNA extraction, the lab bench was wiped down with 70% ethanol and RNaseZap (Invitrogen, #AM9780) to create an RNase-free environment. RNA extraction was performed on snap frozen cell pellets using the ReliaPrep RNA Miniprep kit (Promega,

#Z6010), following manufacturer's protocol. To extract total RNA, 250 µl of BL + TG lysis buffer was added to the frozen cell pellet before thawing on ice. Once thawed, the lysates were pipetted 3-4 times to shear the DNA, then 85 µl of Isopropanol was added and the lysed sample was vortexed for 5 sec. Lysates were then transferred to a ReliaPrepTM Minicolumn, placed on top of a collection tube and centrifuged at 13,000 × g for 30 sec at RT. 500 µl of RNA Wash solution was then added to the column, centrifuged at 13,000 × g for 30 sec and the contents of the collection tube discarded. In a sterile nuclease free tube, DNase I incubation mix consisting of 24 µl of yellow core buffer, 3 µl of 0.09M $MnCl_2$ and 3 µl of DNase I enzyme (per sample) was prepared. The DNase I incubation mix (30 µl/sample) was added onto the membrane of the ReliaPrepTM Minicolumn and incubated for 15 mins at RT. After incubation, 200 µl of Column Wash Solution was added to the column and centrifuged at 13,000 × g for 15 sec. The column was washed twice with RNA Wash solution (500 µl and 300 µl), replacing the collection tube with a fresh tube before the second wash, and centrifuging at 13,000 × g for 30 sec after each wash. The column was then placed onto an elution tube and RNA was collected by adding 30 µl of nuclease-free water to the membrane and centrifuging at 13,000 g for 1 minute. Yield and quality of the purified RNA was measured using a NanoDrop (Thermo Scientific, #ND-ONE-W). Using this protocol, pure RNA had A260/A280 ratios between 1.7–2.1 and A260/A230 ratios between 1.8–2.2. RNA was stored at –20°C for immediate use or –80°C for long-term use.

2.4.2 Complementary DNA (cDNA) synthesis

Purified RNA was reverse transcribed into complementary DNA (cDNA) with SuperScript III First-Strand Synthesis System (Invitrogen, #18080051), following manufacturers

protocol. To prepare the cDNA synthesis mix, 2 µl of the enzyme mix containing reverse transcriptase, 10 µl reaction buffer and 1µg total RNA was added to a PCR tube. Nuclease free water was added to make up 20 µl final volume and the contents mixed. The PCR tube was then placed in a Thermo Cycler (Thermo Fisher, #A37834) to incubate for 10 mins at 25 °C, 30 mins at 50 °C and 5 mins at 85 °C. After the reaction, the tubes were chilled on ice (5 mins), centrifuged (13,000 × g for 15 sec to collect condensation and 1 µl RNase H was added to degrade any non-transcribed RNA. After incubation at 37 °C for 20 mins cDNAs were stored at -20 °C.

2.4.3 Primer design and validation

Primers for quantitative reverse-transcription PCR (qRT-PCR) were designed using National Centre for Biotechnology Information (NCBI) Primer-BLAST (www.ncbi.nlm.nih.gov/tools/primer-blast). The mRNA reference sequence (ReSeq RNA) accession numbers were used to generate primer pairs which produced a PCR product of 100-170 base pairs (bp), with melting temperatures (T_m) of 58-62°C, and a maximum of 2°C T_m difference between primer pairs. They were also designed to span an exon-exon junction, have GC content between 50-65% with potential to amplify mRNA splice variants. The primers were synthesised by Integrated DNA Technologies (IDT) and are listed in Chapter 4. Lyophilised primers were resuspended in nuclease free water to make 100 µM primer stocks. A target gene primer mix (12.5 µM) was prepared by adding 50 µl of the forward and 50 µl of the reverse primers in 300 µl nuclease free water and stored at -20°C.

Target	Sense	Sequence
IGF1R	Forward	GCCCAAACCCTTAACTGACA
	Reverse	GGACAGGGACAGAGTGAGGA
KLK3 (PSA)	Forward	ATTTCCAATGACGTGTGTGCG
	Reverse	ATCAGAATGACCCACGAGCA
Androgen receptor (AR)	Forward	GCCACTCAGACCCACTTAGC
	Reverse	CCTCACTCTTCGTCCACATCG
CD274 (PD-L1)	Forward	GTGGCATCCAAGATACAAACTCAA
	Reverse	TCCTTCCTCTTGTCACGCTCA
β-Actin	Forward	GATGAGATTGGCATGGCTTT
	Reverse	CACCTTCACCGTTCCAGTTT
B2M	Forward	TGCTGTCTCCATGTTTGATGTATCT
	Reverse	TCTCTGCTCCCCACCTCTAAGT
STAT5A	Forward	ATTCACCACGCGGGATTTCT
	Reverse	AGCTTTAGCCAGCACAGGAG
CXCL8	Forward	TGGAGAAGTTTTTGAAGAGGGCT
	Reverse	ACAGACCCACACAATACATGAAG
CCL5	Forward	GCAGTCGTCCACAGGTCAAG
	Reverse	TCTTCTCTGGGTTGGCACAC
IFNB1	Forward	AGTAGGCGACACTGTTCGTG
	Reverse	GCCTCCCATTCAATTGCCAC
CXCL10	Forward	CCACGTGTTGAGATCATTGCT
	Reverse	TGCATCGATTTTGCTCCCCT
ARG2	Forward	GGAGATTCTCAGTGCTGCGG
	Reverse	CCTTTTCTTTTCTGCCCTTGTGA
IFIT1	Forward	GTGCTTGAAGTGGACCCTGA
	Reverse	CCTGCCTTAGGGGAAGCAAA

Table 2-2 List of primers. Table indicates list and sequence of primers used for qRT-PCR analysis

2.4.4 qRT-PCR

Gene expression was measured using qRT-PCR on the 7500 Fast Real-Time PCR System, (Thermo Fisher, #4351106) using SYBR Green (New England Biolabs, #M3003L). The reaction master mix consisted of 200 µg of cDNA, 10 µl of SYBR green, 1 µl of the target primer mix and nuclease free water to make up a final volume of 20 µl. Each reaction was set up in triplicates and the assay run using the following temperatures: initial denaturation at 95°C for 60 sec, 40-45 cycles of denaturation (95 °C for 15 seconds) and extension (60°C for 30 sec). Every assay also contained a no-template control (NTC) using nuclease-free water instead of cDNA to test for DNA contamination and primer dimer formation. At the end of each PCR run primer specificity was quality checked using the melt curve feature of the qRT-PCR machine, where production of a single peak suggested the presence of a single product.

2.4.5 Relative quantification

The relative quantification as fold change was calculated using $2^{-\Delta\Delta CT}$ method (Livak and Schmittgen, 2001) to show changes in gene expression of the treatment group compared to the control. Expression values from the qRT-PCR were first normalised against the reference/housekeeping gene (specified for each experiment) to correct for differences in the amount of cDNA loaded:

ΔC_T Control = C_T (Control gene) – C_T (Reference gene)

ΔC_T Target = C_T (Target gene) – C_T (Reference gene)

Fold change was then measured as the difference in mRNA expression between the target sample and the control sample. Values were then exponentially transformed.

$\Delta\Delta C_T = \Delta C_T$ Control – ΔC_T Target

$2^{-\Delta\Delta CT}$ = Exponentially transformed value

2.5 Western blot

Cells were grown as monolayers and treated as described in the respective experiments. Cell culture medium was then aspirated and adherent cells washed twice with cold PBS. Monolayers were then scraped using disposable plastic scrapers (Fisher-Scientific, #11577692) and collected in 3 ml cold-PBS, pelleted by centrifuging at 400 x g, 4 ºC for 5 mins and the PBS aspirated off. The cell pellet was lysed immediately or snap frozen in dry ice and ethanol to be stored at -80°C.

Cell pellets were lysed in RIPA buffer (Sigma-Aldrich, #R0278-50ML) with protease inhibitor cocktail (Roche, #11873580001), phosphatase inhibitor cocktail 1 (Sigma, #P2850) and phosphatase inhibitor cocktail 2 (Sigma, #P5726). After lysis on ice for 30 mins, eppendorfs were centrifuged at 16,000 x g for 15 mins at 4°C to pellet insoluble debris. Protein concentration was measured using the Pierce BCA Protein Assay Kit (Thermo Fisher, #23227) on the POLARstar Omega plate reader (BMG Labtech, #415-201) at 562 nm absorbance as per manufactures instructions. Samples were normalised for equal protein concentration (usually 70 µg), and denatured in 1x NuPAGE LDS Sample Buffer

(Invitrogen, #NP0007) and 0.1 M Dithiothreitol (DTT) at 95°C. Proteins were then separated by molecular weight by electrophoresis on 7.5% polyacrylamide gels. Proteins were transferred onto nitrocellulose membrane by semi-dry transfer using the Trans-Blot Turbo device (Bio-Rad, #1704155) and the accompanying transfer kit (Bio-Rad, #1704271). The nitrocellulose membrane was then blocked for an hour at RT with Intercept blocking buffer (Li-Cor, #927-90001) to reduce non-specific antibody binding. After blocking, the membrane was incubated with primary antibodies overnight at 4°C. List of antibodies and their dilutions are given in Table 2-3.

The following day, membranes were washed with PBS-T (1X PBS and 0.1% Tween) thrice for 5 mins each and incubated for one hour at RT with secondary IRDye antibody (Li-Cor, anti-Rabbit: #926-68073, anti-Mouse: #926-68072). After incubation, membranes were washed again with PBS-T (3 times, 5 mins). Following this, bound antibodies were visualised on the Odyssey Quantitative Fluorescence Imaging System. Western blot band intensities were quantified using Fiji Image J (version 2.0) by normalising the target protein intensity to the loading control.

Name	Host and isotype	Provider	Catalogue number	Dilution
Phospho-IGF-I Receptor β (Tyr1135/1136)	Rabbit IgG	CST	3024	1:1000
IGF-I Receptor β	Rabbit IgG	CST	3027	1:1000
Phospho-Akt (Ser473)	Rabbit IgG	CST	4058,4060	1:1000
Akt	Rabbit IgG	CST	9272	1:1000
β-Tubulin	Mouse IgG	CST	86298	1:1000
Phospho-p44/42 MAPK (Erk1/2) (Thr202/Tyr204)	Rabbit IgG	CST	9101	1:1000
p44/42 MAPK (Erk1/2)	Mouse IgG	CST	4696	1:1000
Androgen Receptor	Rabbit IgG	CST	5153	1:1000
Phospho-S6 Ribosomal Protein (Ser235/236)	Rabbit IgG	CST	2211	1:1000
S6 Ribosomal Protein	Rabbit IgG	CST	2217	1:1000
STING	Rabbit IgG	CST	13647S	1:1000
Phospho-IRF-3 (Ser396)	Rabbit IgG	CST	4947S	1:1000
IRF-3	Rabbit IgG	CST	4302S	1:1000
Phospho-STAT1 (Tyr701)	Rabbit IgG	CST	9167S	1:1000
STAT1	Rabbit IgG	CST	14994S	1:1000
Phospho-TBK1/NAK (Ser172)	Rabbit IgG	CST	5483S	1:1000
TBK1	Rabbit IgG	CST	3013S	1:1000

Table 2-3 List of western blot primary antibodies. Table indicated the primary antibodies used for western blot assays, their host, provider, catalogue number and dilutions.

2.6 Flow cytometry

PD-L1 surface expression was measured using flow cytometry. Cultured cells were dissociated with 2 mM Ethylenediamine tetraacetic acid (EDTA, Sigma, #324506) diluted in PBS at 37 °C and collected in cold MACs buffer (1XPBS+ 0.5% BSA+ 2mM EDTA) to prevent cell aggregation. This suspension was centrifuged for 5 mins at 400 g and resuspended with fresh MACs buffer. The cell suspension was centrifuged again with the same settings as before and resuspended in Phycoerythrin (PE) conjugated anti-human PD-L1 (BioLegend, #329705) or PE IgG2b isotype control (BioLegend, #400312), diluted in MACs buffer at 1:100 and 1:50 respectively. PE conjugated anti-mouse PD-L1 (BioLegend, #124307) and PE isotype control (BioLegend, #400607) were both diluted in MACs buffer at 1:50. Fluorophore conjugated antibodies were incubated with the cells for 30 mins in the dark at RT. MACs buffer was then added and the samples were centrifuged for 5 mins at 400 g, 4°C. Cells were washed by resuspending with MACs buffer, centrifuged again and fixed with 10% Neutral buffered formalin (NBF) in PBS for 10 mins. Fixed cells were centrifuged (5 mins at 400 g), resuspended in fresh MACs buffer at 200 µL final volume and stored in the dark at 4°C until flow cytometry analysis. PD-L1 surface expression was measured on the Attune NxT Flow Cytometer and data were analysed using FlowJo 10.8.1.

2.7 Clinical samples

2.7.1 Fixed tissues

Immunohistochemistry (IHC), *in situ* hybridization (ISH, RNAScope), multi-spectral immunofluorescence and RNA sequencing were performed on formalin-fixed paraffin-embedded (FFPE) sections of radical prostatectomies from patients recruited to the Prostate Cancer Mechanisms of Progression and Treatment (ProMPT) study (UK MREC number 01/4/61). Samples were collected for this specific work under the Oxford Radcliffe Biobank (ORB) approved study 20/A028, and 4 μm sections were cut at the Oxford Centre for Histopathology Research (OCHRe). IGF-1R IHC was also conducted on tissue microarray (TMA) slides made from RPs from patients recruited to the European Prospective Investigation into Cancer and Nutrition (EPIC) study. The TMA sections were provided by Prof Clare Verrill and this work was conducted under REC-approved study 07/H0606/120: 'The role of insulin-like growth factor (IGF) signaling in tumour biology'. Samples used for this study were from a narrow Gleason grade group between 3+4 and 4+3.

2.7.2 Fresh tissues

For single-cell transcriptional profiling, we set up a fresh prostate tissue collection pipeline via the Oxford Radcliffe Biobank (study 20/A032), with the help of surgeons Prof Freddie Hamdy and Dr Alastair Lamb. Prostatectomies were taken unfixed by ORB tissue collector Miriam O'Hanlon to the Pathology Department, John Radcliffe Hospital. Briefly, punch biopsies (~4 mm^3) were taken by Prof Clare Verrill, Dr Richard Colling or Dr Gill Pelvender from the index tumour of 12 prostate cancers using Prof Verrill and Dr Gill's protocol for

research sampling of radical prostatectomies (Gill et al., 2012). Fresh tumours were collected in MACS Tissue Storage Solution (Miltenyi Biotec, #130-100-008) and kept at 4°C until ready for processing.

2.8 Immunohistochemistry

IGF-1R- β immunohistochemistry (IHC) was performed as per the protocol optimised in our laboratory (Aleksic et al., 2016). To check the specificity of the antibody, control sections were made using IGF-1R siRNA depleted DU145 cells and IGF-1R CRISPR knocked out DU145 cells (generated by Dr Eliot Osher). To prepare these control FFPE sections, cells were fixed in 10% neutral buffered formalin (NBF) overnight at 4°C and moved to 70% ethanol for an additional 24 hrs. Cell pellets were then processed and paraffin embedded by Marcus Green, Histopathology facility, Department of Oncology, University of Oxford. Processed FFPE blocks were cut into 5 µm sections using the microtome (Leica, RM2125), mounted onto charged slides (Leica, #75809-488) and dried overnight at 37 °C.

Tissue and control cell pellet sections were incubated at 60 °C for 15 mins, dewaxed using Citroclear (TCS Biosciences Ltd, # HC5005-5L) and rehydrated in decreasing concentrations of ethanol (2 mins each in 100%, 95% 80%, 70% and 50%) and distilled water (dH_2O). Heat based antigen retrieval was performed in 50 mM Tris-Cl, 2 mM Ethylenediaminetetraacetic acid (EDTA) pH 9 buffer (TE) at 125°C for 2 mins and 85°C for 10 mins using a decloaking chamber (Biocare Medical, #DC2002). Slides were then chilled on ice for 15 mins to bring to room temperature (RT) and blocked with 3 % hydrogen peroxide (H_2O_2) in dH_2O for 10 min (RT) to prevent non-specific background staining

produced from endogenous peroxidase. Slides were then washed with PBS thrice for 5 mins each and blocked with 5% bovine serum albumin (BSA), 5% goat serum in PBS for 1 hr at RT. Tissue areas on the slides were marked with a hydrophobic barrier pen and placed onto a humidefied chamber. Slides were then incubated with IGF-1R-β antibody (CST, #9750), diluted 1:50 in blocking solution, overnight at 4 °C.

Following incubation with the primary antibody, slides were washed in PBS (3 times, 5 mins each) and bound antibody was detected using the MP-531-M3R25 kit from Menarini Diagnostics. This involved adding 3 drops of rabbit probe for 15 mins at RT, followed by PBS washes (3 times, 5 mins each) and incubating with rabbit HRP polymer for 15 mins at RT. Slides were then washed in PBS (3 times, 5 mins each) and colour developed using 3,3'-Diaminobenzidine (DAB) substrate (Envision, # K346711-2) for 5-7 mins. Excess DAB was washed away in tap water (3 times, 2 mins each) and slides were counter stained in Mayer's haematoxylin (Vector Laboratories, # MHS32-1L) for 20 sec. Slides were washed in tap water to remove excess stain and then dehydrated in increasing concentrations of ethanol (2 mins each in 50%, 70%, 80%, 95% and 100%) and Citroclear (5 mins). Finally, coverslips were mounted onto slides with DPX reagent (Sigma, 1005790500) and left to air dry overnight at RT. Once the slides dried, excess mounting medium was cleared using a blade and slides were scanned using the Aperio brightfield ScanScope digital slide scanner at 40x magnification. The scanned images were scored for IGF-1R staining by Prof Clare Verrill, scoring for IGF-1R expression in the cell membranes, cytoplasm and nuclei. These scores were summed to produce total IGF-1R immunoreactive score.

2.9 Colorimetric *In Situ* Hybridisation using RNAScope

RNAScope was used to quantify *IGF1R* mRNA expression in FFPE tissue sections using RNAscope 2.5 assay kit (Bio-Techne, #322350) according to the manufacturer's protocol. RNA Scope is an improved RNA *in situ* hybridisation technique with a reduced signal-to-noise ratio due to target specific amplification. Target probes for specific genes can bind and hybridise to the target RNA. The double-Z design of the target probes allows for binding of sequential fluorophore conjugated amplicons to it and ultimately signal can be visualised using a florescent microscope (Wang et al., 2012). Experiments were conducted on tissues from the ProMPT cohort and sections were cut with RNase-free precautions by Marcus Green. To test the specificity of the *IGF1R* probe, control sections were used of FFPE IGF-1R depleted or null cells as in Section 2.2.2.

Slides were baked at 60°C for 15 mins and deparaffinised by immersion in Xylene (2 times, 5 mins each) and 100% ethanol (2 times, 1 min each) and left to airdry at RT for 15 mins. Once dry, slides were treated with 5-8 drops of RNAscope Hydrogen Peroxide to reduce non-specific binding and washed in dH_2O. A water bath was set up with two slide holders, the first filled with dH_2O and the second with RNAscope target retrieval reagent (Bio-Techne, #322350). The water in the water bath was heated to at least 99°C. Slides were immersed first in dH_2O for 10 sec to equilibrate to the temperature and then placed in the target retrieval holder for 30 mins. After antigen retrieval, slides were rinsed with dH_2O and incubated in 100% ethanol (3 mins, RT) and left to dry for 5 mins in the 60°C incubator. A temperature resistant hydrophobic barrier was drawn around the tissues with ImmEdge barrier pen (Vector laboratories, #H-4000) and left to dry at RT for 10 mins. Slides were

treated with 5 drops of RNAscope Protease Plus reagent and baked at 40°C for 30 mins to digest nucleases. Slides were then washed in dH_2O and incubated with *IGF1R* (ACDBio, #471961) or *PPIB* (ACDBio, #313901) mRNA probes for 2 hrs at 40°C. The Peptidylprolyl Isomerase B (*PPIB)* gene is expressed at low levels in most tissues, and the *PPIB* probe was the recommended positive control to check the integrity of RNA in the tissue sections (https://acdbio.com/control-slides-and-control-probes-rnascope). After incubation with the probes, tissues were hybridised with sequential amplicons (Hybridize Amp 1-6, as per the protocol recommended time and temperature) to intensify the target signal. Slides were washed with the wash buffer provided and RNAscope red detection reagent was added for 10 mins at RT. Once colour developed after 10 mins, sections were washed in tap water, counter stained for 20 seconds with 50% Haematoxylin and blued by rinsing in 0.02% Ammonia water. Finally, slides were dried by incubating at 60°C for 15 mins, dipped in fresh Xylene and coverslips mounted using EcoMount (Biocare Medical, #PBC-BRR897L). As in the IHC protocol, excess mounting medium was cleaned off the dried slides and slides were scanned using the Aperio brightfield ScanScope digital slide scanner at 40x magnification.

Tumour areas were manually marked on the images by Uro-Pathologist Prof Clare Verrill. Digital image analysis was conducted by Dr Nasullah Khalid Alham, Clinical Informatician, University of Oxford using the Visiopharm Integrator System platform (version 2018.4.3.4480, Hoersholm, Denmark), and image analysis protocols were implemented as analysis protocol packages (APPs) as described by Rao et al (Rao et al., 2020). The APPs were used to detect the benign areas and mark the outer and inner margins of the benign and tumour areas. After quantifying the areas (μm^2) of the centre of the tumour, inner margin,

outer margin and benign areas, the software produced measurements (μm^2) of positive *IGF1R* mRNA staining in these areas.

2.10 Multiplex Immunofluorescence

Multiplex immunofluorescence (M-IF) was performed on 4 μm FFPE sections of radical prostatectomies from the ProMPT cohort by Leticia Campo, with the support of Dr Alistair Easton and Leticia Campo in the Translational Histopathology Laboratory, University of Oxford. The experiments were conducted using the OPAL protocol (AKOYA Biosciences) on the Leica BOND RX autostainer. Staining was performed in six successive cycles using the primary antibody and their assigned opal fluorophore pairings listed in Table 2-4. In brief, antigen retrieval was performed at 100 °C for 20 mins followed by Epitope Retrieval (ER) with solutions 1 or 2 (Leica Biosystems, ER1 AR9961, ER2 #AR9640). Slides were incubated with primary antibodies for an hour at RT and colour detected using the BOND Polymer Refine Detection System (Leica Biosystems, #DS9800), replacing the DAB for the specific Opal fluorophores with ten-minute incubation at RT. Following this, sections were incubated with spectral DAPI (Akoya Biosciences, #FP1490) for 10 mins and mounted with Vectashield Vibrance Antifade Mounting Medium (Vector Laboratories, #H-1700-10). After all the staining were performed, slides were scanned by Leticia Campo on the AKOYA Biosciences Vectra Polaris.

Primary Antibody	Dilution	Antigen Retrieval	Assigned Opal	Opal Dilution
PD-L1 (CST, Cat# 13684)	1:1600	ER2/ 20 mins	520	1:150
CD4 (Leica, Cat# NCL-L-CD4-368)	1:100	ER2/ 20 mins	540	1:150
FoxP3 (Abcam, Cat# ab20034)	1:100	ER2/ 20 mins	620	1:150
CD8 (Dako, Cat # M7103)	1:400	ER2/ 20 mins	650	1:500
Pan-Cytokeratin (Dako, Cat# M3515)	1:1000	ER2/ 20 mins	690	1:150
Cytokeratin 5 (Leica, Cat# NCL-L-CK5)	1:200	ER1/ 20 mins	620	1:150

Table 2-4 Antibodies used for M-IF. Table shows list of M-IF antibodies, their dilution, antigen retrieval epitope retrieval (ER) solution used and timings, assigned secondary Opal antibodies and their dilution. M-IF assay was optimised and performed by Leticia Campo, Translational Histopathology Laboratory.

2.11 HALO Image analysis

Immunofluorescence images were merged by Leticia on inForm 2.4.8 (Akoya Biosciences). Training in multispectral image analysis was provided by Dr Alistair Easton, Translational Histopathology Laboratory. The analysis was performed using using the HALO platform.

The first step involved Uro-Pathologist Clare Verrill marking areas of cancer and percentage cancer content on the images of parallel H&E stained sections from the same cases on which multiplex imaging was performed. I then annotated cancer areas on the multiplex images on the HALO platform, making the remaining areas as benign. Following this, I taught the platform to differentiate between areas of epithelium, stroma and artifact using the MiniNet AI classifier. Classification of tumour and benign glands at single-gland level was also performed using epithelial markers Pan-cytokeratin (PCK, luminal cell marker) and Cytokeratin 5 (CK5, basal cell marker, positive in benign glands). Cell detection and quantification were performed using the HighPlex FL v3.1.0 module and results were then analysed using Prism.

2.12 RNA Extraction from FFPE tissue sections

FFPE sections (4 μm) of radical prostatectomies from the ProMPT cohort were cut by OCHRe using RNase-free conditions. The malignant areas were marked on images of H&E stained sections by Uro-Pathologist Prof Clare Verrill. Slides were deparaffinised by immersion in Histoclear for 2 mins. Following this, marked malignant areas were scraped from the slide with a scalpel and transferred into a 1.5 ml nuclease-free eppendorf containing 800 ul xylene. Four adjacent replicate slides sectioned at 4 μm thickness were used per sample. RNA extraction was performed using the High Pure FFPET RNA Isolation Kit (Roche, #06650775001) as per manufacturer's instructions. Briefly, eppendorfs containing the scraped tissues were vortexed and then 400 μl absolute ethanol was added. Samples were centrifuged for 2 mins at 16,000 x g, RT, and the supernatant was discarded. The pellet was resuspended with 1 ml ethanol, vortexed, and centrifuged again for 2 mins at 16,000 x g.

The supernatant was discarded and the tissue pellet was dried for 20 mins at 56°C with the eppendorf cap open.

Then, 100 µl RNA Tissue Lysis Buffer, 16 µl 10% SDS, and 40 µl Proteinase K were added to each tissue pellet, which was vortexed and incubated for 30 mins at 85 °C with shaking (600 rpm). The mixture was cooled to below 55 °C before adding 80 µl Proteinase K and incubating for 40 mins at 55°C with shaking (600 rpm). RNA Binding Buffer (325 µl) and 325 µl absolute ethanol were added to the lysate, vortexed, transferred to a High Pure filter tube containing a glass fibre fleece membrane and placed on a High Pure collection tube. The sample was centrifuged for 30 sec at 6,000 × g, collection tube replaced with a fresh tube and centrifuged again for 2 mins at 16,000 × g to dry the filter. The dried filter tube was placed onto a fresh collection tube and 100 µl DNase was added and samples incubated at RT for 15 mins. The columns were washed once with 500 µl Wash Buffer I, and twice with 500 µl Wash Buffer II, with centrifugation (20 sec at 6,000 × g) after each wash to discard the flow through. The filter tube was dried by centrifugation for 2 mins at 16,000 × g and placed onto a 1.5 ml eppendorf. Then 25 µl of elution buffer was added to the centre of the fleece membrane, incubated for one minute at RT and RNA was eluted by centrifuging for one minute at 6,000 × g. RNA concentrations were measured using the Invitrogen Qubit 4 Fluorometer, and the A260/A280 and A260/A230 ratios were measured using a Nanodrop (Thermo Scientific, #ND-ONE-W). The eluted RNA was stored at -70°C.

2.13 RNA library preparation and sequencing

RNA library preparation and sequencing were performed at the Oxford Genomics Centre at the Wellcome Centre for Human Genetics, University of Oxford. Briefly, the extracted RNA was quantified using RiboGreen (Invitrogen, #R11490) on the FLUOstar OPTIMA plate reader (BMG Labtech) and the size profile and integrity analysed on the 2200 or 4200 TapeStation (Agilent, RNA ScreenTape). Input material was normalised to 30 ng prior to library preparation. The RNA was depleted of ribosomal RNA using NEBNext rRNA Depletion Kit (NEB, #E6350L) following manufacturer's instructions. Strand specific library preparation was completed using NEBNext Ultra II mRNA kit (NEB, #E7770L) following manufacturer's instructions. Libraries were amplified (17cycles) on a Tetrad (Bio-Rad) using in-house unique dual indexing primers. Individual libraries were normalised using Qubit, and the size profile was analysed on the 2200 or 4200 TapeStation. Individual libraries were normalised and pooled together accordingly. The pooled library was diluted to ~10 nM for storage. The 10 nM library was denatured and further diluted prior to loading on the sequencer. Paired end sequencing was performed using a NovaSeq6000 platform (Illumina, NovaSeq 6000 S2/S4 reagent kit v1.5, 300 cycles).

2.14 RNA-sequencing data processing and analysis

I was trained in RNA Sequencing analysis by Dr Avigail Taylor, Bioinformatician, Macaulay group. FASTQ-format files containing paired end reads were first concatenated and reads aligned to the human reference genome, hg38 using the STAR gene mapper (Dobin et al., 2013). Cutadapt software was then used to remove adapter sequences and

unwanted primers from the mapped sequence. Unique reads were then mapped using featureCounts and differential expression analysis performed using DESeq2 (version 3.14). Pathways were generated from differentially expressed genes using Over Representation Analysis using KEGG pathways, WikiPathway, Biocarta and Gene set enrichment analysis (GSEA) using the KEGG pathway.

2.15 Fresh tissue processing for single-cell sequencing

Punch biopsies (~4 mm^3) from radical proctectomies were obtained as mentioned in Section 2.7. From each radical prostatectomy, the Uro-Pathologist sampled areas of index tumour and adjacent benign tissue, and the benign biopsy was used as control for the downstream flow cytometry process. Fresh tissue was disaggregated with the Human tissue dissociation kit (Miltenyi Biotec Inc., #130-095-929). First, a master mix of the dissociation buffer was made in c-tubes (Miltenyi Biotec, #130-093-237) using 2.2 mL serum-free RPMI-1640, 100 µl Enzyme H, 50 uL Enzyme R and 12.5 uL Enzyme A from the tissue dissociation kit. The tissue samples were then cut into 1cm^3 pieces and transferred into the c-tubes, which were placed onto the gentleMACS Octo Dissociator with Heaters. The heating unit was placed on top of the c-tube and tissues were dissociated using the 37C_h_TDK_2 programme. Once the run was complete, the c-tubes were centrifuged at 300 x g for 10 mins (4°C) to collect the sample at the bottom of the tube. While samples were centrifuged, a 70 µm strainer was placed onto a 50 mL falcon tube and pre-wet with cold PBS.

After the first centrifugation, samples were resuspended in cold PBS (10 mL) and the cell suspension was filtered through the strainer to remove cell debris, clumped cells and any

undigested adipose tissue. The filter was washed twice with cold PBS and the filtered cell suspension was centrifuged again at 300 x g for 10 mins (4°C). Cells were resuspended in 1 mL cold PBS and stored at 4 °C until flow cytometric sorting the following day.

On the next day, samples were vortexed and an aliquot of 200 uL was taken from the benign sample to use as a live-dead control. An aliquot of 100 uL was heated at 95 °C for 1 min and then chilled on ice for another minute. This was then mixed back with the remaining 100 uL aliquot to make 200 uL of live-dead control. Another 100 uL was taken from the benign sample to use as unstained control. Live-dead/Fc receptor blocking solution was prepared by mixing 1 mL cold PBS and 1 uL fixable viability dye eFluor 450 (eBioscience, #65-0863-14). Onto 220 uL of this solution, 10 uL of Fc receptor blocking solution, human truStain FcX (BioLegend, #422301) was added. The cancer, benign, live-dead control and unstained control single cell samples were centrifuged at 300 x g for 10 mins and cancer, benign and live-dead control samples resuspended in 70 uL live-dead stain/Fc receptor blocking mix. The unstained sample was re-suspended in cold PBS. Samples were then incubated for 10 mins at 4 °C, the stain was diluted by adding 1 mL cold PBS and samples were centrifuged at 300g for 10 mins (4°C). After centrifugation, samples were resuspended in 200 uL 0.04% BSA in PBS solution that had been passed through a 0.02 μm. Following staining, samples were sorted for live cells at the Weatherall Institute of Molecular Medicine (WIMM) flow cytometry core. Benign and malignant live cells were sorted and collected separately, counted using a haemocytometer and 20,000 cells from each benign and malignant cell suspension were resuspended in 40 uL 0.04% BSA in PBS.

2.16 Single-cell sequencing with 10X genomics

Immediately following cell sorting, downstream library preparation for 10X genomics single-cell sequencing was performed by Dr Neil Ashley at the Weatherall Institute of Molecular Medicine (WIMM) Single-cell Facility, University of Oxford. Single cell suspensions were loaded onto the 10X genomics chromium controller where cells were lysed and mRNA was reverse transcribed into individual gel bead emulsions (GEM) to generate cDNA using the Single Cell 5' Kit v2 (10X genomics, #1000265) and Next GEM Chip K Single Cell Kit (10X genomics, #1000286). Sample quality was analysed on the Agilent 4200 system and sequencing was performed on the Illumina NovaSeq sequencer, S4 by Genewiz (Essex UK).

2.17 Single-cell sequencing analysis

Single-cell sequencing analysis was performed by Ashwin Jainarayanan, The Kennedy Institute of Rheumatology. Briefly, sequencing data were processed using the 10x genomics Cell Ranger (version 6.1.0) pipeline and aligned to the human genome (GRCh38). Gene matrices with expression count data were then imported onto the Seurat pipeline (v3.2.2) on R Studio (cersion 1.4.1106), and filtered for cells with lower library size and high mitochondrial transcripts. Data was quality tested and cells with less than 200 genes or mitochondrial level of 5% or greater were excluded. Data was normalised, scaled and batch effects removed using the Seurat package. Doublet cells were also removed using DoubletFinder99 (version 2.0.3). Principal component analysis (PCA) was performed on the highly variable genes identified using the FindVariableGenes parameter in Seurat. Cell

clusters were obtained using the Uniform Manifold Approximation and Projection (UMAP) function and cell types identified based published datasets and work previously done by Ashwin Jainarayanan. Violin plots were generated for genes of interest using the default Seruat settings.

2.18 Statistical Analysis

All statistical analyses were performed using GraphPad Prism v9. Statistical significance between two treatment groups were calculated using a t-test and differences between three or more treatment groups were calculated using one-way ANOVA with Tukey's multiple comparison test to compare between individual treatment groups. P values of <0.05 were considered statistically significant.

3 Chapter III: Investigating the association between circulating levels of IGF-1 and IGF-1 receptor expression in prostate cancer.

3.1 Introduction

As described in Chapter 1, previous work in the laboratory has suggested that there is an association between high circulating levels of IGF-1 and upregulation of IGF-1R protein (shown by IHC) in malignant but not benign prostatic epithelium (Figure 1-2). To check this association and understand the mechanism of altered IGF-1R expression, it will be necessary to use a larger validation cohort and test whether the upregulation of IGF-1R is consistent at the transcriptional level. Understanding the association between high circulating IGF-1 and IGF-1R could help to elucidate the role of IGF-1 in promoting prostate cancer risk and progression to lethal disease (Travis et al., 2016; Ahearn et al., 2018; Watts et al., 2020).

To investigate these aims, I have first checked the specificity of the IGF-1R antibody used for IHC and tested for the distribution of IGF-1R expression in malignant and benign prostate epithelium in an independent cohort. To test if IGF-1R expression was upregulated at the mRNA level, I used a chromogenic *in situ* hybridization (ISH) technique called RNAScope to test for *IGF1R* mRNA levels on the same sections in which the IHC for IGF-1R had been performed previously. The association between IGF-1 supply and IGF-1R expression was also studied using prostate cancer *in vitro* models.

3.2 Results

3.2.1 Testing IGF-I Receptor β antibody in IHC

Prior to testing the effects of IGF-1 on IGF-1R expression, the specificity of the IGF-1R β antibody (CST 9750), was checked, using DU145 prostate cancer cells where IGF-1R was depleted using siRNA or deleted using CRISPR, the latter made using genome editing by Dr Eliot Osher, Postdoctoral Scientist, Macaulay group. Efficiency of the receptor knockout and knockdown was tested using a western blot (Figure 3-1a)

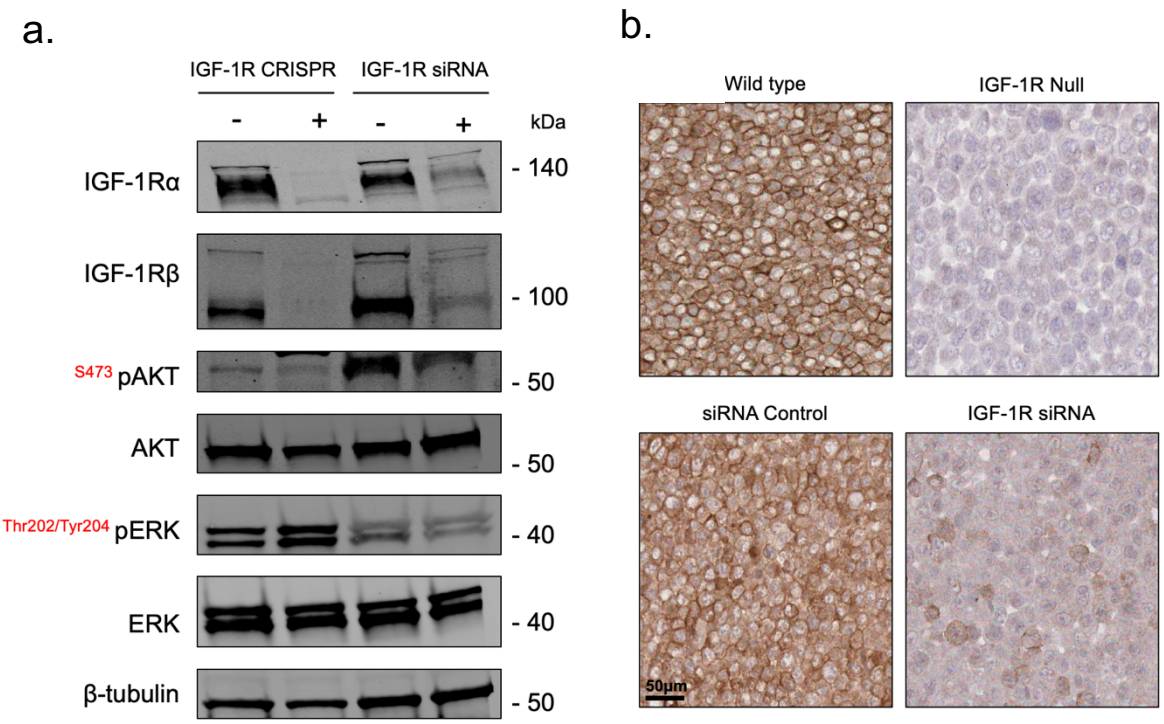


Figure 3-1 Testing IGF-1R antibody specificity. Validation was conducted using DU145 cells 48 hr after transfection with control or IGF-1R siRNA and wild type or IGF-1R CRISPR knockout cells made by Dr Eliot Osher. Cell pellets were collected, lysed and protein expression tested using western blot. (a) Western blot confirming IGF-1R deletion and knockdown in DU145 cells. (b) Cell pellets were also formalin fixed and paraffin embedded and receptor expression tested using IGF-1R IHC.

The western blot confirmed the reduction of receptor expression following IGF-1R siRNA transfection and absence of IGF-1R in CRISPR knockout cells. There was also reduced phosphorylation of AKT in these cells compared to controls, which indicated reduction in downstream signalling. Minor reduction in ERK phosphorylation was seen in IGF-1R siRNA transfected cells but not IGF-1R null cells, possibly due to compensation for long-term IGF-1R loss. IGF-1R IHC was performed on FFPE cell pellets of IGF-1R knockout and knockdown cells, using a heat-based antigen retrieval method previously optimised and published by Dr Tamara Aleksic in our group (Aleksic et al., 2016). Results from the IHC confirmed strong membrane IGF-1R staining and detectable cytoplasmic staining in both the controls (Figure 3-1b). Furthermore, the IGF-1R knockdown cells showed partial staining, while the null cells displayed absence of IGF-1R staining, supporting the specificity of the antibody.

3.2.2 Investigating IGF-1R localisation in prostate cancer.

IGF-1R staining and its distribution in benign vs malignant epithelium was also tested in an independent cohort of prostate cancer cases. The ProMPT cohort originally tested comprised 150 cases of which 139 were interpretable. Attempts were made to access larger cohorts for validation. These included cases collected by Prof John Kelly and Dr Andrew Feber at University College London, and by Prof Tuomas Mirtti, University of Helsinki. However the former had only a limited number of fresh frozen tumours (Dinneen et al., 2021) with whole blood saved for circulating tumour DNA, and while the latter had tissue microarrays of >460 cases (Blom et al., 2019) there were no paired serum samples. The only cohort we

could identify with available FFPE tissue and known serum IGF-1 was a small tissue microarray (TMA) made from 50 cores from prostate cancers in 12 subjects recruited to the EPIC study (Figure 3-2a**)**. Each tissue had been sampled in the centre and invasive margin of the dominant tumour centre, any other tumour area, adjacent benign peripheral zone and distant benign peripheral zone. The TMA section was provided via collaboration with Profs Ruth Travis and Tim Key, Cancer Epidemiology Unit Oxford and Prof Clare Verrill, Consultant Uro-Pathologist, John Radcliffe Hospital Oxford. IGF-1R IHC was performed as above and receptor expression was scored by Prof Verrill for intensity (0-3) and percentage positivity (0-4) in the plasma membranes, cytoplasm and nucleus as described (Aleksic et al., 2016, 2018). The products of these values gave a maximum score for each compartment of 12 and a maximum total score of 36. IGF-1 receptor total expression was calculated by summing the membrane, cytoplasmic and nuclear- IGF-1R immunoreactive scores. Amongst these 12 cases, only 6 cases were evaluable of which 5 contained both benign and malignant epithelium. The other cases lacked malignant epithelium and/or had dropouts of tumour or benign punches. Furthermore, Prof Verrill also encountered difficulty deciding whether some of the benign glands were true benign or malignant from the histopathology of the specimens.

The results indicated stronger staining in epithelium than stroma, consistent with other reports (Figure 3-2a) (Hellawell et al., 2002; Aleksic et al., 2018). There was nuclear IGF-1R staining in one epithelial gland thought by Prof Verrill to be benign (Figure 3-2a), however its adjacent tumour section had dropped out and this case could not be used for paired analysis. In the 5 cases where IGF-1R was scored in benign and malignant epithelium, all but one contained more IGF-1R in the malignant epithelium, but the difference was not

significant (Fig 3-2b). Previously, larger cohorts had shown a significant difference (Hellawell et al., 2002; Aleksic et al., 2018). There was also a trend to increased IGF-1R expression in the cytoplasmic compartment in the tumour sections compared to the benign areas (Figure 3-2c), confirming our previous work (Aleksic et al., 2018). Upon binding to IGF-1, IGF-1R activation is followed by receptor internalisation and, in some cases, nuclear translocation (Aleksic et al., 2018, 2010; Mills et al., 2021). The increased cytoplasmic localisation of IGF-1R in the malignant epithelium could be suggestive of its increased activation from circulating or tissue resident IGF-1 sources.

There was no difference between the membrane IGF-1R content of the tumour and benign areas (Figure 3-2d) and there was no detectable nuclear IGF-1R in any of the 6 tumour samples. The previously published data from our group showed nuclear IGF-1R in ~30% of primary prostate cancers and only weak nuclear signal in <10% of benign areas (Aleksic et al., 2018). Lack of nuclear IGF-1R detection here may be due to technical issues or small sample size, which also prevented validation of the previous finding of association between high circulating IGF-1 and IGF-1R expression in malignant epithelium, as the circulating IGF-1 levels for these patients were not available. Testing the association of serum IGF-1 with IGF-1R expression in a larger validation cohort may help understand whether these measures are linked.

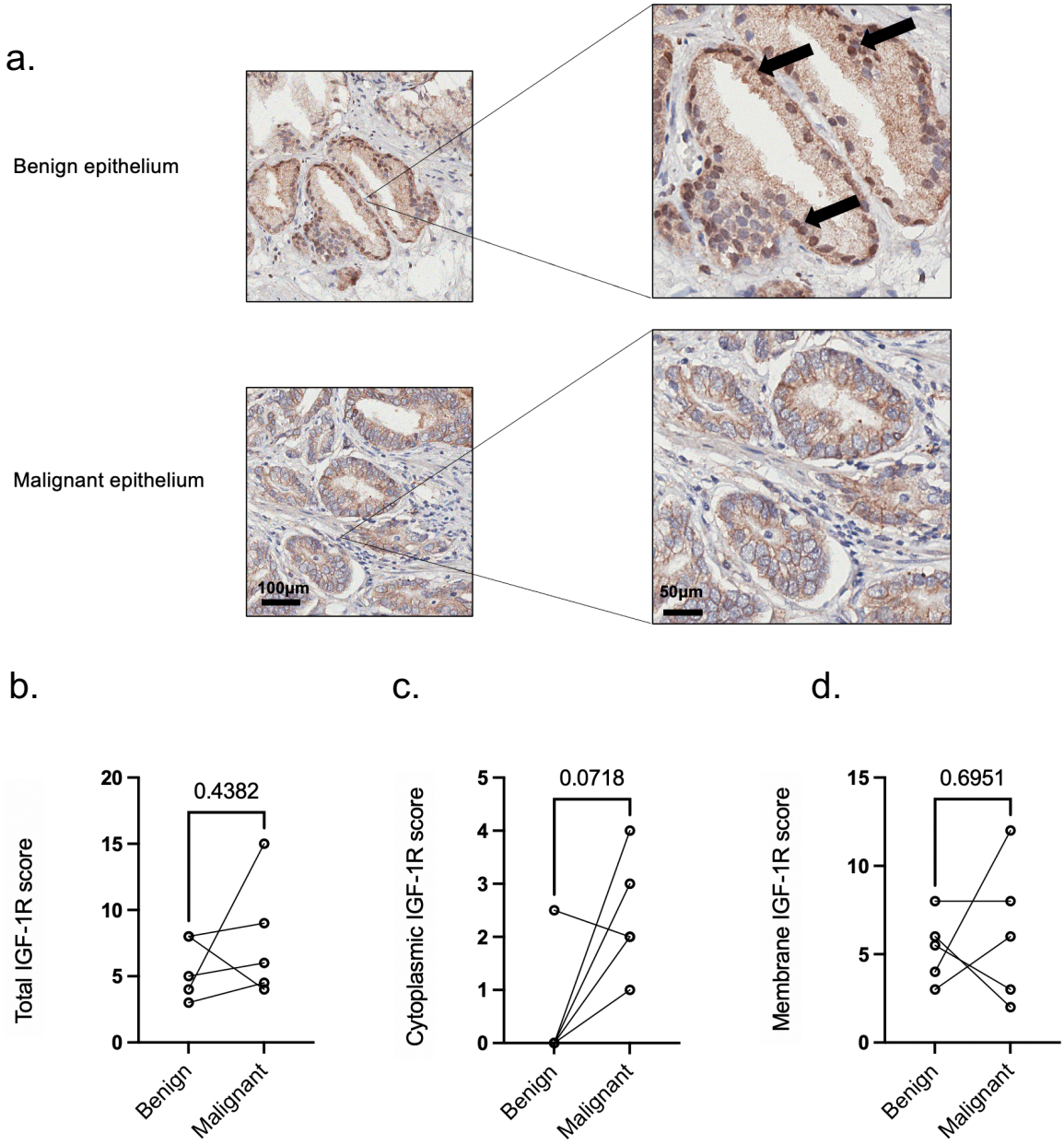


Figure 3-2 IGF-1R IHC performed on EPIC TMA. IGF-1R staining of EPIC TMA showing (a) low power view of individual cores showing area of benign prostate epithelium, gland judged to be benign by Prof Verrill showing weak membrane, cytoplasmic and strong nuclear (black arrows) IGF-1R, and malignant prostate epithelium showing membrane and cytoplasmic IGF-1R staining. (b) Quantification of total (nuclear, cytoplasmic plus membrane) IGF-1R, (c) cytoplasmic IGF-1R and (d) membrane IGF-1R in the EPIC cohort. Graphs show mean ± SEM, n=5 paired samples analysed by two-tailed paired T-Test.

3.2.3 Investigating whether *IGF1R* mRNA parallels IGF-1R protein detected by IHC in prostate cancer

To investigate if *IGF1R* is transcriptionally upregulated in parallel with increased IGF-1R seen in malignant prostate tissue by IHC, an *in-situ* hybridisation technique, RNAScope, was used to detect *IGF1R* mRNA. RNAScope was performed on 8 radical prostatectomies with high (16-30) and 9 samples with low (0-6) malignant IGF-1R immunoreactive score, using FFPE sections of ProMPT cases previously tested by Dr Tamara Aleksic and scored by Prof Clare Verrill. Peptidyl-prolyl cis-trans isomerase B (PPIB), a protein involved in regulating protein folding and maturation, was used as a positive control to check the integrity of the mRNA in the tissues. RNAScope quantification was performed by Dr Nasullah Khalid Alham and an overview of the analysis is described in Materials and Methods. Briefly, tissue sections were marked for tumour area by Prof Verrill and divided into benign, outer margin, inner margin and tumour area for quantification (Figure 3-3). The amount of red *IGF1R* staining was calculated from scanned images and total expression was measured as the staining intensity per μm^2.

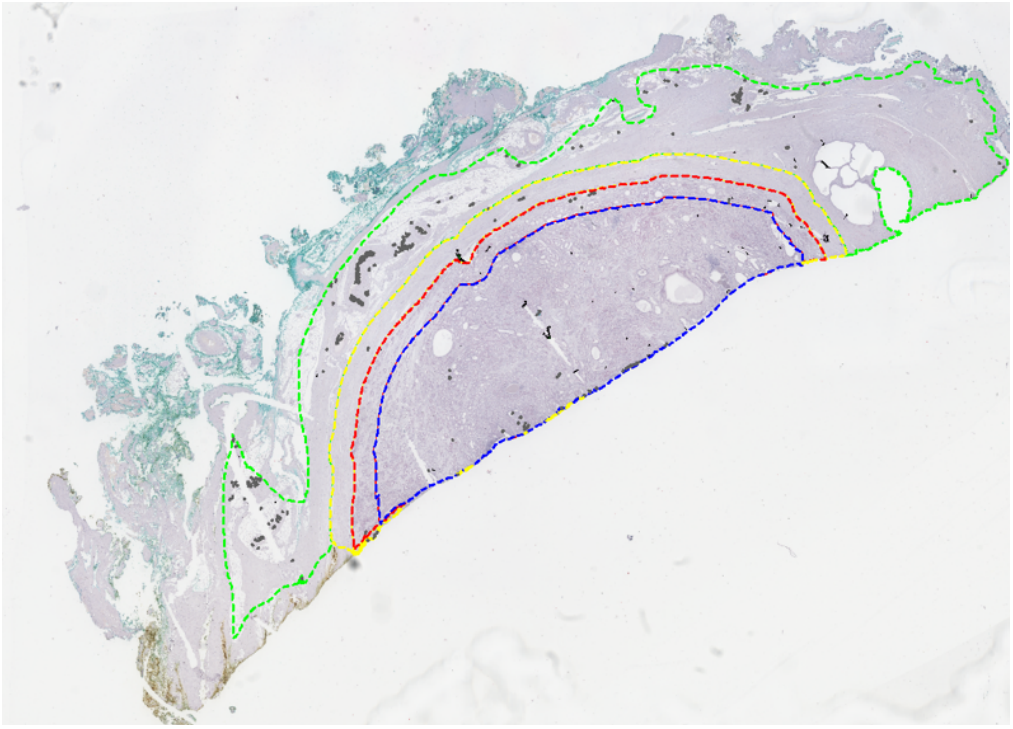


Figure 3-3 Sample output from Visiopharm. Image output from Visiopharm shows prostate cancer tissue with malignant (red lines), outer margin (yellow line), inner margin (blue line) and benign margin (green line) marked by Prof Verrill.

Specificity of the *IGF1R* probe was validated using the same cell pellets used to validate IGF-1R β antibody for IHC (Figure 3-1b). In samples where IGF-1R was depleted using siRNA, there was the expected reduction in *IGF1R* mRNA expression (Figure 3-4a), again supporting the ability of the antibody to detect downregulated IGF-1R. Comparable *PPIB* signal between the control and siRNA treatment confirmed the presence of stable RNA in both the sections (Figure 3-4a). RNAScope was then performed on the ProMPT tissue sections (Figure 3-4b). Signal from the *PPIB* probe was similar between low and high IGF-1R tumours.

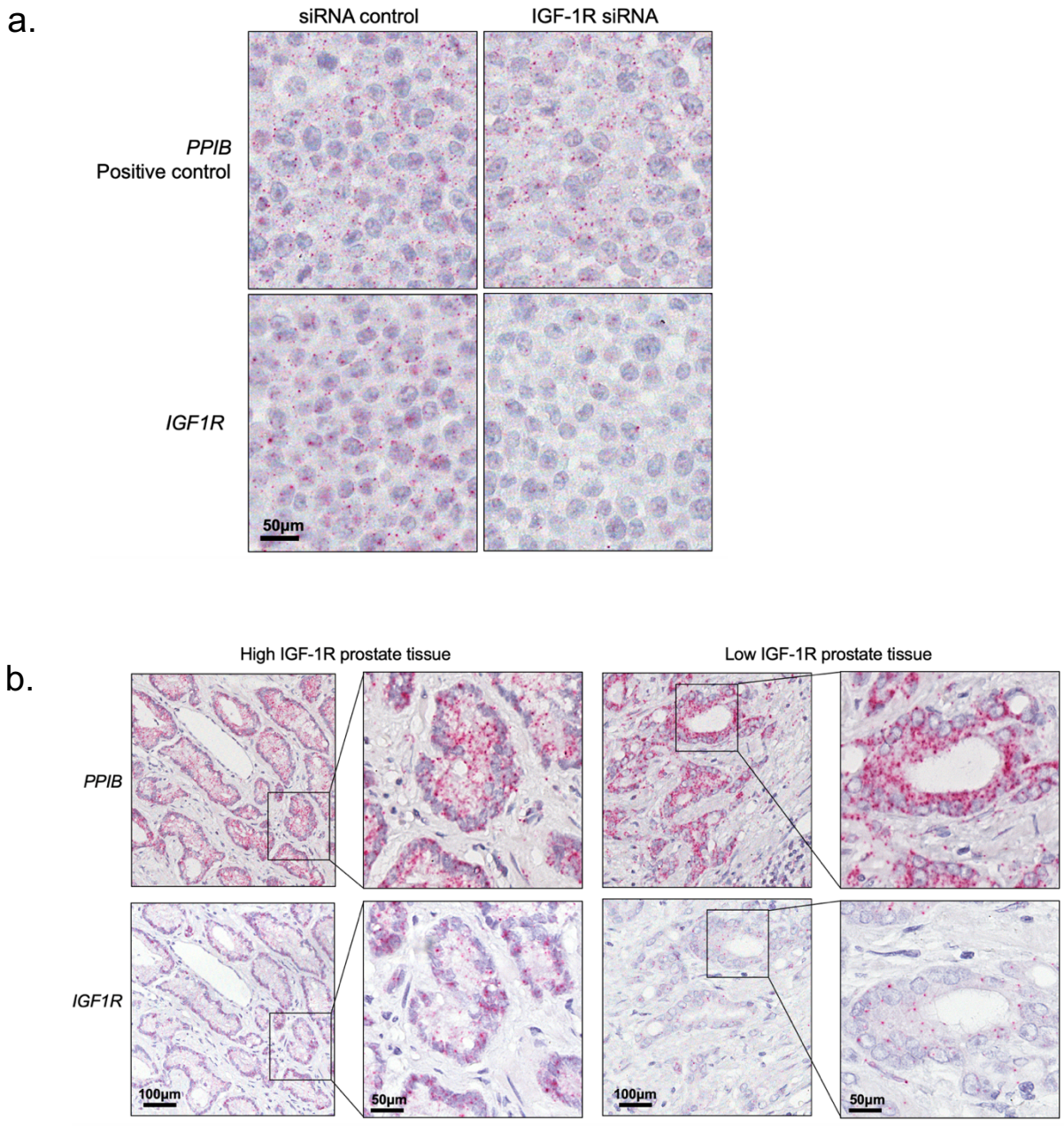


Figure 3-4 IGF1R mRNA detected by RNA Scope. (a) Specificity of *IGF1R* RNAScope probe was validated using IGF-1R siRNA depleted DU145 cells and mRNA integrity confirmed using the *PPIB* positive control. (b) *IGF1R* mRNA levels were tested on prostate cancers from the ProMPT study with low or high IGF-1R score as previously assessed by Prof Verrill (Aleksic et al., 2018).

Results of *IGF1R* mRNA levels from the RNAScope analysis, parallel IGF-1R protein immunoreactive scores and circulating IGF-1 levels of the patient are displayed in **Table 3-1**. Analysis showed a significant increase in *IGF1R* mRNA levels within the tumour compartment (inner margin+ tumour), when compared to the benign compartment (Figure 3-5a). This is in line with the parallel IGF-1R protein expression in the same sections previously measured by IHC (Aleksic et al., 2018). However, there was no difference in *IGF1R* mRNA expression in tumours with high vs low IGF-1R protein expression (Figure 3-5b). No apparent association was detected between *IGF1R* expression and circulating IGF-1 levels, Gleason grade or PSA (Figure 3-5c,d,e). This study was performed with only 17 samples and a larger cohort would be necessary to investigate if *IGF1R* is transcriptionally upregulated in high IGF-1R tumours from men with high circulating IGF-1. This information could help us understand if the IGF-1R upregulation seen in high IGF-1 patients are a result of post translational modificans leading to reduced receptor degradation or due to transcriptional upregulation of *IGF1R*. This can contribute to the understanding of how increased IGF-1 promotes prostate cancer risk.

No.	IGF-1R Nuclear Score	IGF-1R Cytoplasmic Score	IGF-1R Membrane Score	IGF-1R Total score	*IGF1R* mRNA intensity	IGF-1 Levels (nmol/L)
1	0	0	0	0	0.01	10.98
2	0	0	1	1	0.14	14.1
3	0	0	2	2	0.03	20.18
4	0	0	2	2	0.05	26.76
5	0	1	2	3	0.1	16.56
6	0	0	3	3	0.06	25.01
7	0	0	4	4	0.06	7.19
8	0	0	4	4	0.12	12.9
9	0	1	3	4	0.01	13.83
10	0	0	12	12	0.06	20.3
11	0	6	12	18	0.08	10.14
12	4	4	12	20	0.06	14.3
13	0	9	12	21	0.04	30.44
14	9	8	6	23	0.08	15.33
15	4	8	12	24	0.18	25.76
16	6	12	12	30	0.05	11.84
17	6	12	12	30	0.06	26.35

Table 3-1 Tumour IGF-1R immunoreactive score, Tumour *IGF1R* mRNA intensity and circulating IGF-1 levels from ProMPT subjects. Table shows IGF-1R nuclear, cytoplasmic, membrane and total (nuclear+cytoplasmic+membrane) immunoreactive scores, *IGF1R* mRNA intensity and serum IGF-1 levels. IGF-1R immunoreactive scores were obtained from IHC on the tumour areas performed Dr Aleksic and scored by Prof Verrill (Aleksic et al., 2018). *IGF1R* mRNA intensity was obtained fom RNAScope assays I conducted on the parallel sections in which IGF-1R IHC was perfomed.

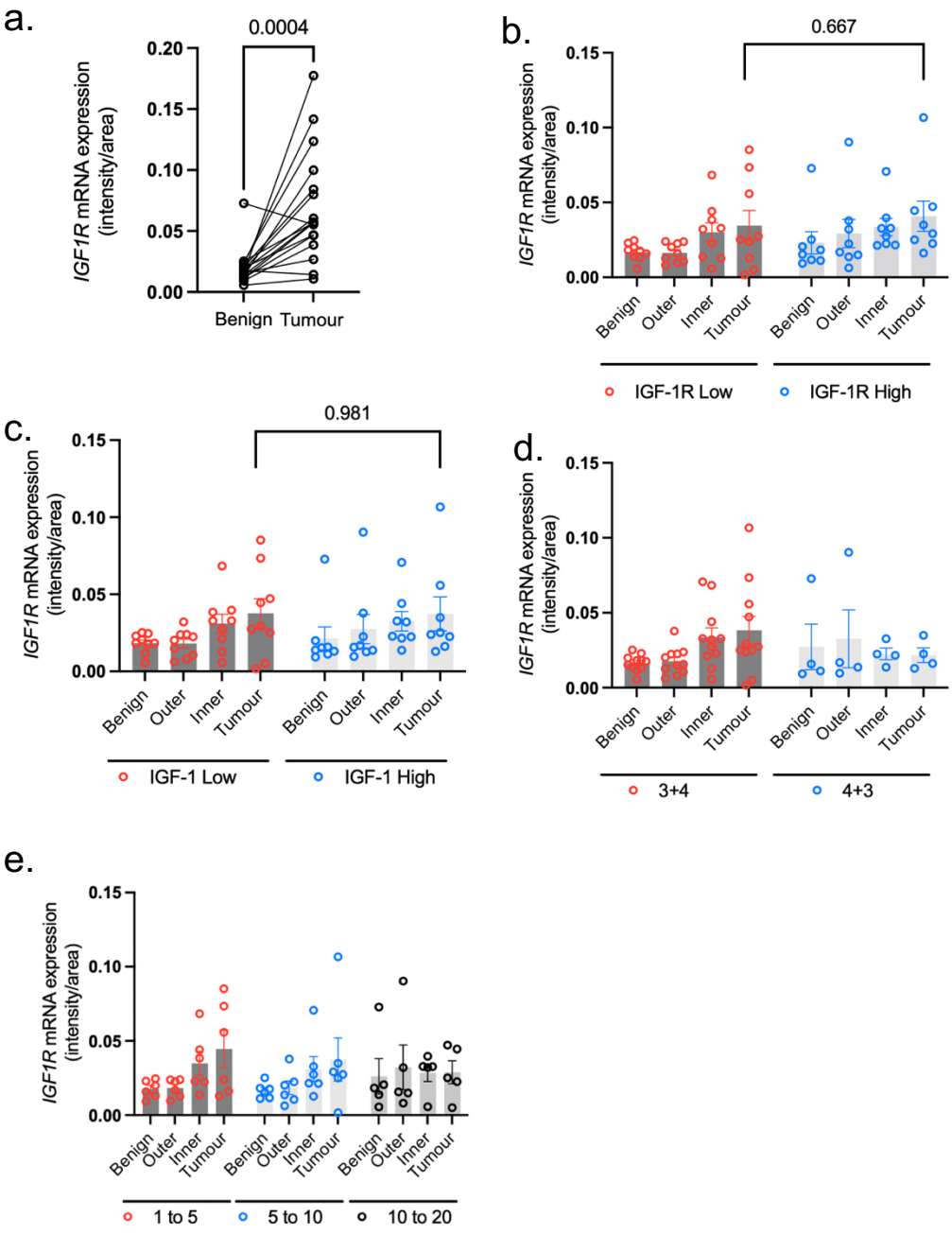


Figure 3-5 Analysis of IGF1R mRNA expression in ProMPT cohort using RNA Scope. (a) *IGF1R* expression distribution in benign and tumour (inner + tumour) areas in prostate cancer. (b) *IGF1R* mRNA expression in tissues with high (12-30) or low (0-4) total IGF-1R protein expression measured by IHC (see Table 3.1). (c) *IGF1R* expression in tissues with high (21.7-31.5 nmol/L) or low (7.2-12.0 nmol/L) circulating IGF-1 levels . (d) *IGF1R* expression in Grade Group 2 (3+4) and Grade Group 3 (4+3) prostate cancers. (e) *IGF1R* expression across ranges of PSA (ng/mL) levels in prostate cancer. Graphs show mean ± SEM, analysed by unpaired two-tailed T-Test, except (a) analysed by paired two-tailed T-Test.

3.2.4 Testing *in vitro* association between IGF-1 and IGF-1R in prostate cancer cell line models

The next aim of the project was to develop a cell line model to test whether IGF-1 regulates IGF-1R expression *in vitro*, to understand the mechanism of association between high circulating IGF-1 and IGF-1R expression in malignant epithelium. To test this, androgen independent DU145 and androgen dependent VCaP prostate cancer cells were used. Initial experiments involved investigating the effects of short term (4-24 hrs) treatment of DU145 and VCaP cells with 30 nM IGF-1, a concentration similar to the upper end of the normal range (6.4 -31 nM) in adult men (Bidlingmaier et al., 2014). Cells were serum starved for 24 hrs and treated with IGF-1. IGF-1R expression was measured at protein and mRNA levels using western blot and qRT-PCR. Short term IGF-1 treatment of DU145 cells showed increased phosphorylation of IGF-1R and AKT, greater at 4 hrs than 24 hrs, suggesting activation of the IGF axis (Figure 3-6a). At 24 hrs VCaP cells also displayed increased phosphorylation of IGF-1R, but reduced phosphorylation of AKT in comparison to the control (Figure 3-6b), possibly suggesting a negative feedback loop following receptor activation. There were trends to variation in IGF-1R protein expression but no significant differences in both cell lines (Figure 3-6c, d), and mRNA expression was unchanged in DU145 cells after 4-24 hrs (Figure 3-7a). However, analysis of *IGF1R* mRNA levels in VCaP cells showed a significant decrease in expression following 24 hrs IGF-1 treatment (Figure 3-7b).

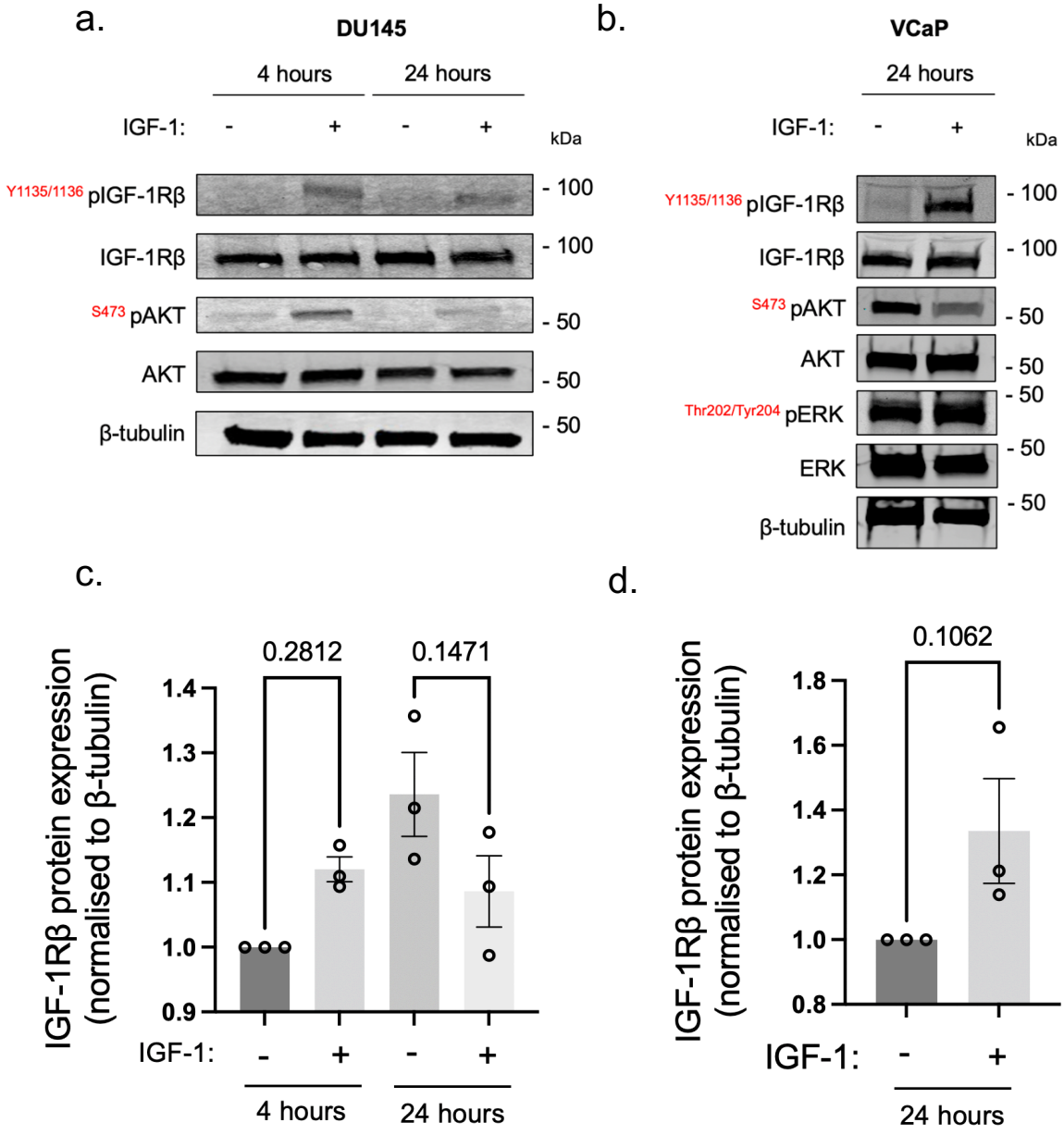


Figure 3-6 IGF-1R protein expression after short term treatment of prostate cancer cells with 30 nM IGF-1. Prostate cancer cells were treated with 30 nM IGF-1 for the indicated times. Representative western blot of n=3, with the same result obtained in three independentely prepared lysates of (a) DU145 and (b) VCaP cells showing activation of the IGF axis, and IGF-1R protein levels. IGF-1R expression quantified in (c) DU145 and (d) VCaP cells after normalisation to β-tubulin using FIJI Imaje J. Gaph shows mean with SEM and significance calculated using a (c) one way ANOVA and (d) unpaired two-tailed T-Test.

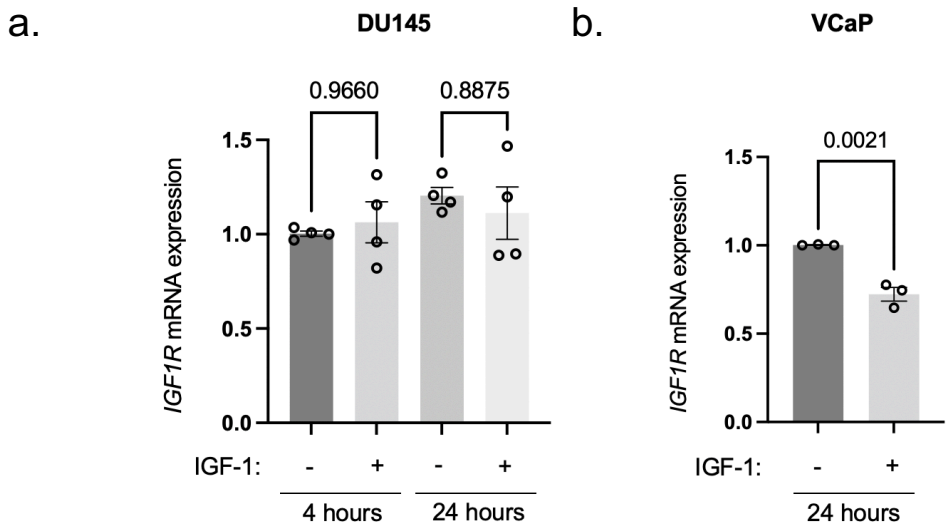


Figure 3-7 *IGF1R* expression after short term IGF-1 treatment of prostate cancer cells with 30 nM IGF-1. Prostate cancer cells (a) DU145 and (b) VCaP were treated as before for the indicated times and *IGF1R* mRNA quantified by qRT-PCR (n=3 independent experiments). Sample distribution represented using SEM and analysed using (a) one way ANOVA and (b) unpaired two-tailed T-Test.

Aiming to develop a cell line model that more closely resembles chronic IGF exposure *in vivo*, DU145 and VCaP cells were treated with or without 30 nM IGF-1 for 8-12 weeks (Figure 3-8a,b). DU145 cells were adapted to grow in 0.2% FBS culture before IGF-1 treatment. VCaP cells did not grow in 0.2% FBS conditions and hence were grown in 10% FBS before IGF-1 treatment. DU145 cells have been reported to produce endogenous IGF-1 (Kawada et al., 2006). To check whether cultures in low serum would upregulate endogenious IGF-1 production, IGF-1 was measured from samples of fresh and conditioned media from both cell lines by Prof Tim James, Biochemistry Laboratory, John Radcliffe Hosital. Compared with fresh medium, there was no evidence that culture in medium with 0.2% FBS caused upregulation of endogenous IGF-1 secretion (not shown).

After 8-12 weeks of IGF-1 treatment, IGF-1R protein and mRNA levels were measured. In both cell line models, there was reduced receptor expression at both protein (Figure 3-8a,b) and mRNA levels (Figure 3-8c,d). Western blot analysis revealed reduced phosphorylation of AKT in the IGF-1 treated cells, consistent with results of 24 hrs IGF-1 treatment in VCaP cells. The detected decrease in IGF-1R expression could be due to its internalisation and degradation after constant activation upon ligand stimulation, and this has been reported (Schillaci et al., 1998; Girnita et al., 2005). Degredation of the receptor does not explain the reduction in mRNA levels and this may be a consequence of feedback downregulation or IGF-1R gene silencing. IGF-1R gene silencing by hypermethylation has been previously reported but not in the context of pathway activation as seen here (Katz et al., 2015). Methylation of the *IGF1R* promoter could be tested by peforming DNA methylation sequencing on these samples, however this is was not pursued given that the cell line data did not parallel data obtained from tissue level analysis (Figure 1.2).

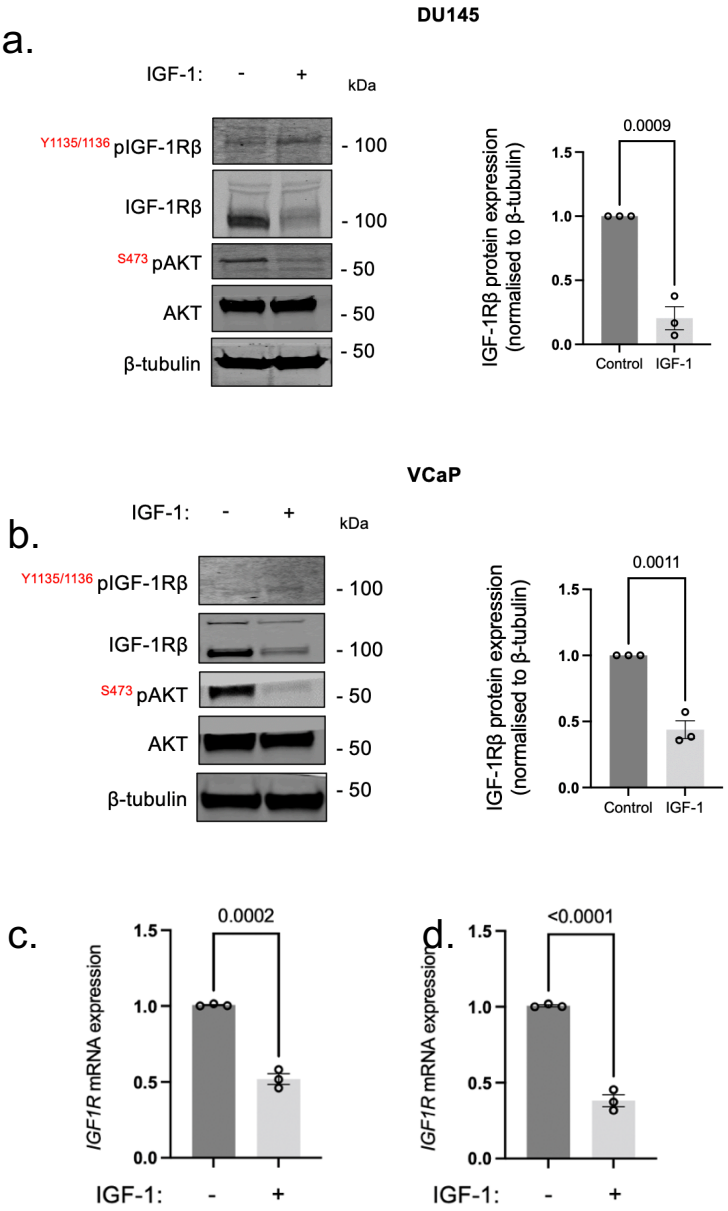


Figure 3-8 Expression and activation of signalling proteins in DU145 & VCaP cells after 8-12 weeks culture in 30 nM IGF-1. DU145 cells were adapted to grow in 0.2% FBS and cultured in 30 nM IGF-1 or solvent (control) for 8-12 weeks. VCaP cells were grown in 10% FBS and treated with 30 nM IGF-1 or solvent (control). Cultures were trypsinised and cells washed in cold PBS, lysed with RIPA for downstream analysis. One representative western blots of n=3 independent repeats of (a) DU145 and (b) VCaP cells. Graphs represent IGF1-R quantification after normalisation to β-tubulin using FIJI Imaje J. *IGF1R* mRNA quantified by qRT-PCR, in (c) DU145 and (d) VCaP (n=3 independent repeats). Sample distribution represented by SEM and significance calculated using an unpaired two-tailed T-Test.

Both short term (24 hrs) and long term (8-12 weeks) IGF-1 treatment caused downregulation of the IGF-1R, not consistent with the preliminary finding of association of serum IGF-1 with IGF-1R in clinical tissue (Figure 1-2). In the clinical setting, effects of IGF-1 may be modified by the presence of testosterone, and cross talk between IGF-1R and androgen receptor (AR) has been well documented in prostate cancer (Wu et al., 2006; Yanase and Fan, 2009; Fan et al., 2007; Wu and Yu, 2014; Bakin et al., 2003). To understand whether AR activation can promote IGF-1R receptor expression after ligand activation, androgen dependent VCaP cells were co-treated for 24 hrs with 30 nM IGF-1 and 28 nM dihydrotestosterone (DHT). DHT was used at 28 nM to mimic the upper range of testosterone levels detected in adult male (data from the NHS). However, DHT is 2.4 times more potent than testosterone and for the subsequent experiments DHT was used at 10 nM (Wright et al., 1996). Control cells treated with IGF-1 alone showed the same pattern as before (Figure 3-6b), with increased IGF-1R phosphorylation and reduced IGF-1R protein and AKT phosphorylation (Figure 3-9a). IGF-1R was significantly upregulated by DHT alone. Stimulation of VCaP cells with both IGF-1 and DHT caused enhanced activation of IGF-1R and rescued IGF-1R downregulation caused by IGF-1 alone (Figure 3-9a), and this was consistent at both protein and mRNA level (Figure 3-9b,c). However, both IGF-1R protein and mRNA levels were lower in co-treated cells, when compared to treatment with DHT alone. At the mRNA level IGF-1 stimulation significantly increased *AR* expression, and similar to the effect of IGF-1 on IGF-1R expression, AR activation by DHT (alone or with IGF-1) downregulated *AR* mRNA (Figure 3-9d). Activation of the AR by DHT was confirmed by increased *KLK3* expression, which encodes for prostate-specific antigen (PSA), a downstream target of AR (Figure 3-9e). It was also noted that IGF-1 downregulated *KLK3* and partially reversed the upregulation caused by DHT (Figure 3-9e).

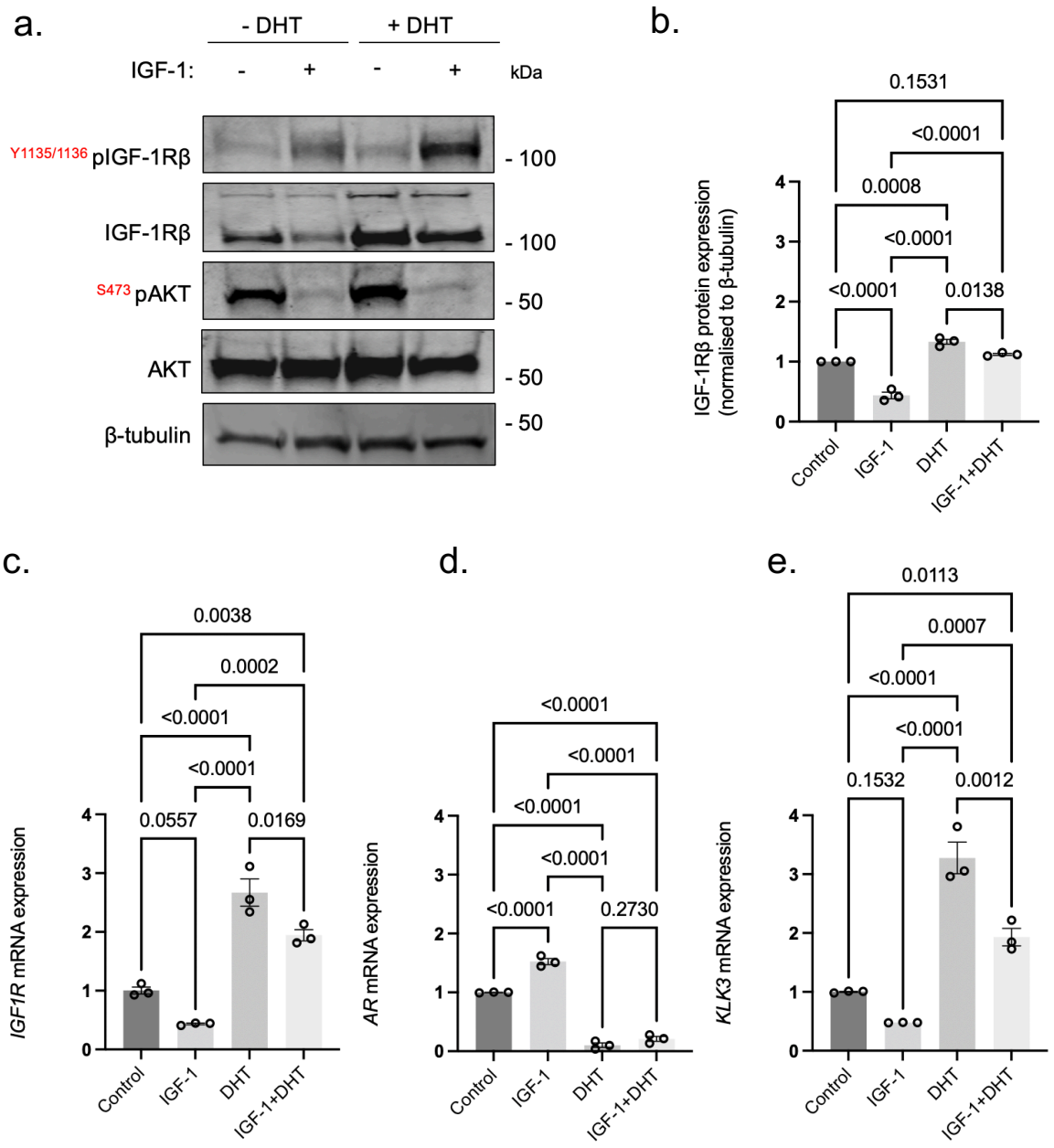


Figure 3-9 IGF-1R expression after co-stimulation with 30 nM IGF-1 and 28 nM DHT. VCaP cells were serum starved for 24 hours and treated with solvent (control), 30 nM IGF-1, 28 nM DHT or a combination of IGF-1 and DHT. (a) Protein expression was measured using a western blot and (b) bands quantified by normalising expression to the loading control β-Tubulin (n=3 independent repeats). qRT-PCR was also performed on RNAs extracted from parallel cell cultures to measure (c) *IGF1R*, (d) *AR* and (e) PSA (*KLK3*) mRNA expression (n=3 independent repeats). Graphs show SEM distribution and significance calculated using a one-way ANOVA with Tukey's post hoc test for multiple comparisons.

Since DHT is 2.4 times more potent than testosterone (Wright et al., 1996) I repeated the assessment of IGF-1 and DHT co-treatment, treating VCaP cells with increasing concentrations of IGF-1 in the presence or absence of 10 nM DHT. Stimulation of VCaP cells with increasing concentrations of IGF-1 resulted in decrease of IGF-1R, similar to the previous results (Figure 3-10a). The effect was apparent even with 1 nM IGF-1 and two-way ANOVA showed statistical difference between the +DHT and -DHT treatment. DHT alone caused significant IGF-1R upregulation as before (Figure 3-9a), an effect that was reduced at both the protein and mRNA levels by IGF-1 (Figure 3-10b,c). These experiments supported previous reports that the AR influences IGF-1R expression in prostate cancer (Yanase and Fan, 2009; Sayeed et al., 2012; Wu et al., 2006; Fan et al., 2007), although the IGF-1R expression in cells treated with IGF-1 did not follow the pattern seen in tissues (Figure 1-2).

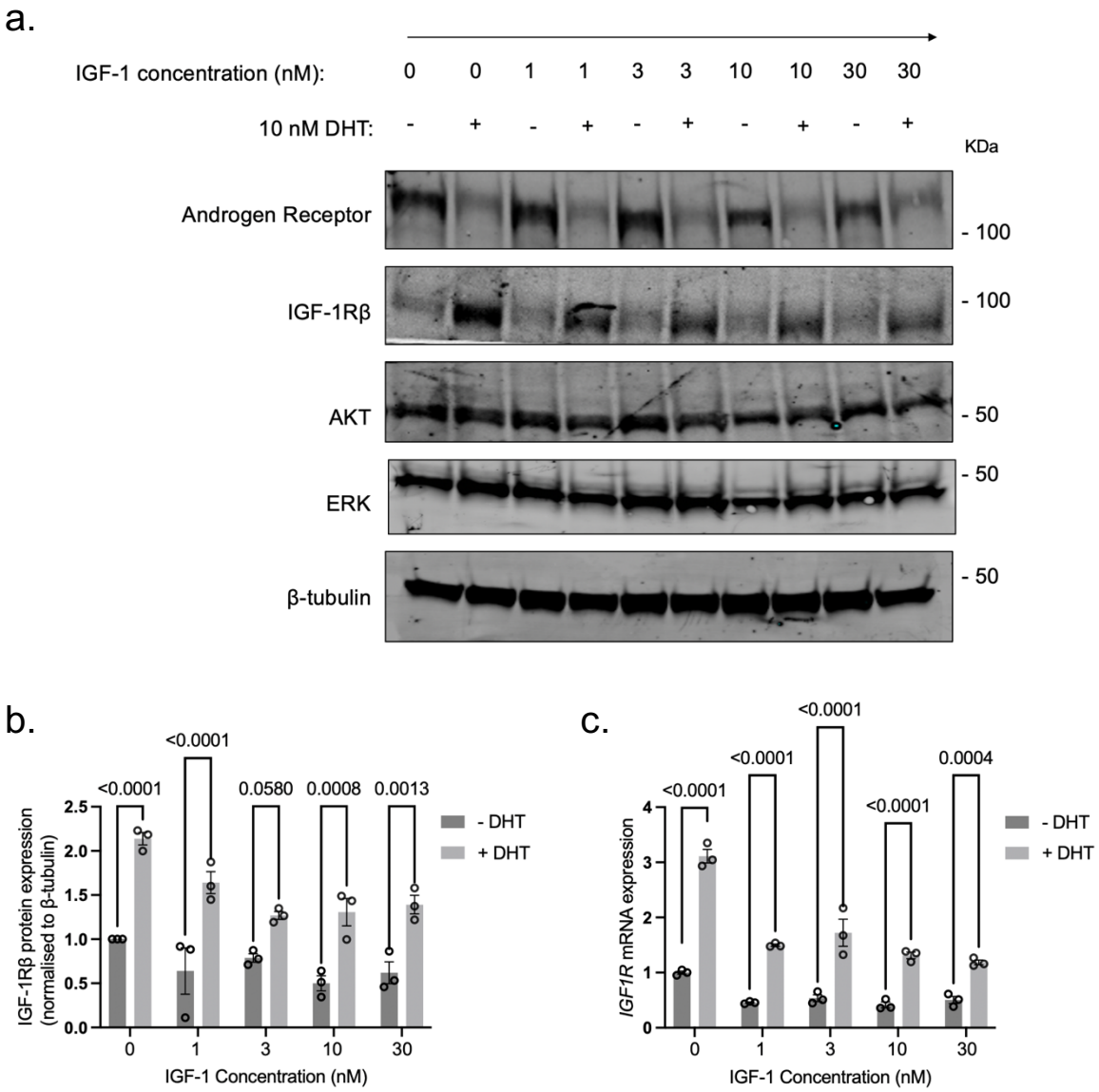


Figure 3-10 Effect of increasing concentration of IGF-1 on IGF-1R expression in the presence or absence of DHT. VCaP cells were serum starved for 24 hours, and treated with increasing concentrations of IGF- 1, with or without 10 nM DHT. IGF-1R expression levels were measured using (a) western blot and (b) quantified by normalising to loading control, β-tubulin, expressing as a fraction of levels in untreated control cells (n=3). (c) In parallel cultures *IGF1R* mRNA expression was measured using qPCR (n=3 independent repeats). Graphs show SEM and and significance was measured using a two-way ANOVA with Šídák's multiple comparisons test. The two-way ANOVA showed overall statistical difference between +/- DHT treatments (p= <0.0001) and graph shows significance at individual IGF-1 concentrations.

To further test the association between IGF-1 supply and IGF-1R axis in clinical samples, I interrogated publicly available Prostate Adenocarcinoma TCGA Firehose Legacy dataset derived from analysis of radical prostatectomies (n=500). Serum IGF-1 data were not available, so patients were divided based on highest or lowest quartile of tumour endogenous *IGF1* mRNA (log2 fold change between -3.04 - -0.64 and 0.51-3.19) and *IGF1R* (log2 fold change between -5.31 - -0.64 and 0.72-2.78). Dividing the patients based on the highest or lowest quartile *IGF1* expression resulted in 249 cases available for analysis. However, high tumour expression of *IGF1* displayed no association with tumour *IGF1R* (Figure 3-11a). High *IGF1* mRNA was significantly associated with *KLK3* (PSA) expression, a marker that could suggest activation of AR pathway (Figure 3-11a). Similarly, patients with high tumour *IGF1R* also had a significantly increased co-expression of *AR* and its downstream target *KLK3* (PSA, Figure 3-11b), further supporting the interplay between the IGF axis and the AR pathway.

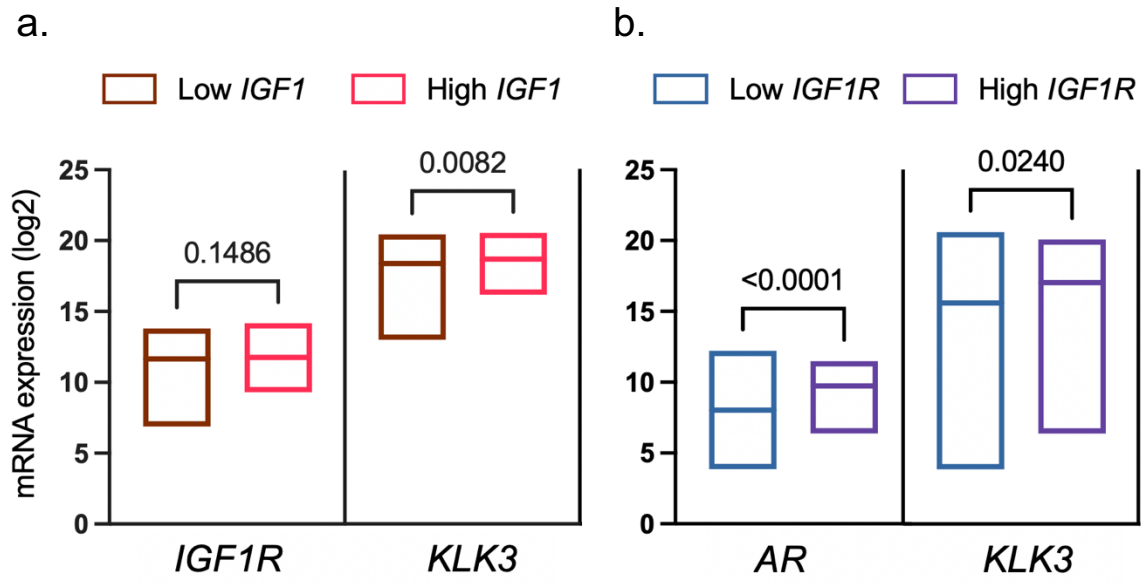


Figure 3-11 Prostate cancer TCGA analysis investigating association of endogenous *IGF1* and *IGF1R* mRNA expression. Patients from TCGA Prostate Adenocarcinoma, Firehose Legacy cohort were divided on highest and lowest quartile mRNA expression of (a) *IGF1* and (b) *IGF1R* (n=249). Associated mRNA co-expression between (a) *IGF1R* and *KLK3* were measured in high vs low *IGF1* patients and (b) *AR* and *KLK3* expression was measured in patients with high or low *IGF1R*. Box plots repesent mean with SEM and statistical significance was calculated using an unpaired two-tailed T-Test .

3.2.5 Effect of IGF-1 concentration on IGF-1R subcellular localisation.

Activation of IGF-1R by IGF-1 was shown by our group and others to lead to internalisation and nuclear translocation of the receptor (Aleksic et al., 2010, 2018; Sehat et al., 2010). In prostate cancer, nuclear IGF-1R was also shown to be detectable predominantly in the malignant glands and associated with advanced tumour stage (Aleksic et al., 2018). Furthermore, nuclear IGF-1R was shown to interact with RNAPol2 and to be recruited to promoters of genes including *JUN* and *FAM21*, which mediate tumour survival and migration (Aleksic et al 2018).

The final aim of this chapter was to test effects of long term IGF-1 stimulation *in vitro*, to understand if a high ligand environment can promote and maintain nuclear translocation of the receptor. VCaP cells were cultured in 30 nM IGF- 1 for 8-12 weeks, stained for IGF-1R, DAPI and actin and analysed using IF confocal microscopy (Figure 3-12a). Images were quantified using Fiji Image J to calculate the staining intensity and percentage increase was estimated against the mean intensity of the control samples. Long-term IGF-1 treated cells appeared to contain more internalised IGF-1R in comparison to the solvent (control) treated cells (Figure 3-12b). These findings suggest increased IGF-1R nuclear localisation in high IGF-1 conditions, which could promote tumour survival and migration. It is possible that the localisation of IGF-1R in the nucleus and its binding to the the chromatin could make less receptor protein available for lysis and detection by western blot, contributing to reduction in IGF-1R protein in IGF-treated cells as seen in Figure 3-8b. However, this would not affect *IGF1R* mRNA levels or explain the *IGF1R* mRNA downregulation seen after IGF-1 treatment (Figure 3-8d).

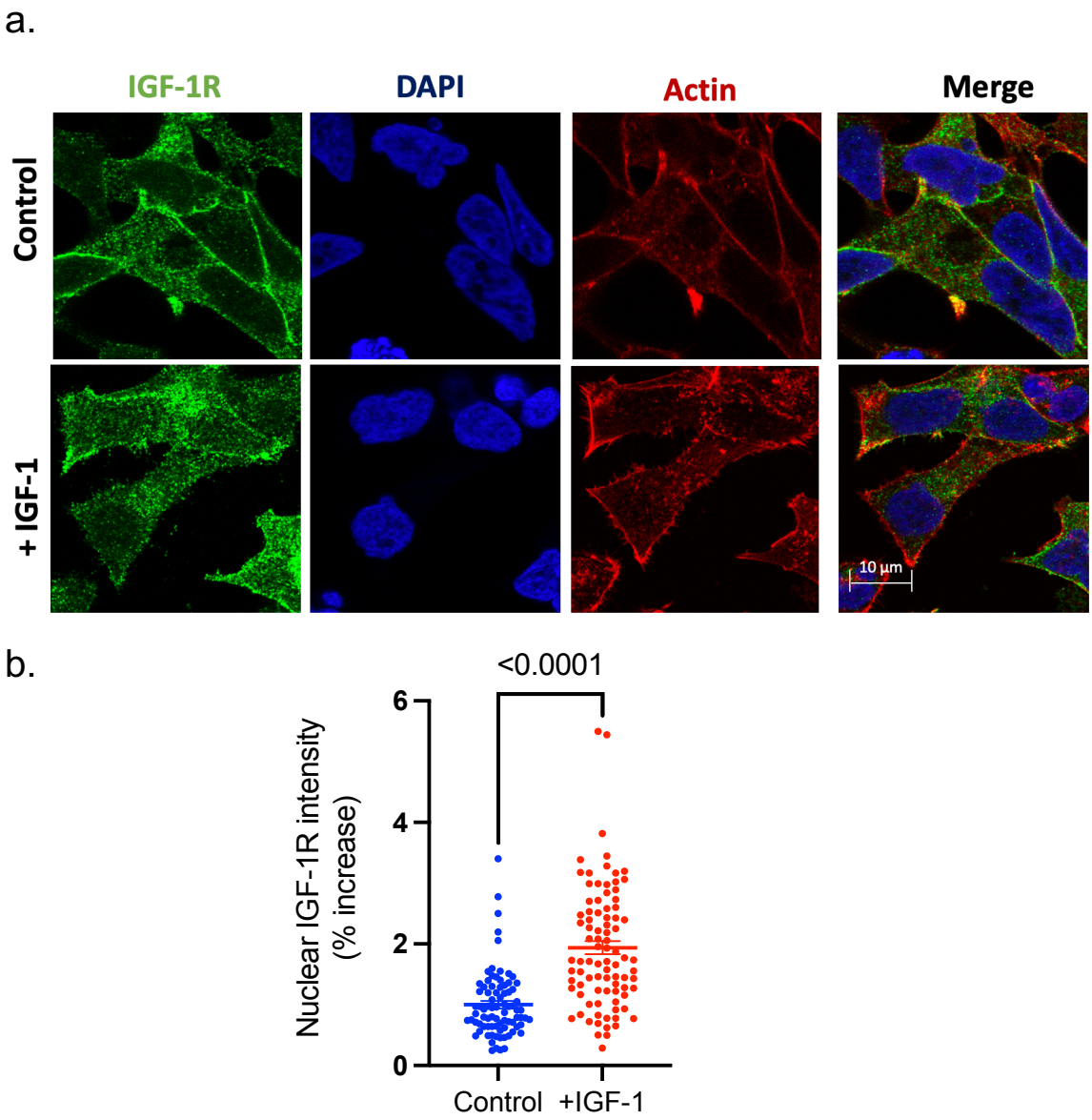


Figure 3-12 IGF-1R Immunofluorescent staining of VCaP cultures treated for 8-12 weeks with 30 nM IGF-1 or solvent. VCaP cells cultured in either 30 nM IGF-1 or solvent control for 8-12 weeks were stained for IGF-1R (green), DAPI (blue) and Actin (red, to define plasma membranes), and (a) IGF-1R subcellular localisation was assessed using IF. (b) IGF-1R localised into the nucleus was quantified if co-localised in the nucleus using DAPI. Analysis performed in a total of ≥ 82 cells per condition done on 3 independently prepared cultures. Graph shows SEM distribution and significance calculated using an unpaired two-tailed T-Test.

3.3 Discussion

The aim of this chapter was to understand the biological significance of IGF-1R upregulation in the malignant epithelium of high IGF-1 patients (Figure 1-2). Findings from this chapter indicate a trend to association of higher IGF-1R and internalised IGF-1R in the malignant areas (Figure 3-2), and this upregulation likely to be transcriptional (Figure 3-5a). No association was found between IGF-1R immunoreactive scores, circulating IGF-1 levels and *IGF1R* mRNA in the malignant epithelium (Figure 3-5b,c). The effects seen at the tissue level could not be recapitulated using cell line models but long-term IGF-1 cultures displayed increased nuclear translocation (Figure 3-12b), consistent with previous results published from the lab after acute IGF-1 stimulation (Aleksic et al., 2018).

Analysis of the tissue level data showed a trend towards increased IGF-1R in the malignant epithelium of prostate cancer and internalised cytoplasmic IGF-1R and its localisation in the malignant epithelium. This is also consistent at the mRNA level as results show increased *IGF1R* mRNA within the tumour compartment when compared to the benign and outer margins. IGF-1R upregulation in the malignant epithelium compared to the benign areas are also in agreement with previous reports published from the Macaulay lab (Hellawell et al., 2002; Aleksic et al., 2018). The increased *IGF1R* expression within the malignant epithelium compared to benign epithelium supports upregulation at the transcriptional level, although in individual tumours there was no correlation between *IGF1R* mRNA and IGF1R protein expression. Receptor upregulation and increased receptor internalisation could suggest that IGFs are drivers of tumorigenesis. Upon activation, ligand internalisation could promote tumorigenesis via the two downstream AKT and ERK pathways and aberrant

regulation of these pathways have been reported to promote tumorigenesis (Chitnis et al., 2008; Vivanco and Sawyers, 2002; Guo et al., 2020). Contrary to what was reported at the protein level by IHC from the lab, RNAScope showed no association between circulating IGF-1 and tumour *IGF1R* mRNA. There was also no association seen between *IGF1R* mRNA levels and PSA or Gleason grade. However, these experiments were performed only on limited (n=17) samples, which may not be a large enough cohort to test this association. Further investigation using a larger cohort would be needed to test whether if the increased receptor protein expression is a result of mRNA upregulation, and whether there is an association between tumour IGF-1R content and serum IGF-1.

The next aim of this chapter was to test the effects of acute and long term IGF-1 stimulation on IGF-1R expression in prostate cancer cells. Short term (24 hrs) treatment with IGF-1 did not affect receptor expression in DU145 cells but reduced IGF-1R expression in VCaP cells. Aiming to make a representative model of lifelong high IGF-1 exposure, VCaP and DU145 cells were cultured with or without IGF-1 supplementation for 8-12 weeks. DU145 cells were adapted to grow in 0.2% FBS before long term IGF-1 cultures. VCaP cells did not grow in 0.2% FBS and hence were cultured with IGF-1 long term in 10% FBS. There was no reduction in viability for DU145 cells grown in 0.2% FBS and all cultures maintained 95-100% viability throughout the study. This model of long term *in vitro* IGF-1 treatment had been used previously, generating clinically relevant data regarding the propensity of IGF-1 to promote bone metastases in triple negative breast cancer (H-F Zhang et al., 2013). Long term (8-12 weeks) IGF-1 treatment of both DU145 and VCaP cells displayed a significant reduction in receptor expression at both protein and mRNA levels. There is conflict in the literature regarding effects of IGF-1 on IGF-1R expression. Similar to my

results, IGF-1 induced IGF-1R downregulation was seen in human T lymphocytes (Schillaci et al., 1998). IGF-1R downregulation by polyubiquitination and degradation was also observed after treatment with IGF-1 in IGF-1R overexpressing mouse cells (Girnita et al., 2005). On the contrary, IGF-1 (3.9 nM) upregulated *IGF1R* in rat granulosa cells *in vitro* (deMoura et al., 2000). IGF-1R was also reported to translocate into the nucleus and up-regulate *IGF1R* expression by binding to its own promoter in breast cancer cells (Sarfstein et al., 2012). Reduced phosphorylation of AKT was also observed in long term IGF-1 cultures, even though they displayed IGF-1R phosphorylation. The reduction in AKT phosphorylation in IGF-1 treated cells could be due to initial IGF-1R-PI3K-AKT-mTOR activation, leading to negative phosphorylation by mTOR effector S6K of IRS-1 at Ser-312 and/or Ser-636/639 residues, leading to depletion of IRS1 and inhibition of AKT signalling (Zhang et al., 2008; Shah and Hunter, 2006). However, the subsequent decrease in AKT activation should prevent its inhibitory phosphorylation of transcription factor FOXO, allowing FOXO transcription factors to upregulate IGF-1R (O'Neill et al., 2016; Chandarlapaty et al., 2011). My results are not consistent with this model as there was no observed increase in IGF-1R with reduced AKT phosphorylation.

The cross talk between AR and IGF-1R is well characterised and AR and IGF-1R are known to regulate each other's expression and function in prostate cancer (Yanase and Fan, 2009; Fan et al., 2007; Wu and Yu, 2014; Bakin et al., 2003). Consisted with published data, DHT treatment upregulated the expression of IGF-1R and IGF-1 treatment upregulated the expression of *AR* (Fan et al., 2007; Pandini et al., 2005; Sayeed et al., 2012; Wu and Yu, 2014). Short term treatment of VCaP cells with IGF-1 and DHT resulted in the upregulation of IGF-1R expression that had been reduced by IGF-1 treatment alone. Co-treatment with

IGF-1 and DHT also resulted in lower IGF-1R protein and mRNA levels compared to treatment with DHT alone. Investigation of publicly available data sets showed no difference between cancer endogenous *IGF1* levels and *IGF1R* expression. However, high *IGF1* tumours had increased expression of *KLK3* (PSA), a downstream target of AR pathway. High *IGF1R* patients also had a significant association with increased *AR* and *KLK3* (PSA) expression. These results are consistent with studies that show androgen stimulation upregulates IGF-1R expression (Pandini et al., 2009; Sayeed et al., 2012). The results obtained here demonstrates a clear interaction between the IGF axis and the AR pathway that could contribute towards the progression of prostate cancer, however, they do not reflect the preliminary observation from the lab of IGF-1R upregulation seen in clinical tissues in men with high IGF-1. In future, there is scope to test the effects of IGF-1 stimulation on receptor expression in prostate cancer explant models, as they resemble a closer *in vivo* setting than cell line models. Making a representative *in vivo* model that replicates the results seen in tissues could help us understand how increased serum IGF-1 influence IGF-1R expression, function and risk of prostate cancer.

Previous results in the lab suggest a non-significant trend (p=0.095) to association of high serum IGF-1 and nuclear IGF-1R (unpublished). Long term treatment (8-12 weeks) of VCaP cells with IGF-1 induced a significant increase in receptor translocation to the nucleus, consistent with reports of IGF effects in short term culture (Aleksic et al., 2018; Sehat et al., 2010; Sarfstein et al., 2012). Receptor internalisation after activation has been shown to induce IGF-1R binding to the regulatory regions of DNA, interaction with RNA Polymerase II and expression of JUN and FAM21 (Aleksic et al., 2018). Thus long-term exposure to

high IGF-1 could maintain nuclear translocation, mediate tumour survival and migration, and contribute to the association of high IGF-1 and prostate cancer risk.

4 Chapter IV: Investigating the association of IGF-1 and immunosuppression in prostate cancer epithelium

4.1 Introduction

Recent advances in T cell targeted checkpoint inhibitors have shown promising outcomes in melanoma, bladder and kidney cancer, but have been largely unsuccessful in prostate cancer (Kwon et al., 2014a; Vitkin et al., 2019). The tumour microenvironment of prostate cancer has been classified as lacking T cell infiltration or as "immune-cold" and this phenotype could contribute to its reduced response to immunotherapy (Danaher et al., 2018). Additionally, tumour cells have the ability to secrete chemokines and cytokines, and express immunosuppressive molecules on their cell surface, which can aid in immune evasion and promote cytotoxic T cell anergy (Kohli et al., 2021; Shen et al., 2019). Improved understanding of factors that induce release of immune-modulatory cytokines and influence the function of infiltrating immune cells could shed light on the association of high IGF-1 with risk of cancer and on novel mechanisms of resistance to current immunotherapies, leading to better outcomes in men with prostate cancer.

Work from the previous chapter did not support the preliminary finding from previous work in the lab of a link between high IGF-1R expression within the tumour compartment and high circulating IGF-1, known to associate with prostate cancer risk (Travis et al., 2016; Watts et al., 2021). IGFs have also been implicated in promoting an immunosuppressive tumour microenvironment in several cancer types and in suppressing auto-immune diseases (Trojan et al., 1993; Kooijman and Coppens, 2004; Chaudhry et al., 2011; Bilbao et al.,

2014a; Johannesson et al., 2014; Lopes et al., 2016; Nordstrand et al., 2017b; Ajona et al., 2020; Vernieri et al., 2021). The work described in this chapter aimed to understand effects of IGF-1 on the immune microenvironment of prostate cancer by investigating its effects on the tumour epithelium. This was done by testing IGF-1 induced effects on prostate cancer expression of chemokines, cytokines and immune checkpoint ligand PD-L1, using *in vitro cell* line models and publicly available transcriptional datasets from prostate cancer clinical samples.

4.2 Results

4.2.1 Effects of IGF-1 on the expression of immune-modulatory cytokines in prostate cancer cell lines

Cytokines and chemokines are important in eliciting an effective immune response against cancer. Their dysregulation can often be seen in various cancers, aiding in recruitment of immunosuppressive cells to the tumour microenvironment (Kohli et al., 2021; Ozga et al., 2021). Effects of IGF-1 on expression of cytokine genes were tested using androgen independent DU145 and androgen dependent VCaP prostate cancer cells (Figure 4-1a-b). Briefly, DU145 (Figure 4-1a) and VCaP (Figure 4-1b) cells were serum starved for 24 hrs and stimulated with IGF-1 for 4, 24 and 48 hours. As in work shown in the previous chapter, these experiments used 30 nM IGF-1, comparable to the upper end of the normal range in adult men (Bidlingmaier et al., 2014) RNAs were extracted and used in qRT-PCR to test expression of chemokine C-C motif ligand 5 (*CCL5*), chemokine C-X-C motif ligands

(*CXCL8*, *CXCL10*) and immune modulatory targets Signal Transducer And Activator Of Transcription 5A (*STAT5A)*, Interferon β (*IFNB1)*, Interferon Induced Protein With Tetratricopeptide Repeats 1 (*IFIT1)* and Arginase 2 (*ARG2*) (Figure 4-1b). These genes were selected as they were downstream targets of the NF-κB and cGAS-STING pathways (Parkes et al., 2017; Reisländer et al., 2019; Pires et al., 2018; Cheng et al., 2018; Wickremasinghe et al., 2004; Hinz et al., 2002; Ho et al., 2017; Lawrence, 2009). Expression patterns of genes varied with time, and with exception of *STAT5A* expression in VCaP cells, all genes were upregulated by IGF-1 at least 1.5-fold compared with controls. IGF-1 stimulation upregulated *IFNB1* expression, maximum at 24 hrs, in both cell lines. Expression of *CCL5* and *ARG2* were both upregulated, with the greatest increase at 48 hours in DU145 cells. *IFIT1* upregulation was the highest after 24 hours IGF-1 stimulation in both cell lines; *STAT5A* showed a similar trend in DU145 cells but with only minor changes in VCaP. *CXCL10* expression was upregulated with increasing time in DU145 cells, while VCaP cells showed the greatest difference after 4 hours.

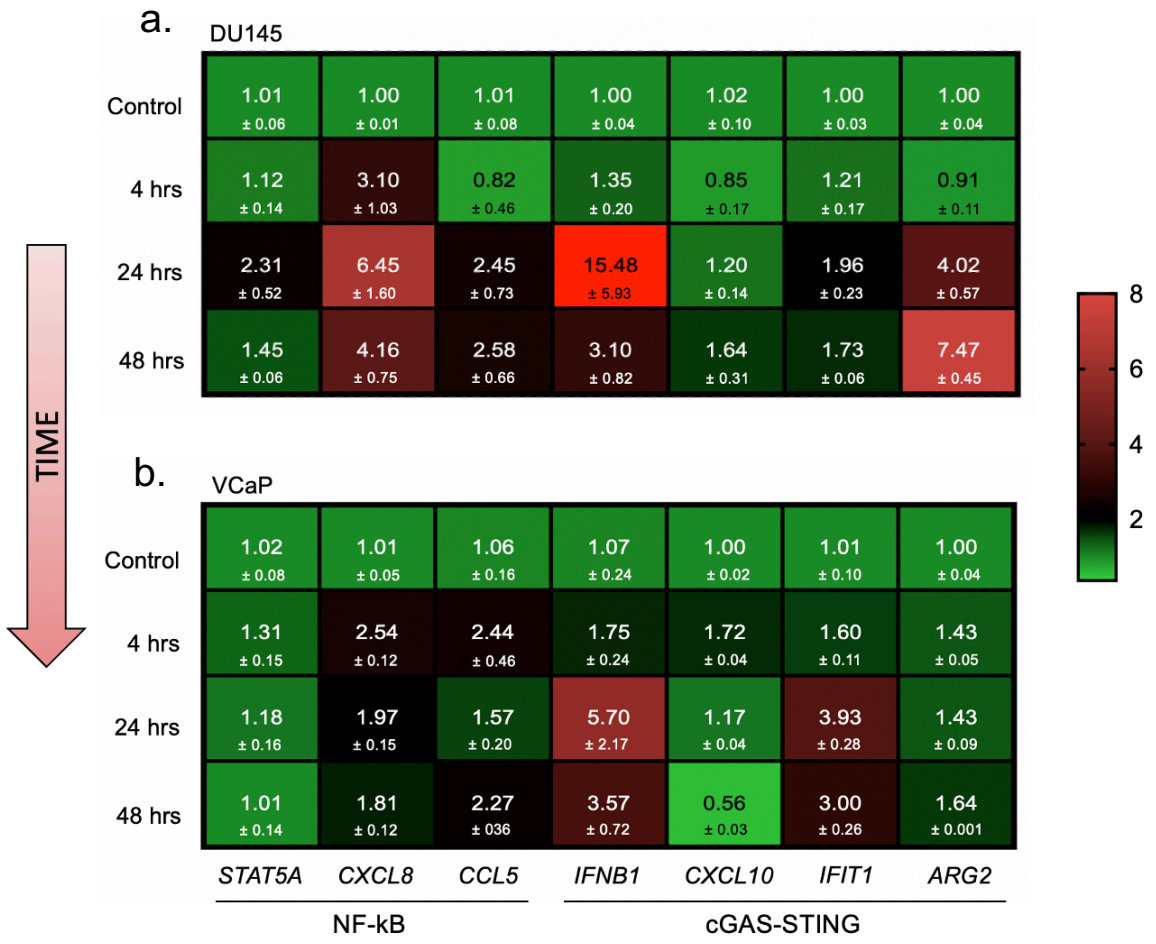


Figure 4-1 Effect of IGF-1 on expression of cytokines and immunomodulatory targets. (a) DU145 and (b) VCaP cells were serum starved for 24 hrs and treated with 30 nM IGF-1 for 4, 24 and 48 hours and gene expression was measured using qRT-PCR. Fold change from solvent-treated control cells was calculated for each gene (mean ± SEM, n=3 independent repeats) and a higher expression was denoted in red (scale on the right). Genes were classified as associated with the NF-κB or cGAS-STING pathway.

4.2.2 Investigating effect of IGF-1 on cGAS-STING pathway

Results from Figure 4-1 suggest that IGF-1 stimulation upregulates genes downstream of the cGAS-STING and NF-kB pathways. To test whether IGF-1 influences the cGAS-STING pathway, DU145 cells were serum starved for 24 hrs, stimulated with 30 nM IGF-1 or solvent (control) and activation of cGAS-STING pathway measured using western blot

(Figure 4-2a). There was detectable IGF-1R phosphorylation in response to IGF-1, as expected, and this was still detectable at 48 hrs. IGF-1 stimulation resulted in time-dependent increase in phosphorylation of TBK1 and IRF3 (Figure 4-2b,c). There was also a significant upregulation of total STING protein (Figure 4-2d). The phosphorylation of TBK1 is known to contribute to the activation of the NF-kB pathway by its negative phosphorylation of IκBα, signalling IκBα ubiquitination and degradation and, translocation of NF-κB proteins into the nucleus (Liu et al., 2017b). Additionally, 4 hrs IGF-1 stimulation resulted in increased phosphorylation of STAT1 (Figure 4-2e). STAT 1 is a surrogate marker for expression of inflammatory signalling as well a mediator of the induction of type 1 interferons after the accumulation of cytosolic DNA (Harding et al., 2017; Erdal et al., 2017).

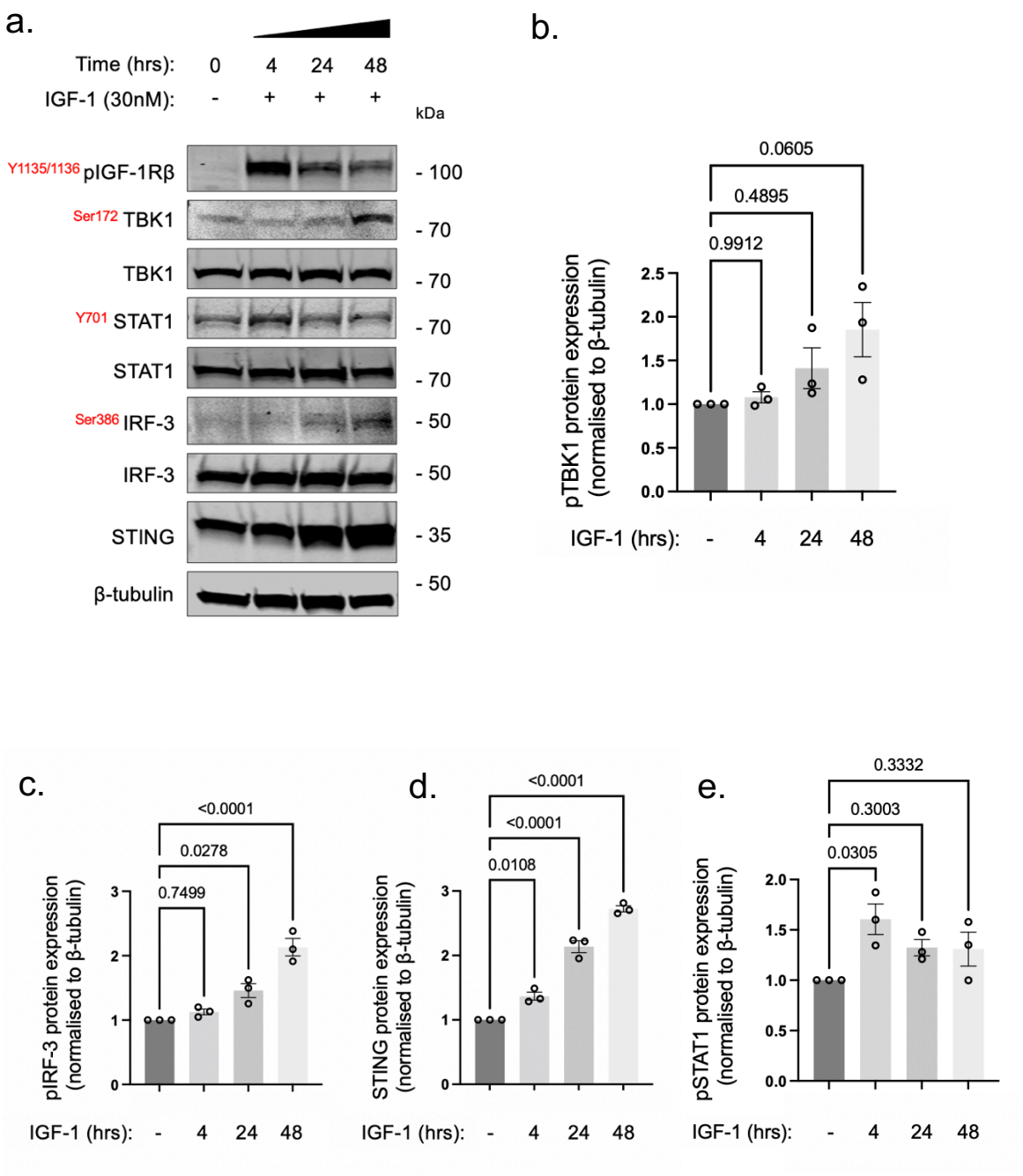


Figure 4-2 IGF-1 induced activation of the cGAS-STING pathway measured using western blot. (a) DU145 cells were serum starved for 24 hrs and treated with 30 nM IGF-1 for 4, 24 and 48 hrs, cells collected, lysed and proteins involved in the cGAS-STING pathway were measured using western blot (n=3 independent repeats). Phosphorylated (b)TBK1, (c) phosphorylated IRF3, (d) STING and (e) phosphorylated STAT1 were quantified after normalisation to the loading control β-tubulin using FIJI ImageJ. Graphs represent SEM and statistical significance was determined using a one-way ANOVA.

The cGAS-STING pathway is commonly activated as a response to the detection of cytosolic DNA by cGAS, seen most often as a result of replication stress (Li and Chen, 2018; Reisländer et al., 2019). Replication stress has been reported to promote DNA damage and contribute to both microsatellite destabilisation and hypermutation (Matsuno et al., 2019). Recent results from our group show that IGF-1 upregulates RRM2, compromising function of RNR while IGF blockade leads to RRM2 downregulation (Rieunier et al., 2021). Both effects can cause dNTP pool imbalance, and an imbalance can be mutagenic (Kumar et al., 2011). Furthermore, unpublished data (Rieunier, Macaulay) also suggests that 24 hr IGF-1 stimulation increases damage marker γ-H2AX and accelerates replication fork progression, which has been shown by others to induce replication stress causes by oncogenes such as MYC, Cyclin E, RAS (Vafa et al., 2002; Kotsantis et al., 2016; Bester et al., 2011). To test whether IGF-1 induces generation of cytosolic DNA and/or micronuclei, future work would make use of DNA stain Picogreen. This assay could not be performed due to time constraints. Cells would be treated with 30 nM IGF-1 for different durations and stained with Picogreen (DNA) and mitotracker (mitochondria) and DAPI (nucleus) (Ho et al., 2016a). DNA localised to the mitochondria and nucleus will be excluded from the analysis and the remaining cytosolic DNA will be quantified.

4.2.3 Investigating effects of IGF-1 on the expression of immune checkpoint ligand PD-L1 *in vitro*

Activation of the cGAS-STING, NF-kB, PI3K-AKT and MAPK/ERK pathways have all been implicated in regulating PD-L1 expression (Shen et al., 2019; Chen et al., 2015; Sato et al., 2017; Abdelhamed et al., 2016). The PI3K-AKT, MAPK/ERK and NF-kB pathways

are well-known to be activated by the IGF axis (Chitnis et al., 2008), as may be cGAS-STING based on findings from Figure 4-2. The next aim was to investigate IGF-1 induced effects on PD-L1 expression in prostate epithelium and prostate cancer cell line models.

To characterise the effects of IGF-1 stimulation on PD-L1 expression, I selected prostate cancer DU145 cells and colorectal cancer NCI-H747 (H747) cells based on their detectable *CD274* (PD-L1) and *IGF1R* mRNA expression. This was obtained from TCGA cancer cell line encyclopaedia (Broad, 2019) (Figure 4-3). There other multiple cell lines that displayed similar or higher *IGF1R* and *CD274* expression, however, DU145 and H747 cells were chosen as they were available in the laboratory.

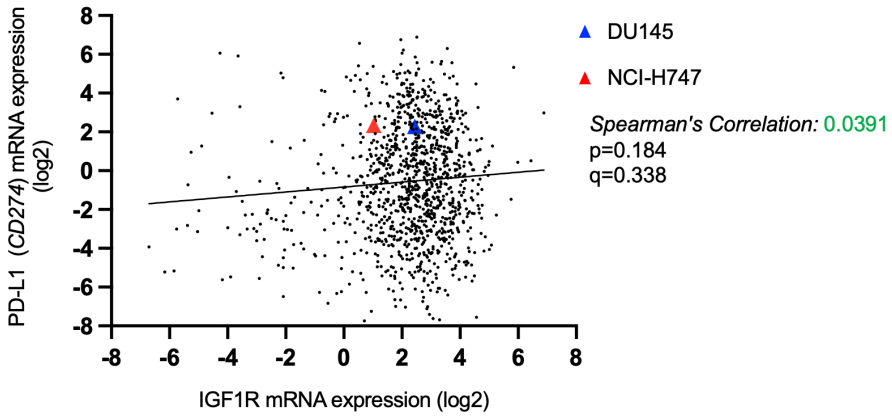


Figure 4-3 Identifying cell lines to test for IGF-1 induced PD-L1 expression. Cell lines were selected from the TCGA cancer cell line encyclopaedia based on their mRNA expression of *IG1R* and *CD274* (PD-L1). Prostate cancer DU145 cells (blue) and colorectal cancer NCI-H747 cells were selected to study effects of IGF-1 PD-L1 expression.

4.2.3.1 Effects of serum starvation on PD-L1 expression

To test the effect of IGF-1 in an *in vitro* setting, DU145 and H747 cells were serum starved for 24 hrs and PD-L1 surface expression was measured using flow cytometry. Expression levels were presented as Median Fluorescence Intensity (MFI). Unstained and fluorophore-labelled isotype controls were used to test the specificity of the antibody staining.

Serum starvation reduced PD-L1 surface expression in both DU145 (Figure 4-4a) and H747 cells (Figure 4-4b). IGFs represent an important (but not the only) component of serum bioactivity. Bovine IGF-1 is identical to human IGF-1 and bovine IGF-2 is identical to human IGF-2 apart from 3 of 67 residues. (Honegger and Humbel, 1986). To understand how IGF-1 contributed to the differences in PD-L1 between serum starved and full medium culture, the IGF-1 concentration in FBS was quantified at the Biochemistry Laboratory, John Radcliffe Hospital using the IDS-iSYS Insulin like Growth Factor-I (IGF-I) assay, supervised by Professor Tim James. After analysis of 3 samples the concentration was reported to be 9.3 nM ±0.58 (SEM). Therefore, compared with culture in 10% FBS, serum starvation would result in a decrease in IGF-1 exposure of ~1 nM.

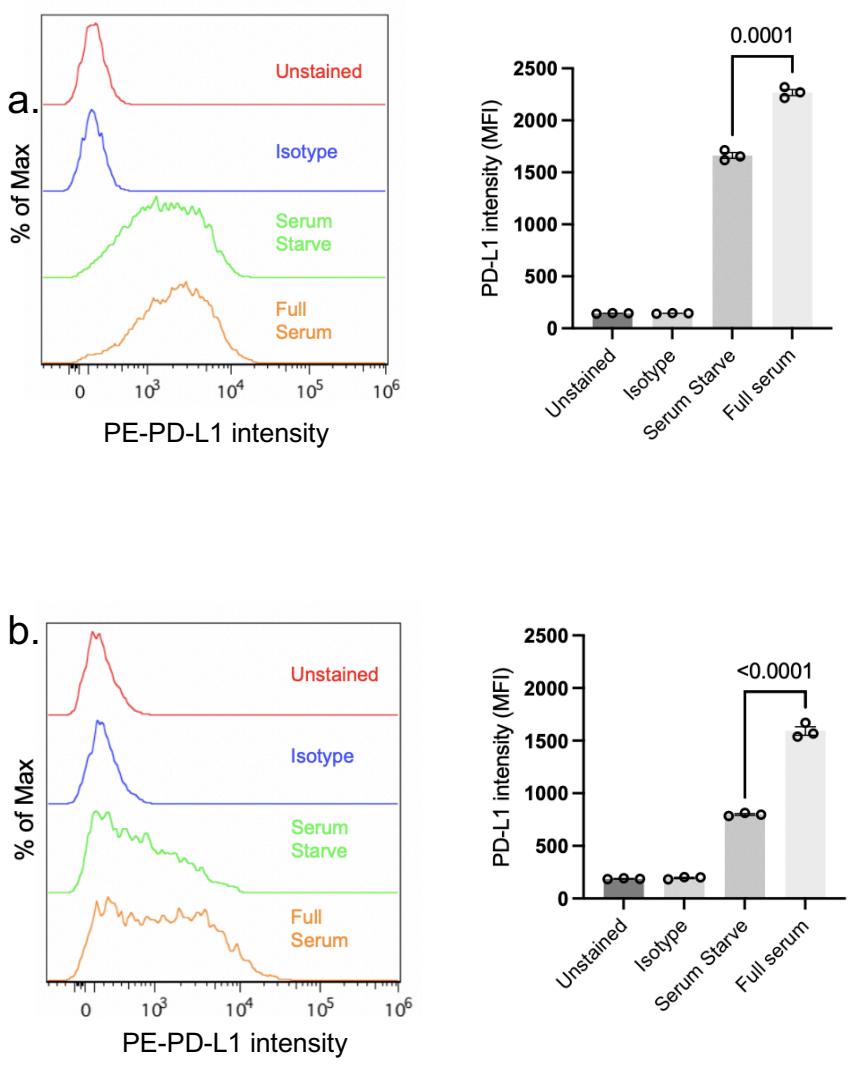


Figure 4-4 Effects of short-term serum starvation on PD-L1 surface expression. PD-L1 surface expression was measured using flow cytometry in (a) DU145 and (b) H747 cells, collected after culture in full medium with 10% FBS or after serum starvation for 24 hrs. Expression levels were calculated using Flow Jo software as Median Fluorescence Intensity (MFI). Y axis represents cell counts scaled as a percentage of the maximum count. Graphs to right: MFI values (mean ± SEM) from 3 independent experiments. Statistical significance was calculated using a one-way ANOVA with Tukey's post-hoc test for multiple comparisons.

4.2.3.2 Effects of IGF-1 on PD-L1 surface expression

Full medium (10% FBS) condition was shown to significantly upregulate the expression of PD-L1 (Figure 4-4) and is known to contain mitogenic factors in addition to IGFs (Zheng et al., 2006; Shanskii et al., 2013). Therefore, I investigated IGF-1 specific effects on PD-L1 surface expression. Cells were treated with 30 nM IGF-1 for 0.5 to 48 hrs in serum starved or full medium (10% FBS) conditions and PD-L1 surface expression was measured using flow cytometry. In serum starved conditions, IGF-1 stimulation resulted in the increase of PD-L1 surface expression in both DU145 (Figure 4-5a) and H747 (Figure 4-5b) cells, with the greatest difference seen after 24 hrs stimulation. Consistent with the findings in serum starved conditions, IGF-1 stimulation in the presence of 10 % FBS also resulted in PD-L1 surface expression. The most significant upregulation was seen in H747 cells, with statistically significant although relatively minor changes in DU145 cells.

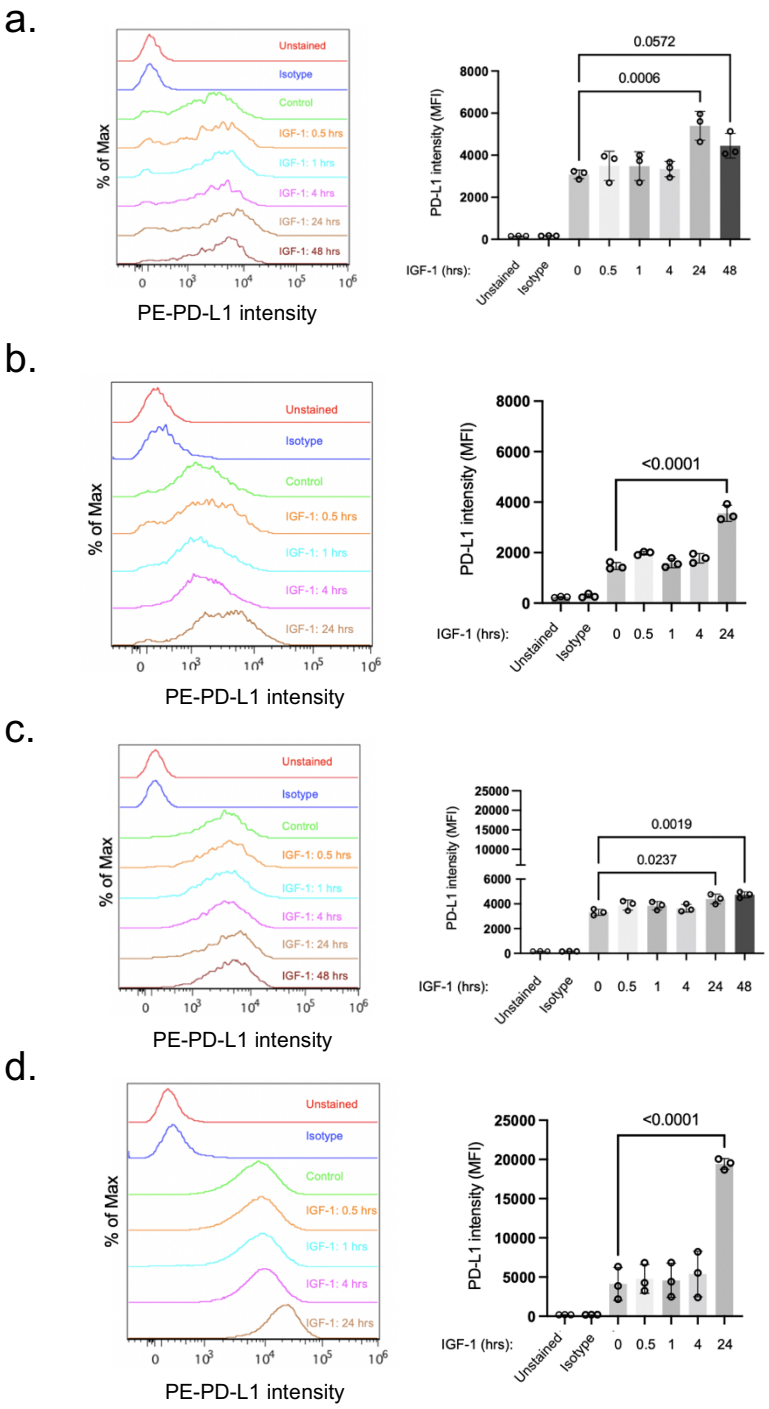


Figure 4-5 Effect of IGF-1 on PD-L1 surface expression (a) DU145 and (b) H747 cells were serum starved for 24 hrs, stimulated with 30 nM IGF-1 for the indicated times and PD-L1 surface expression was measured using flow cytometry. Experiments shown in a-b were repeated in both (c) DU145 and (d) H747 cells after 30 nM IGF-1 stimulation in full medium (10% FBS). Expression levels were measured as MFI. Graphs to right show MFI values (mean ± SEM) from 3 independent experiments. Statistical significance was calculated using a one-way ANOVA with Tukey's test for multiple comparisons.

4.2.3.3 Investigating if PD-L1 is transcriptionally upregulated by IGF-1

To understand the mechanism through which PD-L1 expression is upregulated by IGF-1, transcription was inhibited using Actinomycin D (Act D) and PD-L1 surface expression was measured using flow cytometry as before (Sobell, 1985). Briefly, DU145 (Figure 4-6a-c) and H747 (Figure 4-6b-d) cells were pre-treated with or without 1 μg/mL Actinomycin D for 2 hrs and stimulated with IGF-1 for 24 hrs, a duration which produced the highest expression of PD-L1(Figure 4-5). Experiments were repeated in serum starved (24 hrs) and full medium (10% FBS) conditions.

Consistent with results of Figure 4-5, IGF-1 stimulation resulted in the increase of PD-L1 surface expression in both DU145 and H747 cells in serum starved and full serum conditions (Figure 4-6a-d). The IGF-induced increase in surface PD-L1 was similar in the two cell lines in serum-starved cultures, and greater in H747 in full medium. Blocking transcription with Actinomycin D prevented IGF-1 induced upregulation of PD-L1 in both DU145 (Figure 4-6a,c) and H747 (Figure 4-6b,d) cell lines. These results suggested that the upregulation of PD-L1 surface expression was due to a transcriptional change.

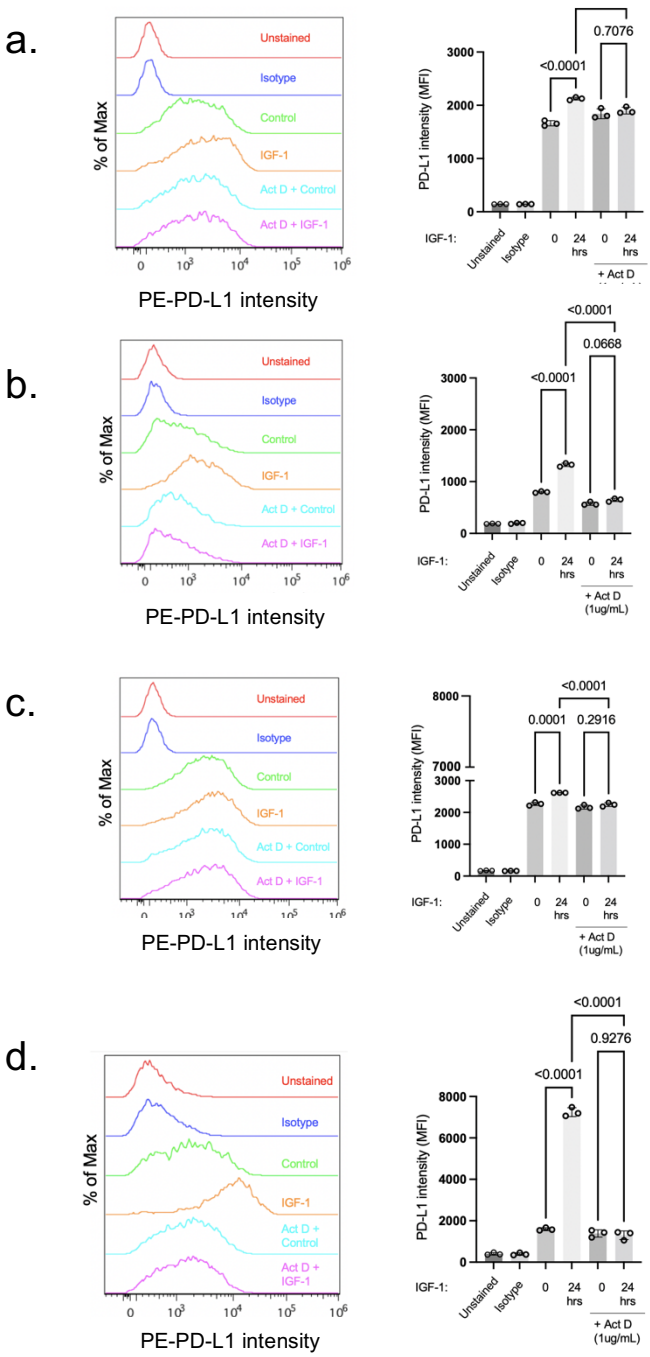


Figure 4-6 Effect of transcriptional inhibition on IGF-stimulated increase in PD-L1 surface expression. DU145 (a) and H747 (b) cells were serum starved for 24 hrs, pre-treated with 1 µg/mL Actinomycin D for 2 hrs and stimulated with 30 nM IGF-1 for 24 hrs. Actinomycin D was left on the cells during the 24 hrs IGF-1 treatment. After stimulation, PD-L1 surface expression was measured using flow cytometry. Experiments were repeated in both (c) DU145 and (d) H747 cells after 30 nM IGF-1 stimulation in 10% FBS. As before, expression levels are shown as MFI (left) and quantified (mean ± SEM, right) from 3

independent experiments. Statistical significance calculated using a one-way ANOVA with Tukey's post hoc test.

4.2.3.4 Effects of IGF-1 on PD-L1 surface expression in additional prostate cancer cells

Effects of IGF-1 on PD-L1 expression were tested in spontaneously immortalised mouse prostate epithelial cells (MPEC) (Haughey et al., 2020), primary mouse prostate cancer cells (MyC-CaP) and metastatic human prostate cancer cells (DU145 and VCaP) using qRT-PCR and flow cytometry. To test for IGF-1 induced effects on expression of *CD274*, the gene encoding PD-L1, DU145 (Figure 4-7a), MyC-CaP (Figure 4-7b) and VCaP (Figure 4-7c) cells were serum starved, treated with IGF-1 for 24 hrs and extracted RNAs were used for qRT-PCR. IGF-1 stimulation led to upregulation of *CD274* mRNA in all three cell lines, with DU145 cells showing the greatest upregulation (4.6-fold change compared with serum-starved controls). PD-L1 surface expression was also measured using flow cytometry in MPEC (Figure 4-7d) and MyC-CaP (Figure 4-7e) cells after serum starvation and IGF-1 stimulation for 24 hrs. IGF-1 increased PD-L1 surface expression in both cell lines, though the increase seen was considerably lower than the upregulation seen in DU145 cells (Figure 4-6a).

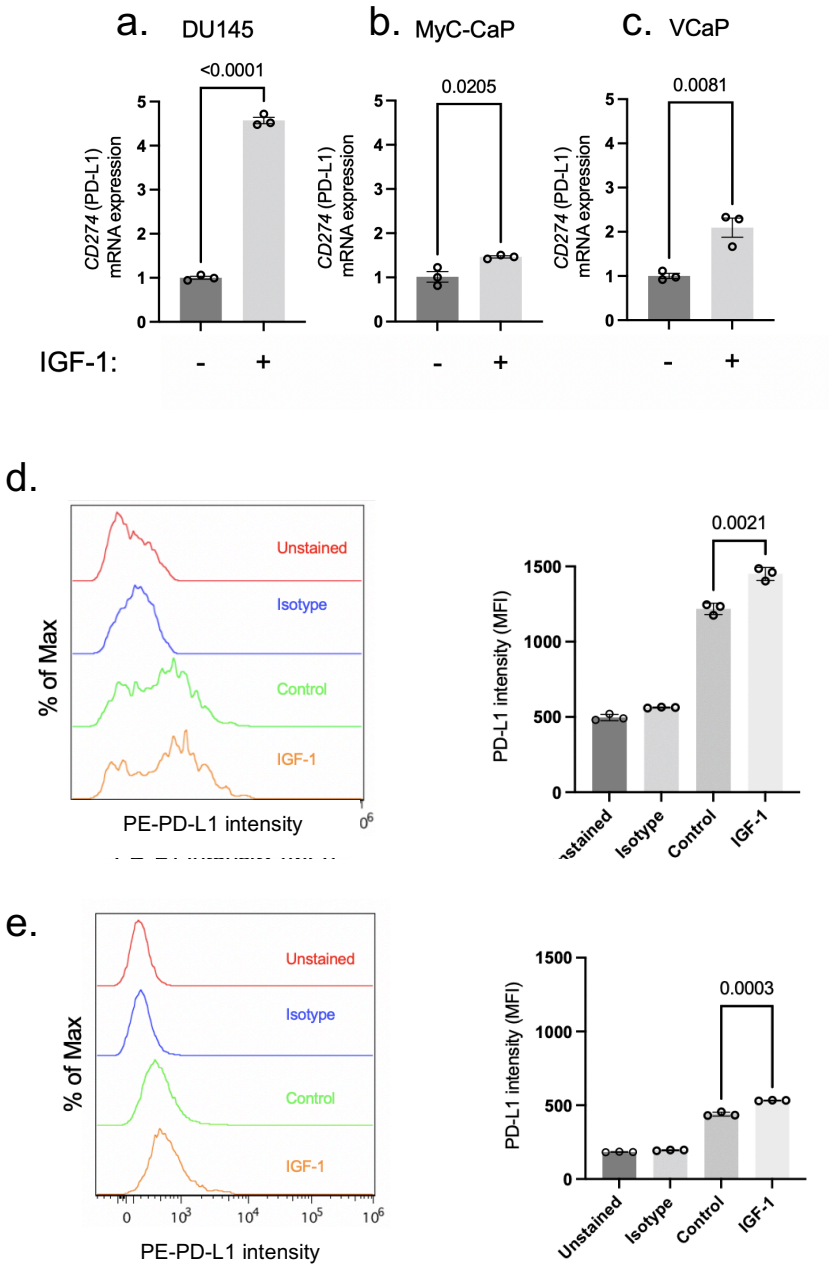


Figure 4-7 Effects of IGF-1 stimulation on PD-L1 expression in prostate cancer cell lines. Prostate cancer cell lines (a) DU145, (b) MyC-CaP and (c) VCaP cells were serum starved for 24 hrs, stimulated with 30 nM IGF-1 for 24 hours and *CD274* (PD-L1) mRNA expression was measured using qRT-PCR (n=3 independent repeats). Graphs show ± SEM with significance determined using an unpaired two-tailed T test. (d) MPEC benign prostate epithelium cells and (e) MyC-CaP prostate cancer cells were treated as in (a-c) and PD-L1 surface expression was measured using flow cytometry. PD-L1 surface expression levels shown as MFI (left) and quantified (mean ± SEM, right) from 3 independent experiments. Statistical significance tested using a one-way ANOVA with Tukey's post hoc test.

4.2.3.5 Investigating the mechanism of IGF-1 induced PD-L1 upregulation.

To investigate how IGF-1 induced PD-L1 upregulation, IGF-1R and its downstream pathways, PI3K-AKT and MAPK/ERK were inhibited and PD-L1 expression was measured using qRT-PCR and flow cytometry. DU145 cells were pre-treated in full medium (10% FBS) for 1 hr with IGF-1R tyrosine kinase inhibitor BMS-754807, allosteric AKT inhibitor AZD5363 and MEK1/2 inhibitor trametinib, and then 30 nM IGF-1 was added for 24 hrs. PD-L1 surface expression was measured using flow cytometry and *CD274* mRNA expression tested using qRT-PCR. As seen previously (Figure 4-7), IGF-1 upregulated *CD274* mRNA and PD-L1 membrane expression (Figure 4-8a). Blocking IGF-1R activity using BMS-754807 prevented the IGF-induced increase in both *CD274* mRNA and surface expression, supporting the idea that IGF-1 induces PD-L1 via its activity on IGF-1R (Figure 4-8a,b). Furthermore, inhibition of downstream PI3K-AKT and MAPK/ERK prevented IGF-1 stimulated PD-L1 upregulation. MAPK/ERK inhibition using trametinib resulted in a significant decrease in *CD274* mRNA, lower than IGF-1R inhibition alone (Figure 4-8a). IGF-induced increase in PD-L1 membrane expression was also significantly reduced after inhibition with BMS-754807, AZD5363 and trametinib, though the changes were not as large when compared to the mRNA levels and there were no significant differences between the effects of the three inhibitors (Figure 4-8b).

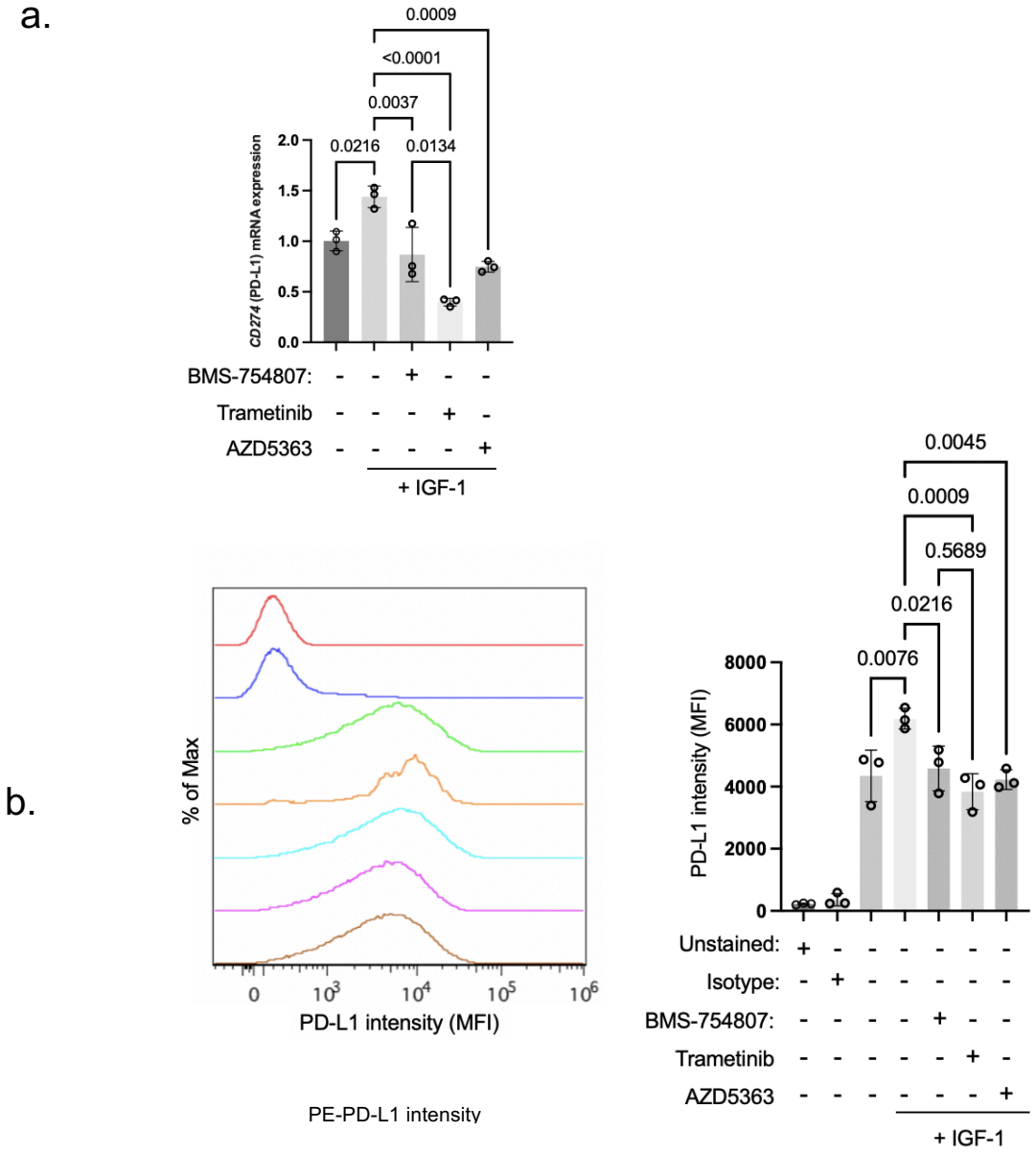


Figure 4-8 Investigating the mechanism of IGF-1 induced upregulation of PD-L1 expression. DU145 cells were grown in 10% supplemented FBS and pre-treated with 300 nM of BMS-754807, 5µM AZD5363 and 50 nM trametinib for 1 hr and then 30 nM IGF-1 was added for 24 hrs. (a) PD-L1 mRNA levels were measured using qRT-PCR and (b) surface expression levels were measured using flow cytometry. PD-L1 surface levels was measured as (left) MFI and expression of 3 independent repeats were graphed (MFI mean ± SEM, right). Statistical significance in (a) and (b) were calculated using a one-way ANOVA with Tukey's test for multiple comparisons.

4.2.4 Investigating the association between tumour endogenous *IGF1R*, *IGF1* and the expression of cytokines and *CD274* (PD-L1) from publicly available data.

Results in this chapter suggested that IGF-1 stimulation led to the upregulation of chemokines in prostate cancer cell lines (Figure 4-1) and PD-L1 in prostate and colorectal cancer cells (Figure 4-5, Figure 4-7). To test these associations in larger cohorts, I analysed publicly available TCGA Firehose Legacy datasets on gene expression in clinical cohorts of primary prostate adenocarcinoma (n=499) and primary colorectal adenocarcinoma (n=592). Patients' tumours were divided based on the highest and lowest quartiles of their *IGF1R* and *IGF1* expression levels (prostate n=149, colon n= 296).

Using this TCGA prostate cancer dataset I assessed expression of immune-modulatory cytokines (*STAT5A, CXCL8, IFNB1, CXCL10, IFIT, ARG2* and *CCL5*), which had been tested using q-RT PCR in Figure 4-1 and additional cytokines (Sphingosine-1-phosphate (*S1P)*, chemokine C-X-C motif ligand 12 (*CXCL12),* chemokine C-C motif ligand 21 (*CCL21*) and chemokine C-C motif ligand 4 (*CCL4)*) involved in immune cell infiltration. In patients whose tumours expressed high *IGF1*, there was significantly higher expression of *STAT5A, IFIT1, ARG2, S1P, CXCL12, CCL5* and *CCL4* (Figure 4-9). There was also a trend towards upregulation of *CCL21* in high *IGF1* tumours (Figure 4-9). Amongst the genes previously tested after IGF-1 stimulation on prostate cancer cell lines (Figure 4-1), *STAT5A, IFIT1, ARG2* and *CCL5* expression was significantly higher in high *IGF1* tumours. Finally, cytokines which have been associated with immunosuppressive cell recruitment into tumours were also assessed (Figure 4-9). These cytokines are responsible for the recruitment into the tumour of cells such as Treg (*S1P*, *CXCL12*), M2 Macrophage (*CXCL12*, *CCL21*)

and MDSCs (*CCL5*, *CCL4*), which commonly infiltrate prostate cancer (Zhou et al., 2020; Lin et al., 2019; Argyle and Kitamura, 2018; Ruytinx et al., 2018; Fleming et al., 2018; Erlandsson et al., 2019; Calcinotto et al., 2018; Vitkin et al., 2019) .

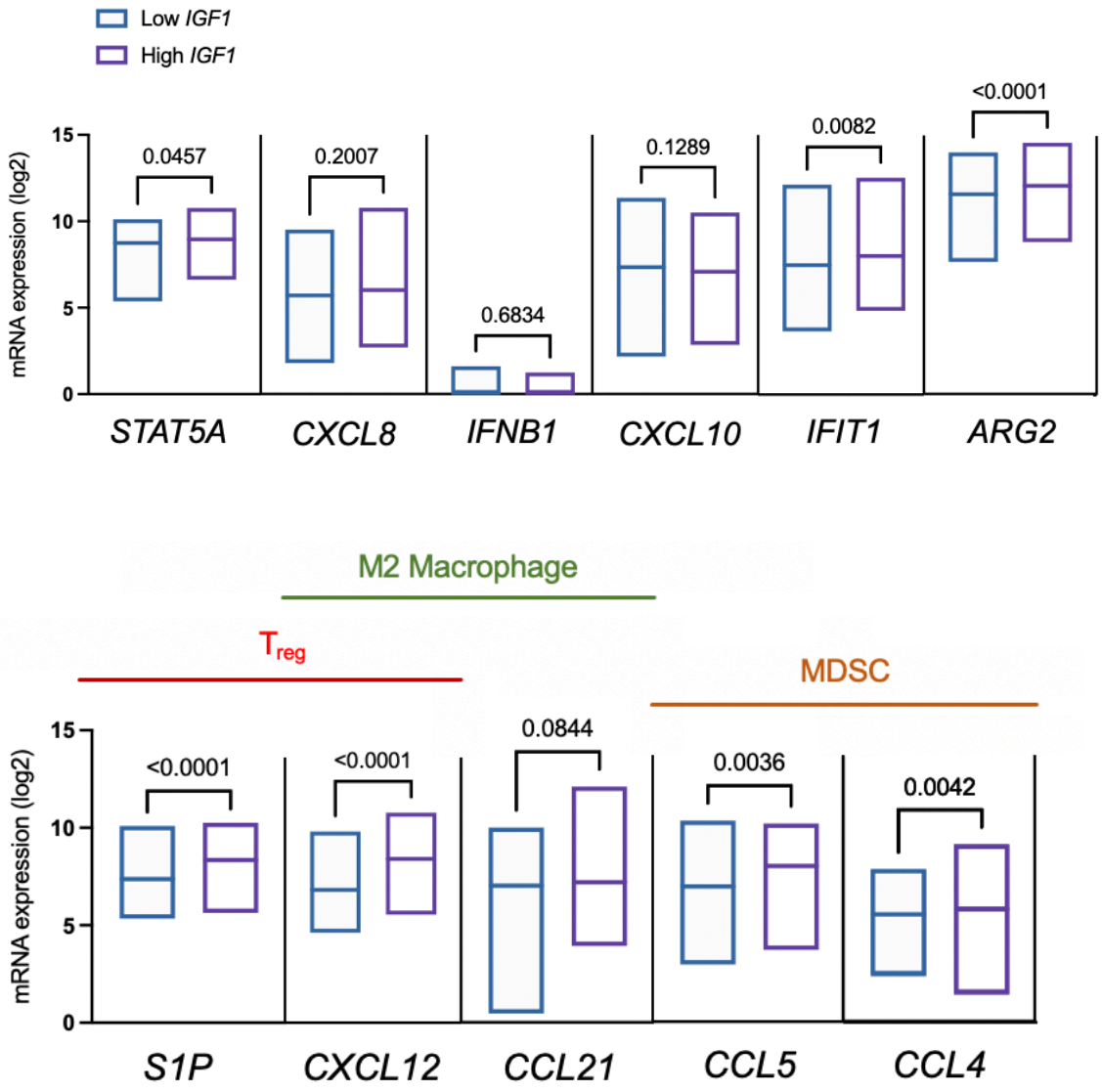


Figure 4-9 Gene expression of immune-modulatory cytokines in high vs low *IGF1* prostate cancer tumours from TCGA. TCGA primary prostate adenocarcinoma Firehose Legacy dataset (n=499) was divided into highest (n=123) and lowest (n=124) quartiles of tumour expression of *IGF1*. Association between levels of IGF1 and cytokines were calculated using log2 mRNA expression. In the graphs, the bar indicates mean log2 mRNA expression with the box representing the SEM. Statistical significance was calculated using an unpaired two-tailed T test.

Similarly, expression of *CD274* was also tested in high vs low *IGF1* and *IGF1R* tumours in prostate and colorectal cancer datasets. In prostate cancer, patients whose tumours had high *IGF1R* and *IGF1* levels displayed significantly higher *CD274* mRNA than the lowest quartile subgroups (Figure 4-10a,b). Colorectal cancers with high endogenous *IGF1* levels displayed ~~a~~ significantly higher *CD274* mRNA when compared to the cancers in the lowest quartile for *IGF1* expression (Figure 4-10c), but there was no difference in *CD274* expression in colorectal cancers that had high *IGF1R* mRNA levels (Figure 4-10d).

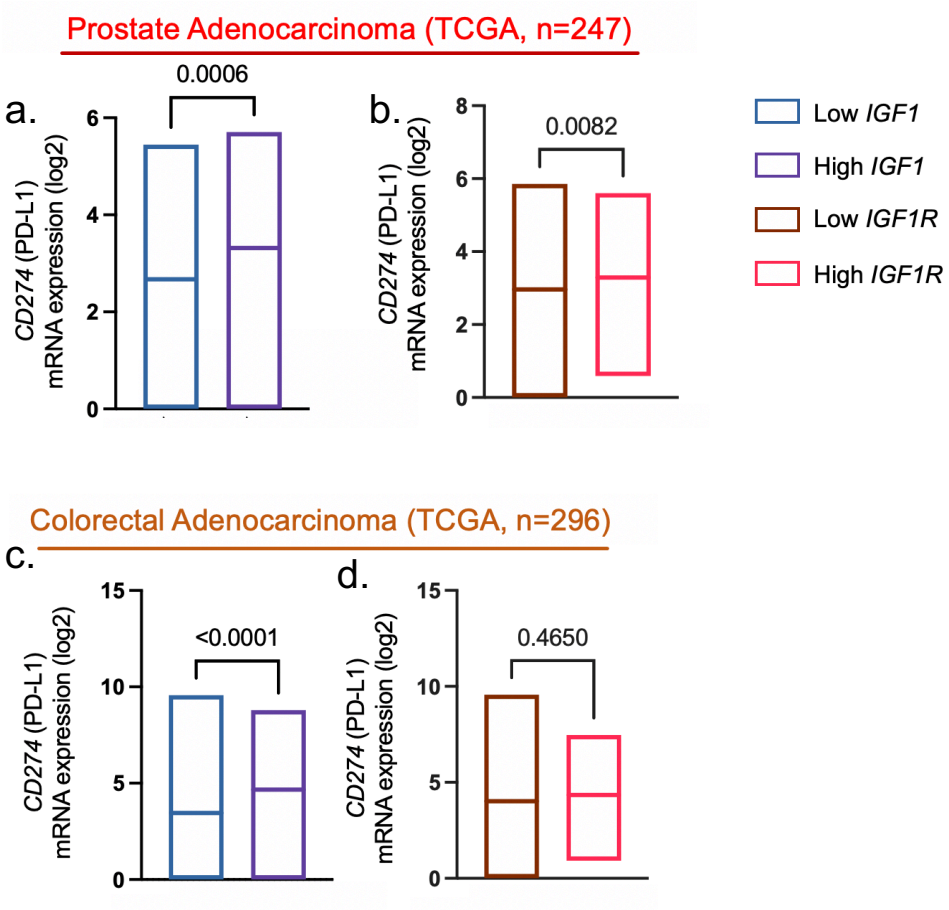


Figure 4-10 *CD274* (PD-L1) expression in prostate and colorectal tumours with high or low *IGF1R* and *IGF1* expression. Tumours from TCGA prostate adenocarcinoma (n=499) were divided based on highest and lowest quartiles of tumour (a) *IGF1* (n= low:124, high=123) and (b) *IGF1R* (n=low:124, high=123) mRNA to test for any association with *CD274* expression. Colorectal adenocarcinomas (TCGA, n=592) were also divided based on their highest and lowest quartiles of (c) *IGF1* (n=low:148, high=148) and (d) *IGF1R* (n=low:148, high=148) levels and *CD274* mRNA expression was analysed between the highest and lowest subgroups. Graphs show mean expression (bar) with distribution represented by SEM (boxes). Statistical significance calculated using an unpaired two-tailed T test.

4.2.4.1 Effects of MYC inhibition and co-treatment with IGF-1 stimulation on PD-L1 surface expression.

PD-L1 surface expression has been reported to be regulated by MYC (Zou et al., 2018; Liang et al., 2020; Casey et al., 2016; Han et al., 2019). In a previous experiment (Figure 4-7e) using MyC-CaP cells established from primary prostate cancer in a MYC-driven transgenic mouse model (Watson et al., 2005b), IGF-1 resulted in only a marginal increase (~21%) in PD-L1 surface levels . To test if MYC had a dominant effect on PD-L1, MyC-CaP cells were treated with 30 nM IGF-1, 8 μM MYCi975, as used in by Casey et al. 2016, or a combination of both for 48 hrs and PD-L1 surface expression was measured using flow cytometry. As seen in Figure 4-7e, IGF-1 resulted in the increase of PD-L1 surface levels (Figure 4-11). MYC inhibition with MYCi975 also upregulated PD-L1 surface expression (Figure 4-11). There were no significant differences in PD-L1 surface expression between IGF-1 stimulation and MYC inhibition single treatments. The combination of IGF-1 stimulation and MYC inhibition resulted in a similar increase in membrane PD-L1 expression, however no additive effect was seen (Figure 4-11).

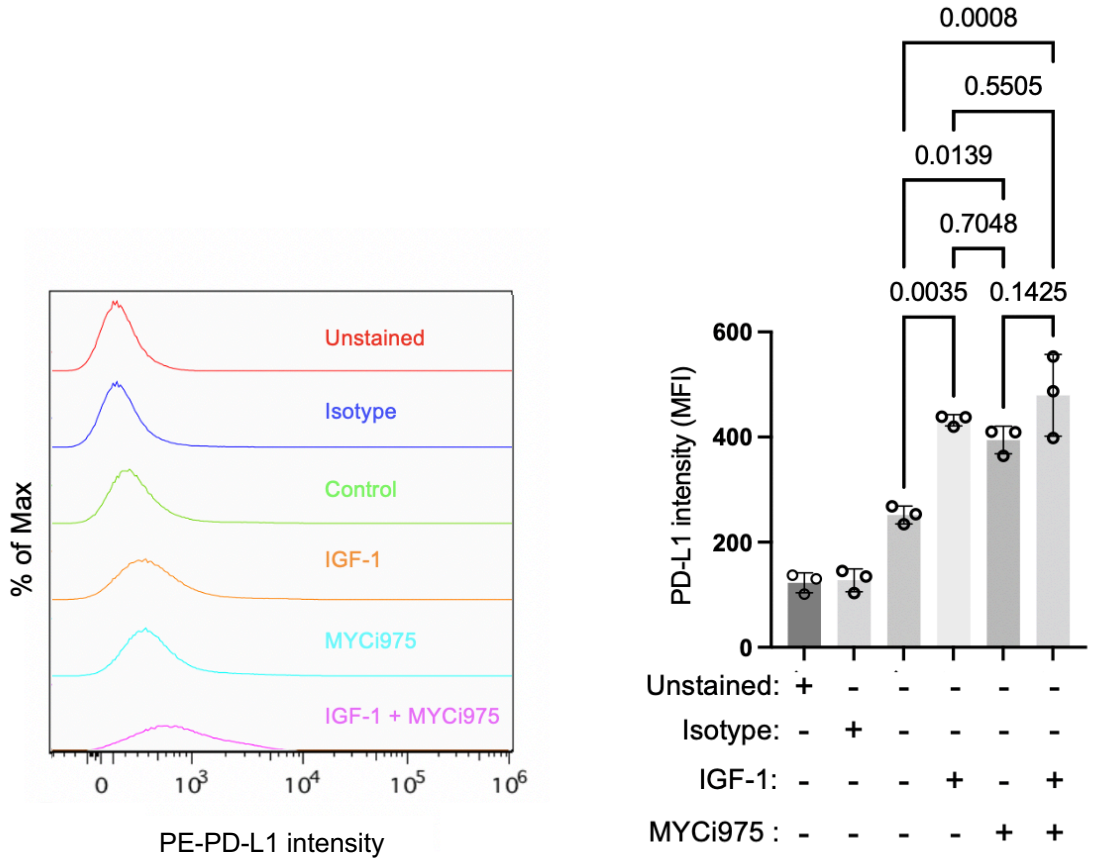


Figure 4-11 Effect of MYC inhibition with IGF-1 stimulation on PD-L1 surface expression. MyC-CaP cells grown in 10% FBS supplemented medium were stimulated with 30 nM IGF-1, 8 µM MYCi975 or a combination of both for 48 hrs and PD-L1 surface expression was measured using flow cytometry. Surface levels represented as MFI (left) and expression of 3 independent repats quantified (right, mean ± SEM). Statistical significance was determined using a one-way ANOVA with multiple testing using Tukey's post hoc test.

4.3 Discussion

The main findings from this chapter suggest that the IGF-1 stimulation can upregulate the expression of immune-modulatory cytokines (Figure 4-1) and immune checkpoint ligand PD-L1 (Figure 4-5). IGF-1 affected expression of genes downstream of both NF-κB (*STAT5A, CCL5*) and cGAS-STING (*IFIT1*, *ARG2*) pathways (Parkes et al., 2017; Reisländer et al., 2019; Pires et al., 2018; Wickremasinghe et al., 2004; Hinz et al., 2002). The expression of *STAT5A, CCL5, IFIT1* and *ARG2* were upregulated after IGF-1 stimulation (Figure 4-1) and these genes were also highly expressed in prostate cancer tumours expressing high *IGF1* compared to low *IGF1* (Figure 4-9). STAT5, encoded by the *STAT5A* gene has confounding roles in cancer and this may be context specific. Phosphorylation of STAT5 associated with decreased E-cadherin levels and was reported to increase prostate cancer metastasis using *in vivo* modes. *STAT5A* is also expressed in 61% of prostate cancer distant metastases (Gu et al., 2010). Furthermore, phosphorylated STAT5 can increase nuclear translocation of AR and has been reported to protect anti-androgen liganded AR from proteasomal degradation (Hoang et al., 2015). Conversely, phosphorylation of STAT5 in CD8 effector cells results in secretion of immune stimulatory IFNγ, important for eliciting an anti-tumour immune response (Verdeil et al., 2019; Lin et al., 2012). Similarly, CCL5 is produced by T cells, fibroblasts and cancer cells in the tumour microenvironment. It has been reported to act as a growth factor promoting cancer proliferation and angiogenesis in a paracrine and autocrine manner (Aldinucci and Colombatti, 2014). CCL5 is also associated with metastasis of breast, melanoma and gastric cancers and acts as a chemoattractant for Tregs and MDSCs into the tumour (Chen et al., 2020; Fu et al., 2021; Ruytinx et al., 2018; Dituri et al., 2011; Kohli et al., 2021; Nagarsheth

et al., 2017). Furthermore, inhibition of PI3K, a pathway downstream of the IGF axis resulted in the downregulation of CCL5 secretion (Meadows et al., 2012). Expression of *IFIT1*, an interferon-stimulated gene promoted metastasis and epithelial-mesenchymal transition of oral squamous cell carcinomas (Pidugu et al., 2019). Arginase 2 encoded by *ARG2* is commonly produced by myeloid cells but has also been reported to be produced by prostate cancer cells after androgen stimulation (Grzywa et al., 2020). Arginase 2 can metabolise L-Arginine which is crucial for T cell metabolism, survival and anti-tumour immunity. Increased expression of Arginase 2 has been reported to inhibit T cell proliferation, resulting an impaired anti-tumour immune response (Geiger et al., 2016; Gannon et al., 2010; Modolell et al., 2009). These results may suggest that IGF-1 induced expression of CCL5 could aid in infiltration of immune suppressive cells and deplete L-Arginine expression by upregulating Arginase 2. This hypothesis could be tested by using a migration assay to test for IGF-1 induced Treg and myeloid cell motility and chemotaxis, and T cell proliferation assays after co-culturing T cells with IGF-1 stimulated cancer cells.

Contrary to its immunosuppressive role, IGF-1 stimulation also upregulated the expression of *IFNB1* (Figure 4-1) and STING protein (Figure 4-2). IFN-β encoded by *IFNB1* has anti-cancer roles by preventing proliferation, inducing apoptosis, promoting autophagy and stimulating cytotoxic immune cell (Borden et al., 2007; Caraglia et al., 2009; Ambjørn et al., 2013). Expression of type 1 interferons is also associated with improved T cell infiltration into the tumour (Corrales et al., 2017). Similarly, STING is important in regulating innate immunity and its activation can induce the expression of IRF3, IFN-β and interferon stimulatory genes that promote anti-cancer immunity (Zhu et al., 2019). Furthermore, STING agonists are currently being tested in numerous clinical trials

(Amouzegar et al., 2021). These results suggest that role of IGFs in inducing anti-cancer immunity could be context specific, depending on the tumour microenvironment. In a T cell inflamed environment, IGFs could upregulate *IFNB1* and STING and promote anti-cancer immunity.

IGF stimulation has previously been reported to activate the NF-κB pathway (Heck et al., 1999; Chetty et al., 2006b). Numerous publications have also implicated pathways downstream of the IGF axis, PI3K-AKT and MAPK/ERK in activating NF-κB signalling (Bai et al., 2009; Hussain et al., 2012; Dan et al., 2008; Ramalingam et al., 2020; Schulze-Osthoff et al., 1997; Saha et al., 2007). AKT signalling can phosphorylate IKK, which then phosphorylates IκBα (Salminen and Kaarniranta, 2010). Phosphorylated IκBα is tagged for ubiquitination and proteasome mediated degradation, resulting in the nuclear translocation and transcriptional activity of NF-κB (Liu et al., 2017b). Similarly, MAPK signalling has also been reported to phosphorylate IKK (Hussain et al., 2012; Ramalingam et al., 2020). MAPK activation cascade also resulted in p38 phosphorylation which was shown to activate the NF-κB pathway (Chen et al., 2016; Norris and Baldwin, 1999). If time had permitted, further research would have been conducted into the localisation of NF-κB to the nucleus to assess activation of the NF-κB pathway after IGF-1 stimulation.

IGF-1 stimulation also resulted in the activation of the cGAS-STING pathway and transcription of downstream genes. This pathway is activated by the presence of cytosolic DNA, commonly seen as a consequence of replication stress (Li and Chen, 2018; Van Vugt and Parkes, 2021). Previous work from the lab has shown that IGF-1 inhibition induces replication stress by downregulating the RRM2 subunit of ribonucleotide reductase,

required for dNTP synthesis, while conversely IGF-1 treatment upregulates RRM2 leading to dNTP pool imbalance (Rieunier et al., 2021). Preliminary data suggest that this imbalance also causes replication stress (Rieunier and Macaulay, unpublished) which has been reported in other models to cause genome instability (Kumar et al., 2011). This could suggest that IGF-1 activates the cGAS-STING pathway partly by contributing to replication stress leading to the release of cytosolic DNA. To assess this, further research needs to be conducted to check whether IGF-1 induces replication stress in prostate cancer models and causes subsequent release of cytosolic DNA and presence of micronuclei. This could be tested by staining IGF-1 stimulated prostate cancer cell lines with Picogreen, which detects double stranded DNA (Ho et al., 2016a). The possible long-term consequences of replication stress could be tested using *in vitro* mutagenesis assays such as the classical hypoxanthine-guanine phosphoribosyltransferase (*HPRT*) gene mutation test (Johnson, 2012), or a more recently-described rapid assay based on a mutation biosensor ('CherryOFF'), where red fluorescence is activated by a specific A/T-G/C nucleotide transition (Birnbaum et al., 2018)

Apart from activation via cytosolic DNA, the cGAS-STING pathway has also been reported to be activated by PI3K-AKT and MAPK/ERK (Joung et al., 2011; Moore and Petro, 2013; Zhang et al., 2009). AKT has been shown to be downstream of TBK1 activation, which lead to the phosphorylation of IRF3 (Joung et al., 2011). Similarly, ERK has been reported to directly phosphorylate IRF3 and indirectly phosphorylate IRF3 via its effects on p38 MAPK and JNK (Moore and Petro, 2013; Zhang et al., 2009). This could also prove to be a mechanism by which IGF-1 stimulation could lead to the activation of the cGAS-STING pathway. To test whether PI3K-AKT and MAPK/ERK contribute to IGF-1 effects on the cGAS-STING pathway, prostate cancer cells could be stimulated with IGF-1 with inhibition

of downstream AKT and MAPK pathways. Effects on phosphorylation on TBK1 and IRF3 could be measured using western blots to investigate cGAS-STING pathway activation. Furthermore, through NF-κB and cGAS-STING pathways, IGFs could also cause secretion of cytokines responsible for the recruitment of immunosuppressive cells such as Tregs, M2 Macrophages and MDSCs, which commonly infiltrate 'immune cold' prostate cancer. (Erlandsson et al., 2019; Calcinotto et al., 2018; Vitkin et al., 2019; Zhou et al., 2020; Lin et al., 2019; Argyle and Kitamura, 2018; Ruytinx et al., 2018; Fleming et al., 2018). As mentioned previously, this hypothesis can be tested by using migration and chemotaxis assays.

IGF-1 induced the upregulation of PD-L1 in prostate cancer cells, with data shown in Figure 4-8 to support involvement of both the PI3K-AKT and MAPK/ERK pathways in this effect. This is consistent with reports which indicate that activation of PI3K-AKT and MAPK/ERK can lead to PD-L1 upregulation (Coelho et al., 2017; Lastwika et al., 2016; Stutvoet et al., 2019; Mittendorf et al., 2014; Chen et al., 2015). Though prostate cancer has been classified to display lower PD-L1 levels compared to other cancers, patients whose tumours have high IGF axis activation could exhibit increased PD-L1 expression, known to assist in tumour immune evasion (Haffner et al., 2018). Effects of circulating IGF-1 and tumour endogenous *IGF1* on PD-L1 expression will be assessed in Chapter 5.

Having investigated the effects of IGF-1 on the tumour epithelial compartment, the next aim was to investigate the effects and associations of IGF axis activity on the immune compartment in prostate cancer tissues.

5 Chapter V: Investigating the association of IGF axis components with prostate cancer immune infiltration.

Results from the previous chapter highlighted potentially immunosuppressive effects of IGF-1 on the prostate tumour epithelium via upregulating cytokines and PD-L1. The IGF axis has also been reported to dampen the anti-tumour immune response by acting on cells within the tumour microenvironment. Inhibiting IGF axis activity resulted in tumour infiltration of CD8+ cytotoxic T cells in murine models of rat glioblastoma and mouse breast cancer and neuroblastoma cells (Trojan et al., 1993; Resnicoff et al., 1994; Liu et al., 1998; Schillaci et al., 2006). IGFs can induce the polarisation of M2 macrophages and proliferation and cell stability of FOXP3+ Tregs, which commonly infiltrate prostate cancer (Bilbao et al., 2014b; DiToro et al., 2020; Erlandsson et al., 2019). Therefore, it is possible that high IGF-1 may promote the immune-cold tumour microenvironment in prostate cancer populated by Tregs, M2 macrophages and MDSCs (Erlandsson et al., 2019; Vitkin et al., 2019; Lu et al., 2017; Calcinotto et al., 2018). The aim of this chapter was to investigate the association of IGF-1 and IGF-1R with immune cells in the prostate cancer tumour microenvironment.

To study the association of circulating IGF-1 on the immune compartment in prostate cancer, I used M-IF imaging to identify tumour infiltrating lymphocytes in FFPE sections of radical prostatectomies. In parallel, RNA was also extracted and sequenced from the cancer regions of FFPE sections from the same prostatectomies to test for transcriptomic changes in patients with high vs low circulating IGF-1. This also enabled me to test for cancer endogenous expression of *IGF1* mRNA and any associations with immune

infiltration. Finally, in a separate series of fresh frozen prostate tissues, single-cell sequencing was used to characterise the prostate cancer microenvironment and test for the expression of IGF axis components in the immune infiltrating cells.

5.1 Characterising the T lymphocyte population in primary prostate cancer

Of the 139 radical prostatectomies from ProMPT cases previously used to investigate possible association between serum IGF-1 and tissue IGF-1R (Figure 1.2) I was able to access additional sections from 126 cases. After ranking by serum IGF-1, I selected the 16 cases with the highest IGF-1 and 16 with the lowest IGF-1. Selection of tissue markers was made in discussion with Professor Clare Verrill. She advised use of epithelial markers Pan-cytokeratin (PCK, luminal cell marker, positive in all glands) and Cytokeratin 5 (CK5, basal cell marker, positive only in benign glands). Benign areas contain intact basal cells, CK5 and luminal marker, PCK, whereas malignant cells lack basal cells, are usually more compact and only stain for PCK (Rao et al., 2019). I selected immune markers, CD4, CD8, FOXP3 and PD-L1. Optimisation of antibodies to these markers together with DAPI to mark nuclei was conducted on tonsil tissues by Leticia Campo (Figure ***5-1***), with supervision of Dr Alistair Easton in the Translational Histopathology Laboratory, University of Oxford.

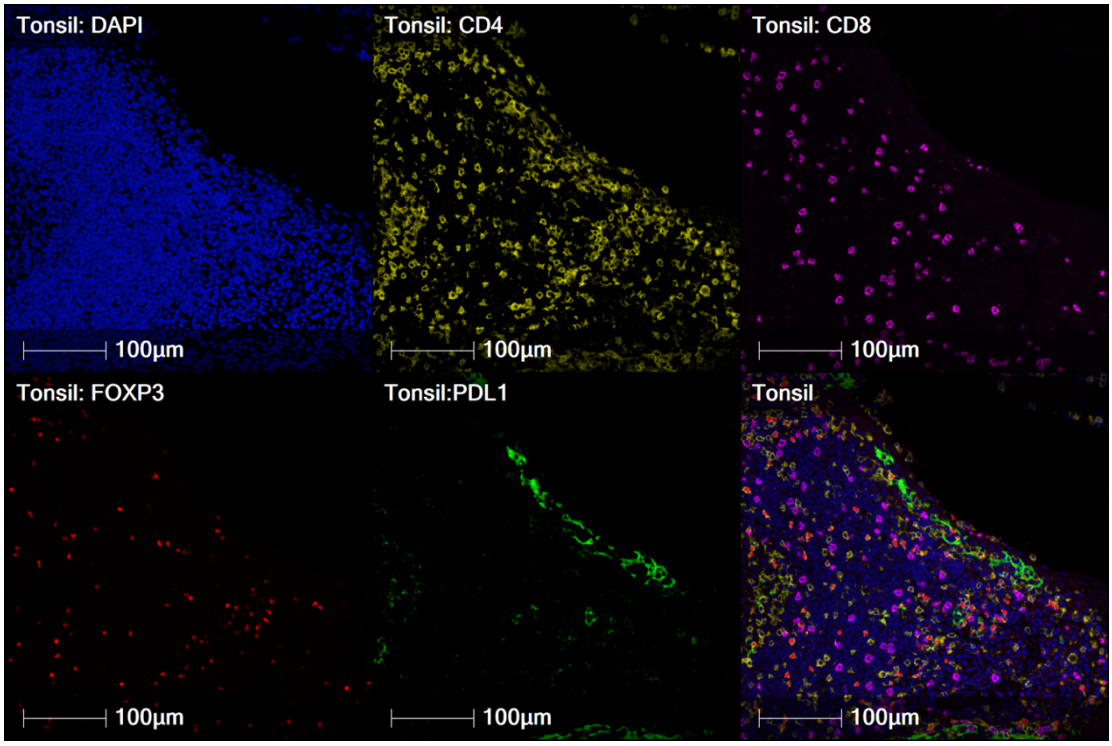


Figure 5-1 Initial optimisation of multiplex immunofluorescence for immune markers. Image of Tonsil tissue stained by Leticia Campo for DAPI and to optimise antibodies to CD4, CD8, FOXP3 and PD-L1.

M-IF staining and scanning of FFPE sections was performed by Leticia Campo. Once images were scanned, I then conducted the imaging analysis on the HALO platform using the pipeline illustrated (Figure 5-2). First, parallel H&E sections of the multiplexed images were marked for areas of cancer and percentage cancer content by Uro-Pathologist Professor Clare Verrill (Figure 5-2a). Marked cancer areas were then annotated onto the multiplexed images and the remaining areas were labelled benign. I then trained the HALO software to differentiate between areas of epithelium, stroma and artifact using the MiniNet AI classifier (Figure 5-2b). This differentiation allowed me to quantify the localisation of the immune

cells in the epithelial vs stromal compartment. Finally, classification of the tumour was also performed at a single-gland level using PCK and CK5 (Figure 5-2c).

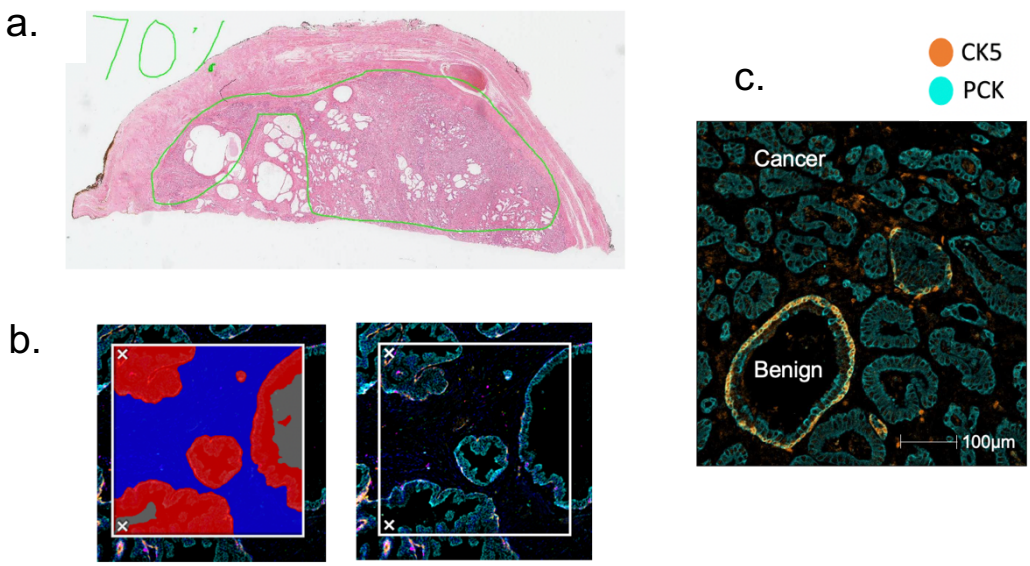
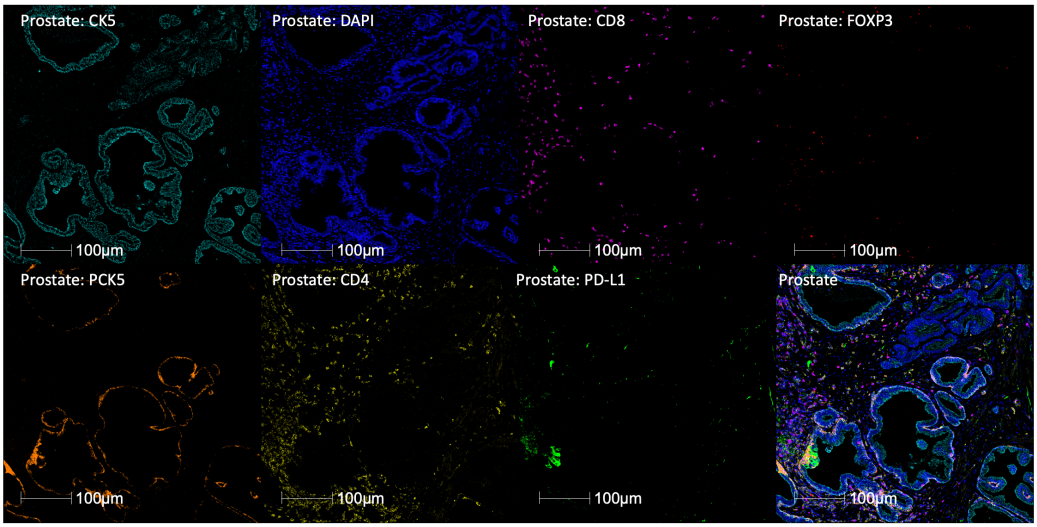


Figure 5-2 Multiplex immunofluorescence workflow on HALO (a) H&E-stained radical prostatectomy of the parallel slide in which M-IF was performed marked by Prof Verrill for tumour area and % tumour within marked area. (b) HALO MiniNet AI classifier detecting epithelial areas (red), stromal areas (blue) and glass (grey). (c) Benign and cancer glands were detected using CK5+ positive basal cells (benign epithelium) and PCK+, CK5- staining (malignant epithelium).

Once the antibodies were optimised and I had developed the analysis pipeline on the HALO software, M-IF was performed by Leticia Campo on FFPE sections of 32 radical prostatectomy samples of patients recruited to the ProMPT study in whom circulating IGF-1 levels had been assayed as stated previously (Figure 1.2). Deconvoluted images are presented in Figure 5-3a showing lymphocyte markers: CD8, FOXP3 (Tregs), CD4, prostate epithelial markers: CK5, PCK, and immune marker: PD-L1. A representative high power

merged image with all the above markers highlighting a junction between benign and cancer gland is displayed on Figure 5-3b.

a.



b.

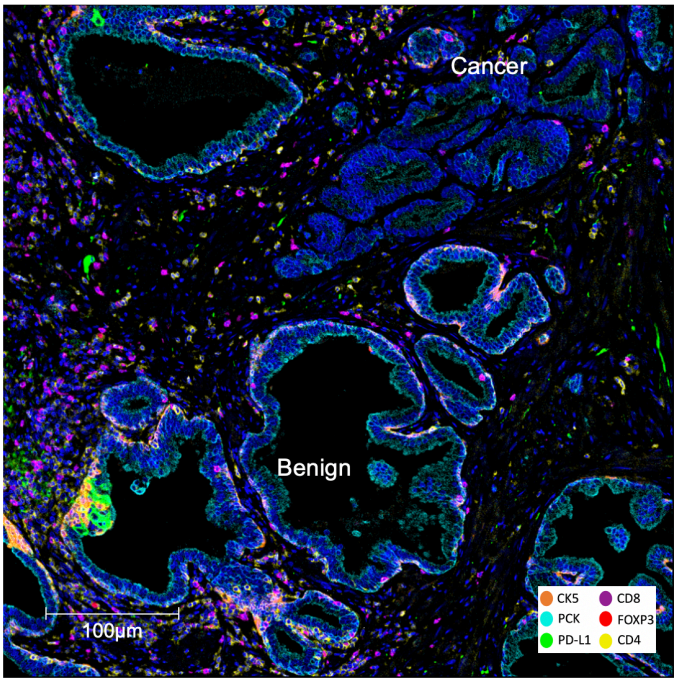


Figure 5-3 Multiplex imaging of radical prostatectomy. (a) Deconvoluted M-IF image visualised using the HALO platform showing T cell markers: CD8, FOXP3, CD4 and epithelial markers: CK5, PCK and immune marker: PD-L1. (b) Higher-power view of merged M-IF image showing the junction between the benign (PCK+, CK5+) and malignant (PCK+, CK5-) glands.

Once the M-IF methods were optimised and the slides stained and scanned, I then performed all the subsequent analysis on the HALO platform. Expression of CD4+, CD8+ and FOXP3+ T cells are represented as the total number of cells positive for the marker per mm^2 to normalise for the size of the specimen. Cells expressing any amounts of PD-L1 were marked as PD-L1 positive and expression levels are represented as total number of PD-L1 positive cells per mm^2. Immune infiltration and PD-L1 expression were analysed on the benign and malignant compartments of prostate cancer using the areas annotated by Professor Verrill (Figure 5-2a). In the 32 samples, three samples did not contain paired benign/cancer areas and hence were excluded from subsequent analysis. Analysis of the remaining 29 showed relatively low numbers of infiltrating immune cells, and displayed no significant differences between CD4, CD8, FOXP3+ Tregs and PD-L1 expression when comparing the benign and cancer compartments in prostate cancer (Figure 5-4a-d). Expression of these markers was also tested with respect to their localisation in the epithelial and stromal areas. Analysis indicated no differences in immune infiltration and PD-L1 expression in the benign vs malignant areas in both the stromal and epithelial compartments (Table 5-1). Since no significant differences were seen between the benign vs cancer compartments, all following analyses were performed only on the malignant areas compartment of the FFPE sections.

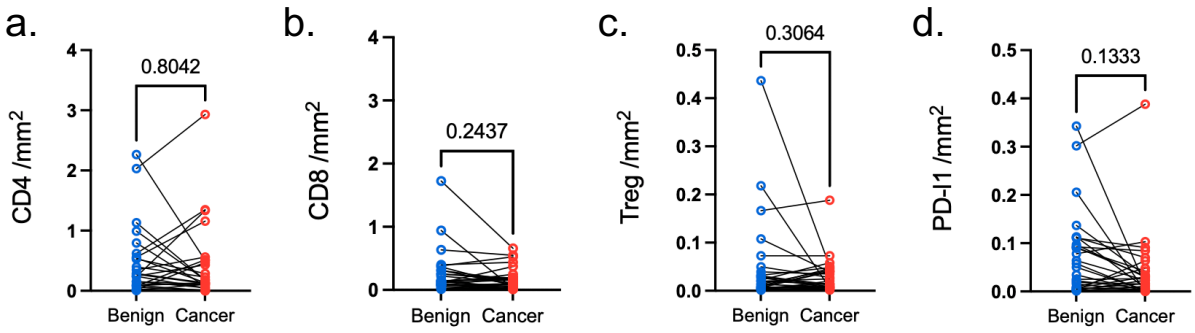


Figure 5-4 T cell infiltration and PD-L1 expression in benign and malignant compartments of prostate cancer. Infiltration of (a) CD4, (b) CD8, (c) FOXP3+ Tregs and (d) PD-L1 were measured as positive cells per mm^2 in benign and malignant areas of radical prostatectomies using HALO analysis of M-IF images. Samples (n=29) were analysed using two-tailed paired T tests and sample distribution represented using standard error of mean (SEM).

Benign vs Cancer			
Location	Marker	Benign vs Cancer Mean ± SEM positive cells/mm^2	P value
Epithelium	CD4	0.47 ± 0.13 vs 0.48 ± 0.16	0.9672
	CD8	0.28 ± 0.08 vs 0.18 ± 0.04	0.2254
	Treg	0.05 ± 0.02 vs 0.02 ± 0.01	0.2928
	PD-L1	0.04 ± 0.02 vs 0.02 ± 0.01	0.3676
Stroma	CD4	0.38 ± 0.09 vs 0.29 ± 0.07	0.4585
	CD8	0.22 ± 0.04 vs 0.18 ± 0.03	0.5007
	Treg	0.04 ± 0.01 vs 0.04 ± 0.01	0.5264
	PD-L1	0.11 ± 0.02 vs 0.06 ± 0.02	0.1390

Table 5-1 T cell and PD-L1 expression in benign and malignant compartments of prostate cancer stroma and epithelium. Table showing the number T cells and PD-L1-positive cells per mm^2 in the epithelium and stromal compartments of prostate cancer. Graphs of the tabulated results are displayed in Appendix 7.1. As before, samples (n=29) were analysed using two-tailed paired T tests and sample distribution represented using SEM.

Association of circulating IGF-1 on immune infiltration and PD-L1 expression were also tested in these 29 samples. All serum IGF-1 values were within the normal range (Bidlingmaier et al., 2014). Out of the 29 samples, 14 patients had relatively low circulating IGF-1 (7.2-12.0 nmol/l) and 15 patients had circulating IGF-1 (21.7-31.5 nmol/l) at the upper end of the normal range. Analysis suggested that patients with high circulating IGF-1 had increased CD4 infiltration in their tumours (Figure 5-5a). There were no significant differences between CD8 and Treg infiltration in the tumours in high vs low IGF-1 patients (Figure 5-5b-c). Results also suggested a non-significant trend to increased PD-L1 expression in high IGF-1 patients (Figure 5-5d).

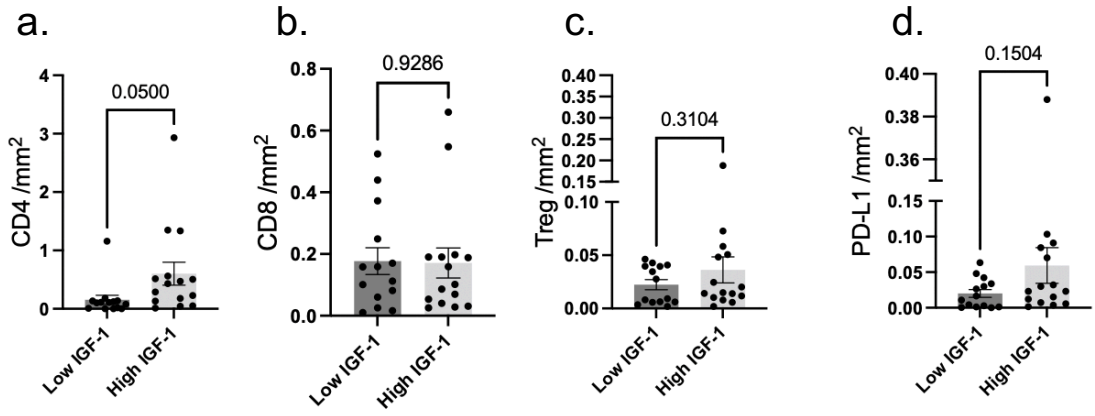


Figure 5-5 Testing associations of circulating IGF-1 with T cells and PD-L1 positivity in prostate cancer. (a) – (d) Patients were divided on their median circulating IGF-1 levels and M-IF imaging using the HALO platform was used to measure the number of cells positive for (a) CD4 (b) CD8 (c) FOXP3+ Tregs and (d) PD-L1 per mm^2. Statistical significance was determined using a two-tailed T test.

Association of immune infiltration and PD-L1 expression was also tested with respect to median IGF-1R expression in the cancer, assayed previously using IHC by Dr Tamara Aleksic and Professor Clare Verrill. As stated previously, no difference was observed between the epithelial and stromal compartments in the analysis of T cells and PD-L1 positive cells per mm^2 and all further analysis were performed on the total areas (epithelium + stroma) (Table 5-1). Results indicated a trend to association between increased Tregs in low IGF-1R patients and no differences between any other markers (Table 5-1a). There was also no statistical difference in association of Gleason score and PSA levels with immune infiltration or PD-L1 expression (Table 5-1b,c).

Low vs High IGF-1R protein expression			
Location	Marker	Low vs High IGF-1R Mean ± SEM positive cells/mm^2	P value
Total: Epithelium + Stroma	CD4	0.47 ± 0.19 vs 0.3 ± 0.12	0.4761
	CD8	0.16 ± 0.04 vs 0.19 ± 0.05	0.6085
	Treg	0.04 ± 0.01 vs 0.02 ± 003	0.0670
	PD-L1	0.06 ± 0.02 vs 0.02 ± 0.01	0.1367
Gleason Score: ≤3+4 vs ≥ 4+3			
Location	Cell type	≤3+4 vs ≥ 4+3 Mean ± SEM	P value
Total: Epithelium + Stroma	CD4	0.38 ± 0.14 vs 0.41 ± 0.19	0.8934
	CD8	0.17 ± 0.04 vs 0.18 ± 0.06	0.9038
	Treg	0.03 ± 0.01 vs 0.03 ± 0.01	0.7667
	PD-L1	0.05 ± 0.02 vs 0.02 ± 0.004	0.3177
PSA: 1 to 6 vs 6 to 20			
Location	Cell type	1-6 vs 6-20 Mean ± SEM	P value
Total: Epithelium + Stroma	CD4	0.4 ± 0.24 vs 0.39 ± 0.12	0.9439
	CD8	0.19 ± 0.06 vs 0.16 ± 0.04	0.7281
	Treg	0.03 ± 0.01 vs 0.03 ± 0.01	0.7825
	PD-L1	0.03 ± 0.01 vs 0.05 ± 0.02	0.4460

Table 5-2 Testing associations between tumour IGF-1R, Gleason score and PSA vs T cell and PD-L1 positivity in prostate cancer. Patients were divided on median tumour endogenous (a) IGF-1R, (b) Gleason score and (c) PSA levels to assess CD4, CD8, Treg and PD-L1 positive cells per mm^2. Graphs for the tabulated results are displayed in Appendix 7.2-7.3. Statistical significance was determined using a two-tailed T test.

5.2 Analysing the transcriptomic profile of tumours from patients with high vs low circulating IGF-1.

RNA sequencing was performed on the parallel FFPE sections from the 32 tumours in which M-IF was conducted. Briefly, RNA was extracted from the tumour annotated areas of the FFPE sections (Figure 5-2a) and sequenced at the Wellcome Centre for Human Genetics, University of Oxford (Figure 5-2a). Extraction of RNA from FFPE samples resulted in

samples with varying quality indicated by RNA Integrity Number (RIN) between 1.2 and 8.3, with average RIN of 2.85. RIN is a 1-10 standardised scale indicating the quality of RNA and a lower value signifies degraded RNA (Schroeder et al., 2006). Extraction of RNA from FFPE has been reported to produce highly fragmented and degraded RNA. Furthermore, multiple reports have stated that the integrity of the RNA generated from FFPE tissues decreases with increasing storage time of the paraffin blocks (Pennock et al., 2019; Mathieson and Thomas, 2020; Groelz et al., 2018; Zhao et al., 2019; Von Ahlfen et al., 2007). FFPE samples obtained from this experiment were collected between 2011-2015, which may have contributed to the reduced RNA integrity. To accommodate for the lower RIN values in the samples, ribodepletion library preparation method was used for RNA sequencing rather than 3'RNA sequencing as originally planned.

I was trained to analyse the RNA sequencing data by Dr Avigail Taylor, bioinformatician in the Macaulay group. Sequencing reads were quality checked, trimmed for adapter sequences and aligned to the human genome as mentioned in Chapter 2. Samples which produced library sizes lower than 10,000,000 reads were removed from the downstream analysis (Figure 5-8a). This resulted in 21 samples, of which 9 belonged to patients with high circulating IGF-1 and 11 to patients with low circulating IGF-1. Pre-processing of the FFPE RNA sequencing revealed a high proportion of genes (>20000) with no reads assigned to them in any of the 21 samples (Figure 5-8b). The increased zero counts may arise from high fragmentation of the FFPE RNA, resulting in RNA probes unable to bind to the target region of the transcript (Mathieson and Thomas, 2020). After discussion with Dr Avigail Taylor, I made the assumption that genes with zero read-counts across the majority of samples were

likely to yield unreliable expression levels, and therefore filtered out any genes with zero read-counts in > 11 samples.

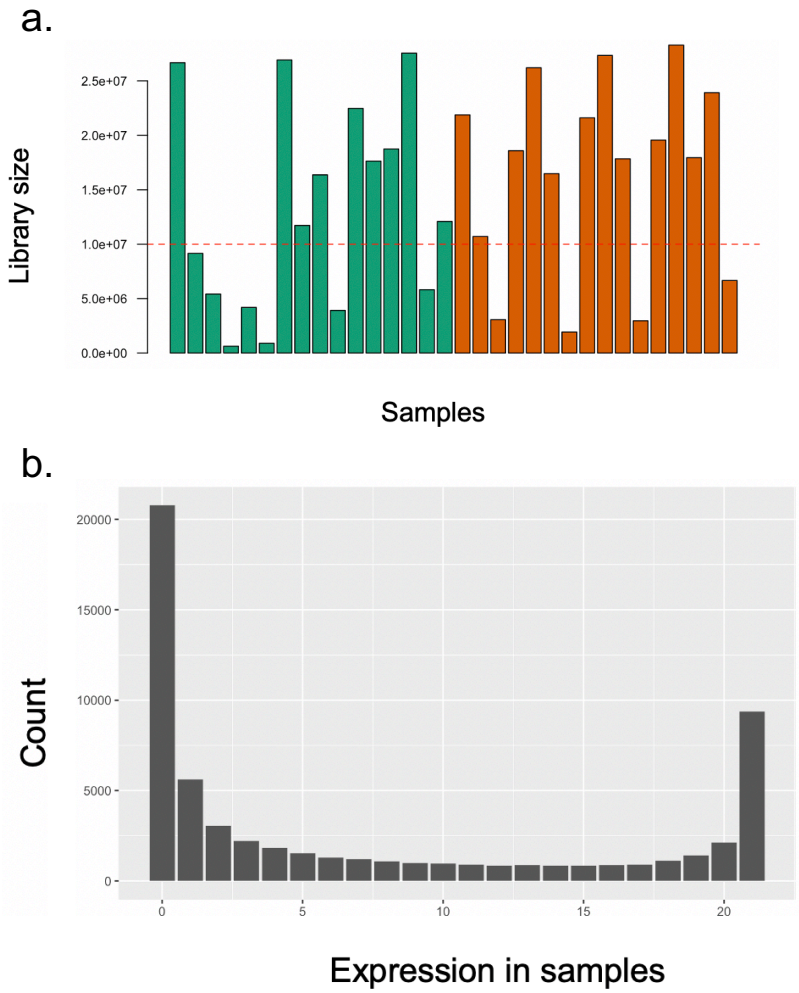


Figure 5-6 FFPE RNA Sequencing filtering threshold. (a) Library size generated from RNA sequencing of 32 FFPE radical prostatectomy sections, showing threshold (red dashed line) used to exclude samples with library size below 10,000,000 reads. (b) Distribution of number of samples per gene recording any expression of that gene, i.e., having read-count > 0; note that a gene can be expressed in a maximum of 21 samples, corresponding to the filtered 21 FFPE samples with library size greater than 10,000,000.

The DESEQ2 pipeline (as described in Chapter 2) was used to identify differentially expressed genes (DEGs). Analysis was performed to identify DEGs in tumours of patients with high vs low circulating IGF-1 levels, but no significantly differentially expressed genes were identified. This may be attributed to the poor quality of the FFPE RNA samples or may be a reflection of the true underlying biology.

Apart from systemic production in the liver, IGF-1 can also be produced by macrophages and fibroblasts within the tumour microenvironment and has been reported to induce resistance to chemotherapy (Ireland et al., 2016; Quail et al., 2016). High tumour endogenous *IGF1* was also reported to associate with reduced overall survival in a TCGA bladder cancer cohort (Chen et al., 2020). Therefore, differential expression analysis was performed comparing tumours with high vs low endogenous *IGF1* mRNA based on median *IGF1* normalised gene expression (read count 3806, Figure 5-7). Gene normalised counts were obtained using DESEQ2's default normalisation pipeline. Principal component analysis (PCA) was used to visualise the high dimensional data, where samples with similar transcriptomic profiles clustered together. PCA analysis of the 21 samples showed minimal separation between high vs low *IGF1* tumours (Figure 5-8a). Normalised gene expression across samples was also visualised using a heatmap, hierarchically clustered by sample (X-axis) and by gene (Y-axis) (Figure 5-8b). The heatmap illustrated the separation between the two different groups, although one low *IGF1* tumour clustered with the high *IGF1* group. Using the DESEQ2 pipeline, differential expression analysis produced 220 upregulated and 126 downregulated genes. Genes which passed the threshold of $P<0.05$ after multiple correction using the Benjamini-Hochberg method were classified as differentially expressed. Top 10 upregulated and downregulated genes are displayed in Table 5-3 and the

full list in Appendix Table 7.1,2. A volcano plot was used to display genes of interested related to the IGF axis and prostate cancer (Figure 5-8c). Analysis confirmed upregulation of *IGF1*, which is expected as I had divided the samples based on median normalised *IGF1* levels. Other upregulated genes of interest included IGF pathway related genes *IGFBP5*, *FOXO1*, *BCL2, ZEB1* (Zinc finger E-box-binding homeobox 1), immune chemokine *CXCL12* (C-X-C Motif Chemokine Ligand 12), prostate cancer associated genes *WFDC1* (WAP Four-Disulfide Core Domain 1), *FGFR2* (Fibroblast growth factor receptor 2) and *EZH1* (Enhancer Of Zeste 1 Polycomb Repressive Complex 2 Subunit). Differentially downregulated genes included *TAP1* (Transporter associated with antigen processing 1), which is crucial for peptide transport and MHC Class 1 presentation by cancer cells, transcription factor *SOX4* (SRY-Box Transcription Factor 4) and regulator of NF-κB, *TRAF4* (TNF receptor-associated factor 4).

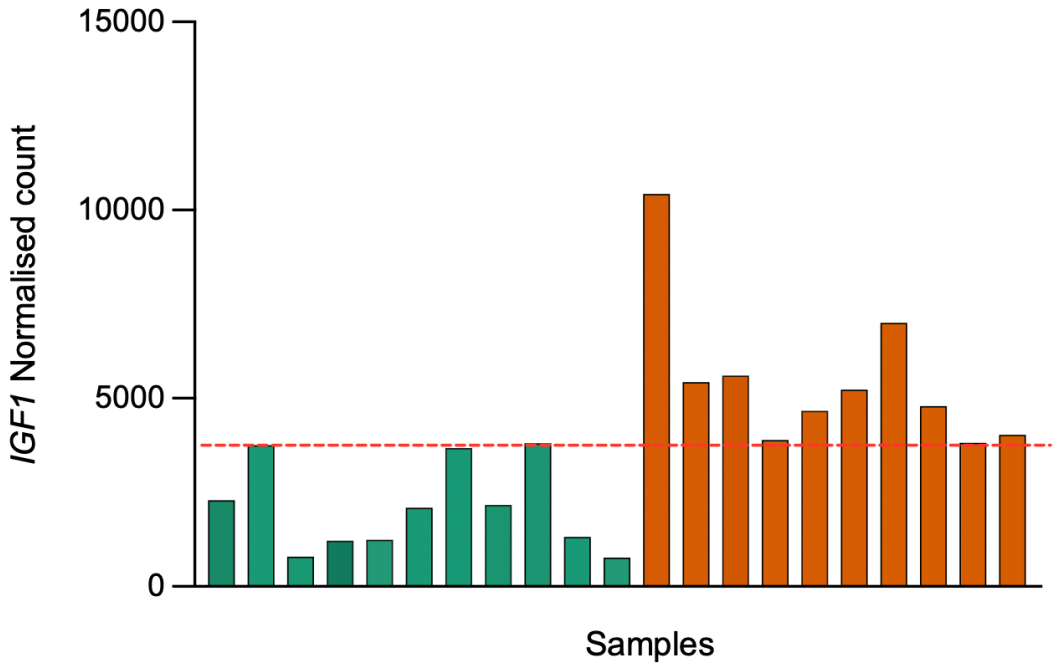


Figure 5-7 *IGF1* normalised count obtained from RNA sequencing analysis. Bar chart representing the *IGF1* normalised count obtained from the DESEQ2 pipeline. Samples were divided using their median IGF1 counts (3806, red line) into low *IGF1* (green, n=11) and high *IGF1* (orange, n=10) tumours.

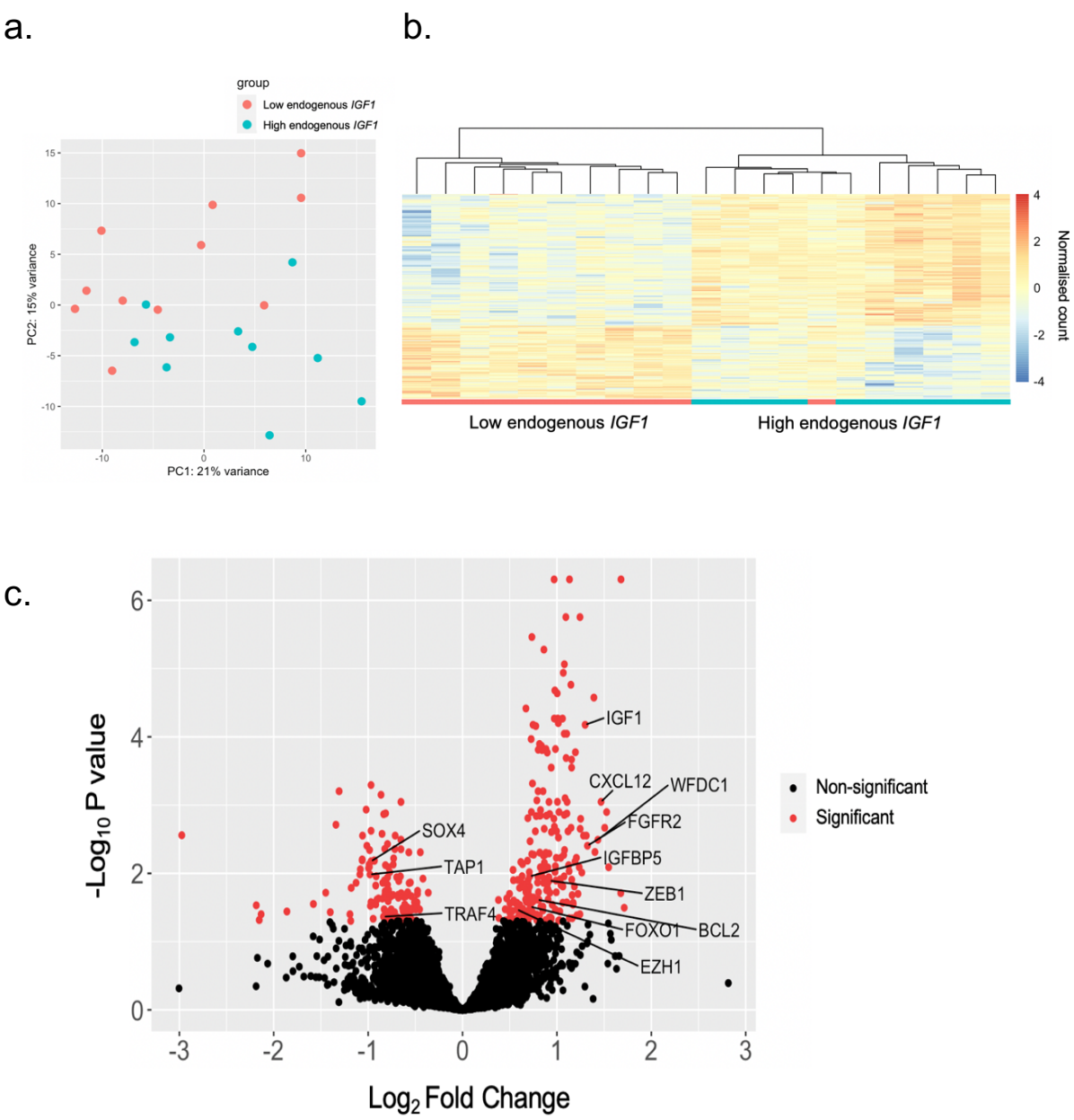


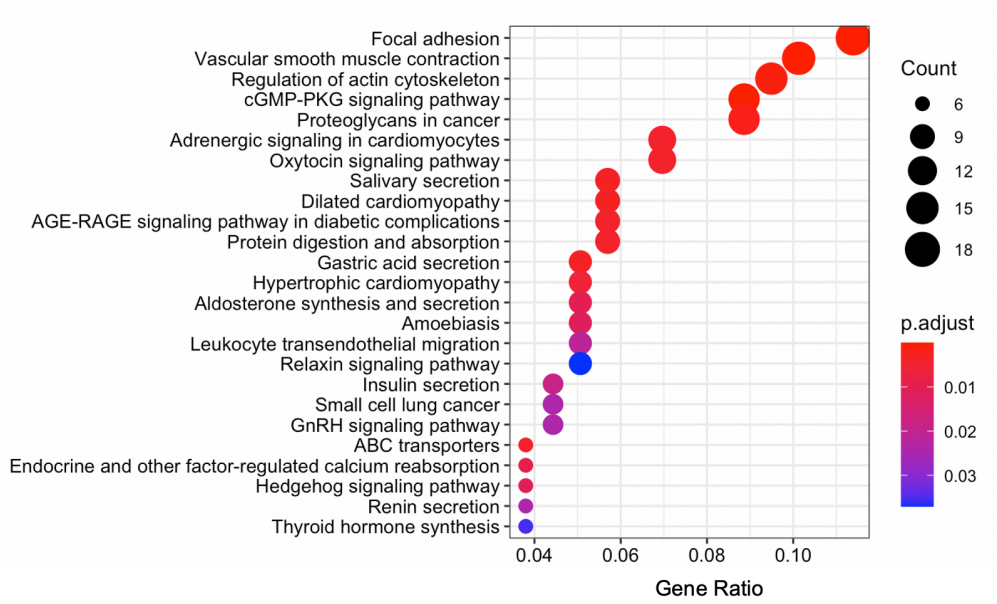
Figure 5-8 RNA Sequencing analysis of prostate cancers with high vs low endogenous *IGF1* mRNA. (a) PCA plot visualising the clustering of tumours with low (red) vs high (blue) tumour endogenous *IGF1*. (b) Normalised gene expression heatmap displaying the transcriptomic clusters in high vs low IGF1 tumours using the Pheatmap package on R studio. (c) Volcano plot displaying the differentially expressed genes (red) with P adjusted value <0.05 (-Log10 P adjusted value >1.3).

Upregulated	Log_2 Foldchange	Adjusted P value	Downregulated	Log_2 Foldchange	Adjusted P value
HLF	1.71284153	0.03191786	*GRAMD4*	-2.9748382	0.00276303
HSPB6	1.67846641	4.94E-07	*ACSM1*	-2.1856995	0.02937761
LSM11	1.67596214	0.01947629	*HK2*	-2.1539357	0.04828428
STOX2	1.54760674	0.00812757	*F5*	-2.1340245	0.03974116
EYA1	1.52617917	0.00126306	*ASRGL1*	-1.8610156	0.036173
TMEM47	1.50610695	0.0021494	*SIPA1L2*	-1.5804815	0.02810647
CXCL12	1.46694272	0.00089657	*AEN*	-1.4496337	0.01918223
WFDC1	1.43362178	0.00321785	*ABCG1*	-1.4015968	0.03705799
GSTM2	1.4025491	0.00487168	*PRSS8*	-1.3417415	0.00193892
CHRDL1	1.39133262	2.66E-05	*MAP2K3*	-1.3078195	0.00062629

Table 5-3 Top 10 differentially expressed genes in high IGF-1 tumours. Top 10 upregulated and downregulated genes in high IGF1 tumours, identified as those with an adjusted P value < 0.05 using Benjamini-Hochberg multiple correction method.

Over-Representation Analysis (ORA) was performed with Kyoto Encyclopedia of Genes and Genomes (KEGG) pathways using the DEGs obtained from DESEQ2 pipeline to identify deregulated pathways and molecular interactions. ORA analysis produced multiple functional pathways of which the pathways of interest included the focal adhesion, regulation of actin cytoskeleton, proteoglycans in cancer, leukocyte transendothelial migration, insulin secretion and hedgehog signalling (Figure 5-9a). Looking at pathways of interest previously stated, it can be seen that overlapping sets of DEGs contribute to the observed over-representation of regulation of actin cytoskeleton pathway with leukocyte transendothelial migration and focal adhesion (Figure 5-9b). However, there were also other pathways with greater DEG-set overlaps, as seen by the thickness of the edges connecting them.

a.



b.

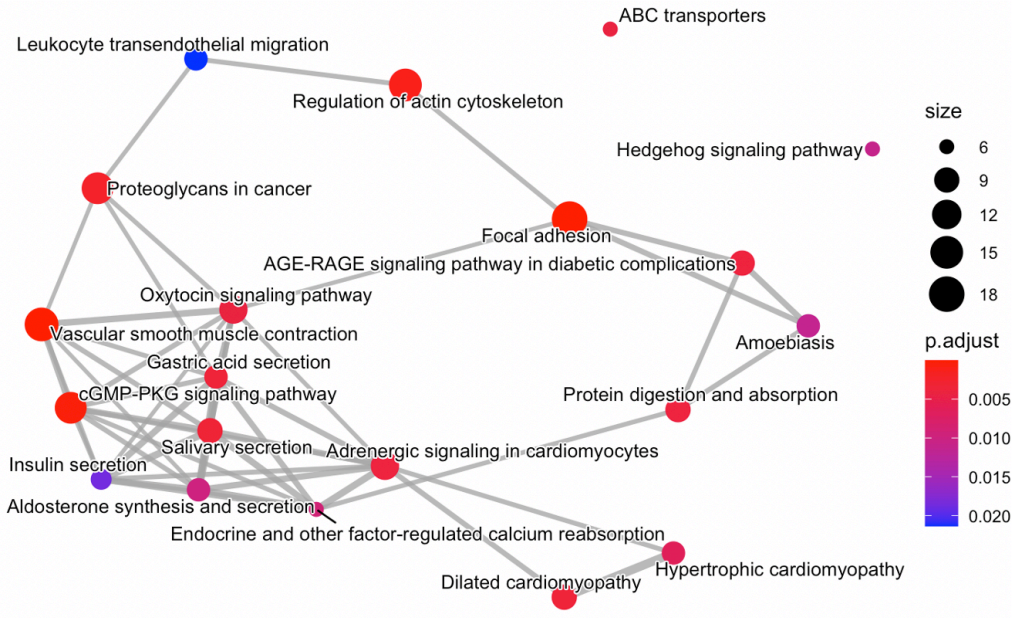


Figure 5-9 Over Representation Analysis using KEGG pathways. Pathway analysis was performed using the differentially expressed genes generated from comparing patients with high vs low *IGF1* levels. (a) List shows the top 25 KEGG pathways generated from DEGs. X axis indicates the ratio between genes overlapping a specific pathway to the total number of genes in the pathway. (b) Interactions between the listed KEGG pathways. Size of cluster represents the number of genes within it. P adjusted value generated using Benjamini-Hochberg test for multiple correction.

Similarly, functional enrichment analysis of the DEGs was also conducted using the WikiPathways and Biocarta webtools. WikiPathways analysis indicated enrichment of focal adhesion and Hedgehog signalling. It also displayed enrichment of signalling via VEGF-A and its receptor VEGFR-2 and, macrophage associated IL-18 pathway (Figure 5-10a). Notable pathways found to be deregulated using Biocarta included chemokine and macrophage associated CCR5 pathway, cancer associated PYK2 and Agrin pathways (Figure 5-10b). Finally, a Gene set enrichment analysis (GSEA) of KEGG pathways amongst the DEGs was conducted. Compared to ORA, GSEA does not use a cut-off value to define differentially expressed genes (Subramanian et al., 2005). Using this method, genes were ordered on their differential expression comparing high *IGF1* to low *IGF1*. This is followed by GSEA “walking down the list" increasing a running -sum statistic if a gene belongs to the pathway or decreasing if it does not. Enrichment score is then calculated as the maximum deviation from zero measured during the “walk down”. A higher enrichment score is represented if there is an overrepresentation of genes associated with the pathway of interest at the top of the gene list. Statistical significance of the enrichment score is calculated using a permutation test and false positives are controlled by adjusting for multiple hypothesis testing with FDR q value < 0.25. Notable significantly pathways produced from GSEA include focal adhesion, pathways in cancer and hedgehog signalling (Figure 5-10c-e).

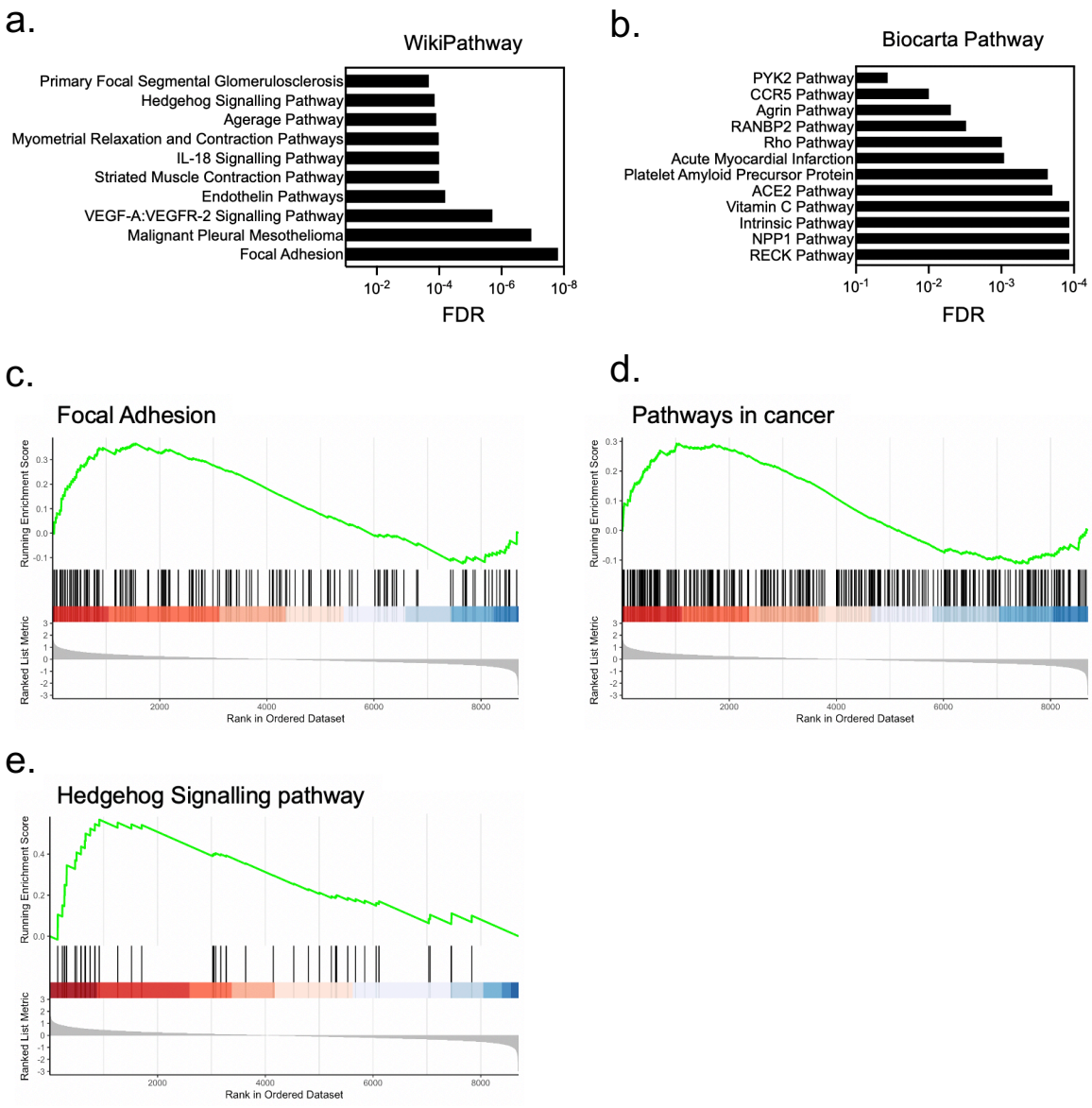


Figure 5-10 Functional enrichment analyses of genes deregulated in high *IGF1* mRNA tumours using Biocarta and Wikipathway functional enrichment analyses and GSEA with the KEGG database. Functional pathways enriched amongst the DEGs were identified using the (a) WikiPathway and (b) Biocarta online tools. The False discovery rate (FDR) was controlled at q-values < 0.05 using the Benjamini-Hochberg method for multiple correction. GSEA using the KEGG database was performed using on the DEGs and enrichment of (c) focal adhesion, (d) pathways in cancer and (e) hedgehog signalling pathway are displayed. The X-axis/ "rank in ordered dataset" denotes the rank of the gene in the list ordered by $\log_2$ fold change from high (red) to low (blue). Green line represents the enrichment score, which increases when a gene associated with the pathway is upregulated in the sample. Vertical black lines on the X-axis indicates the number of genes associated with the particular pathway.

Association between tumour endogenous *IGF1* and other genes of interest was tested by dividing the patients based on their median *IGF1* normalised gene expression, obtained from RNA sequencing. IGF-1 in circulation and tissues is bound to by IGFBPs that regulate the bioavailability and function of IGF-1 (Baxter, 2014). Measuring circulating IGF-1 levels alone may not signify activation of the IGF axis as the assay does not differentiate between bound and unbound IGF-1. Several reports have indicated that IGF axis activation results in the increased tissue expression of *IGFBP5* (Mohrin et al., 2021; Duan et al., 1996; Fleming et al., 2005; Kuemmerle, 2000; Ye and D'Ercole, 1998). Therefore, *IGFBP5* expression could be used as a surrogate for activation of the IGF axis. Tumours with high *IGF1* were found to express significantly increased *IGFBP5* mRNA compared with low *IGF1* tumours (Figure 5-11a). The association of high endogenous *IGF1* and *IGFBP5* may indicate that high *IGF1* tumours may have an increased activation of the IGF axis. Given the findings shown in Chapter 4 suggesting that IGF-1 upregulated PD-L1 in prostate cancer cells (Figure 4-7-9), this association was also tested. There was a trend to association between high tumour *IGF1* and *CD274* (PD-L1) expression (Figure 5-11b). Expression of IGF-1 stimulated cytokines identified in Chapter 4 were also investigated, however only *STAT5A* and *IFIT1* genes produced sufficient counts for downstream analysis. No statistical difference could be observed between *STAT5A* and *IFIT1* in high vs low *IGF1* tumours (Figure 5-11c,d).

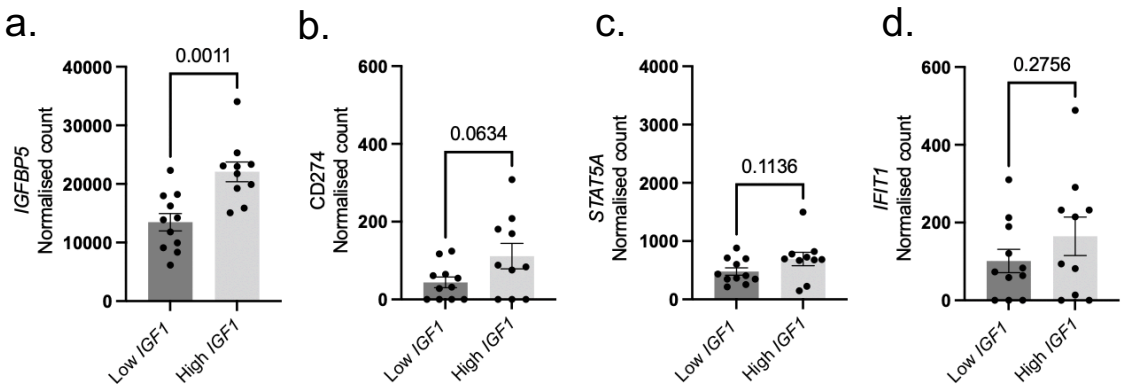


Figure 5-11 Testing association between tumour endogenous *IGFBP5, CD274*, STAT5A and *IFIT1* with tumour *IGF1* mRNA expression. Tumours were divided based on their median tumour endogenous *IGF1* expression and associations were tested with (a) *IGFBP5*, (b) *CD274*, (c) *STAT5A* and (d) *IFIT1*. Statistical significance calculated using a two-tailed unpaired T test.

5.3 Investigating associations of tumour endogenous *IGF1* with T cell infiltration and PD-L1 positivity in M-IF.

As before, patients were divided based on their median tumour endogenous *IGF1* expression and association with T cell infiltration and PD-L1 expression analysed using the parallel FFPE samples in which M-IF was performed. Results indicated no significant differences between *IGF1* levels and immune infiltration, though there was a non-significant trend to association of high *IGF1* with CD4 and with Treg infiltration (Figure 5-12a-c). Similarly, no statistical association was observed between high *IGF1* and PD-L1 expression, though there was a non-significant trend to increased epithelial PD-L1 (Figure 5-12d-f).

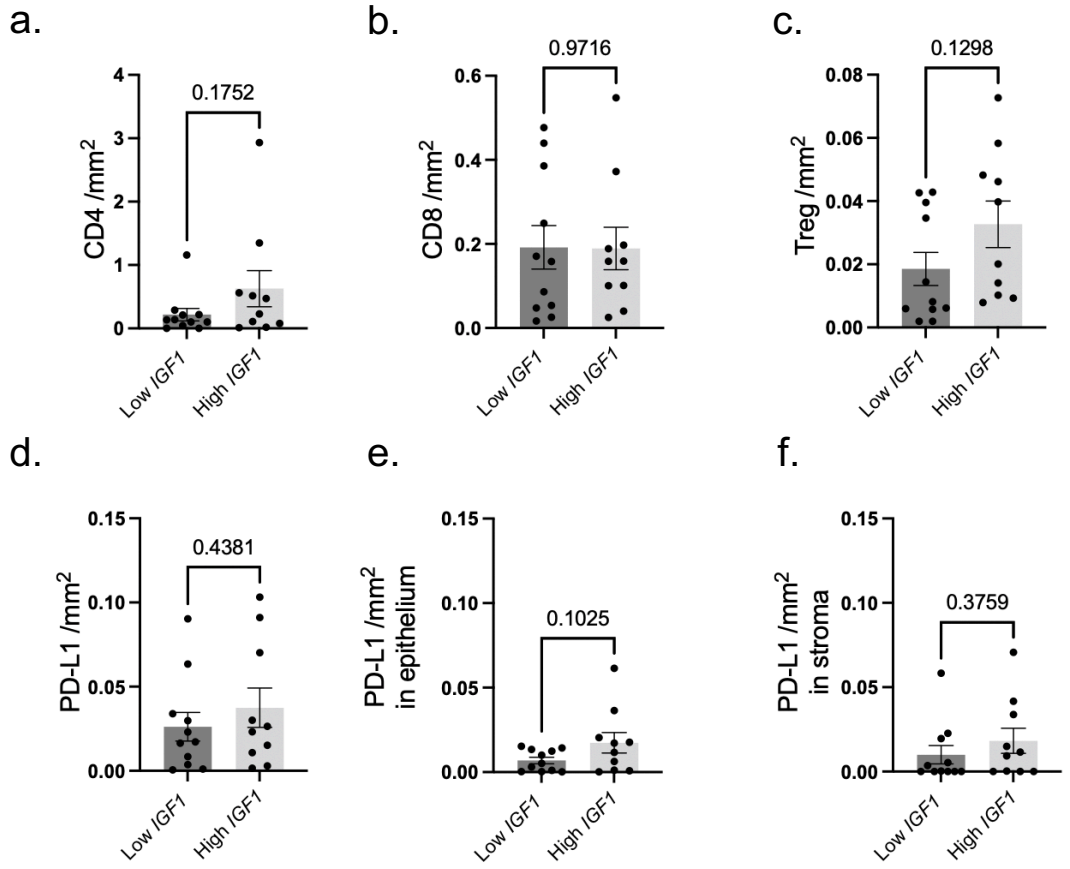


Figure 5-12 M-IF analysis of tumours with high vs low tumour endogenous *IGF1*. Patients were divided on their median tumour endogenous *IGF1* levels as before and parallel FFPE sections were used to quantify cells positive for (a) CD4, (b) FOXP3+ Tregs, (c) CD8 and (d) PD-L1 per mm^2. HALO MiniNet AI classifier was also used to assess PD-L1 positivity in the (e) tumour epithelium and (f) stromal compartments. Statistical significance was determined using a two-tailed unpaired T-test.

5.4 Single-cell sequencing of fresh prostate cancers to characterise the tumour microenvironment

Single-cell sequencing was performed on 3 benign and 8 malignant samples to identify the cell types infiltrating the prostate cancer microenvironment. This involved setting up a fresh prostate tumour tissue collection pipeline at Oxford with the help of staff of the Oxford Centre for Histopathology Research (OCHRe) and pathologists Professor Clare Verrill and Dr Richard Colling. Briefly, patients were asked to give NHS consent for use of surplus tumour tissue in ethically-approved research. From consenting patients, ~4mm^3 punch biopsies of benign and malignant areas were sampled from fresh, unfixed radical prostatectomies by the pathologists (Figure 5-13a). Malignant labelled samples were used for single-cell sequencing, however based on the later histopathological analysis of H&E stained sections, 3 samples were re-classified as benign. Within 1 hr of the punch biopsy being taken, I performed enzymatical disaggregation using a modified GentleMACS protocol detailed in Chapter 2. The resulting single-cell suspension was incubated at 4 °C overnight and the next morning stained using the eFluor 450 viability dye. Live cells were sorted by Craig Waugh, Kevin Clark and Sally-Ann Clark at the Flow Cytometry facility at The MRC Weatherall Institute of Molecular Medicine (WIMM), Oxford. Cells were gated to remove debris and doublets, and the live single cell population was positively sorted (Figure 5-13b). All live cells collected were resuspended in 0.04% BSA in PBS to prevent cell aggregation. Live cells underwent RNA extraction, barcoding and reverse transcription at the WIMM Single Cell facility by Facility Manager Dr Neil Ashley and Research Assistant Shayla Venkaya. DNAs were single-cell sequenced at GENEWIZ (Essex UK).

Analysis of the of single-cell sequencing data was performed in collaboration with Ashwin Jainarayanan, The Kennedy Institute of Rheumatology.

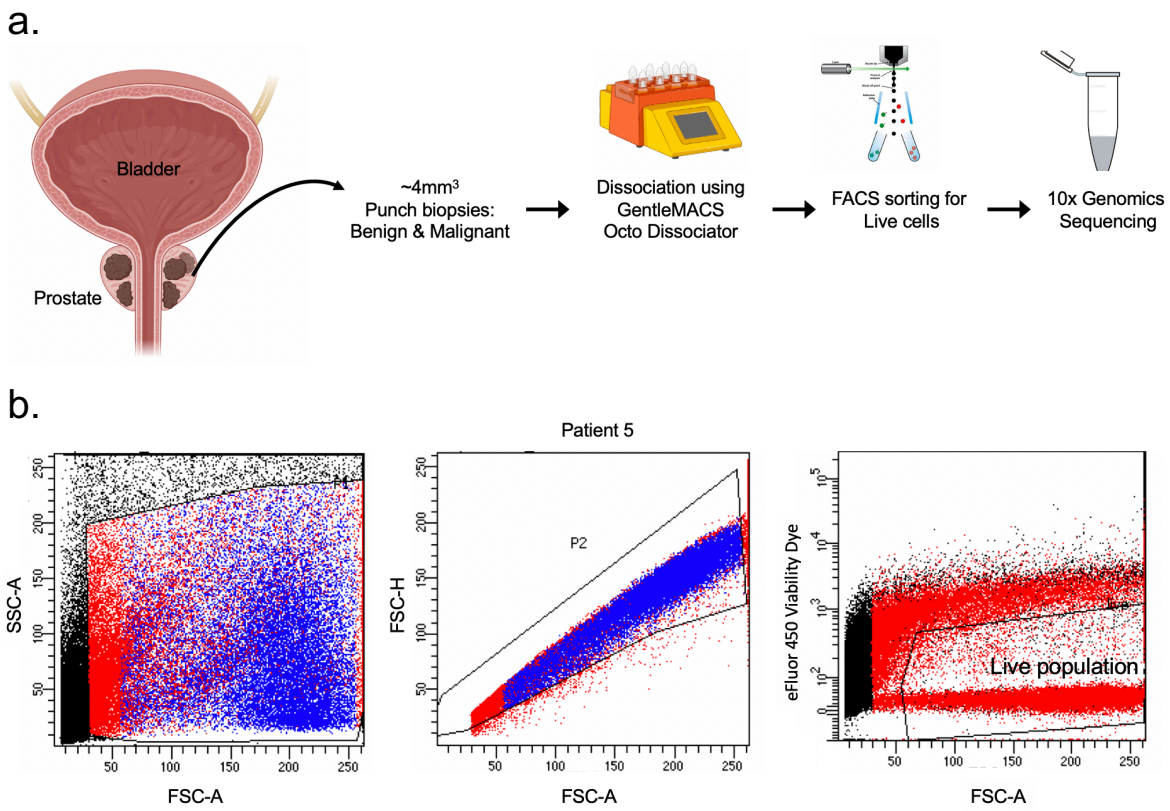


Figure 5-13 Prostate cancer single-cell sequencing workflow. (a) Fresh prostate radical prostatectomy punch biopsies were disaggregated using the GentleMacs Octo Dissociator, stained with the eFluor 450 viability dye and FACS sorted for live cells. Live cells were resuspended in 0.04% BSA in PBS and submitted for 10x sequencing. (b) One representative repeat of flow cytometry gating settings used to sort for the live population performed by Craig Waug at the WIMM Flow Cytometry facility.

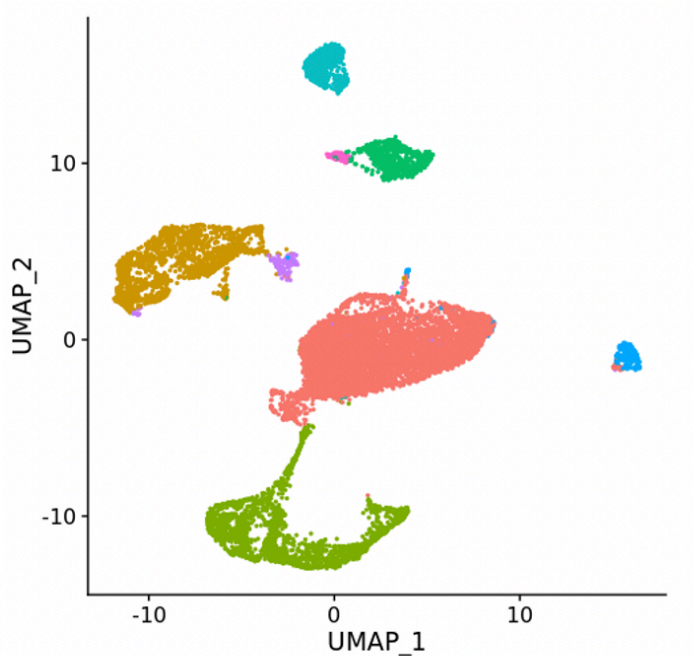
Single-cell sequencing data analysis was performed using the Seurat pipeline (Butler et al., 2018; Stuart and Satija, 2019). Briefly, cells with unique feature counts were filtered to remove doublets and, cells expressing greater than 5% mitochondrial genes were removed. Filtered data were normalised and cells with highly variable gene expression identified using the integrated Seurat pipeline to differentiate cell populations. Non-linear dimensional

reduction technique Uniform Manifold Approximation and Projection (UMAP) was performed to generate clusters of the cell populations. These clusters were annotated into different cell types based on their gene expression using references from published single-cell studies and gene sets (Kfoury et al., 2021; Chen et al., 2021; Song et al., 2022) previously used by Ashwin Jainarayanan (Figure 5-14a). Analysis produced a total of 11,859 cells split between 1,545 cells from benign and 10,314 cells from malignant prostate samples. Among the total infiltrating cells, there were 6,060 T cells (51%), 2,060 epithelial (17.4%), 1,823 myeloid (15.4%), 683 smooth muscle (5.8%), 639 endothelial (5.4%), 304 mast (2.6%), 176 B cells (1.5%) and 114 Fibroblasts (~1%).

Percentage cell composition per patient indicates T cells as the majority population followed by the epithelial and myeloid population (Figure 5-14a,b). This distribution was not consistent with relative cell composition identified in M-IF (Figure 5.3) or with previously published literature evaluating prostate cancer using single-cell sequencing, which displayed the epithelial cells as the majority population (Kfoury et al., 2021; Chen et al., 2021; Song et al., 2022). The cell filtration part of the tissue disaggregation method and doublet removal in live cell sorting may have enriched for the T cell population, and a lower ratio of epithelial cells and fibroblasts, which may be more prone to aggregate together. Furthermore, the mechanical and enzymatic disaggregation of cells from solid tumours cemented in extracellular matrix may result in altered mRNA levels leading to artefactual results (Haque et al., 2017). As far as I am aware, the resulting 6,660 cells form the largest dataset of tumour infiltrating T cells sequenced at a single-cellular level in primary prostate cancer based on current literature (Song et al., 2022; Kfoury et al., 2021; Chen et al., 2021). The normalised gene expression was used to generate a heatmap illustrating cell annotation-based clusters

and genes expressed in the identified clusters (Figure 5-15). Analysing the three dominant populations, T cells displayed enrichment of genes such as *CD8A*, *IFNG CCL5*, *CCL4* and *IL7R*. Epithelial cells were enriched for *TMPRSS2*, *KLK2*, *MSMB*. Myeloid cells were enriched for *LYZ*, *CD74* and *IL1B* (Figure 5-15).

a.



b.

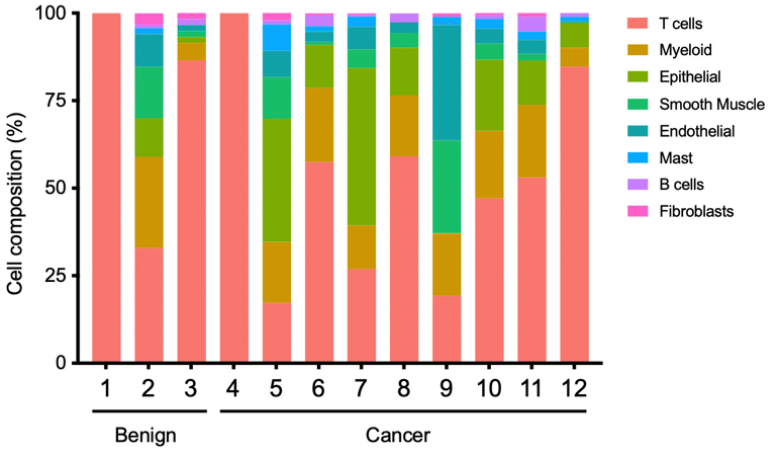


Figure 5-14 Single-cell sequencing analysis characterising prostate cancer microenvironment. (a) UMAP overview of the major cell types in prostate cancer identified based on their transcriptomic clustering. (b) Cell type composition per patient normalised to 100%

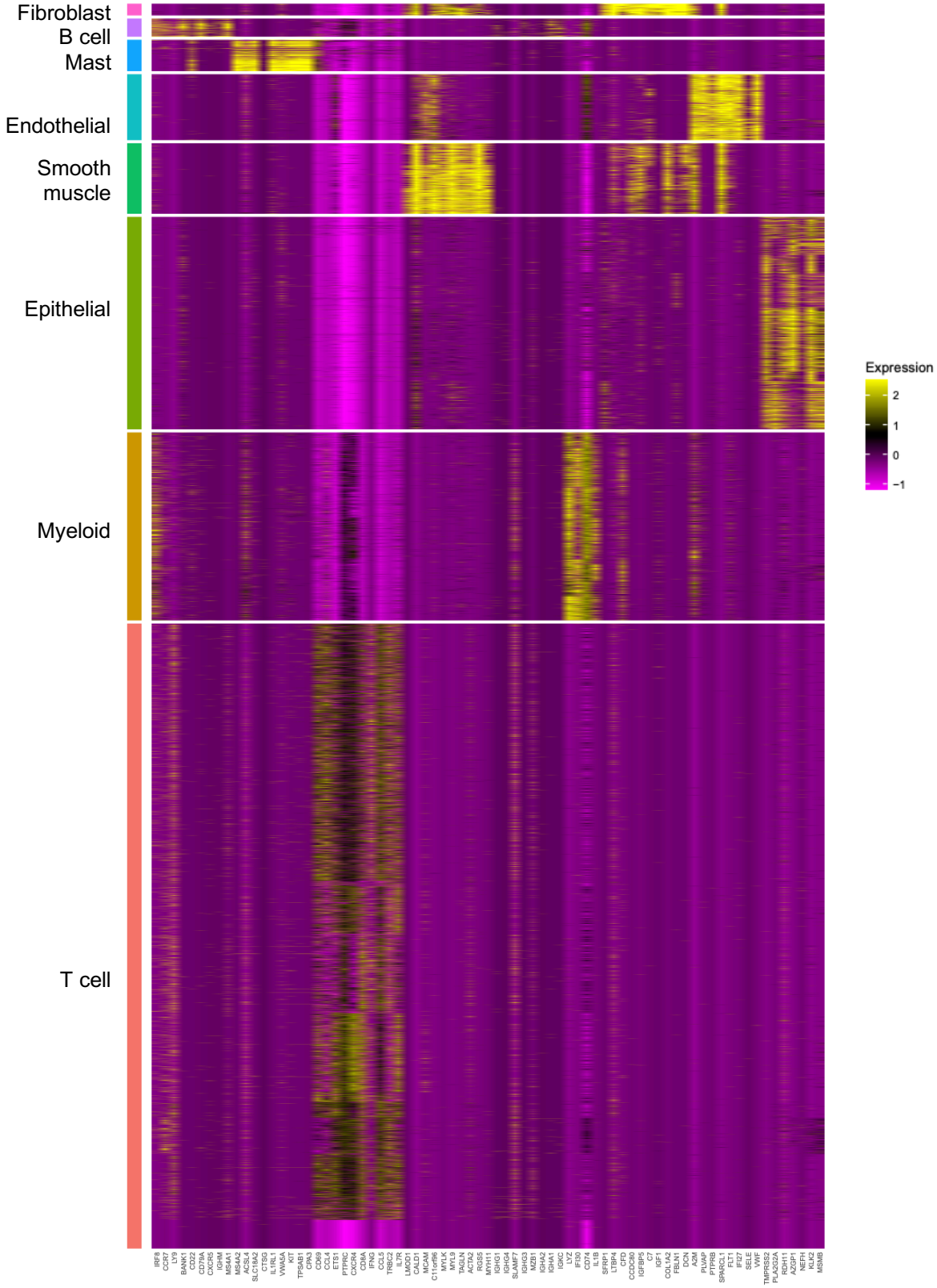


Figure 5-15 Heatmap of single-cell sequencing cell population clusters. Heatmap illustrating the expression of the marker genes used to annotate each cell population.

5.5 Expression of IGF axis associated genes in prostate cancer infiltrating cells

Expression of IGF axis associated ligands *IGF1* and *IGF2*, receptors *IGF1R* and *IGF2R* and binding protein *IGFBP3* were analysed across the clustered cell types. Analysis was performed using the normalised gene expression obtained from the Seurat pipeline and illustrated using violin plots and feature expression UMAPs. Expression of *IGF1* was enriched in fibroblasts and by a lower proportion of epithelial and myeloid cells (Figure 5-16a). In comparison, *IGF2* levels were not detected across clusters (Figure 5-16b). Expression of *IGF1R* was enriched in the epithelial cells (Figure 5-16c). Levels of *IGF2R* were enriched across multiple cell types including epithelial cells, myeloid cells, smooth muscle, fibroblasts and T cells (Figure 5-16d). Increased expression levels of *IGFBP3* was also seen in epithelial and endothelial cells (Figure 5-16e). Given the association between endogenous *IGF1* and *IGFBP5* identified in the RNA sequencing data from FFPE tissue of ProMPT subjects (Figure 5-11a), it will be interesting to investigate any similar association here.

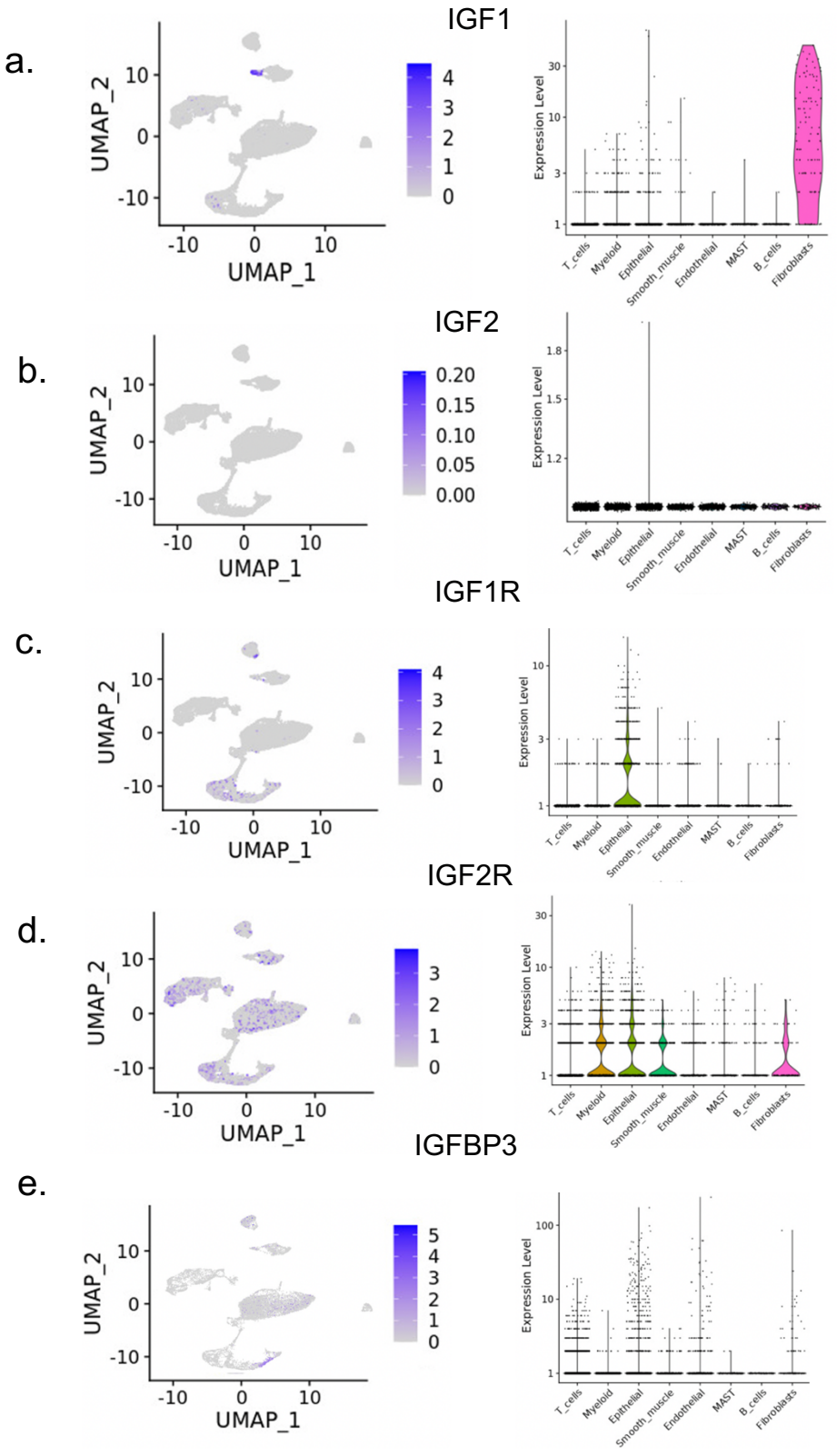


Figure 5-16 IGF axis expression across cell types. UMAP (left) and violin plot (right) showing the normalised gene expression of (a) IGF1, (b) IGF2, (c) IGF1R, (d) IGF2R and

(e) IGFBP3 across the annotated cell types. UMAP plots show the location of cells expressing each gene of interest, and violin plots indicate gene expression probability distributions across cell types, both generated using the Seurat pipeline.

5.6 Characterising the myeloid infiltrating population in prostate cancer.

The myeloid infiltrating population (1,823 cells, 15.4%) was isolated and clustered based on their gene expression profiles and visualised using the UMAP (Figure 5-17a). Cell based annotations were assigned from published literature as previously mentioned (Kfoury et al., 2021; Chen et al., 2021; Song et al., 2022). Analysis identified populations of monocytes, dendritic cells (DC), hematopoietic stem and progenitor cells (HSPC) and platelets.

The monocyte population was further differentiated into the classical CD14 high monocytes and non-classical CD16 high monocytes. Classical monocytes are reported to be the major (~70%) monocytic population and are progenitors to tissue resident macrophages. (Robinson et al., 2021; Kapellos et al., 2019; Olingy et al., 2019). They also contribute to the generation of an immune response. Non-classical subset functions as the patrolling monocytes in the vasculature, regulating tumour growth and preventing metastasis (Hanna et al., 2015; Olingy et al., 2019; Mukherjee et al., 2015). Classical CD14 high monocytes have also been reported to differentiate into CD16 high non-classical monocytes. The role of non-classical monocytes in cancer is not well characterised (Thomas et al., 2016; Mukherjee et al., 2015; Robinson et al., 2021).

The dendritic cells detected here were further classified into conventional DC type 1 (cDC1) and type 2 (cDC2) and, plasmacytoid DCs (pDCs). The cDC1 lineage cells are responsible for cross presentation of MHC Class I antigens to cytotoxic CD8+ T cells to promote anti-

tumour immunity. The cDC2 cells are involved presenting MHC Class II antigens to CD4+ T cells. Finally, pDCs have been reported to be potent producers of type 1 interferons and could enhance the anti-tumour functions of cDC1 cells (Del Prete et al., 2020; Guilliams et al., 2016; Mildner and Jung, 2014). However, tumour inflammatory DCs have been reported to be immunosuppressive, aiding the growth of cancer cells and inducing Tregs (Del Prete et al., 2020). Classical CD14 monocytes and cDC2 cells were the majority population observed in the single-cell analysis (Figure 5-17a). Amongst the DC population observed after single-cell sequencing, cDC2 was observed to be the majority population (Figure 5-17a). There were considerably fewer erythrocytes, HSPC and platelets in the prostate cancer tumour microenvironment.

Prostate cancer has been reported to be infiltrated by immunosuppressive M2 macrophages and MDSCs and their presence associated with tumour progression (Vitkin et al., 2019; Calcinotto et al., 2018; Erlandsson et al., 2019). To test for the functional status of the infiltrating myeloid population, expression of M2 macrophage associated genes *CD163* (Cluster of Differentiation 163) and *MRC1* (Mannose Receptor C-Type 1) and MDSC associated genes *S100A9* (S100 calcium-binding protein A9), *S100A8* (S100 calcium-binding protein A9) and *IFITM1* (Interferon Induced Transmembrane Protein 1) were investigated in the dataset (Gong et al., 2021; Alshetaiwi et al., 2020; Zhao et al., 2012; Zhang et al., 2020; Pombo Antunes et al., 2021). Expression of M2 associated genes was enriched in the macrophage progenitor CD14 monocytes and cDC2 population (Figure 5-17b,c). Analysis was only performed using the M2 genes and future work will investigate the expression and characteristics of the infiltrating M1 population. MDSCs are composed of a heterogeneous myeloid population consisting of monocytes, immature macrophages

and immature dendritic cells (Gabrilovich and Nagaraj, 2009). Analysis of MDSC associated genes on our single-cell sequencing data indicated the presence of MDSC gene enrichment in the CD14 classical and CD16 non-classical monocytes with lower expression also seen across the cDC2 population (Figure 5-17d-f).

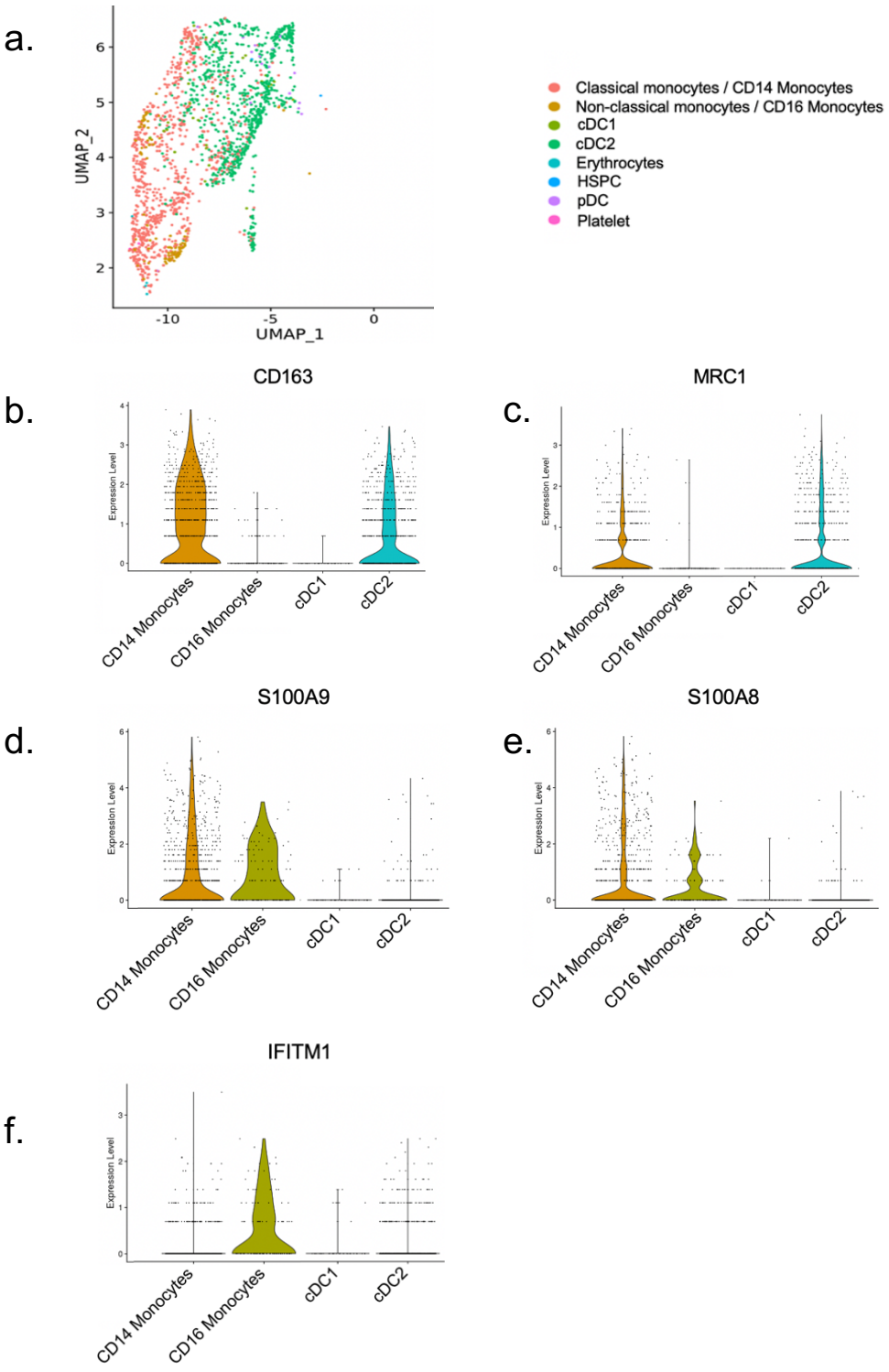


Figure 5-17 Characterisation of the tumour infiltrating myeloid subpopulation. (a) UMAP illustrating the clustering of the myeloid population based on their transcriptomic profile. (b) – (f): Violin plots indicating the expression of M2 associated markers (b) *CD165* and (c) *MRC1* and MDSC associated markers (d) *S100A9*, (e) *S100A8* and (f) *IFTM1* across

the myeloid population. The Y-axis of the violin plot represents gene expression probability distributions across cell types.

5.7 Characterising the lymphoid infiltrating population in prostate cancer.

The major cell population in our dataset were T cells with 6,060 cells (51%) of all cells sequenced. Tumour-infiltrating lymphoid cells (TILs) were analysed to identify their functional status by assessing the expression of cytotoxic and immunosuppressive markers. The lymphoid population was isolated and clustered based on their gene expression profiles into multiple sub-populations consisting of CD4 T cells, CD8 T cells, double negative T cells (dnT), γδ T cells, MAIT cells, NK cells including the cytokine producing CD56 bright population and Tregs (Figure 5-19a). The CD4 population was further classified into cytotoxic CD4 (CD4 CTL) cells, proliferating CD4, central memory associated CD4 (CD4 TCM) and effector memory associated CD4 (CD4 TEM). Similarly, CD8 T cells were classified into naïve, proliferating, central memory associated CD8 (CD8 TCM) and effector memory associated CD8 (CD8 TEM). Cell composition per patient revealed that the majority of the TILs belonged to the CD8 TEM subtype (47% of lymphocytes), followed by CD8 TCM (19%), CD4 TCM (15%) and NK cells (7.5%) (Figure 5-19b). The remaining population consisted of MAIT cells (2.4%), CD4 TEM (2%), Tregs (1.4%), NK CD56 bright (1.2%), dnT (1.1%) and less than 0.5% of CD4 CTL, CD4 proliferating, CD8 Naïve, CD8 proliferating, γδ T cells and NK proliferating cells. Classifying these cell types into broader categories also indicated a majority of CD8s, followed by CD4s and NK cells (Figure 5-19c).

Cytotoxic potential of lymphocytes was assessed by testing for expression of granzyme A (*GZMA*) and granzyme B (*GZMB*) genes. Granzyme A triggers cell death via caspase independent mechanisms, causing mitochondrial dysfunction and single-stranded DNA damage, while Granzyme B initiates apoptosis through caspase mediated interactions (Zhu et al., 2009). *GZMA* expression was enriched in the CD8 naïve, TCM and TEM subsets, NK cells, MAIT cells and within the CD4 TCM and TEM cells (Figure 5-19a). *GZMB* expression was consistently enriched within the CD8 and NK population, but not in the CD4 cells (Figure 5-19b).

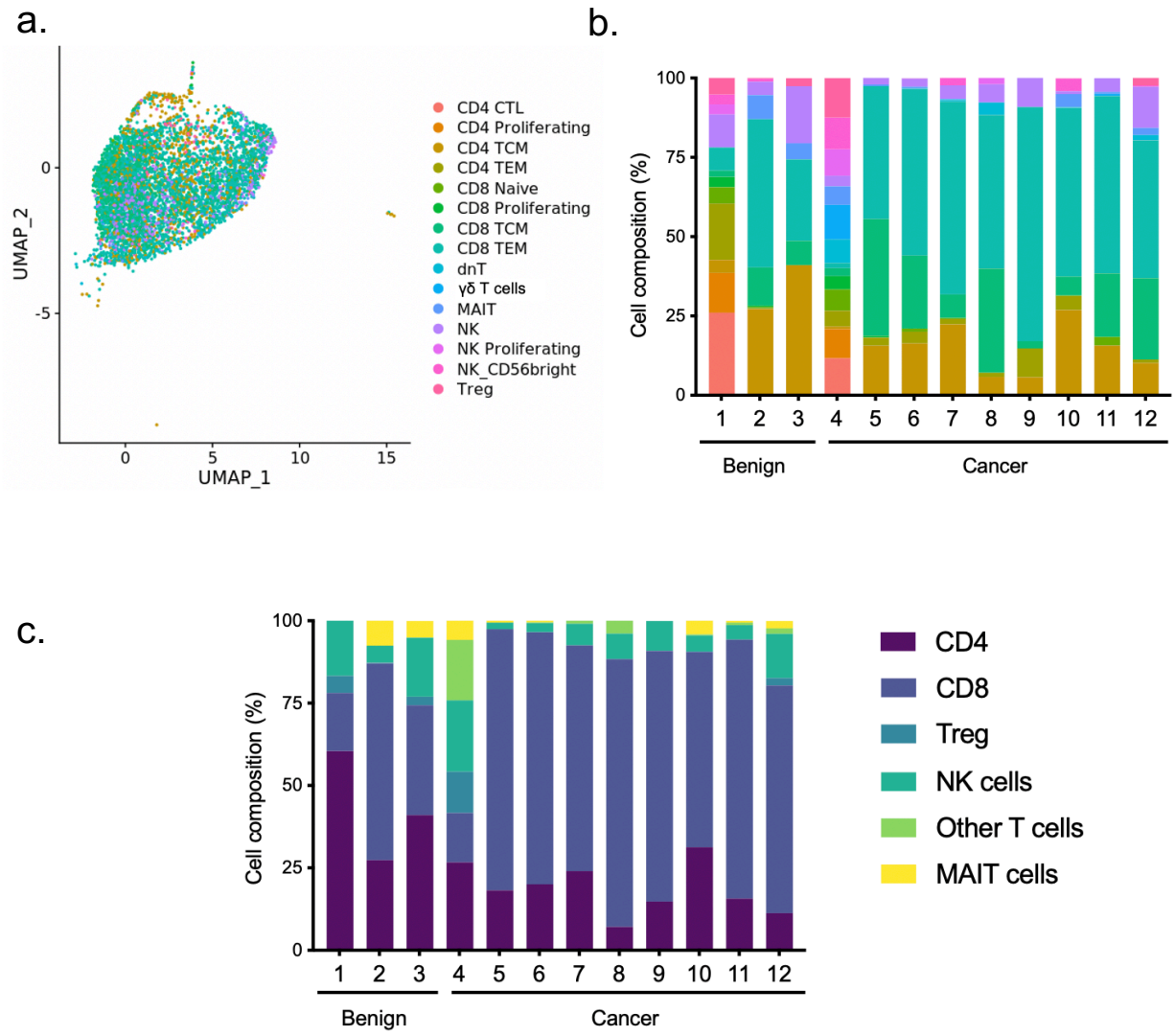


Figure 5-18 Characterising the tumour infiltrating lymphocytes in prostate cancer. (a) UMAP illustrating the lymphocyte cell types indicated by their colour. (b) Composition of infiltrating lymphocytes shown as % of total lymphocytes per tumour. (c) Composition of infiltrating lymphocytes per tumour grouped into broader clusters, normalised as in b) to 100%.

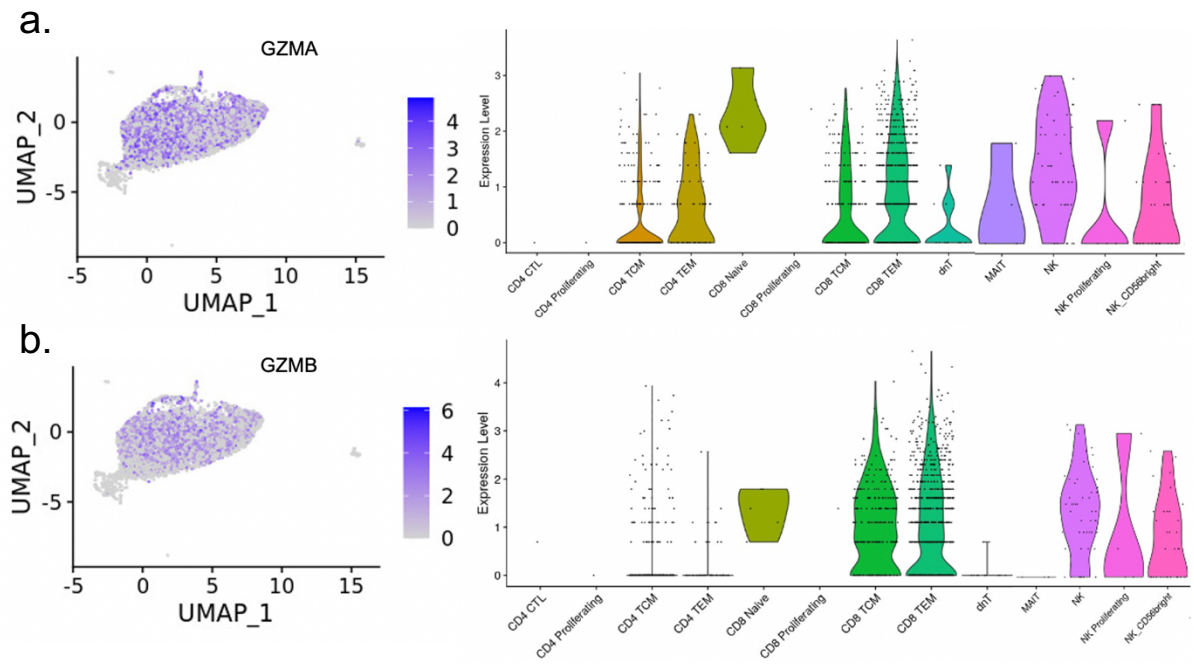


Figure 5-19 Expression of cytotoxic markers in the tumour infiltrating lymphocyte population. Expression of cytotoxic markers (a) GZMA and (b) GZMB across the lymphocytes illustrated using UMAP (left) and violin plots (right).

In parallel to assessment of the expression of cytotoxic markers, expression of immune checkpoint ligands was also measured across the lymphoid population. Analysis revealed expression of *CTLA4* in the CD4 TCM, CD8 Naïve, dnT cells and proliferating NK cells (Figure 5-20a). Expression of PD-1, encoded by its gene *PDCD1* was enriched in TEM and TCM subsets of both CD4 and CD8 T cells, naïve CD8s and MAIT cells (Figure 5-20b). Finally, *LAG3* expression was detected across CD8 TEM and TCM cells, MAIT cells and NK proliferating cells (Figure 5-20c). The expression of immune checkpoints ligands was lower in the NK subsets compared to the T cells, which may imply less intrinsic suppression of NK associated vs T cell associated anti-tumour cytotoxicity. Further analysis needs to be performed on the T cell population to identify if *GZMA*/*GZMB* expressing T cells concurrently express checkpoint ligands *CTLA4*, *PDCD1* and *LAG3* or if these are two

different populations. If they are concurrently expressed, this could be suggestive of a negative feedback loop to prevent T cell overactivation, commonly seen after TCR activation (Oyewole-Said et al., 2020; Tian et al., 2015; Simon and Labarriere, 2018).

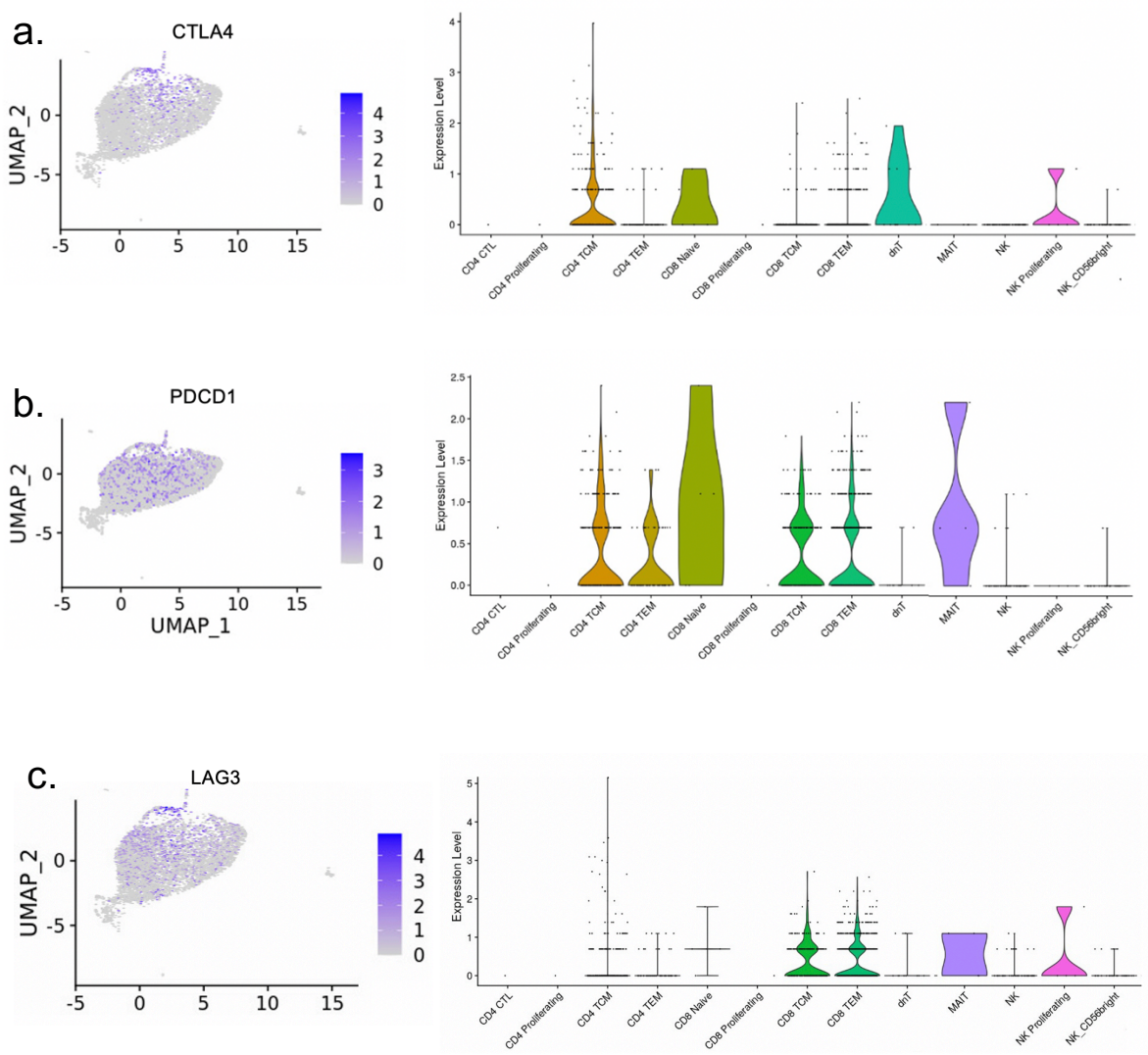


Figure 5-20 Expression of immune checkpoints across the lymphocyte populations. Expression of (a) *CTLA4*, (b) *PDCD1* and (c) *LAG3* across the lymphocyte population illustrated by ~~a~~ UMAP (left) and violin plots (right).

5.8 Expression of IGF axis ligands and receptors across the lymphocyte population.

Expression of IGF axis ligands IGF1 and IGF2, receptors IGF1R, IGF2R and binding protein IGFBP3 was analysed across the lymphocyte population and visualised using violin plots. Expression of *IGF1, IGF2* and *IGF1R* were minimal across the lymphocyte population, though a small proportion of CD8 TCM and TEM cells showed higher expression of *IGF1* and *IGF2* (Figure 5-21a-d). Expression of *IGF2R* was enriched across the CD8 and NK proliferating cells as well as the γδ T cells (Figure 5-21d). Finally, higher *IGFBP3* levels were seen in the CD8 TCM and TEM populations (Figure 5-21e).

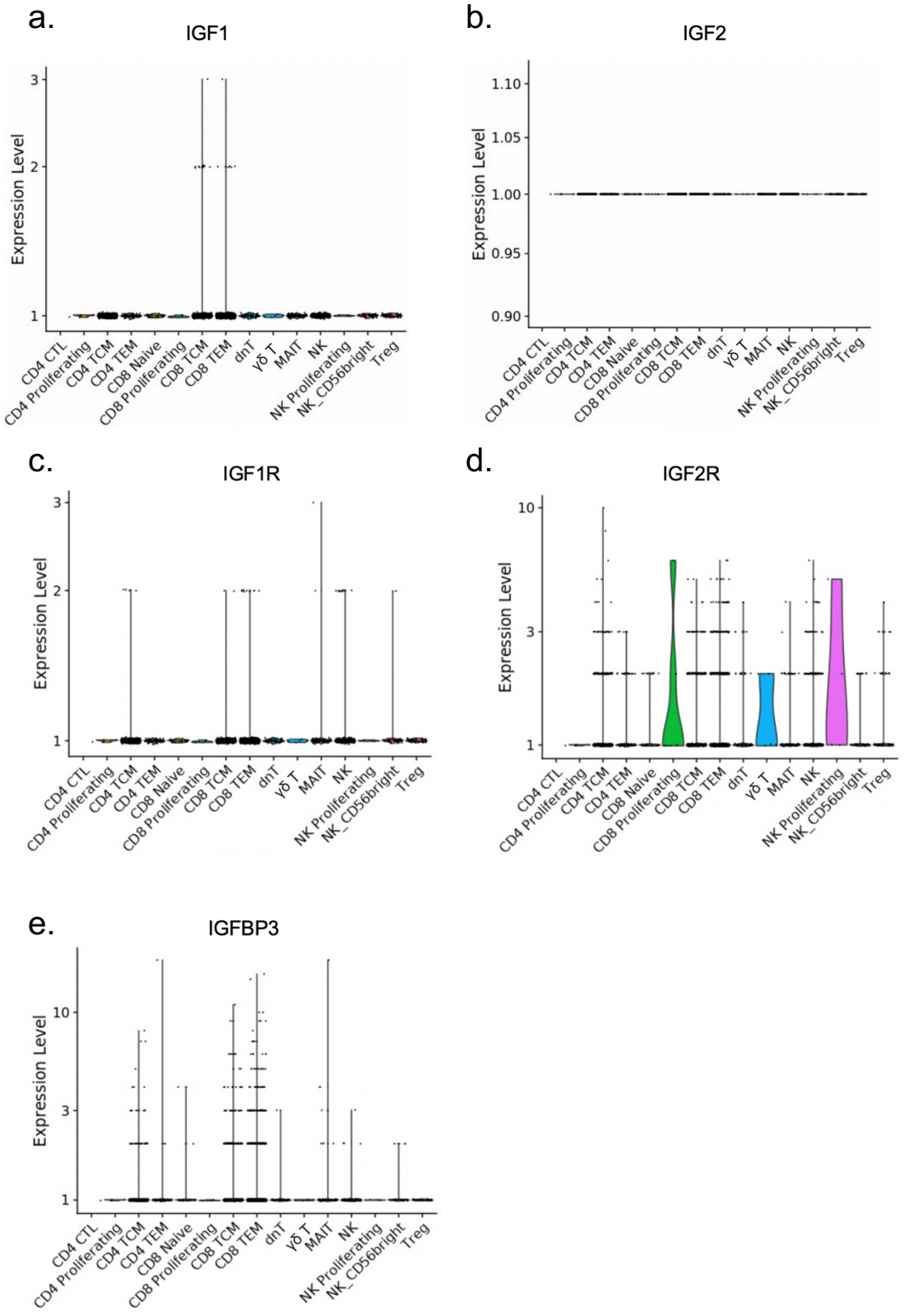


Figure 5-21 Expression of IGF axis markers across the lymphocyte population. Violin plots illustrating the expression of (a) *IGF1*, (b) *IGF2*, (c) *IGF1R*, (d) *IGF2R* and (e)

IGFBP3 across the infiltrating lymphocyte population. The Y-axis represents the gene expression probability distributions across cell types.

5.9 Discussion

In this chapter, three approaches were used to investigate the immune microenvironment of prostate cancer. First, we used M-IF to quantify the tumour infiltrating T cell population in 32 prostate cancer samples. Results indicated no differences in T cell infiltration between areas of benign and cancer tissue, Gleason grade group or PSA levels. Classifying patients on their circulating IGF-1 levels, high IGF-1 patients displayed a significant increase in tumour infiltrating CD4 T cells and a non-significant trend to PD-L1 upregulation ($p=0.1504$). Results obtained in Chapter 4 revealed PD-L1 expression to be upregulated by IGF-1 *in vitro* and analysis for TCGA prostate and colorectal datasets showed a significant association between high tumour *IGF1* and *CD274* (PD-L1) mRNA (Chapter 4-7-10). Similarly in this chapter, high circulating IGF-1 and tumour endogenous *IGF1* was shown to be linked to increased PD-L1 expression, though not statistically significant. These results may imply that tumour with increased IGF axis activity could express immunosuppressive PD-L1 and patients with increased IGF axis activity may benefit from anti-PD1 blockade, previous shown to be unsuccessful in prostate cancer (Bilusic et al., 2017). However, these results need to be tested on a larger validation cohort as the association between circulating IGF-1 and endogenous *IGF1* was not statistically significant, which could be due at least in part to the small number of samples analysed.

Secondly, RNA was extracted and sequenced from the parallel cancer annotated areas of the FFPE sections from cases in which M-IF was performed, aiming to identify the transcriptomic profile of tumours from patients with high vs low circulating IGF-1. No differentially expressed genes were identified in association with circulating IGF-1 levels. This may be due to several factors. RNA extracted from FFPE samples produced low RIN values and a high number of genes with zero read counts in the RNA sequencing data. FFPE extracted RNA has been reported to be highly fragmented and to decrease in quality with increasing age of the paraffin block (Pennock et al., 2019; Mathieson and Thomas, 2020; Groelz et al., 2018; Zhao et al., 2019; Von Ahlfen et al., 2007). The samples we obtained were from 2011-2015 and the storage duration may have affected the quality of extracted RNA. For future experiments involving FFPE samples, a targeted sequencing approach involving specialised probes such as the Nanostring platform may be preferable to characterise gene expression. The epidemiological studies that reported the association of high circulating IGF-1 with risk of prostate cancer comprised of a sample size of ~18,000 subjects in the meta-analysis by Travis et al. 2016 and ~200,000 subjects from the UK Biobank and, ~140,000 subjects from EPIC and The Prostate Cancer Association Group to Investigate Cancer Associated Alterations in the Genome (PRACTICAL) consortium in Watts et al 2021 (Travis et al., 2016; Watts et al., 2021). Therefore, the lack of DEGs expressed in a smaller dataset of 21 patients used in my analysis may suggested larger cohorts are necessary to characterise differences.

As an alternative approach, I decided to compare gene expression in tumours with high vs low endogenous *IGF1* expression obtained from normalised gene counts. Tumours with high *IGF1* mRNA displayed upregulation of IGF pathway related genes *IGFBP5*, *FOXO1*,

BCL2 and *ZEB1*, chemokine *CXCL12*, prostate cancer associated genes *WFDC1*, *FGFR2* and *EZH1*. *WFDC1* encodes for prostate stromal 20 secreted protein and has been reported to promote proliferation of LNCaP prostate tumour cells but induce apoptosis of stromal cells (Hickman et al., 2016). No association has been previously reported about the interaction between *WFDC1* and the IGF axis. *FGFR2* overexpression is associated with gastric cancer with higher N-Stage (Ahn et al., 2016). Both IGF-1R and FGFR-2 signal via the PI3K-AKT and MAPK pathways and activation of IGF-1 has been reported to stimulate the expression of expression of ligands associated to FGFR2 (Melnik, 2009). EZH1 is encoded by *EZH1* a core subunit of polycomb repressive complex 2 (PRC2) and promotes transcriptional repression by histone trimethylation (Nakagawa and Kitabayashi, 2018). EZH1 is an alternative EZH2 subunit, and dual inhibition of EZH1 and EZH2 have been reported to sensitise prostate tumours to proteasome inhibition (Rizq et al., 2017; Kook et al., 2017). *EZH2* has been previously reported to bind to the *IGF1R* promoter and upregulate its expression (Kosalai et al., 2019)

Results of RNA-seq on FFPE tissues also displayed downregulation of MHC Class I associated gene *TAP1*, *SOX4* and NF-κB regulator *TRAF4* (Figure 5-8). Functional pathway analysis indicated differential regulation of pathways including those associated with migration (focal adhesion, regulation of actin cytoskeleton and proteoglycans in cancer pathways), immunity (leukocyte transendothelial migration, CCR5 and IL-18 pathways), IGF axis (insulin secretion pathway, VEGF signalling, hedgehog signalling) and cancer (PYK2 and Agrin pathways) (Yeo et al., 2017; Zhang et al., 2010; Shi et al., 2015; Matz-Soja et al., 2014; Lipinski et al., 2005). Furthermore, patients with high *IGF1*

endogenous expression displayed increased *IGFBP5* expression, which as mentioned above is upregulated in response to IGF axis activation (Mohrin et al., 2021).

High *IGF1* tumours also showed a trend to upregulation of *CD274* (p=0.0634), consistent with results shown in prostate cancer cells (Chapter 4-7-8. Integrating the sequencing results with the M-IF data, we found a non-significant trends to association of high tumour *IGF1* with increased infiltration of CD4 T cells (P=0.1720), FOXP3+ Tregs (p=0.1298) and PD-L1 epithelial positivity (P=0.1025) (Figure 5-11). Though upregulation of PD-L1 by IGF-1 has not been reported before, the pathways downstream of the IGF axis has been linked to upregulating PD-L1 expression (Mittendorf et al., 2014; Chen et al., 2015; Kang et al., 2019).

Finally, single-cell sequencing was performed to characterise the infiltrating cells within prostate cancer microenvironment. Analysis revealed infiltration of T cells, epithelial, myeloid, endothelial, smooth muscle, B cells and fibroblasts in prostate tumours. The samples were highly enriched for T cells, which may have resulted from the tumour disaggregation and sorting strategies. However, the data provided the largest collection of prostate tumour infiltrating T cells to date (6,660 cells). Previous publications of primary prostate cancer single cell analysis revealed a T cell population of 3,116 cells (8.6%, Chen et al. 2021), ~1,400 cells (6.4%, Song et al. 2022) and 1694 cells (10.9%, Tuong et al. 2021), with epithelial cells being the major cell type (Tuong et al., 2021; Song et al., 2022; Chen et al., 2021).

Analysis also revealed the presence of M2 and MDSC associated phenotypes and T cell expression, activation and immune checkpoint markers. Expression of *IGF1* was enriched in the fibroblasts, consistent with reports that stromal fibroblasts secrete IGF-1, contributing to chemotherapy resistance and associating with reduced overall survival in bladder cancer (Ireland et al., 2016; Quail et al., 2016; Chen et al., 2020). Results also found a novel enrichment of *IGF2R* expression in the myeloid, epithelial and fibroblast populations, and with CD8 and proliferating NK cells (Figure 5-15,20).

IGF-1 has been reported to promote the proliferation and differentiation of CD4 Th17 cells (DiToro et al., 2020). IGF-1 stimulation has also been reported to induce immunosuppressive IL-10 secretion in Th1 CD4 cells(Kooijman and Coppens, 2004). In the work reported here, high circulating IGF-1 associated with increased CD4 infiltration in M-IF analysis (Figure 5-5a), and in RNA-seq analysis of the same cases, tumours with high endogenous *IGF1* displayed a trend towards increased CD4 and Treg infiltration (Figure 5-12a,c). Aside from this trend there were no identified links between the IGF-1 axis and Treg infiltration, in contrast to functional associations reported previously (Bilbao et al., 2014b; Miyagawa et al., 2017; Johannesson et al., 2014; Farabaugh et al., 2015; Lu et al., 2014). It is possible however that high IGF axis activity may aid in the recruitment of CD4 T cells into the tumour. This hypothesis is supported by RNA sequencing results which indicated chemokines *CXCL12* and enrichment of leukocyte transendothelial migration pathway in high *IGF1* patients. CXCL12 via its interaction with CXCR4 receptor regulates migration of T cells and has also been reported to induce CD4 T cell activation and proliferation by upregulating CD25, CD69, CD154 and and IFNγ (Ottoson et al., 2001; Borge et al., 2013; Lin et al., 2009). Using single-cell RNA sequencing, we characterised

that the CD4 infiltrating cells expressed activation markers *GZMA* (Figure 5-19) as well as anergy markers *CTLA4* and *PDCD1* (Figure 5-20a,b). For future work, effects of IGF-1 on the infiltrating CD4 T cells could be tested by *in vitro* assays testing for gene and surface expression using qRT-PCR and flow cytometry after IGF-1 treatment, to determine if IGF-1 could influence markers associated with anergy in the CD4 infiltrating T cells such as PD-1, CTLA-4 and LAG-3 (Crespo et al., 2013).

The role of IGFs in regulating migration and motility of epithelial cells have been well documented (Chitnis et al., 2008; Brodt et al., 2001) Consistent with this, high *IGF1* tumours showed deregulation of migration associated pathways such as focal adhesion and regulation of actin cytoskeleton and increased chemokine *CXCL12* and activation of immune associated: leukocyte transendothelial migration, CCR5 and IL-18 pathways (Figure 5-8,9). However, these results do not confirm if the *CXCL12* expression in enriched in the malignant cells or stromal cells. IGF-1 induced expression of *CXCL12* by prostate tumour cells can be tested using q-RT PCR and these results could also be compared to the expression levels of cell types identified using single-cell RNA sequencing. For future work, chemotaxis effects of IGF-1 on T cell populations could be tested using Ibidi's chemotaxis chambers (Yang et al., 2020). For this assay, prostate cancer cells will be labelled with cell tracker dyes, stimulated or not with IGF-1 and placed onto one chamber. Leukocytes or macrophages can then be seeded onto the other chamber and cell migration towards the cancer cells can be measured using microscopy. Due to time constraints, differentially expressed genes could not be validated *in vitro* in prostate cancer cell cultures using q-RT PCT and future work should address this. If results from the chemotaxis assays show that IGF-1 promotes

chemotaxis of specific cell populations, genes for validation could include *CXCL12, CCR5, IL18* identified from the deregulated pathways.

Downregulation of the IGF axis and downstream MAPK pathway has been reported to upregulate MHC Class I antigen presentation has been reported in glioma and head and neck squamous cell carcinoma (Trojan et al., 1996; Kang et al., 2019). Consistent with IGF effects on antigen presentation, results from this chapter suggested downregulation of the MHC Class I associated *TAP1* gene in high *IGF1* patients. TAP1 complexes with TAP2 and is required for peptide transport and loading onto MHC Class I molecules with β_2 microglobulin, for trafficking to the cell surface (Dhatchinamoorthy et al., 2021). TAP1/2 deficiency is associated with immunodeficiency associated with granulomatous lesions with high NK cell infiltration leading to tissue damage (Moins-Teisserenc et al., 1999; Teisserenc et al., 1997; Law-Ping-Man et al., 2018; Gadola et al., 2000). TAP deficiency has been reported to cause immune escape and poor prognosis in colorectal cancer (Ling et al., 2017). The consequence of IGF axis downregulation of TAP1 could be tested by measuring the surface expression of MHC Class I in cancer cells using flow cytometry with the W6/32 monoclonal antibody which recognises the HLA/ β_2 macroglobulin complex on the cell surface (Teisserenc et al., 1997).

The RNA sequencing analysis of RNAs extracted from FFPE tissue sections was conducted comparing tumours with high vs low *IGF1*. Samples were divided based on the median *IGF1* counts obtained from DESEQ2 normalisation. This resulted in *IGF1* being a DEG, obtained as a result of dividing the samples using median count. Analysing pathways associated with DEGs, *IGF1* was involved in the gene set associated with pathways of

interest including focal adhesion pathway, insulin secretion and proteoglycans in cancer pathways (Figure 5-9, Figure 5-10). The inclusion of *IGF1* may have influenced the identification of these pathways as being of interest. For future analysis, *IGF1* gene could be removed from the downstream analysis to produce an unbiased set of genes. Alternatively, samples could be divided using expression of IGF axis activation marker such as IGFBP5, which could be checked at the protein level by performing IHC on the parallel slides in which FFPE RNA sequencing was performed.

Single-cell analysis suggested that the infiltrating T cell population expressed both activation and exhaustion markers (Calcinotto et al., 2018; Erlandsson et al., 2019). It is unclear whether the T cells are expressing the activation and exhaustion markers concurrently or if they are two separate populations and future single-cell analysis should be conducted to examine this. This is because both PD-L1 and CTLA-4 are expressed after TCR activation of the T cells as a negative feedback loop. Therefore, concurrent expression of PD-L1 and CTLA-4 could signify activation rather than exhaustion of T cells (Chikuma, 2017; Simon and Labarriere, 2018). Finally, results from RNA sequencing of FFPE samples indicated activation of macrophage associated CCR5 and IL-18 pathways. Single-cell analysis identified a myeloid population expressing M2 and MDSC markers, consistent with published data (Calcinotto et al., 2018; Song et al., 2022; Kfoury et al., 2021; Erlandsson et al., 2019). Associations of *IGF1* with macrophage phenotypes could also be tested on the single-cell sequencing data, dividing patients by their endogenous *IGF1* levels.

Due to time constraints, the further analysis of associations between IGF axis and immune infiltrating cells could not be performed in the single-cell data. In future single cell work,

ideally in a larger series, prostate cancers could divided by endogenous *IGF1* or IGF axis activation marker *IGFBP5*, or by IGF-1R phosphorylation assessed by IHC to analyse expression of specific markers of lineage and function by different components of the immune TME. IGF axis specific effects could also be studied using spatial transcriptomics on the FFPE samples from the ProMPT cohort in which we have assayed serum IGF-1, tissue IGF-1R, and expression of *IGF1R*, *IGF1* and *IGFBP5* mRNA. Spatial transcriptomics is very expensive particularly at the single-cell level (Marx, 2021). However, it may be possible to access existing datasets (Berglund et al., 2018; Chelebian et al., 2021), which could enable us to test associations of IGF axis gene expression with phenotypes of immune cells, to guide future investigations.

6 Chapter VI: Discussion & Future work

The principal aim of this project was to understand whether there is any evidence to suggest whether IGFs could promoting prostate cancer risk and progression through its effects on the tumour epithelium and the microenvironment. High circulating IGF-1 has been reported to be associated with increased risk to breast, colorectal and prostate cancer (Key et al., 2010; Rinaldi et al., 2010; Travis et al., 2016; Hankinson et al., 1998; Ma et al., 1999; Knuppel et al., 2020). Recent evidence also suggests that the association of high IGF-1 with prostate cancer may be causative of both cancer risk and lethality (Watts et al., 2020). Exploring this association in prostate cancer, previous work from the lab indicated that high circulating IGF-1 levels were associated with increased IGF-1R in the malignant epithelium but not in benign areas of radical prostatectomies from ProMPT study subjects (Aleksic, Verrill, Macaulay, unpublished). Work in Chapter 3 investigated the association between IGF-1 and IGF-1R expression in a small cohort of EPIC subjects. Analysis of radical prostatectomy tissues indicated a trend towards increased IGF-1R and an association with internalised IGF-1R in the malignant epithelium of prostate cancer, compared with benign areas. These findings are comparable to previously published reports of IGF-1R upregulation in prostate cancer (Hellawell et al., 2002; Aleksic et al., 2018). In parallel, using a subset of the previously studied ProMPT cases, *IGF1R* mRNA was found to be upregulated in the malignant glands suggesting regulation at the transcriptional level in clinical prostate cancers, and this finding is new. Contrary to the findings from IHC, RNAScope studies showed no association between circulating IGF-1 and increased *IGF1R* mRNA, though this may be due to the limited number of samples used in the study (n=17).

As an alternative way of testing whether high IGF-1 affects IGF-1R expression, we cultured prostate cancer cells in IGF-supplemented medium for 24 hrs and 8-12 weeks. Long term culture in IGF-1 was used here to mimic the lifelong high IGF-1 supply associated with prostate cancer risk, and had been used to identify clinically relevant phenotypes in breast cancer (H-F Zhang et al., 2013). However, both acute and long term IGF-1 stimulation resulted in IGF-1R downregulation, which may occur as a consequence of IGF-1R activation resulting in receptor degradation (Schillaci et al., 1998; Girnita et al., 2005). This result was inconsistent with the tissue level findings, but did reveal a novel finding that long term IGF-1 treatment resulted in IGF-1R nuclear translocation. Nuclear IGF-1R has been reported to be associated with advanced tumour stage in prostate cancer and can bind to regulatory regions of DNA, interact with RNA Polymerase II and upregulate *JUN* and *FAM21* (Aleksic et al., 2018). These results may suggest that chronic IGF-1 supply can lead to IGF axis activation, as indicated by receptor nuclear translocation, and contribute to the association between IGF-1 and prostate cancer risk. No association was found between high IGF-1 and nuclear IGF-1R in 139 ProMPT cases in which IGF-1R IHC was performed (Aleksic, Verrill, Macaulay, unpublished). Despite multiple attempts it was not possible to obtain a larger cohort of clinical cases with serum for IGF-1 assay, which would be very useful to further test the association of serum IGF-1 with IGF-1R expression and localisation.

Work then turned to investigating IGF axis effects on immune responses to prostate cancer, using cell lines and clinical tissues. The initial focus was the malignant epithelium, studied by investigating IGF-1 induced expression of cytokines and PD-L1. Results from Chapter 4 uncovered that IGF-1 stimulation of prostate cancer cells lead to the upregulation of

cytokines including *CXCL8, CXCL10*, *CCL5* and immune associated genes *IFNB1* and *ARG2*. These targets have been implicated as promoting immunosuppression in cancers such as melanoma and lung cancer, but not previously reported in prostate cancer (Nagarsheth et al., 2017; Maio et al., 2019; Grzywa et al., 2020; Morimoto et al., 2018; Garcia-Diaz et al., 2017). Additionally, analysis of public datasets revealed that tumours with high *IGF1* mRNA had increased expression of *S1P*, *CXCL12*, *CCL5* and *CCL4*, which have been associated with increased infiltration of immunosuppressive Tregs, M2 macrophages and MDSCs, commonly found to infiltrate prostate cancer. (Zhou et al., 2020; Lin et al., 2019; Argyle and Kitamura, 2018; Ruytinx et al., 2018; Fleming et al., 2018; Erlandsson et al., 2019; Calcinotto et al., 2018; Vitkin et al., 2019). IGF-1 stimulation also led to the phosphorylation of TBK1 and IRF3, and STING upregulation. These findings suggested activation of the cytosolic DNA sensing cGAS-STING pathway, which I speculated could be the result of IGF-1 induced replication stress. This is consistent with recent report from our group that IGF-1 upregulates RRM2, compromising the function of RNR leading to dNTP pool imbalance, shown in models to be mutagenic (Rieunier et al., 2021; Kumar et al., 2011). However, further tests need to be conducted to confirm the presence of cytosolic DNA after IGF-1 stimulation. This could be tested by stimulating prostate cancer cells with IGF-1 and measuring the release of cytosolic DNA and micronuclei after staining with double stranded DNA dye Picogreen (Ho et al., 2016b).

One of the effects of cGAS-STING pathway activation is to upregulate the immune checkpoint PD-L1 (Wang et al., 2017; Deng et al., 2014; Du et al., 2022). Indeed, IGF-1 stimulation was found to result in transcriptional mediated upregulation of PD-L1 surface

expression in prostate and colorectal cancer cells. Though PD-L1 expression was upregulated in both cancer cell lines, the increase in expression in colorectal cancer cells was higher than in DU145 prostate cancer cells, where PD-L1 was upregulated five-fold at the mRNA level but only ~1.7-fold at the cell surface by flow cytometry, with more modest PD-L1 upregulation (~1.2 fold) in other human and murine prostate cell lines. These experiments were only conducted in two prostate cancer and one colorectal cancer cell line and it is important to test these effects in other cell lines.

Future work should assess the functional consequences of PD-L1 upregulation in prostate cancer using CD8 T cell - cancer cell co-culture models and measuring T cell apoptosis as used by Chen et al (Chen et al., 2015). This would allow us to examine the T cell killing in a high IGF-1 environment. If IGF-1 is found to suppress T cell killing, involvement of PD-L1 could be assessed by blocking its effector immune checkpoint receptor PD-1 in the co-culture assays. It should also be noted that IGF-1 stimulation may have different effects on T cells and this could influence the interpretation of the result (Bilbao et al., 2014b; Miyagawa et al., 2017; Johannesson et al., 2014; Farabaugh et al., 2015; Lu et al., 2014; DiToro et al., 2020). Inhibition of IGF-1R has been reported to sensitise lung cancers to anti-PD1 treatment and resulted in tumour regression (Ajona et al., 2020). Similarly, work from others in our lab is currently assessing the combination effects of IGF-1 and PD-1 inhibition on prostate cancer using murine models. These experiments could also be repeated in colorectal cancer models where high serum IGF-1 associates with cancer risk and where, using an *in vitro* model, we have shown IGF-1 to upregulate PD-L1 expression (Knuppel et al., 2020; Rinaldi et al., 2010). With increasing numbers of patients developing adaptive

resistance to immunotherapy, many preclinical studies and clinical trials are testing checkpoint inhibitors in combination with other drugs and it is possible that combination with IGF axis inhibition may offer survival benefit (Aldea et al., 2021).

Finally, the association of serum and endogenous IGF-1 with components of the immune tumour microenvironment was analysed by characterising infiltrating cells including T lymphocytes into primary prostate tumours. Firstly, results from M-IF suggested that patients with high circulating IGF-1 had increased CD4 T cell infiltration, a potentially novel finding, and non-significant trend to PD-L1 upregulation (p=0.1504) in their tumours. Transcriptomic analysis of these tumours indicated that patients with high tumour *IGF1* displayed upregulation of IGF axis activation marker *IGFBP5*, chemokine *CXCL12* and downregulation of *TAP1*, required for antigen transport and presentation (Chen et al., 1996; Ling et al., 2017). Pathway analysis of transcriptomic data in high *IGF1* tumours suggested deregulation of focal adhesion, leukocyte transendothelial migration and multiple macrophage associated pathways. Finally, single-cell sequencing analysis of fresh prostate tumours showed infiltration of immunosuppressive M2 macrophages and MDSCs. This is consistent with other prostate cancer single-cell studies that have reported their infiltration (Chen et al., 2021; Song et al., 2022).

My results also found enrichment of *IGF1* in prostate cancer fibroblasts, which has been previously shown to be upregulated by AR in prostate cancer fibroblasts (Yu et al., 2013). We also found expression of *IGF2R* in the myeloid cells, CD8 proliferating and NK proliferating cells. IGF-2 via its action on IGF-2R has been shown to be important for macrophage maturation by sustaining oxidative phosphorylation resulting in anti-

inflammatory properties (Wang et al., 2020b; Du et al., 2019). DCs with increased IGF-2R expression were also associated with increased apoptosis (Suen et al., 2020). Increased IGF-2R expression in T cells were associated with uptake of apoptosis inducing Granzyme B and IGF-2R downregulation has been reported to promote CD8 T cell survival (Ahmed et al., 2015). The association of serum IGF-1 with CD4 infiltration and PD-L1 expression is supported by the *in vitro* data from Chapter 4, which showed that IGF-1 upregulated expression of multiple chemokines and PD-L1. By upregulating the expression chemokine ligands such as *CXCL8, CXCL10, CCL5* and *CCL4*, IGF-1 may attract leukocytes into the tumour (Gales et al., 2013; Huang et al., 2021; Bai et al., 2020; Zhang et al., 2021a). However, these cytokines have been predominantly associated with infiltration of immunosuppressive immune cells (Nagarsheth et al., 2017; Kohli et al., 2021; Ozga et al., 2021). Therefore, the functional status of the infiltrating CD4 cells need to be investigated to understand the effects serum IGF-1 may have on immune infiltration. This hypothesis that serum IGF-1 can influence immune infiltration can be tested by using chemotaxis assays where cancer cells will be stimulated with IGF-1 and migration of CD4 T cells can be measured.

Several findings from this project suggest that a high IGF-1 environment may induce immunosuppression by upregulating chemokines, PD-L1 and downregulating MHC Class I associated *TAP1*. This model is supported by previous work which reported IGF axis inhibition to induce MHC Class I upregulation and make murine tumours non-tumorigenic (Trojan et al., 1993; Resnicoff et al., 1994; Liu et al., 1998; Schillaci et al., 2006). Similarly, activation of PI3K-AKT and MAPK pathways downstream of the IGF axis has also been implicated in upregulating PD-L1 and chemokines (Kim and Suresh, 2013; Abdullah et al.,

2021; Xue et al., 2008; O'Donnell et al., 2018b; a; Hähnel et al., 2008; Sun et al., 2010; De Souza et al., 2014; Dituri et al., 2011). Experiments performed here using inhibitors of PI3K-AKT and MAPK suggest that both pathways contribute to IGF-induced PD-L1 expression in prostate cancer cells. However, some of the results are inconsistent with the idea that IGF-1 is an immunosuppressive cytokine. High serum IGF-1 associated with increased CD4 T cell infiltration, which depending on the phenotype of these cells could be immunosuppressive Tegs or tumour suppressive CD4 helper cells (Tay et al., 2020; Koretzky, 2010). Furthermore, *in vitro* IGF-1 stimulation led to the upregulation of *IFNB1*. In melanoma and colorectal cancer models, increased CD4 T cell infiltration has been reported to be important for anti-tumour immunity as they promote the function of CD8 T cells and B cells and are also involved in direct tumour cytotoxicity (Tay et al., 2020). Similarly, interferon beta encoded by *IFNB1*, has also been reported to suppress tumour growth by increasing the infiltration of CD8+ cells, inhibiting angiogenesis and proliferation, and blocking cancer stem cell associated properties (Enomoto et al., 2017; Lee et al., 2021; Doherty et al., 2017; Lu et al., 2019). Therefore, the above-mentioned functionality assays and immune migration experiments can help shed better insights into the specific role of IGF axis in each component of the immune tumour microenvironment. Experiments could also be conducted using prostate cancer patient derived organoids, which could be stimulated with IGF-1 *ex vivo* to examine the effects on individual immune cell components (Servant et al., 2021).

The main aim of this project was to investigate how a high IGF-1 environment could promote prostate cancer risk. It was not feasible to study the prostates of men prior to their cancer diagnosis, and given that IGF-1 has been associated with prostate cancer progression

and lethality, it was decided to study early localised cancers instead (Watts et al., 2020). Based on the results obtained in this work, it is possible that the association of IGF-1 and cancer risk and progression may be attributed at least partly to its immunosuppressive effects on the tumour microenvironment. As mentioned above, there are also confounding results to this hypothesis. An immunosuppressive role of IGF axis is supported by studies in other tumour types which have investigated the effects of fasting and caloric restriction on tumour growth. Fasting or caloric restriction has been reported to reduce the circulating levels of IGF-1 and has shown to promote anti-tumour effects in breast cancer and melanoma patients, and murine models of breast cancer, lung cancer and glioma (Caffa et al., 2020; Lee et al., 2012; Di Biase et al., 2016; Lee et al., 2010; Ajona et al., 2020; de Groot et al., 2020). Furthermore, the anti-tumour effects of diet restriction have been partly reported to involve the immune microenvironment. A recent cancer clinical trial reported that a fasting mimicking diet resulted in ~30% reduction in serum IGF-1, with reduced amounts of blood circulating immunosuppressive MDSCs and Tregs, and increased cytotoxic lymphocytes and NK cells (Vernieri et al., 2022). Analysis of breast cancer tumours from patients that underwent a fasting mimicking diet displayed reduction of IGF-1R and IGF-1R phosphorylation, with increased leukocyte infiltration estimated from transcriptional data using the XCell programme. Future work on the effects of circulating IGF on the immune system can use murine models which express a 3-fold elevation of serum Igf-1 due to expression of a hepatic Igf-1 transgene (Cannata et al., 2010). This transgenic 'HIT' mouse model has been previously used in our group to assess high Igf-1 effects on the transcriptional and mutational profiles of prostate cancer, which are currently being analysed. This model could be used to compare the immune profile of tumour infiltrating cells in prostate cancer tissue and the immune cells in circulation.

Though the association of the IGF axis with prostate cancer risk has been shown by analysis of serum IGF-1 levels (Watts et al., 2020; Travis et al., 2016), high serum IGF-1 may not necessarily represent high IGF axis activity as the bioactivity of free IGF-1 is regulated in blood and tissues by IGFBPs (Travis et al., 2016; Baxter, 2014). IGF-1 induced IGF-1R activation lead to receptor internalisation, required for downstream signalling (Romanelli et al., 2007)

and associated in previous work from our lab with clinical radioresistance (Aleksic et al., 2017), and in some cells to nuclear translocation (Aleksic et al., 2010; Sehat et al., 2010; Aleksic et al., 2018; Mills et al., 2021). Additionally, IGF axis activation has also reported to upregulate the expression of *IGFBP5* (Mohrin et al., 2021; Duan et al., 1996; Fleming et al., 2005; Kuemmerle, 2000; Ye and D'Ercole, 1998). Results from this project suggested increased IGF-1R internalisation in the malignant prostate epithelium as well as high *IGFBP5* in tumours with high endogenous *IGF1*. The methods optimised in this work, including M-IF and RNA-sequencing from FFPE tissues, will contribute to the upcoming windows trial of IGF blockade in men with early prostate cancer, funded by Prostate Cancer UK, with IGF neutralising antibody provided by Boehringer Ingelheim.

In summary, future work priorities are:

- → Test for the presence of cytosolic DNA and micronuclei after IGF-1 stimulation to characterise IGF-1 induced replication stress and activation of the cGAS-STING pathway.
- → Test for effects of IGF-1 induced PD-L1 expression in other prostate cancer and colorectal cancer cell lines.
- → Functional consequences of PD-L1 upregulation by IGF-1 in prostate cancer cell lines using CD8 T cell - cancer cell co-culture models.
- → Co-inhibition of IGF-1 and immune checkpoint PD-1 using prostate cancer murine models. This work is currently being performed in the lab.
- → Immune migration assays to test for IGF-1 induced migration of CD4 T cells and macrophages.
- → Characterising effects of high circulating IGF-1 on the immune infiltration and tumour mutational burden using murine models with 3-fold elevated serum Igf-1 levels (HIT mice).
- → Validating the genes identified using of the bulk RNA sequencing of patients with high vs low tumour endogenous *IGF1* using qT-PCR.
- → Validating the results of the single-cell sequencing on a second prostate cancer cohort. We are currently in collaboration with Dr Charlie Massie, University of Cambridge to access a second prostate cancer single-cell data (Tuong et al., 2021).

In conclusion, results from our work supports previous data showing that high IGF-1 environment can promote nuclear translocation of IGF-1R (Aleksic et al., 2010; Sehat et al., 2010; Aleksic et al., 2018; Mills et al., 2021). Furthermore, we found evidence that IGF-1 upregulates the expression of immunosuppressive cytokines and PD-L1 in prostate cancer cells, and in tissues associates with increased infiltration of CD4 T cells and downregulated expression of MHC Class I associated *TAP1* in the malignant prostatic cancer. Further work will be required to test the functional consequences of these associations, which if confirmed to be IGF-induced may contribute to tumour immune suppression. This effect could promote the growth of occult tumours to become clinically significant, and may also be relevant to prostate cancer treatment.

7 Chapter VII: Appendix

7.1 T cell infiltration and PD-L1 expression in cancer vs benign prostate sections

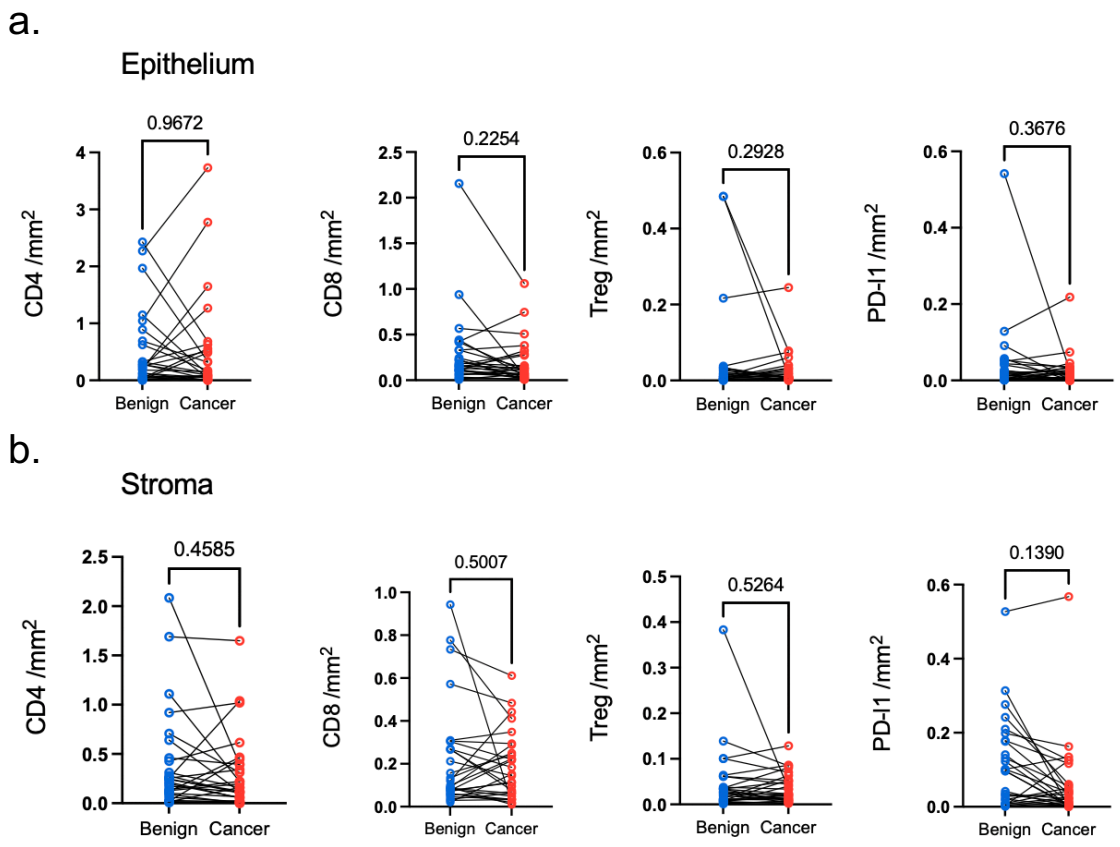


Figure 7-1 Immune infiltration and PD-L1 expression in prostate cancer. T cell infiltration in the (a) epithelium and (b) stromal compartment in cancer vs benign radical prostatectomy sections. Statistical significance was tested on the paired samples using a two tailed T Test.

7.2 T cell infiltration and PD-L1 expression in high vs low IGF-1R tumour areas

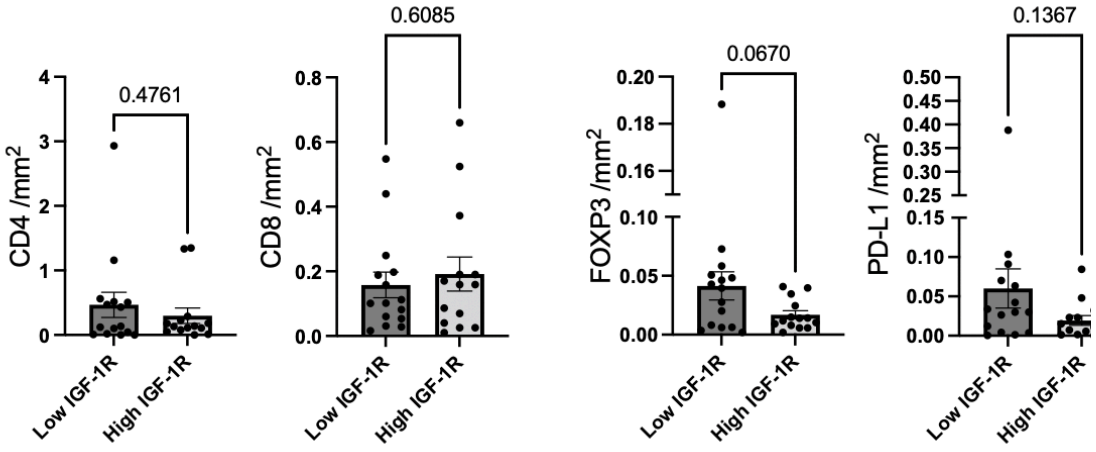


Figure 7-2 Association between IGF-1R expression, T cell infiltration and PD-L1 expression. CD4, CD8, FOXP3+ Treg and PD-L1 expression was measured on the cancer areas in radical prostatectomy samples split based on the median cancer expression of IGF-1R protein measured by IHC. Statistical significance was calculated using a two-tailed T test.

7.3 Analysis of T cell infiltration and PD-L1 expression with Gleason grade group and PSA.

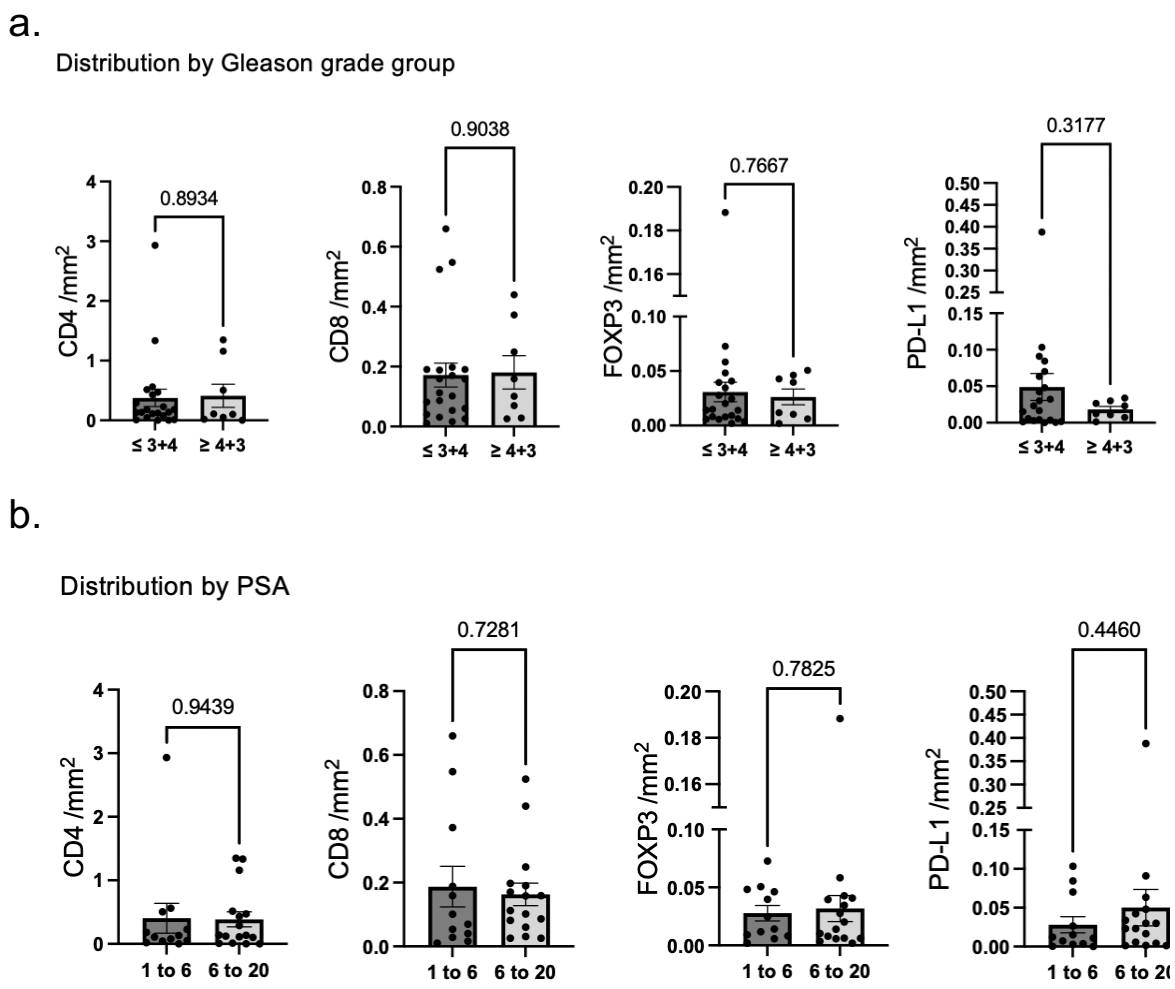


Figure 7-3 Associations between Gleason grade group and PSA levels on T cell infiltration and PD-L1 expression. (a) Radical prostatectomy samples were divided based on their Gleason grade group and T cell population and, PD-L1 expression was measured. The ≥ 4+3 group only had 8 samples compared to 21 samples in the ≤ 3+4 group. (b) T cell infiltration and PD-L1 expression was measured in radical prostatectomies where patients were divided based on their median PSA levels. As before, a two-tailed T test was used to analyse statistical significance.

7.4 List of differentially upregulated genes in patients with high endogenous *IGF1*

Symbol	Log2 Fold Change	Adjusted P value
HLF	1.712841529	0.03191786
HSPB6	1.678466408	4.94E-07
LSM11	1.675962136	0.01947629
STOX2	1.547606735	0.00812757
EYA1	1.526179168	0.00126306
TMEM47	1.506106951	0.0021494
CXCL12	1.466942724	0.00089657
WFDC1	1.433621782	0.00321785
GSTM2	1.402549099	0.00487168
CHRDL1	1.391332621	2.66E-05
FGFR2	1.323010435	0.00394187
BNC2	1.310444049	0.00280005
IGF1	1.298450579	6.66E-05
FAM153CP	1.281481589	0.00280005
COL4A6	1.263724804	0.00973634
LINC00578	1.251082319	0.00158791
PGR	1.246254671	0.00222397
PDE5A	1.244264244	1.76E-06
COL18A1-AS1	1.243564267	0.03974116
HSPB8	1.236212824	0.00812757

Symbol	Log2 Fold Change	Adjusted P value
NTRK2	1.222645039	0.01996205
GSTO2	1.212143958	0.04119804
AOX1	1.20586149	0.00591819
OGFRL1	1.195661779	0.00016792
ITIH5	1.191211809	0.00671254
GREB1L	1.184655664	0.01556595
KCNN3	1.171353877	0.028447
EYA4	1.171262748	0.02689601
EPB41L3	1.169585627	0.02869312
PI15	1.162148541	0.04539539
SLC8A1-AS1	1.160923825	0.02086744
NR2F2-AS1	1.157025036	0.01234924
CRYAB	1.15539537	0.00028198
EHD2	1.15508831	0.00021502
PCDH7	1.149606435	0.0021494
DMD	1.147894177	1.72E-05
MYLK	1.133027179	4.94E-07
CACNB4	1.131153715	0.04539539
RBFOX3	1.12907205	0.00928699
LSAMP	1.123549301	0.00758462
MCAM	1.117360486	0.00242103
DZIP1	1.10752698	0.0008989

Symbol	Log2 Fold Change	Adjusted P value
ATP1A2	1.104910705	0.00132786
PGM5	1.10393773	0.0265351
SYNPO2	1.103023498	9.01E-05
SLC8A1	1.097069215	0.00020423
SORBS1	1.094068485	1.76E-06
SYNM	1.086036746	0.00079313
PNMA1	1.080391644	0.00454997
MSRB3	1.078630282	8.64E-06
BRF2	1.078044135	0.00139337
MEIS1	1.07684264	9.01E-05
POLR2M	1.07505223	0.01108453
HDAC9	1.071949344	0.00537524
MYL9	1.067074751	1.15E-05
LINC02210	1.062961427	0.01556595
AHNAK2	1.062394653	0.02686501
KLHL5	1.058967876	5.39E-05
FHOD3	1.04704755	0.01444691
CPEB3	1.042325533	0.01482067
CLIP4	1.039341118	0.00591819
CLIP3	1.032522104	0.01224486
CERK	1.029942579	0.03594525
ARHGEF6	1.025332288	0.04865561

Symbol	Log2 Fold Change	Adjusted P value
CCDC80	1.021613964	0.0012624
PMP22	1.017970592	0.04919924
SPEG	1.015956126	0.00299004
MYH11	1.014226921	6.29E-05
NDE1	1.008519101	5.39E-05
FZD7	1.004915105	0.00089657
ACTA2-AS1	1.002563231	2.30E-05
FRMD6	0.996006994	0.00241382
MYLK-AS1	0.992560034	0.00591819
SELENOM	0.992543591	0.01889468
CPED1	0.989902228	0.01275744
LIMS2	0.983675863	0.00015092
ADAM33	0.983058224	0.00783137
ACOT11	0.982888511	0.03375809
MFAP4	0.979442884	0.00955539
ACTA2	0.977887107	2.09E-05
ACTG2	0.973137962	0.00206606
PBX1	0.972150289	5.39E-05
CSRP1	0.970049614	4.94E-07
ZNF483	0.967812437	0.00158001
CLMP	0.950768242	0.02889096
KCNMA1	0.941709394	0.00248034

Symbol	Log2 Fold Change	Adjusted P value
SMC6	0.939984903	0.04539539
IRAG1	0.939161803	0.00028198
ZRANB3	0.933798704	0.04875169
GAS1	0.931355564	0.04404452
MGST3	0.924510037	0.01923788
CDC42EP3	0.922423429	0.00134912
ZEB1	0.920015819	0.01275744
AOC3	0.918144604	0.04404452
LAMA4	0.915740423	0.0008989
ADAMTS9-AS2	0.914912315	0.00512479
COL4A4	0.913923361	0.01138736
ITGA7	0.911558262	0.01234924
FAT3	0.905791431	0.01724254
GFOD1	0.905788374	0.02408989
MEIS2	0.903224069	0.00817268
MAP1A	0.899066385	0.01433159
PTGIS	0.898065446	0.01662372
SH3PXD2B	0.897337044	0.00016973
PRRX1	0.890048431	0.01768349
MEG3	0.888736142	0.00142844
FERMT2	0.884268472	0.00015092
LMOD1	0.882779071	0.00500031

Symbol	Log2 Fold Change	Adjusted P value
IGSF9B	0.881783181	0.00877437
PTGDS	0.880902744	0.04832475
ACACB	0.874896177	0.00533438
COL4A3	0.866635303	0.00697683
ZMAT1	0.865281188	0.00222397
NR2F1-AS1	0.861875717	0.01195635
TAGLN	0.861812291	5.28E-06
SCRN1	0.860106221	0.00531566
MMP2	0.856478429	0.0137513
CDKL1	0.856017535	0.00546376
CNN1	0.852398046	0.00062629
FLRT2	0.851519838	0.03493639
OSGEP	0.8504524	0.0306553
TPM1	0.841764997	0.00015633
FHL1	0.840451172	0.00962286
PPP1R12B	0.835996504	0.00013582
ABCC9	0.830685685	0.0306553
PRKACA	0.825672463	0.00118079
FLNA	0.825003225	0.00141675
CLK4	0.824460695	0.00815004
DPYSL3	0.819529007	0.00142844
TPM2	0.818102112	0.00497173

Symbol	Log2 Fold Change	Adjusted P value
CALD1	0.815104194	0.00012726
STARD9	0.813860843	0.04173191
ZC3H6	0.809226351	0.02419555
PLEKHA1	0.804188502	0.01889468
ABCA5	0.80124474	0.00015457
CAVIN1	0.799884824	0.00062629
BOC	0.798569838	0.01123595
CELF2	0.794802385	0.0136369
BCL2	0.793134757	0.02424047
SMTN	0.787152354	0.00085443
PLEKHO1	0.786400945	0.04017232
MFF-DT	0.786004007	0.04828428
DPY19L4	0.782048221	0.04442747
RBPMS	0.780715503	0.00144759
TNS1	0.776137784	6.95E-05
DENND2B	0.771314043	0.00242103
DENND3	0.752876968	0.00532785
KCTD12	0.750701015	0.02257166
GLI3	0.747629071	0.02559531
ATP2B4	0.74679396	6.66E-05
MMP14	0.74152173	0.03718591
VCL	0.740465102	0.00048176

Symbol	Log2 Fold Change	Adjusted P value
MKNK1	0.734640232	0.04173191
PCSK7	0.734251966	3.45E-06
SERPINF1	0.733911435	0.04156128
FBLN1	0.732954414	0.00523024
EDNRA	0.731431221	0.02679989
SETBP1	0.729173844	0.00126306
TSC22D3	0.726591453	0.0001078
NKD1	0.724460642	0.03376063
FOXO1	0.716853858	0.0306553
FILIP1L	0.715860949	0.02192633
TIMP2	0.71502874	0.00338474
EVA1C	0.711671486	0.0280816
IGFBP5	0.711308889	0.01108453
PLPP3	0.709082781	0.01558913
DES	0.707347155	0.00958611
VSTM4	0.704413973	0.036173
NFASC	0.696462915	0.01792717
PRKCA	0.6945625	0.0170485
ALDH3A2	0.694162221	0.01537169
MIR99AHG	0.694101493	0.02013611
EPB41L2	0.693766668	0.04977766
ABLIM1	0.692786141	0.01275744

Symbol	Log2 Fold Change	Adjusted P value
NFIA	0.691545868	0.00155381
CALM1	0.687634859	0.00653566
COL14A1	0.68286469	0.03594525
DCN	0.682680316	0.0149974
MXRA7	0.676377886	0.04472116
JCAD	0.675046689	0.02604207
COL27A1	0.672394808	0.03846976
PARM1	0.671217231	0.01889468
PARVA	0.671209191	3.84E-05
BACE1	0.669611311	0.01743017
LOC101927060	0.668031743	0.02408989
KLF7	0.665318168	0.03974116
CLIC4	0.658600096	0.01556595
ARHGAP10	0.647803726	0.01576389
CCND2	0.639850388	0.03313157
EHBP1L1	0.635561952	0.00731743
DST	0.632902431	0.01400862
PALLD	0.630965991	0.01100447
KANK1	0.62351424	0.03717935
FBN1	0.616989537	0.00682724
PDLIM7	0.6075436	0.03718591
ERC1	0.604288167	0.01632798

Symbol	Log2 Fold Change	Adjusted P value
PIAS1	0.604237122	0.02889096
TIMP3	0.603046419	0.04505199
PDCD4	0.592506394	0.04248586
KANK2	0.58459911	0.01247786
SPARCL1	0.576134219	0.02701027
EZH1	0.575650465	0.03376063
ZFP36L1	0.555612149	0.02692239
ANO6	0.542228359	0.02499177
COL4A5	0.539273059	0.01262784
ATXN1L	0.53504211	0.00889164
PPIG	0.533924324	0.04626966
GSN	0.52813239	0.03547268
RBFOX2	0.502025152	0.0275306
QKI	0.501224535	0.04505199
ALG13	0.499298482	0.03718591
RORA	0.497312177	0.0199452
MSN	0.492299696	0.03477778
PPP1R12A	0.487513115	0.04828428
TACC1	0.480893189	0.04970025
LPP	0.468079971	0.02329247
FBXO32	0.4559485	0.04886196
SORBS2	0.451864363	0.03357846

Symbol	Log2 Fold Change	Adjusted P value
SNX27	0.384850859	0.04505199
ARID1B	0.380202936	0.02454661

Table 7-1 List of differentially upregulated genes in high *IGF1* patients. Patients were divided based on their median normalised tumour endogenous *IGF1* expression obtained from RNA sequencing. Differential gene expression was calculated using the DESEQ2 pipeline and genes with P adjusted value < 0.05 after multiple testing with Benjamini-Hochberg method were called as significant.

7.5 List of differentially downregulated genes in patients with high endogenous *IGF1*

Symbol	Log2 Fold Change	Adjusted P value
GRAMD4	-2.974838163	0.00276303
ACSM1	-2.185699529	0.02937761
HK2	-2.153935749	0.04828428
F5	-2.134024536	0.03974116
ASRGL1	-1.861015593	0.036173
SIPA1L2	-1.580481452	0.02810647
AEN	-1.449633741	0.01918223
ABCG1	-1.401596786	0.03705799
PRSS8	-1.341741541	0.00193892
MAP2K3	-1.307819472	0.00062629
FARSA	-1.193161782	0.03974116
FSIP1	-1.184509238	0.04970025
NUDT9	-1.179468584	0.01632798
PKP3	-1.128203159	0.0137513
ITPKC	-1.087847718	0.01035772
IFRD2	-1.083222533	0.00872418
SNX22	-1.063766328	0.00645111
GNL3	-1.062764772	0.00624833

Symbol	Log2 Fold Change	Adjusted P value
TMC5	-1.059666326	0.00280005
ARHGEF38	-1.021582269	0.00116458
FNIP2	-1.01372652	0.00394187
CLDN4	-0.995678251	0.00838131
HELZ2	-0.990637532	0.00742831
ENTR1	-0.987103049	0.00803038
PYCR1	-0.985240628	0.00454997
TAP1	-0.980935493	0.01039673
GNL2	-0.976037362	0.02999703
SOX4	-0.97030785	0.00667226
MAL2	-0.970213695	0.0262971
SHROOM3	-0.969803119	0.00050814
GUCY1A1	-0.969437151	0.0023785
CIB1	-0.946705164	0.04626966
RAP1GAP	-0.935137806	0.00656714
RRP12	-0.93483872	0.00645111
TMEM30B	-0.920098311	0.0150818
LINC00662	-0.919760729	0.02854719
ZDHHC9	-0.91554331	0.01102741
LDHA	-0.90642628	0.02408989

Symbol	Log2 Fold Change	Adjusted P value
NCDN	-0.890886988	0.02329247
SLC44A4	-0.864020541	0.00070608
MCTP2	-0.853113809	0.0026361
LDLR	-0.849411441	0.02344356
SLC37A1	-0.845276033	0.0137513
TRAF4	-0.838240404	0.04310803
DNMBP	-0.835065219	0.00135782
UGDH	-0.83088984	0.03361254
PPIB	-0.826695642	0.0126466
ABCC4	-0.82434618	0.00438617
RALGAPA2	-0.821348097	0.0199452
ALCAM	-0.82013718	0.01820271
SGMS2	-0.817290867	0.03594525
EPS8L2	-0.817106936	0.00758462
ST14	-0.815165332	0.00131944
ARFGAP3	-0.814159597	0.02147208
RASEF	-0.801953795	0.03990529
FURIN	-0.799470491	0.02257166
EDRF1	-0.797221091	0.04828428
SEL1L3	-0.795633294	0.02408989

Symbol	Log2 Fold Change	Adjusted P value
CEMIP2	-0.795471384	0.01464431
RPN2	-0.795196913	0.01148573
DIAPH1	-0.795188938	0.00371712
LINC01128	-0.788545916	0.02559531
CHPF2	-0.785649944	0.00812757
ARFGEF3	-0.78419634	0.01754395
RHPN2	-0.775007415	0.01996205
FAM83H	-0.771901791	0.03631432
SERINC5	-0.771584671	0.00962286
PSMB5	-0.771041285	0.03594525
PVR	-0.767083855	0.04173191
POR	-0.763419313	0.02192982
GFOD2	-0.75548288	0.03370762
KRT18	-0.736735091	0.02075653
EZR	-0.734517565	0.00742831
CCT2	-0.731998366	0.04471371
DHCR24	-0.730149707	0.00602462
MBOAT2	-0.719322697	0.03718591
ARHGAP32	-0.718037043	0.00441366
CAMKK2	-0.71428675	0.04906104

Symbol	Log2 Fold Change	Adjusted P value
DTX3L	-0.713881744	0.00280005
HSPA5	-0.698164862	0.01138736
KRT8	-0.683653101	0.04440433
TMC6	-0.681937886	0.02066849
MBD3	-0.679314178	0.02272517
SPTBN2	-0.675911645	0.0129434
ECE1	-0.659246526	0.01108453
SEC16A	-0.653672622	0.00320361
RBM47	-0.653262386	0.00442561
ATP1A1	-0.65282474	0.0008989
MLPH	-0.650324369	0.01947629
BRI3	-0.647983322	0.04865561
GRHL2	-0.635418296	0.03242064
MAP7	-0.62956577	0.03594525
ZNF692	-0.623149213	0.02192982
UNC13B	-0.621474513	0.02185687
STK40	-0.621423612	0.04739563
ITPR3	-0.613239141	0.02842267
ENO1	-0.612251174	0.03705799
GPAT4	-0.603597656	0.0399242

Symbol	Log2 Fold Change	Adjusted P value
PIEZO1	-0.601679494	0.02163804
RACK1	-0.598450354	0.03405603
ZBTB7B	-0.593824028	0.04112184
DOP1B	-0.586477547	0.0312864
ABCC1	-0.581558545	0.03832473
AGPAT3	-0.581070209	0.01889468
GCN1	-0.569192992	0.00492476
FOXA1	-0.565753581	0.01387817
PHC2	-0.562176401	0.04183242
TOP3A	-0.556491979	0.04404452
POLR1A	-0.55313053	0.0136369
CYFIP1	-0.543424723	0.02155228
ATP1A1-AS1	-0.536715927	0.03275187
PHF12	-0.533492086	0.04828428
RANBP2	-0.530645932	0.03376063
PLXNA3	-0.509429546	0.0265351
KIAA1522	-0.507077728	0.02499177
KDELR2	-0.495242779	0.03375809
RPL7L1	-0.490733052	0.04919924
TMEM214	-0.489245445	0.0328105

Symbol	Log2 Fold Change	Adjusted P value
TULP4	-0.484385371	0.02950612
ATP5F1B	-0.48340934	0.0265351
UTRN	-0.477657266	0.0199452
GSPT1	-0.477116802	0.01803598
SURF4	-0.454835031	0.03376063
BRD2	-0.447213956	0.00491221
TLE3	-0.419642235	0.01195635
GOLGA3	-0.363563501	0.01918223

Table 7-2 List of differentially downregulated genes in high *IGF1* patients. Patients were divided based on their median normalised tumour endogenous *IGF1* expression obtained from RNA sequencing. Differential gene expression was calculated using the DESEQ2 pipeline and genes with P adjusted value < 0.05 after multiple testing with Benjamini-Hochberg method were called as significant.

References

Abdelhamed, S., K. Ogura, S. Yokoyama, I. Saiki, and Y. Hayakawa. 2016. AKT-STAT3 pathway as a downstream target of egfr signaling to regulate PD-l1 expression on NSCLC cells. *J. Cancer*. 7:1579–1586. doi:10.7150/jca.14713.

Abdullah, L., L.B. Hills, E.B. Winter, and Y.H. Huang. 2021. Diverse Roles of Akt in T cells. *Immunometabolism*. 3. doi:10.20900/IMMUNOMETAB20210007.

Adams, T.E., V.C. Epa, T.P.J. Garrett, and C.W. Ward*. 2000. Structure and function of the type 1 insulin-like growth factor receptor. *Cell. Mol. Life Sci.* 57:1050–1093. doi:10.1007/PL00000744.

Agoulnik, I.U., A. Vaid, M. Nakka, M. Alvarado, W.E. Bingman, H. Erdem, A. Frolov, C.L. Smith, G.E. Ayala, M.M. Ittmann, and N.L. Weigel. 2006. Androgens modulate expression of transcription intermediary factor 2, an androgen receptor coactivator whose expression level correlates with early biochemical recurrence in prostate cancer. *Cancer Res.* 66:10594–10602. doi:10.1158/0008-5472.CAN-06-1023.

Ahearn, T.U., S. Peisch, A. Pettersson, E.M. Ebot, C.K. Zhou, R.E. Graff, J.A. Sinnott, L. Fazli, G.L. Judson, T.A. Bismar, J.R. Rider, T. Gerke, J.M. Chan, M. Fiorentino, R. Flavin, H.D. Sesso, S. Finn, E.L. Giovannucci, M. Gleave, M. Loda, Z. Li, M. Pollak, and L.A. Mucci. 2018. Expression of IGF/insulin receptor in prostate cancer tissue and progression to lethal disease. *Carcinogenesis*. 39:1431–1437. doi:10.1093/CARCIN/BGY112.

Von Ahlfen, S., A. Missel, K. Bendrat, and M. Schlumpberger. 2007. Determinants of RNA Quality from FFPE Samples. *PLoS One*. 2:e1261. doi:10.1371/JOURNAL.PONE.0001261.

Ahmed, K.A., L. Wang, P. Griebel, D.D. Mousseau, and J. Xiang. 2015. Differential expression of mannose-6-phosphate receptor regulates T cell contraction. *J. Leukoc. Biol.* 98:313–318. doi:10.1189/JLB.2HI0215-049RR.

Ahn, S., J. Lee, M. Hong, S.T. Kim, S.H. Park, M.G. Choi, J.H. Lee, T.S. Sohn, J.M. Bae, S. Kim, S.H. Jung, W.K. Kang, and K.M. Kim. 2016. FGFR2 in gastric cancer: protein overexpression predicts gene amplification and high H-index predicts poor survival. *Mod. Pathol. 2016 299*. 29:1095–1103. doi:10.1038/modpathol.2016.96.

Ajona, D., S. Ortiz-Espinosa, T. Lozano, F. Exposito, A. Calvo, K. Valencia, M. Redrado, A. Remírez, F. Lecanda, D. Alignani, J.J. Lasarte, I. Macaya, Y. Senent, C. Bértolo, C. Sainz, I. Gil-Bazo, I. Eguren-Santamaría, J.M. Lopez-Picazo, A. Gonzalez, J.L. Perez-Gracia, C.E. de Andrea, S. Vicent, M.F. Sanmamed, L.M. Montuenga, and R. Pio. 2020. Short-term starvation reduces IGF-1 levels to sensitize lung tumors to PD-1 immune checkpoint blockade. *Nat. Cancer*. 1:75–85. doi:10.1038/s43018-019-0007-9.

Al-Saad, S., E. Richardsen, T.K. Kilvaer, T. Donnem, S. Andersen, M. Khanehkenari, R.M. Bremnes, and L.T. Busund. 2017. The impact of MET, IGF-1, IGF1R expression and EGFR mutations on survival of patients with non-small-cell lung cancer. *PLoS One*. 12. doi:10.1371/JOURNAL.PONE.0181527.

Alao, J.P. 2007. The regulation of cyclin D1 degradation: roles in cancer development and the potential for therapeutic invention. *Mol. Cancer*. 6. doi:10.1186/1476-4598-6-24.

Alberts, B., A. Johnson, J. Lewis, M. Raff, K. Roberts, and P. Walter. 2002. Molecular Biology of the Cell. Garland Science, New York.

Aldea, M., F. Andre, A. Marabelle, S. Dogan, F. Barlesi, and J.C. Soria. 2021. Overcoming Resistance to Tumor-Targeted and Immune-Targeted Therapies. *Cancer Discov.* 11:874–899. doi:10.1158/2159-8290.CD-20-1638.

Aldinucci, D., and A. Colombatti. 2014. The Inflammatory Chemokine CCL5 and Cancer Progression. *Mediators Inflamm.* 2014. doi:10.1155/2014/292376.

Aleksic, T., M.M. Chitnis, O. V Perestenko, S. Gao, P.H. Thomas, G.D. Turner, A.S. Protheroe, M. Howarth, and V.M. Macaulay. 2010. Type 1 insulin-like growth factor receptor translocates to the nucleus of human tumor cells. *Cancer Res.* 70:6412–9. doi:10.1158/0008-5472.CAN-10-0052.

Aleksic, T., N. Gray, X. Wu, G. Rieunier, E. Osher, J. Mills, C. Verrill, R.J. Bryant, C. Han, K. Hutchinson, A.G. Lambert, R. Kumar, F.C. Hamdy, U. Weyer-Czernilofsky, M.P. Sanderson, T. Bogenrieder, S. Taylor, and V.M. Macaulay. 2018. Nuclear IGF1R Interacts with Regulatory Regions of Chromatin to Promote RNA Polymerase II Recruitment and Gene Expression Associated with Advanced Tumor Stage. *Cancer Res.* 78:3497–3509. doi:10.1158/0008-5472.CAN-17-3498.

Aleksic, T., A. Ross Worrall, C. Verrill, H. Turley, L. Campo, and V.M. Macaulay. 2016.

Improved Immunohistochemical Detection of Type 1 Insulin-Like Growth Factor Receptor in Human Tumors. *Immunochem. Immunopathol.* 02:1–5. doi:10.4172/2469-9756.1000114.

Aleksic, T., C. Verrill, R.J. Bryant, C. Han, A.R. Worrall, L. Brureau, S. Larré, G.S. Higgins, F. Fazal, A. Sabbagh, S. Haider, F.M. Buffa, D. Cole, and V.M. MacAulay. 2017. IGF-1R associates with adverse outcomes after radical radiotherapy for prostate cancer. *Br. J. Cancer 2017 11711*. 117:1600–1606. doi:10.1038/bjc.2017.337.

Alexandrov, L.B., S. Nik-Zainal, D.C. Wedge, S.A.J.R. Aparicio, S. Behjati, A. V. Biankin, G.R. Bignell, N. Bolli, A. Borg, A.L. Børresen-Dale, S. Boyault, B. Burkhardt, A.P. Butler, C. Caldas, H.R. Davies, C. Desmedt, R. Eils, J.E. Eyfjörd, J.A. Foekens, M. Greaves, F. Hosoda, B. Hutter, T. Ilicic, S. Imbeaud, M. Imielinsk, N. Jäger, D.T.W. Jones, D. Jonas, S. Knappskog, M. Koo, S.R. Lakhani, C. López-Otín, S. Martin, N.C. Munshi, H. Nakamura, P.A. Northcott, M. Pajic, E. Papaemmanuil, A. Paradiso, J. V. Pearson, X.S. Puente, K. Raine, M. Ramakrishna, A.L. Richardson, J. Richter, P. Rosenstiel, M. Schlesner, T.N. Schumacher, P.N. Span, J.W. Teague, Y. Totoki, A.N.J. Tutt, R. Valdés-Mas, M.M. Van Buuren, L. Van 'T Veer, A. Vincent-Salomon, N. Waddell, L.R. Yates, J. Zucman-Rossi, P. Andrew Futreal, U. McDermott, P. Lichter, M. Meyerson, S.M. Grimmond, R. Siebert, E. Campo, T. Shibata, S.M. Pfister, P.J. Campbell, and M.R. Stratton. 2013. Signatures of mutational processes in human cancer. *Nat. 2013 5007463*. 500:415–421. doi:10.1038/nature12477.

Ali, A., A. Hoyle, Á.M. Haran, C.D. Brawley, A. Cook, C. Amos, J. Calvert, H. Douis, M.D. Mason, D. Dearnaley, G. Attard, S. Gillessen, M.K.B. Parmar, C.C. Parker, M.R. Sydes, N.D. James, and N.W. Clarke. 2021. Association of Bone Metastatic Burden With Survival Benefit From Prostate Radiotherapy in Patients With Newly Diagnosed Metastatic Prostate Cancer: A Secondary Analysis of a Randomized Clinical Trial. *JAMA Oncol.* 7:555–563. doi:10.1001/JAMAONCOL.2020.7857.

Alshetaiwi, H., N. Pervolarakis, L.L. McIntyre, D. Ma, Q. Nguyen, J.A. Rath, K. Nee, G. Hernandez, K. Evans, L. Torosian, A. Silva, C. Walsh, and K. Kessenbrock. 2020. Defining the emergence of myeloid-derived suppressor cells in breast cancer using single-cell transcriptomics. *Sci. Immunol.* 5.

doi:10.1126/SCIIMMUNOL.AAY6017/SUPPL_FILE/AAY6017_TABLE_S9.XLSX
.

Alzahrani, A.S. 2019. PI3K/Akt/mTOR inhibitors in cancer: At the bench and bedside. *Semin. Cancer Biol.* 59:125–132. doi:10.1016/J.SEMCANCER.2019.07.009.

Ambjørn, M., P. Ejlerskov, Y. Liu, M. Lees, M. Jäättelä, and S. Issazadeh-Navikas. 2013. IFNB1/interferon-β-induced autophagy in MCF-7 breast cancer cells counteracts its proapoptotic function. *Autophagy*. 9:287. doi:10.4161/AUTO.22831.

Amouzegar, A., M. Chelvanambi, J.N. Filderman, W.J. Storkus, and J.J. Luke. 2021. STING Agonists as Cancer Therapeutics. *Cancers 2021, Vol. 13, Page 2695*. 13:2695. doi:10.3390/CANCERS13112695.

Andersen, M., D. Nørgaard-Pedersen, J. Brandt, I. Pettersson, and R. Slaaby. 2017. IGF1 and IGF2 specificities to the two insulin receptor isoforms are determined by insulin receptor amino acid 718. *PLoS One*. 12:e0178885. doi:10.1371/journal.pone.0178885.

Antonarakis, E.S., J.M. Piulats, M. Gross-Goupil, J. Goh, K. Ojamaa, C.J. Hoimes, U. Vaishampayan, R. Berger, A. Sezer, T. Alanko, R. de Wit, C. Li, A. Omlin, G. Procopio, S. Fukasawa, K. ichi Tabata, S.H. Park, S. Feyerabend, C.G. Drake, H. Wu, P. Qiu, J. Kim, C. Poehlein, and J.S. de Bono. 2020. Pembrolizumab for treatment-refractory metastatic castration-resistant prostate cancer: Multicohort, open-label phase II KEYNOTE-199 study. *J. Clin. Oncol.* 38:395–405. doi:10.1200/JCO.19.01638.

Argyle, D., and T. Kitamura. 2018. Targeting macrophage-recruiting chemokines as a novel therapeutic strategy to prevent the progression of solid tumors. *Front. Immunol.* 9:2629. doi:10.3389/FIMMU.2018.02629/BIBTEX.

Asmane, I., E. Watkin, L. Alberti, A. Duc, P. Marec-Berard, I. Ray-Coquard, P. Cassier, A.V. Decouvelaere, D. Ranchère, J.E. Kurtz, J.P. Bergerat, and J.Y. Blay. 2012. Insulin-like growth factor type 1 receptor (IGF-1R) exclusive nuclear staining: A predictive biomarker for IGF-1R monoclonal antibody (Ab) therapy in sarcomas. *Eur. J. Cancer*. 48:3027–3035. doi:10.1016/J.EJCA.2012.05.009.

Attard, G., L. Murphy, N.W. Clarke, W. Cross, R.J. Jones, C.C. Parker, S. Gillessen, A. Cook, C. Brawley, C.L. Amos, N. Atako, C. Pugh, M. Buckner, S. Chowdhury, Z.

Malik, J.M. Russell, C. Gilson, H. Rush, J. Bowen, A. Lydon, I. Pedley, J.M. O'Sullivan, A. Birtle, J. Gale, N. Srihari, C. Thomas, J. Tanguay, J. Wagstaff, P. Das, E. Gray, M. Alzoueb, O. Parikh, A. Robinson, I. Syndikus, J. Wylie, A. Zarkar, G. Thalmann, J.S. de Bono, D.P. Dearnaley, M.D. Mason, D. Gilbert, R.E. Langley, R. Millman, D. Matheson, M.R. Sydes, L.C. Brown, M.K.B. Parmar, N.D. James, E. Jones, K. Hyde, H. Glen, S. Needleman, U. McGovern, D. Sheehan, S. Paisey, R. Shaffer, M. Beresford, E. Porfiri, D. Fackrell, L. Lee, T. Sreenivasan, S. Brock, S. Brown, A. Bahl, M. Smith-Howell, C. Woodward, M.D. Phan, D. Mazhar, K. Narahari, F. Douglas, A. Kumar, A. Hamid, A. Ibrahim, D. Muthukumar, M. Simms, J. Worlding, A. Tran, M. Kagzi, C. Pezaro, V. Sivoglo, B. Masters, P. Keng-Koh, C. Manetta, D. McLaren, N. Gupta, S. Boussios, H. Taylor, J. Graham, C. Perna, L. Melcher, W. Grant, A. Sabharwal, U. Hofmann, R. Dealey, N. McPhail, R. Brierly, L. Capaldi, N. Sidek, et al. 2022. Abiraterone acetate and prednisolone with or without enzalutamide for high-risk non-metastatic prostate cancer: a meta-analysis of primary results from two randomised controlled phase 3 trials of the STAMPEDE platform protocol. *Lancet (London, England)*. 399:447–460. doi:10.1016/S0140-6736(21)02437-5.

Bach, L.A. 2018. IGF-binding proteins. *J. Mol. Endocrinol.* 61:T11–T28. doi:10.1530/JME-17-0254.

Badolato, R., H.M. Bond, G. Valerio, A. Petrella, G. Morrone, M.J. Waters, S. Venuta, and A. Tenore. 1994. Differential expression of surface membrane growth hormone receptor on human peripheral blood lymphocytes detected by dual fluorochrome flow cytometry. *J. Clin. Endocrinol. Metab.* 79:984–990. doi:10.1210/JCEM.79.4.7962309.

Badzio, A., M.W. Wynes, R. Dziadziuszko, D.T. Merrick, M. Pardo, W. Rzyman, A. Kowalczyk, S. Singh, J. Ranger-Moore, G. Manriquez, F. Gaire, J. Jassem, and F.R. Hirsch. 2010. Increased insulin-like growth factor 1 receptor (IGF1R) protein expression and gene copy number in small cell lung cancer. *J. Thorac. Oncol.* 5:1905. doi:10.1097/JTO.0B013E3181F38F57.

Bai, D., L. Ueno, and P.K. Vogt. 2009. Akt-mediated regulation of NFκB and the essentialness of NFκB for the oncogenicity of PI3K and Akt. *Int. J. Cancer*.

125:2863. doi:10.1002/IJC.24748.

Bai, S., Y.Y. Wu, Y. Yan, H. Kang, J. Zhang, W. Ma, Y. Gao, B. Hui, R. Li, X. Zhang, and J. Ren. 2020. The effect of CCL5 on the immune cells infiltration and the prognosis of patients with kidney renal clear cell carcinoma. *Int. J. Med. Sci.* 17:2917. doi:10.7150/IJMS.51126.

Baker, J., J.P. Liu, E.J. Robertson, and A. Efstratiadis. 1993. Role of insulin-like growth factors in embryonic and postnatal growth. *Cell*. 75:73–82. doi:10.1016/S0092-8674(05)80085-6.

Bakin, R.E., D. Gioeli, R.A. Sikes, E.A. Bissonette, M.J. Weber, R. Vigneri, and A. Belfiore. 2003. Constitutive activation of the Ras/mitogen-activated protein kinase signaling pathway promotes androgen hypersensitivity in LNCaP prostate cancer cells. *Cancer Res.* 63:1981–9. doi:10.1158/0008-5472.can-04-1837.

Balaram, S. 1999. Insulin like growth factor-1 activates nuclear factor-κB and increases transcription of the intercellular adhesion molecule-1 gene in endothelial cells. *Cardiovasc. Surg.* 7:91–97. doi:10.1016/S0967-2109(98)00044-1.

Balk, S.P., Y.J. Ko, and G.J. Bubley. 2003. Biology of prostate-specific antigen. *J. Clin. Oncol.* 21:383–391. doi:10.1200/JCO.2003.02.083.

Bandaru, P., Y. Kondo, and J. Kuriyan. 2019. The Interdependent Activation of Son-of-Sevenless and Ras. *Cold Spring Harb. Perspect. Med.* 9. doi:10.1101/CSHPERSPECT.A031534.

Bansal, D., M.A. Reimers, E.M. Knoche, and R.K. Pachynski. 2021. Immunotherapy and Immunotherapy Combinations in Metastatic Castration-Resistant Prostate Cancer. *Cancers 2021, Vol. 13, Page 334*. 13:334. doi:10.3390/CANCERS13020334.

Barclay, W.W., and S.D. Cramer. 2005. Culture of mouse prostatic epithelial cells from genetically engineered mice. *Prostate*. 63:291–298. doi:10.1002/PROS.20193.

Barrett, J.P., A.M. Minogue, A. Falvey, and M.A. Lynch. 2015. Involvement of IGF-1 and Akt in M1/M2 activation state in bone marrow-derived macrophages. *Exp. Cell Res.* 335:258–268. doi:10.1016/J.YEXCR.2015.05.015.

Baserga, R. 2013. The decline and fall of the IGF-I receptor. *J. Cell. Physiol.* 228:675–679. doi:10.1002/jcp.24217.

Baserga, R., F. Peruzzi, and K. Reiss. 2003. The IGF-1 receptor in cancer biology. *Int. J.*

Cancer. 107:873–877. doi:10.1002/ijc.11487.

Baudler, S., J. Baumgartl, B. Hampel, T. Buch, A. Waisman, C.M. Snapper, W. Krone, and J.C. Brüning. 2005. Insulin-like growth factor-1 controls type 2 T cell-independent B cell response. *J. Immunol.* 174:5516–5525. doi:10.4049/JIMMUNOL.174.9.5516.

Baxter, R.C. 2014. IGF binding proteins in cancer: mechanistic and clinical insights. *Nat. Rev. Cancer 2014 145*. 14:329–341. doi:10.1038/nrc3720.

Beer, T.M., E.D. Kwon, C.G. Drake, K. Fizazi, C. Logothetis, G. Gravis, V. Ganju, J. Polikoff, F. Saad, P. Humanski, J.M. Piulats, P.G. Mella, S.S. Ng, D. Jaeger, F.X. Parnis, F.A. Franke, J. Puente, R. Carvajal, L. Sengeløv, M.B. McHenry, A. Varma, A.J. Van Den Eertwegh, and W. Gerritsen. 2017. Randomized, Double-Blind, Phase III Trial of Ipilimumab Versus Placebo in Asymptomatic or Minimally Symptomatic Patients With Metastatic Chemotherapy-Naive Castration-Resistant Prostate Cancer. *J. Clin. Oncol.* 35:40–47. doi:10.1200/JCO.2016.69.1584.

Behjati, S., P.S. Tarpey, K. Haase, H. Ye, M.D. Young, L.B. Alexandrov, S.J. Farndon, G. Collord, D.C. Wedge, I. Martincorena, S.L. Cooke, H. Davies, W. Mifsud, M. Lidgren, S. Martin, C. Latimer, M. Maddison, A.P. Butler, J.W. Teague, N. Pillay, A. Shlien, U. McDermott, P.A. Futreal, D. Baumhoer, O. Zaikova, B. Bjerkehagen, O. Myklebost, M.F. Amary, R. Tirabosco, P. Van Loo, M.R. Stratton, A.M. Flanagan, and P.J. Campbell. 2017. Recurrent mutation of IGF signalling genes and distinct patterns of genomic rearrangement in osteosarcoma. *Nat. Commun. 2017 81*. 8:1–8. doi:10.1038/ncomms15936.

Von Behring, E., and S. Kitasato. 2015. The early history of B cells. *Nat. Rev. Immunol. 2015 153*. 15:191–197. doi:10.1038/nri3801.

Belfiore, A., F. Frasca, G. Pandini, L. Sciacca, and R. Vigneri. 2009a. Insulin receptor isoforms and insulin receptor/insulin-like growth factor receptor hybrids in physiology and disease. *Endocr. Rev.* 30:586–623. doi:10.1210/ER.2008-0047.

Belfiore, A., F. Frasca, G. Pandini, L. Sciacca, and R. Vigneri. 2009b. Insulin Receptor Isoforms and Insulin Receptor/Insulin-Like Growth Factor Receptor Hybrids in Physiology and Disease. *Endocr. Rev.* 30:586–623. doi:10.1210/ER.2008-0047.

Berglund, E., J. Maaskola, N. Schultz, S. Friedrich, M. Marklund, J. Bergenstråhle, F.

Tarish, A. Tanoglidi, S. Vickovic, L. Larsson, F. Salmén, C. Ogris, K. Wallenborg, J. Lagergren, P. Ståhl, E. Sonnhammer, T. Helleday, and J. Lundeberg. 2018. Spatial maps of prostate cancer transcriptomes reveal an unexplored landscape of heterogeneity. *Nat. Commun.* 9. doi:10.1038/S41467-018-04724-5.

Bester, A.C., M. Roniger, Y.S. Oren, M.M. Im, D. Sarni, M. Chaoat, A. Bensimon, G. Zamir, D.S. Shewach, and B. Kerem. 2011. Nucleotide deficiency promotes genomic instability in early stages of cancer development. *Cell*. 145:435–446. doi:10.1016/J.CELL.2011.03.044.

Bettelli, E., Y. Carrier, W. Gao, T. Korn, T.B. Strom, M. Oukka, H.L. Weiner, and V.K. Kuchroo. 2006. Reciprocal developmental pathways for the generation of pathogenic effector TH17 and regulatory T cells. *Nature*. 441:235–238. doi:10.1038/NATURE04753.

Bharti, S.K., S. Kakkad, P. Danhier, F. Wildes, M.F. Penet, B. Krishnamachary, and Z.M. Bhujwalla. 2019. Hypoxia Patterns in Primary and Metastatic Prostate Cancer Environments. *Neoplasia*. 21:239. doi:10.1016/J.NEO.2018.12.004.

Bhowmick, N.A., E.G. Neilson, and H.L. Moses. 2004. Stromal fibroblasts in cancer initiation and progression. *Nature*. 432:332. doi:10.1038/NATURE03096.

Di Biase, S., C. Lee, S. Brandhorst, B. Manes, R. Buono, C.W. Cheng, M. Cacciottolo, A. Martin-Montalvo, R. de Cabo, M. Wei, T.E. Morgan, and V.D. Longo. 2016. Fasting-Mimicking Diet Reduces HO-1 to Promote T Cell-Mediated Tumor Cytotoxicity. *Cancer Cell*. 30:136–146. doi:10.1016/J.CCELL.2016.06.005.

Bidlingmaier, M., N. Friedrich, R.T. Emeny, J. Spranger, O.D. Wolthers, J. Roswall, A. Körner, B. Obermayer-Pietsch, C. Hübener, J. Dahlgren, J. Frystyk, A.F.H. Pfeiffer, A. Doering, M. Bielohuby, H. Wallaschofski, and A.M. Arafat. 2014. Reference intervals for insulin-like growth factor-1 (igf-i) from birth to senescence: results from a multicenter study using a new automated chemiluminescence IGF-I immunoassay conforming to recent international recommendations. *J. Clin. Endocrinol. Metab.* 99:1712–1721. doi:10.1210/JC.2013-3059.

Bilbao, D., L. Luciani, B. Johannesson, A. Piszczek, and N. Rosenthal. 2014a. Insulin-like growth factor-1 stimulates regulatory T cells and suppresses autoimmune disease . *EMBO Mol. Med.* 6:1423–1435. doi:10.15252/emmm.201303376.

Bilbao, D., L. Luciani, B. Johannesson, A. Piszczek, and N. Rosenthal. 2014b. Insulin-like growth factor-1 stimulates regulatory T cells and suppresses autoimmune disease. *EMBO Mol. Med.* 6:1423–1435. doi:10.15252/emmm.201303376.

Bilusic, M., R.A. Madan, and J.L. Gulley. 2017. Immunotherapy of Prostate Cancer: Facts and Hopes. *Clin. Cancer Res.* 23:6764. doi:10.1158/1078-0432.CCR-17-0019.

Birnbaum, M.D., L. Nemzow, A. Kumar, F. Gong, and F. Zhang. 2018. A Rapid and Precise Mutation-Activated Fluorescence Reporter for Analyzing Acute Mutagenesis Frequency. *Cell Chem. Biol.* 25:1038-1049.e5. doi:10.1016/J.CHEMBIOL.2018.05.010.

Biswas, S.K., and A. Mantovani. 2010. Macrophage plasticity and interaction with lymphocyte subsets: cancer as a paradigm. *Nat. Immunol. 2010 1110*. 11:889–896. doi:10.1038/ni.1937.

Blom, S., A. Erickson, A. Ostman, A. Rannikko, T. Mirtti, O. Kallioniemi, and T. Pellinen. 2019. Fibroblast as a critical stromal cell type determining prognosis in prostate cancer. *Prostate*. 79:1505–1513. doi:10.1002/pros.23867.

de Bono, J., C.C. Lin, L.T. Chen, J. Corral, V. Michalarea, K. Rihawi, M. Ong, J.H. Lee, C.H. Hsu, J.C.H. Yang, H.S. Shiah, C.J. Yen, A. Anthoney, M. Jove, S. Buschke, R. Fuertig, U. Schmid, R.G. Goeldner, N. Strelkowa, D.C.L. Huang, T. Bogenrieder, C. Twelves, and A.L. Cheng. 2020. Two first-in-human studies of xentuzumab, a humanised insulin-like growth factor (IGF)-neutralising antibody, in patients with advanced solid tumours. *Br. J. Cancer*. 122:1324–1332. doi:10.1038/S41416-020-0774-1.

de Bono, J.S., C.J. Logothetis, A. Molina, K. Fizazi, S. North, L. Chu, K.N. Chi, R.J. Jones, O.B. Goodman, F. Saad, J.N. Staffurth, P. Mainwaring, S. Harland, T.W. Flaig, T.E. Hutson, T. Cheng, H. Patterson, J.D. Hainsworth, C.J. Ryan, C.N. Sternberg, S.L. Ellard, A. Fléchon, M. Saleh, M. Scholz, E. Efstathiou, A. Zivi, D. Bianchini, Y. Loriot, N. Chieffo, T. Kheoh, C.M. Haqq, and H.I. Scher. 2011. Abiraterone and increased survival in metastatic prostate cancer. *N. Engl. J. Med.* 364:1995–2005. doi:10.1056/NEJMOA1014618.

de Bono, J.S., N. Mehra, G. V. Scagliotti, E. Castro, T. Dorff, A. Stirling, A. Stenzl, M.T. Fleming, C.S. Higano, F. Saad, C. Buttigliero, I.M. van Oort, A.D. Laird, M. Mata,

H.C. Chen, C.G. Healy, A. Czibere, and K. Fizazi. 2021. Talazoparib monotherapy in metastatic castration-resistant prostate cancer with DNA repair alterations (TALAPRO-1): an open-label, phase 2 trial. *Lancet. Oncol.* 22:1250–1264. doi:10.1016/S1470-2045(21)00376-4.

De Bono, J.S., S. Oudard, M. Ozguroglu, S. Hansen, J.P. MacHiels, I. Kocak, G. Gravis, I. Bodrogi, M.J. MacKenzie, L. Shen, M. Roessner, S. Gupta, and A.O. Sartor. 2010. Prednisone plus cabazitaxel or mitoxantrone for metastatic castration-resistant prostate cancer progressing after docetaxel treatment: a randomised open-label trial. *Lancet (London, England)*. 376:1147–1154. doi:10.1016/S0140-6736(10)61389-X.

Borden, E.C., G.C. Sen, G. Uze, R.H. Silverman, R.M. Ransohoff, G.R. Foster, and G.R. Stark. 2007. Interferons at age 50: past, current and future impact on biomedicine. *Nat. Rev. Drug Discov.* 6:975–990. doi:10.1038/NRD2422.

Borge, M., P.R. Nannini, P.E. Morande, C. Jancic, A. Bistmans, R.F. Bezares, M. Giordano, and R. Gamberale. 2013. CXCL12 is a costimulator for CD4+ T cell activation and proliferation in chronic lymphocytic leukemia patients. *Cancer Immunol. Immunother.* 62:113–124. doi:10.1007/S00262-012-1320-7.

Borish, L.C., and J.W. Steinke. 2003. 2. Cytokines and chemokines. *J. Allergy Clin. Immunol.* 111. doi:10.1067/MAI.2003.108.

Borugian, M.J., J.J. Spinelli, Z. Sun, L.N. Kolonel, I. Oakley-Girvan, M.D. Pollak, A.S. Whittemore, A.H. Wu, and R.P. Gallagher. 2008. Prostate cancer risk in relation to insulin-like growth factor (IGF)-I and IGF-binding protein-3: a prospective multiethnic study. *Cancer Epidemiol. Biomarkers Prev.* 17:252–254. doi:10.1158/1055-9965.EPI-07-2694.

Bowers, L.W., E.L. Rossi, C.H. O'Flanagan, L.A. De Graffenried, and S.D. Hursting. 2015. The role of the insulin/IGF system in cancer: Lessons learned from clinical trials and the energy balance-cancer link. *Front. Endocrinol. (Lausanne).* 6:77. doi:10.3389/FENDO.2015.00077/BIBTEX.

Braulke, T. 1999. Type-2 IGF Receptor: A Multi-Ligand Binding Protein. *Horm. Metab. Res.* 31:242–246. doi:10.1055/s-2007-978725.

Brodt, P., L. Fallavollita, A.M. Khatib, A.A. Samani, and D. Zhang. 2001. Cooperative regulation of the invasive and metastatic phenotypes by different domains of the type

I insulin-like growth factor receptor beta subunit. *J. Biol. Chem.* 276:33608–33615. doi:10.1074/JBC.M102754200.

Bromley, S.K., A. Iaboni, S.J. Davis, A. Whitty, J.M. Green, A.S. Shaw, A. Weiss, and M.L. Dustin. 2001. The immunological synapse and CD28-CD80 interactions. *Nat. Immunol. 2001 212*. 2:1159–1166. doi:10.1038/ni737.

Brzozowski, A.M., E.J. Dodson, G.G. Dodson, G.N. Murshudov, C. Verma, J.P. Turkenburg, F.M. De Bree, and Z. Dauter. 2002. Structural origins of the functional divergence of human insulin-like growth factor-I and insulin. *Biochemistry*. 41:9389–9397. doi:10.1021/BI020084J/SUPPL_FILE/BI020084J_S.PDF.

Bunn, R.C., and J.L. Fowlkes. 2003. Insulin-like growth factor binding protein proteolysis. *Trends Endocrinol. Metab.* 14:176–181. doi:10.1016/S1043-2760(03)00049-3.

Burgering, B.M.T., and P.J. Coffer. 1995. Protein kinase B (c-Akt) in phosphatidylinositol-3-OH kinase signal transduction. *Nature*. 376:599–602. doi:10.1038/376599A0.

Butler, A., P. Hoffman, P. Smibert, E. Papalexi, and R. Satija. 2018. Integrating single-cell transcriptomic data across different conditions, technologies, and species. *Nat. Biotechnol. 2018 365*. 36:411–420. doi:10.1038/nbt.4096.

Caffa, I., V. Spagnolo, C. Vernieri, F. Valdemarin, P. Becherini, M. Wei, S. Brandhorst, C. Zucal, E. Driehuis, L. Ferrando, F. Piacente, A. Tagliafico, M. Cilli, L. Mastracci, V.G. Vellone, S. Piazza, A.L. Cremonini, R. Gradaschi, C. Mantero, M. Passalacqua, A. Ballestrero, G. Zoppoli, M. Cea, A. Arrighi, P. Odetti, F. Monacelli, G. Salvadori, S. Cortellino, H. Clevers, F. De Braud, S.G. Sukkar, A. Provenzani, V.D. Longo, and A. Nencioni. 2020. Fasting-mimicking diet and hormone therapy induce breast cancer regression. *Nat. 2020 5837817*. 583:620–624. doi:10.1038/s41586-020-2502-7.

Calcinotto, A., C. Spataro, E. Zagato, D. Di Mitri, V. Gil, M. Crespo, G. De Bernardis, M. Losa, M. Mirenda, E. Pasquini, A. Rinaldi, S. Sumanasuriya, M.B. Lambros, A. Neeb, R. Luciano, C.A. Bravi, D. Nava-Rodrigues, D. Dolling, T. Prayer-Galetti, A. Ferreira, A. Briganti, A. Esposito, S. Barry, W. Yuan, A. Sharp, J. de Bono, and A. Alimonti. 2018. IL-23 secreted by myeloid cells drives castration-resistant prostate cancer. *Nature*. 559:363–369. doi:10.1038/s41586-018-0266-0.

Cannata, D., D. Lann, Y. Wu, S. Elis, H. Sun, S. Yakar, D.A. Lazzarino, T.L. Wood, and

D. LeRoith. 2010. Elevated Circulating IGF-I Promotes Mammary Gland Development and Proliferation. *Endocrinology*. 151:5751–5761. doi:10.1210/en.2010-0792.

Cao, Z., H. Fan-Minogue, D.I. Bellovin, A. Yevtodiyenko, J. Arzeno, Q. Yang, S.S. Gambhir, and D.W. Felsher. 2011. MYC phosphorylation, activation, and tumorigenic potential in hepatocellular carcinoma are regulated by HMG-CoA reductase. *Cancer Res.* 71:2286–2297. doi:10.1158/0008-5472.CAN-10-3367.

Caraglia, M., M. Marra, P. Tagliaferri, S. Lamberts, S. Zappavigna, G. Misso, F. Cavagnini, G. Facchini, A. Abbruzzese, L. Hofland, and G. Vitale. 2009. Emerging strategies to strengthen the anti-tumour activity of type I interferons: overcoming survival pathways. *Curr. Cancer Drug Targets*. 9:690–704. doi:10.2174/156800909789056980.

Carlin, L.M., E.G. Stamatiades, C. Auffray, R.N. Hanna, L. Glover, G. Vizcay-Barrena, C.C. Hedrick, H.T. Cook, S. Diebold, and F. Geissmann. 2013. Nr4a1-dependent Ly6C(low) monocytes monitor endothelial cells and orchestrate their disposal. *Cell*. 153:362–375. doi:10.1016/J.CELL.2013.03.010.

Carracedo, A., and P.P. Pandolfi. 2008. The PTEN-PI3K pathway: of feedbacks and cross-talks. *Oncogene*. 27:5527–5541. doi:10.1038/ONC.2008.247.

Casey, S.C., L. Tong, Y. Li, R. Do, S. Walz, K.N. Fitzgerald, A.M. Gouw, V. Baylot, I. Gütgemann, M. Eilers, and D.W. Felsher. 2016. MYC regulates the antitumor immune response through CD47 and PD-L1. *Science*. 352:227–231. doi:10.1126/SCIENCE.AAC9935.

Cattrini, C., R. España, A. Mennitto, M. Bersanelli, E. Castro, D. Olmos, D. Lorente, and A. Gennari. 2021. Optimal Sequencing and Predictive Biomarkers in Patients with Advanced Prostate Cancer. *Cancers 2021, Vol. 13, Page 4522*. 13:4522. doi:10.3390/CANCERS13184522.

Cerundolo, V., J. Alexander, K. Anderson, C. Lamb, P. Cresswell, A. McMichael, F. Gotch, and A. Townsend. 1990. Presentation of viral antigen controlled by a gene in the major histocompatibility complex. *Nat. 1990 3456274*. 345:449–452. doi:10.1038/345449a0.

Chan, J.M., M.J. Stampfer, E. Giovannucci, P.H. Gann, J. Ma, P. Wilkinson, C.H.

Hennekens, and M. Pollak. 1998. Plasma insulin-like growth factor-I and prostate cancer risk: a prospective study. *Science*. 279:563–566. doi:10.1126/SCIENCE.279.5350.563.

Chan, S.C., Y. Li, and S.M. Dehm. 2012. Androgen receptor splice variants activate androgen receptor target genes and support aberrant prostate cancer cell growth independent of canonical androgen receptor nuclear localization signal. *J. Biol. Chem.* 287:19736–19749. doi:10.1074/jbc.M112.352930.

Chandarlapaty, S., A. Sawai, M. Scaltriti, V. Rodrik-Outmezguine, O. Grbovic-Huezo, V. Serra, P.K. Majumder, J. Baselga, and N. Rosen. 2011. AKT Inhibition Relieves Feedback Suppression of Receptor Tyrosine Kinase Expression and Activity. *Cancer Cell*. 19:58–71. doi:10.1016/j.ccr.2010.10.031.

Chang, F., J.T. Lee, P.M. Navolanic, L.S. Steelman, J.G. Shelton, W.L. Blalock, R.A. Franklin, and J.A. McCubrey. 2003. Involvement of PI3K/Akt pathway in cell cycle progression, apoptosis, and neoplastic transformation: a target for cancer chemotherapy. *Leuk. 2003 173*. 17:590–603. doi:10.1038/sj.leu.2402824.

Chaudhry, A., R.M. Samstein, P. Treuting, Y. Liang, M.C. Pils, J.M. Heinrich, R.S. Jack, F.T. Wunderlich, J.C. Brüning, W. Müller, and A.Y. Rudensky. 2011. Interleukin-10 Signaling in Regulatory T Cells Is Required for Suppression of Th17 Cell-Mediated Inflammation. *Immunity*. 34:566–578. doi:10.1016/j.immuni.2011.03.018.

Che, W., N. Lerner-Marmarosh, Q. Huang, M. Osawa, S. Ohta, M. Yoshizumi, M. Glassman, J.-D. Lee, C. Yan, B.C. Berk, and J.-I. Abe. 2002. Insulin-Like Growth Factor-1 Enhances Inflammatory Responses in Endothelial Cells Role of Gab1 and MEKK3 in TNF-Induced c-Jun and NF-B Activation and Adhesion Molecule Expression. doi:10.1161/01.RES.0000021127.83364.7D.

Chelebian, E., C. Avenel, K. Kartasalo, M. Marklund, A. Tanoglidi, T. Mirtti, R. Colling, A. Erickson, A.D. Lamb, J. Lundeberg, and C. Wählby. 2021. Morphological Features Extracted by AI Associated with Spatial Transcriptomics in Prostate Cancer. *Cancers (Basel).* 13:4837. doi:10.3390/CANCERS13194837.

Chen, B., J. Liu, T.T. Ho, X. Ding, and Y.Y. Mo. 2016. ERK-mediated NF-κB activation through ASIC1 in response to acidosis. *Oncog. 2016 512*. 5:e279–e279. doi:10.1038/oncsis.2016.81.

Chen, D.S., and I. Mellman. 2017. Elements of cancer immunity and the cancer–immune set point. *Nat. 2017 5417637*. 541:321–330. doi:10.1038/nature21349.

Chen, H.L., D. Gabrilovich, R. Tampé, K.R. Girgis, S. Nadaf, and D.P. Carbone. 1996. A functionally defective allele of TAP1 results in loss of MHC class I antigen presentation in a human lung cancer. *Nat. Genet. 1996 132*. 13:210–213. doi:10.1038/ng0696-210.

Chen, N., W. Fang, J. Zhan, S. Hong, Y. Tang, S. Kang, Y. Zhang, X. He, T. Zhou, T. Qin, Y. Huang, X. Yi, and L. Zhang. 2015. Upregulation of PD-L1 by EGFR Activation Mediates the Immune Escape in EGFR-Driven NSCLC: Implication for Optional Immune Targeted Therapy for NSCLC Patients with EGFR Mutation. *J. Thorac. Oncol.* 10:910–923. doi:10.1097/JTO.0000000000000500.

Chen, S., G. Zhu, Y. Yang, F. Wang, Y.T. Xiao, N. Zhang, X. Bian, Y. Zhu, Y. Yu, F. Liu, K. Dong, J. Mariscal, Y. Liu, F. Soares, H. Loo Yau, B. Zhang, W. Chen, C. Wang, D. Chen, Q. Guo, Z. Yi, M. Liu, M. Fraser, D.D. De Carvalho, P.C. Boutros, D. Di Vizio, Z. Jiang, T. van der Kwast, A. Berlin, S. Wu, J. Wang, H.H. He, and S. Ren. 2021. Single-cell analysis reveals transcriptomic remodellings in distinct cell types that contribute to human prostate cancer progression. *Nat. Cell Biol. 2021 231*. 23:87–98. doi:10.1038/s41556-020-00613-6.

Chen, Z., L. Zhou, L. Liu, Y. Hou, M. Xiong, Y. Yang, J. Hu, and K. Chen. 2020. Single-cell RNA sequencing highlights the role of inflammatory cancer-associated fibroblasts in bladder urothelial carcinoma. *Nat. Commun. 2020 111*. 11:1–12. doi:10.1038/s41467-020-18916-5.

Cheng, N., R. Watkins-Schulz, R.D. Junkins, C.N. David, B.M. Johnson, S.A. Montgomery, K.J. Peine, D.B. Darr, H. Yuan, K.P. McKinnon, Q. Liu, L. Miao, L. Huang, E.M. Bachelder, K.M. Ainslie, and J.P.Y. Ting. 2018. A nanoparticle-incorporated STING activator enhances antitumor immunity in PD-L1–insensitive models of triple-negative breast cancer. *JCI Insight*. 3. doi:10.1172/JCI.INSIGHT.120638.

Cheng, P., C.A. Corzo, N. Luetteke, B. Yu, S. Nagaraj, M.M. Bui, M. Ortiz, W. Nacken, C. Sorg, T. Vogl, J. Roth, and D.I. Gabrilovich. 2008. Inhibition of dendritic cell differentiation and accumulation of myeloid-derived suppressor cells in cancer is

regulated by S100A9 protein. *J. Exp. Med.* 205:2235–2249. doi:10.1084/JEM.20080132.

Chetty, A., G.J. Cao, and H.C. Nielsen. 2006a. Insulin-like growth factor-I signaling mechanisms, type I collagen and alpha smooth muscle actin in human fetal lung fibroblasts. *Pediatr. Res.* 60:389–394. doi:10.1203/01.pdr.0000238257.15502.f4.

Chetty, A., G.J. Cao, and H.C. Nielsen. 2006b. Insulin-like Growth Factor-I signaling mechanisms, type I collagen and alpha smooth muscle actin in human fetal lung fibroblasts. *Pediatr. Res.* 60:389–394. doi:10.1203/01.PDR.0000238257.15502.F4.

Chien, Y.H., R. Jores, and M.P. Crowley. 2003. Recognition by γ/δ T Cells. *http://dx.doi.org/10.1146/annurev.immunol.14.1.511*. 14:511–532. doi:10.1146/ANNUREV.IMMUNOL.14.1.511.

Chikuma, S. 2017. CTLA-4, an Essential Immune-Checkpoint for T-Cell Activation. *Curr. Top. Microbiol. Immunol.* 410:99–126. doi:10.1007/82_2017_61.

Chin, Y.R., and A. Toker. 2009. Function of Akt/PKB Signaling to Cell Motility, Invasion and the Tumor Stroma in Cancer. *Cell. Signal.* 21:470. doi:10.1016/J.CELLSIG.2008.11.015.

Chitnis, M.M., K.A. Lodhia, T. Aleksic, S. Gao, A.S. Protheroe, and V.M. Macaulay. 2014. IGF-1R inhibition enhances radiosensitivity and delays double-strand break repair by both non-homologous end-joining and homologous recombination. *Oncogene*. 33:5262–73. doi:10.1038/onc.2013.460.

Chitnis, M.M., J.S.P. Yuen, A.S. Protheroe, M. Pollak, and V.M. Macaulay. 2008. The Type 1 Insulin-Like Growth Factor Receptor Pathway. *Clin. Cancer Res.* 14:6364–6370. doi:10.1158/1078-0432.CCR-07-4879.

Clemmons, D.R., D.K. Snyder, and W.H. Busby. 1991. Variables Controlling the Secretion of Insulin-Like Growth Factor Binding Protein-2 in Normal Human Subjects. *J. Clin. Endocrinol. Metab.* 73:727–733. doi:10.1210/JCEM-73-4-727.

Codony-Servat, J., M. Cuatrecasas, E. Asensio, C. Montironi, A. Martínez-Cardús, M. Marín-Aguilera, C. Horndler, E. Martínez-Balibrea, M. Rubini, P. Jares, O. Reig, I. Victoria, L. Gaba, M. Martín-Richard, V. Alonso, P. Escudero, C. Fernández-Martos, J. Feliu, J.C. Méndez, M. Méndez, J. Gallego, A. Salud, F. Rojo, A. Castells, A. Prat, R. Rosell, X. García-Albéniz, J. Camps, and J. Maurel. 2017. Nuclear IGF-1R

predicts chemotherapy and targeted therapy resistance in metastatic colorectal cancer. *Br. J. Cancer*. 117:1777–1786. doi:10.1038/bjc.2017.279.

Coelho, M.A., S. de Carné Trécesson, S. Rana, D. Zecchin, C. Moore, M. Molina-Arcas, P. East, B. Spencer-Dene, E. Nye, K. Barnouin, A.P. Snijders, W.S. Lai, P.J. Blackshear, and J. Downward. 2017. Oncogenic RAS Signaling Promotes Tumor Immunoresistance by Stabilizing PD-L1 mRNA. *Immunity*. 47:1083. doi:10.1016/J.IMMUNI.2017.11.016.

Cohen, P., D. Peehl, and R. Rosenfeld. 1994. The IGF Axis in the Prostate. *Horm. Metab. Res.* 26:81–84. doi:10.1055/s-2007-1000777.

Corrales, L., V. Matson, B. Flood, S. Spranger, and T.F. Gajewski. 2017. Innate immune signaling and regulation in cancer immunotherapy. *Cell Res.* 27:96–108. doi:10.1038/CR.2016.149.

Crespo, J., H. Sun, T.H. Welling, Z. Tian, and W. Zou. 2013. T cell anergy, exhaustion, senescence and stemness in the tumor microenvironment. *Curr. Opin. Immunol.* 25:214. doi:10.1016/J.COI.2012.12.003.

Cui, H., M. Cruz-Correa, F.M. Giardiello, D.F. Hutcheon, D.R. Kafonek, S. Brandenburg, Y. Wu, X. He, N.R. Powe, and A.P. Feinberg. 2003. Loss of IGF2 imprinting: A potential marker of colorectal cancer risk. *Science (80-.).* 299:1753–1755. doi:10.1126/SCIENCE.1080902/SUPPL_FILE/CUI.SOM.PDF.

Czech, M.P. 2000. PIP2 and PIP3: Complex Roles at the Cell Surface. *Cell*. 100:603–606. doi:10.1016/S0092-8674(00)80696-0.

Damaschke, N.A., B. Yang, S. Bhusari, M. Avilla, W. Zhong, M.L. Blute, W. Huang, and D.F. Jarrard. 2017. Loss of Igf2 Gene Imprinting in Murine Prostate Promotes Widespread Neoplastic Growth. *Cancer Res.* 77:5236–5247. doi:10.1158/0008-5472.CAN-16-3089.

Damodaran, S., J.M. Lang, and D.F. Jarrard. 2019. Targeting Metastatic Hormone Sensitive Prostate Cancer: Chemohormonal Therapy and New Combinatorial Approaches. *J. Urol.* 201:876–885. doi:10.1097/JU.0000000000000117.

Dan, H.C., M.J. Cooper, P.C. Cogswell, J.A. Duncan, J.P.Y. Ting, and A.S. Baldwin. 2008. Akt-dependent regulation of NF-κB is controlled by mTOR and Raptor in association with IKK. *Genes Dev.* 22:1490–1500. doi:10.1101/GAD.1662308.

Danaher, P., S. Warren, R. Lu, J. Samayoa, A. Sullivan, I. Pekker, B. Wallden, F.M. Marincola, and A. Cesano. 2018. Pan-cancer adaptive immune resistance as defined by the Tumor Inflammation Signature (TIS): Results from The Cancer Genome Atlas (TCGA). *J. Immunother. Cancer*. 6:1–17. doi:10.1186/S40425-018-0367-1/FIGURES/2.

Davidsson, S., O. Andren, A.-L. Ohlson, J. Carlsson, S.-O. Andersson, F. Giunchi, J.R. Rider, and M. Fiorentino. 2018. FOXP3 $^{+}$ regulatory T cells in normal prostate tissue, postatrophic hyperplasia, prostatic intraepithelial neoplasia, and tumor histological lesions in men with and without prostate cancer. *Prostate*. 78:40–47. doi:10.1002/pros.23442.

Davidsson, S., A.L. Ohlson, S.O. Andersson, K. Fall, A. Meisner, M. Fiorentino, O. Andrén, and J.R. Rider. 2012. CD4 helper T cells, CD8 cytotoxic T cells, and FOXP3+ regulatory T cells with respect to lethal prostate cancer. *Mod. Pathol. 2013 263*. 26:448–455. doi:10.1038/modpathol.2012.164.

Demaria, O., S. Cornen, M. Daëron, Y. Morel, R. Medzhitov, and E. Vivier. 2019. Harnessing innate immunity in cancer therapy. *Nat. 2019 5747776*. 574:45–56. doi:10.1038/s41586-019-1593-5.

deMoura, M.D., D. Chamoun, C.E. Resnick, and E.Y. Adashi. 2000. Insulin-like Growth Factor (IGF)-I Stimulates IGF-I and Type 1 IGF Receptor Expression in Cultured Rat Granulosa Cells: Autocrine Regulation of the Intrafollicular IGF-I System. *Endocrine*. 13:103–110. doi:10.1385/ENDO:13:1:103.

Denduluri, S.K., O. Idowu, Z. Wang, Z. Liao, Z. Yan, M.K. Mohammed, J. Ye, Q. Wei, J. Wang, L. Zhao, and H.H. Luu. 2015a. Insulin-like growth factor (IGF) signaling in tumorigenesis and the development of cancer drug resistance. *Genes Dis.* 2:13–25. doi:10.1016/j.gendis.2014.10.004.

Denduluri, S.K., O. Idowu, Z. Wang, Z. Liao, Z. Yan, M.K. Mohammed, J. Ye, Q. Wei, J. Wang, L. Zhao, and H.H. Luu. 2015b. Insulin-like growth factor (IGF) signaling in tumorigenesis and the development of cancer drug resistance. *Genes Dis.* 2:13–25. doi:10.1016/j.gendis.2014.10.004.

Deng, L., H. Liang, B. Burnette, M. Beckett, T. Darga, R.R. Weichselbaum, and Y.X. Fu. 2014. Irradiation and anti-PD-L1 treatment synergistically promote antitumor

immunity in mice. *J. Clin. Invest.* 124:687–695. doi:10.1172/JCI67313.

Denley, A., E.R. Bonython, G.W. Booker, L.J. Cosgrove, B.E. Forbes, C.W. Ward, and J.C. Wallace. 2004. Structural determinants for high-affinity binding of insulin-like growth factor II to insulin receptor (IR)-A, the exon 11 minus isoform of the IR. *Mol. Endocrinol.* 18:2502–2512. doi:10.1210/ME.2004-0183.

Dhatchinamoorthy, K., J.D. Colbert, and K.L. Rock. 2021. Cancer Immune Evasion Through Loss of MHC Class I Antigen Presentation. *Front. Immunol.* 12. doi:10.3389/FIMMU.2021.636568.

Dhillon, A.S., S. Hagan, O. Rath, and W. Kolch. 2007. MAP kinase signalling pathways in cancer. *Oncogene 2007 2622*. 26:3279–3290. doi:10.1038/sj.onc.1210421.

Dinneen, E., A. Haider, J. Grierson, A. Freeman, J. Oxley, T. Briggs, S. Nathan, N.R. Williams, C. Brew-Graves, R. Persad, J. Aning, C. Jameson, M. Ratynska, I. Ben-Salha, R. Ball, R. Clow, C. Allen, D. Heffernan-Ho, J. Kelly, and G. Shaw. 2021. NeuroSAFE frozen section during robot-assisted radical prostatectomy: peri-operative and histopathological outcomes from the NeuroSAFE PROOF feasibility randomized controlled trial. *BJU Int.* 127:676–686. doi:10.1111/BJU.15256.

DiToro, D., S.N. Harbour, J.K. Bando, G. Benavides, S. Witte, V.A. Laufer, C. Moseley, J.R. Singer, B. Frey, H. Turner, J. Bruning, V. Darley-Usmar, M. Gao, C. Conover, R.D. Hatton, S. Frank, M. Colonna, and C.T. Weaver. 2020. Insulin-Like Growth Factors Are Key Regulators of T Helper 17 Regulatory T Cell Balance in Autoimmunity. *Immunity*. 52:650-667.e10. doi:10.1016/J.IMMUNI.2020.03.013.

Dituri, F., A. Mazzocca, G. Giannelli, and S. Antonaci. 2011. PI3K Functions in Cancer Progression, Anticancer Immunity and Immune Evasion by Tumors. *Clin. Dev. Immunol.* 2011. doi:10.1155/2011/947858.

Dobin, A., C.A. Davis, F. Schlesinger, J. Drenkow, C. Zaleski, S. Jha, P. Batut, M. Chaisson, and T.R. Gingeras. 2013. STAR: ultrafast universal RNA-seq aligner. *Bioinformatics*. 29:15–21. doi:10.1093/BIOINFORMATICS/BTS635.

Doherty, M.R., H.J. Cheon, D.J. Junk, S. Vinayak, V. Varadan, M.L. Telli, J.M. Ford, G.R. Stark, and M.W. Jackson. 2017. Interferon-beta represses cancer stem cell properties in triple-negative breast cancer. *Proc. Natl. Acad. Sci. U. S. A.* 114:13792–13797. doi:10.1073/PNAS.1713728114/-/DCSUPPLEMENTAL.

Dong, C., and R.A. Flavell. 2000. Cell fate decision: T-helper 1 and subsets in immune responses. *Arthritis Res.* 2:179–188. doi:10.1186/AR85/FIGURES/1.

Douglas, R.S., V. Naik, C.J. Hwang, N.F. Afifiyan, A.G. Gianoukakis, D. Sand, S. Kamat, and T.J. Smith. 2008. B cells from patients with Graves' disease aberrantly express the IGF-1 receptor: implications for disease pathogenesis. *J. Immunol.* 181:5768–5774. doi:10.4049/JIMMUNOL.181.8.5768.

Dowery, R., D. Benhamou, E. Benchetrit, O. Harel, A. Nevelsky, S. Zisman-Rozen, Y. Braun-Moscovici, A. Balbir-Gurman, I. Avivi, A. Shechter, D. Berdnik, T. Wyss-Coray, and D. Melamed. 2021. Peripheral B cells repress B-cell regeneration in aging through a TNF-α/IGFBP-1/IGF-1 immune-endocrine axis. *Blood*. 138:1817–1829. doi:10.1182/BLOOD.2021012428.

Du, L., L. Lin, Q. Li, K. Liu, Y. Huang, X. Wang, K. Cao, X. Chen, W. Cao, F. Li, C. Shao, Y. Wang, and Y. Shi. 2019. IGF-2 Preprograms Maturing Macrophages to Acquire Oxidative Phosphorylation-Dependent Anti-inflammatory Properties. *Cell Metab.* 29:1363-1375.e8. doi:10.1016/J.CMET.2019.01.006/ATTACHMENT/9A15130F-1F14-49D6-AA1D-14C8489E9F3F/MMC2.XLSX.

Du, S.S., G.W. Chen, P. Yang, Y.X. Chen, Y. Hu, Q.Q. Zhao, Y. Zhang, R. Liu, D.X. Zheng, J. Zhou, J. Fan, and Z.C. Zeng. 2022. Radiation Therapy Promotes Hepatocellular Carcinoma Immune Cloaking via PD-L1 Upregulation Induced by cGAS-STING Activation. *Int. J. Radiat. Oncol. Biol. Phys.* doi:10.1016/J.IJROBP.2021.12.162.

Duan, C., and J.B. Allard. 2018. iGF-Binding Proteins: why Do They exist and why Are There So Many? 9:1. doi:10.3389/fendo.2018.00117.

Duan, C., S.B. Hawes, T. Prevette, and D.R. Clemmons. 1996. Insulin-like growth factor-I (IGF-I) regulates IGF-binding protein-5 synthesis through transcriptional activation of the gene in aortic smooth muscle cells. *J. Biol. Chem.* 271:4280–4288. doi:10.1074/JBC.271.8.4280.

Duffy, M.J. 2020. Biomarkers for prostate cancer: Prostate-specific antigen and beyond. *Clin. Chem. Lab. Med.* 58:326–339. doi:10.1515/CCLM-2019-0693/XML.

Dunn, G.P., L.J. Old, and R.D. Schreiber. 2004. The Immunobiology of Cancer

Immunosurveillance and Immunoediting. *Immunity*. 21:137–148. doi:10.1016/J.IMMUNI.2004.07.017.

Durfort, T., M. Tkach, M.I. Meschaninova, M.A. Rivas, P. V. Elizalde, A.G. Venyaminova, R. Schillaci, and J.-C. François. 2012. Small Interfering RNA Targeted to IGF-IR Delays Tumor Growth and Induces Proinflammatory Cytokines in a Mouse Breast Cancer Model. *PLoS One*. 7:e29213. doi:10.1371/journal.pone.0029213.

Ebong, S., C.R. Yu, D.A. Carper, A.B. Chepelinsky, and C.E. Egwuagu. 2004. Activation of STAT Signaling Pathways and Induction of Suppressors of Cytokine Signaling (SOCS) Proteins in Mammalian Lens by Growth Factors. *Invest. Ophthalmol. Vis. Sci.* 45:872–878. doi:10.1167/IOVS.03-0311.

El-Shewy, H.M., and L.M. Luttrell. 2009. Insulin-like growth factor-2/mannose-6 phosphate receptors. *Vitam. Horm.* 80:667–697. doi:10.1016/S0083-6729(08)00624-9.

Elmore, S. 2007. Apoptosis: a review of programmed cell death. *Toxicol. Pathol.* 35:495–516. doi:10.1080/01926230701320337.

Enomoto, H., L. Tao, R. Eguchi, A. Sato, M. Honda, S. Kaneko, Y. Iwata, H. Nishikawa, H. Imanishi, H. Iijima, T. Tsujimura, and S. Nishiguchi. 2017. The in vivo antitumor effects of type I-interferon against hepatocellular carcinoma: the suppression of tumor cell growth and angiogenesis. *Sci. Reports 2017 71*. 7:1–11. doi:10.1038/s41598-017-12414-3.

Erdal, E., S. Haider, J. Rehwinkel, A.L. Harris, and P.J. McHugh. 2017. A prosurvival DNA damage-induced cytoplasmic interferon response is mediated by end resection factors and is limited by Trex1. *Genes Dev.* 31:353–369. doi:10.1101/GAD.289769.116/-/DC1.

Erlandsson, A., J. Carlsson, M. Lundholm, A. Fält, S.O. Andersson, O. Andrén, and S. Davidsson. 2019. M2 macrophages and regulatory T cells in lethal prostate cancer. *Prostate*. 79:363–369. doi:10.1002/pros.23742.

Fan, W., T. Yanase, H. Morinaga, T. Okabe, M. Nomura, H. Daitoku, A. Fukamizu, S. Kato, R. Takayanagi, and H. Nawata. 2007. Insulin-like Growth Factor 1/Insulin Signaling Activates Androgen Signaling through Direct Interactions of Foxo1 with

Androgen Receptor. doi:10.1074/jbc.M610447200.

Farabaugh, S.M., D.N. Boone, and A. V Lee. 2015. Role of IGF1R in Breast Cancer Subtypes, Stemness, and Lineage Differentiation. *Front. Endocrinol. (Lausanne).* 6:59. doi:10.3389/fendo.2015.00059.

Favelyukis, S., J.H. Till, S.R. Hubbard, and W.T. Miller. 2001. Structure and autoregulation of the insulin-like growth factor 1 receptor kinase. *Nat. Struct. Biol.* 8:1058–1063. doi:10.1038/NSB721.

Feng, M., W. Jiang, B.Y.S. Kim, C.C. Zhang, Y.X. Fu, and I.L. Weissman. 2019. Phagocytosis checkpoints as new targets for cancer immunotherapy. *Nat. Rev. Cancer 2019 1910*. 19:568–586. doi:10.1038/s41568-019-0183-z.

Fernandez, E. V., K.M. Reece, A.M. Ley, S.M. Troutman, T.M. Sissung, D.K. Price, C.H. Chau, and W.D. Figg. 2015. Dual targeting of the androgen receptor and hypoxia-inducible factor 1α pathways synergistically inhibits castration-resistant prostate cancer cells. *Mol. Pharmacol.* 87:1006–1012. doi:10.1124/MOL.114.097477.

Fernandez, M.C., R. Rayes, B. Ham, N. Wang, F. Bourdeau, S. Milette, M. lllemann, N. Bird, A. Majeed, J. Xu, T. Kisselova, and P. Brodt. 2017. The type I insulin-like growth factor regulates the liver stromal response to metastatic colon carcinoma cells. *Oncotarget*. 8:52281. doi:10.18632/ONCOTARGET.12595.

Fernando, R., O. Caldera, and T.J. Smith. 2021. Therapeutic IGF-I receptor inhibition alters fibrocyte immune phenotype in thyroid-associated ophthalmopathy. *Proc. Natl. Acad. Sci. U. S. A.* 118. doi:10.1073/PNAS.2114244118.

Filella, X., and N. Giménez. 2013. Evaluation of [- 2] proPSA and prostate health index (phi) for the detection of prostate cancer: A systematic review and meta-analysis. *Clin. Chem. Lab. Med.* 51:729–739. doi:10.1515/CCLM-2012-0410/PDF.

Firth, S.M., and R.C. Baxter. 2002. Cellular actions of the insulin-like growth factor binding proteins. *Endocr. Rev.* 23:824–854. doi:10.1210/ER.2001-0033.

Fizazi, K., H.I. Scher, K. Miller, E. Basch, C.N. Sternberg, D. Cella, D. Forer, M. Hirmand, and J.S. de Bono. 2014. Effect of enzalutamide on time to first skeletal-related event, pain, and quality of life in men with castration-resistant prostate cancer: results from the randomised, phase 3 AFFIRM trial. *Lancet. Oncol.* 15:1147–1156. doi:10.1016/S1470-2045(14)70303-1.

Flammiger, A., L. Weisbach, H. Huland, P. Tennstedt, R. Simon, S. Minner, C. Bokemeyer, G. Sauter, T. Schlomm, and M. Trepel. 2013. High tissue density of FOXP3+ T cells is associated with clinical outcome in prostate cancer. *Eur. J. Cancer*. 49:1273–1279. doi:10.1016/j.ejca.2012.11.035.

Fleming, J.M., B.J. Leibowitz, D.E. Kerr, and W.S. Cohick. 2005. IGF-I differentially regulates IGF-binding protein expression in primary mammary fibroblasts and epithelial cells. *J. Endocrinol.* 186:165–178. doi:10.1677/JOE.1.06164.

Fleming, V., X. Hu, R. Weber, V. Nagibin, C. Groth, P. Altevogt, J. Utikal, and V. Umansky. 2018. Targeting myeloid-derived suppressor cells to bypass tumor-induced immunosuppression. *Front. Immunol.* 9:398. doi:10.3389/FIMMU.2018.00398/BIBTEX.

Forbes, B.E., P.J. Hartfield, K.A. McNeil, K.H. Surinya, S.J. Milner, L.J. Cosgrove, and J.C. Wallace. 2002. Characteristics of binding of insulin-like growth factor (IGF)-I and IGF-II analogues to the type 1 IGF receptor determined by BIAcore analysis. *Eur. J. Biochem.* 269:961–968. doi:10.1046/J.0014-2956.2001.02735.X.

Foskolou, I.P., C. Jorgensen, K.B. Leszczynska, M.M. Olcina, H. Tarhonskaya, B. Haisma, V. D'Angiolella, W.K. Myers, C. Domene, E. Flashman, and E.M. Hammond. 2017. Ribonucleotide Reductase Requires Subunit Switching in Hypoxia to Maintain DNA Replication. *Mol. Cell*. 66:206-220.e9. doi:10.1016/J.MOLCEL.2017.03.005.

Fraga, A., R. Ribeiro, P. Príncipe, C. Lopes, and R. Medeiros. 2015. Hypoxia and Prostate Cancer Aggressiveness: A Tale With Many Endings. *Clin. Genitourin. Cancer*. 13:295–301. doi:10.1016/J.CLGC.2015.03.006.

Francisco, L.M., V.H. Salinas, K.E. Brown, V.K. Vanguri, G.J. Freeman, V.K. Kuchroo, and A.H. Sharpe. 2009. PD-L1 regulates the development, maintenance, and function of induced regulatory T cells. *J. Exp. Med.* 206:3015–3029. doi:10.1084/JEM.20090847.

Fridman, W.H., L. Zitvogel, C. Sautès-Fridman, and G. Kroemer. 2017. The immune contexture in cancer prognosis and treatment. *Nat. Rev. Clin. Oncol. 2017 1412*. 14:717–734. doi:10.1038/nrclinonc.2017.101.

Fu, C., Y. Lu, Y. Zhang, M. Yu, S. Ma, and S. Lyu. 2021. Intermittent fasting suppressed

splenic CD205+ G-MDSC accumulation in a murine breast cancer model by attenuating cell trafficking and inducing apoptosis. *Food Sci. Nutr.* 9:5517. doi:10.1002/FSN3.2510.

Fuertes Marraco, S.A., N.J. Neubert, G. Verdeil, and D.E. Speiser. 2015. Inhibitory Receptors Beyond T Cell Exhaustion. *Front. Immunol.* 6:310. doi:10.3389/FIMMU.2015.00310.

Fujimoto, N., H. Miyamoto, A. Mizokami, S. Harada, M. Nomura, Y. Ueta, T. Sasaguri, and T. Matsumoto. 2007. Prostate cancer cells increase androgen sensitivity by increase in nuclear androgen receptor and androgen receptor coactivators; a possible mechanism of hormone-resistance of prostate cancer cells. *Cancer Invest.* 25:32–37. doi:10.1080/07357900601130698.

Fukuda, R., K. Hirota, F. Fan, Y. Do Jung, L.M. Ellis, and G.L. Semenza. 2002. Insulin-like growth factor 1 induces hypoxia-inducible factor 1-mediated vascular endothelial growth factor expression, which is dependent on MAP kinase and phosphatidylinositol 3-kinase signaling in colon cancer cells. *J. Biol. Chem.* 277:38205–38211. doi:10.1074/JBC.M203781200.

Gabrilovich, D.I., and S. Nagaraj. 2009. Myeloid-derived-suppressor cells as regulators of the immune system. *Nat. Rev. Immunol.* 9:162. doi:10.1038/NRI2506.

Gadola, S.D., H.T. Moins-Teisserenc, J. Trowsdale, W.L. Gross, and V. Cerundolo. 2000. TAP deficiency syndrome. *Clin. Exp. Immunol.* 121:173–178. doi:10.1046/J.1365-2249.2000.01264.X.

Gajewski, T.F., H. Schreiber, and Y.X. Fu. 2013. Innate and adaptive immune cells in the tumor microenvironment. *Nat. Immunol. 2013 1410*. 14:1014–1022. doi:10.1038/ni.2703.

Gales, D., C. Clark, U. Manne, and T. Samuel. 2013. The Chemokine CXCL8 in Carcinogenesis and Drug Response. *ISRN Oncol.* 2013:1–8. doi:10.1155/2013/859154.

Gannon, P.O., J. Godin-Ethier, M. Hassler, N. Delvoye, M. Aversa, A.O. Poisson, B. Péant, M.A. Fahmy, F. Saad, R. Lapointe, and A.M. Mes-Masson. 2010. Androgen-Regulated Expression of Arginase 1, Arginase 2 and Interleukin-8 in Human Prostate Cancer. *PLoS One*. 5. doi:10.1371/JOURNAL.PONE.0012107.

Gao, J., J.F. Ward, C.A. Pettaway, L.Z. Shi, S.K. Subudhi, L.M. Vence, H. Zhao, J. Chen, H. Chen, E. Efstathiou, P. Troncoso, J.P. Allison, C.J. Logothetis, I.I. Wistuba, M.A. Sepulveda, J. Sun, J. Wargo, J. Blando, and P. Sharma. 2017. VISTA is an inhibitory immune checkpoint that is increased after ipilimumab therapy in patients with prostate cancer. *Nat. Med. 2017 235*. 23:551–555. doi:10.1038/nm.4308.

Garcia-Diaz, A., D.S. Shin, B.H. Moreno, J. Saco, H. Escuin-Ordinas, G.A. Rodriguez, J.M. Zaretsky, L. Sun, W. Hugo, X. Wang, G. Parisi, C.P. Saus, D.Y. Torrejon, T.G. Graeber, B. Comin-Anduix, S. Hu-Lieskovan, R. Damoiseaux, R.S. Lo, and A. Ribas. 2017. Interferon Receptor Signaling Pathways Regulating PD-L1 and PD-L2 Expression. *Cell Rep.* 19:1189. doi:10.1016/J.CELREP.2017.04.031.

Garçon, F., D.T. Patton, J.L. Emery, E. Hirsch, R. Rottapel, T. Sasaki, and K. Okkenhaug. 2008. CD28 provides T-cell costimulation and enhances PI3K activity at the immune synapse independently of its capacity to interact with the p85/p110 heterodimer. *Blood*. 111:1464–1471. doi:10.1182/BLOOD-2007-08-108050.

Ge, R.T., L.H. Mo, R. Wu, J.Q. Liu, H.P. Zhang, Z. Liu, Z. Liu, and P.C. Yang. 2015. Insulin-like growth factor-1 endues monocytes with immune suppressive ability to inhibit inflammation in the intestine. *Sci. Reports 2015 51*. 5:1–7. doi:10.1038/srep07735.

Geiger, R., J.C. Rieckmann, T. Wolf, C. Basso, Y. Feng, T. Fuhrer, M. Kogadeeva, P. Picotti, F. Meissner, M. Mann, N. Zamboni, F. Sallusto, and A. Lanzavecchia. 2016. L-Arginine Modulates T Cell Metabolism and Enhances Survival and Anti-tumor Activity. *Cell*. 167:829. doi:10.1016/J.CELL.2016.09.031.

Giannoukakis, N., C. Deal, J. Paquette, C.G. Goodyer, and C. Polychronakos. 1993. Parental genomic imprinting of the human IGF2 gene. *Nat. Genet.* 4:98–101. doi:10.1038/NG0593-98.

Gibbons, R.M., X. Liu, V. Pulko, S.M. Harrington, C.J. Krco, E.D. Kwon, and H. Dong. 2012. B7-H1 limits the entry of effector CD8(+) T cells to the memory pool by upregulating Bim. *Oncoimmunology*. 1:1061–1073. doi:10.4161/ONCI.20850.

Gill, P.S., I.S. Roberts, L. Browning, R. Perera, A.Y. Warren, F.C. Hamdy, and C. Verrill. 2012. The handling and sampling of radical prostatectomy specimens for reporting and research: the Oxford approach. *J Clin Pathol*. 65:1057–1061.

doi:10.1136/jclinpath-2012-200923.

Girnita, L., S.K. Shenoy, B. Sehat, R. Vasilcanu, A. Girnita, R.J. Lefkowitz, and O. Larsson. 2005. {beta}-Arrestin is crucial for ubiquitination and down-regulation of the insulin-like growth factor-1 receptor by acting as adaptor for the MDM2 E3 ligase. *J. Biol. Chem.* 280:24412–9. doi:10.1074/jbc.M501129200.

Gleason, D.F. 1992. Histologic grading of prostate cancer: A perspective. *Hum. Pathol.* 23:273–279. doi:10.1016/0046-8177(92)90108-F.

Gong, L., D.L.W. Kwong, W. Dai, P. Wu, S. Li, Q. Yan, Y. Zhang, B. Zhang, X. Fang, L. Liu, M. Luo, B. Liu, L.K.Y. Chow, Q. Chen, J. Huang, V.H.F. Lee, K.O. Lam, A.W.I. Lo, Z. Chen, Y. Wang, A.W.M. Lee, and X.Y. Guan. 2021. Comprehensive single-cell sequencing reveals the stromal dynamics and tumor-specific characteristics in the microenvironment of nasopharyngeal carcinoma. *Nat. Commun. 2021 121*. 12:1–18. doi:10.1038/s41467-021-21795-z.

Groelz, D., C. Viertler, D. Pabst, N. Dettmann, and K. Zatloukal. 2018. Impact of storage conditions on the quality of nucleic acids in paraffin embedded tissues. *PLoS One*. 13. doi:10.1371/JOURNAL.PONE.0203608.

de Groot, S., R.T. Lugtenberg, D. Cohen, M.J.P. Welters, I. Ehsan, M.P.G. Vreeswijk, V.T.H.B.M. Smit, H. de Graaf, J.B. Heijns, J.E.A. Portielje, A.J. van de Wouw, A.L.T. Imholz, L.W. Kessels, S. Vrijaldenhoven, A. Baars, E.M.K. Kranenbarg, M.D. de Carpentier, H. Putter, J.J.M. van der Hoeven, J.W.R. Nortier, V.D. Longo, H. Pijl, J.R. Kroep, H. de Graaf, J.B. Heijns, J.E.A. Portielje, A.J. van de Wouw, A.L.T. Imholz, L.W. Kessels, S. Vrijaldenhoven, A. Baars, E. Göker, A.J.M. Pas, A.H. Honkoop, A.E. van Leeuwen-Stok, and J.R. Kroep. 2020. Fasting mimicking diet as an adjunct to neoadjuvant chemotherapy for breast cancer in the multicentre randomized phase 2 DIRECT trial. *Nat. Commun.* 11. doi:10.1038/S41467-020-16138-3.

Gros, G. Le, S.Z. Ben-Sasson, R. Seder, F.D. Finkelman, and W.E. Paul. 1990. Generation of interleukin 4 (IL-4)-producing cells in vivo and in vitro: IL-2 and IL-4 are required for in vitro generation of IL-4-producing cells. *J. Exp. Med.* 172:921–929. doi:10.1084/JEM.172.3.921.

Grzywa, T.M., A. Sosnowska, P. Matryba, Z. Rydzynska, M. Jasinski, D. Nowis, and J.

Golab. 2020. Myeloid Cell-Derived Arginase in Cancer Immune Response. *Front. Immunol.* 11:938. doi:10.3389/FIMMU.2020.00938/BIBTEX.

Gu, L., P. Vogiatzi, M. Puhr, A. Dagvadorj, J. Lutz, A. Ryder, S. Addya, P. Fortina, C. Cooper, B. Leiby, A. Dasgupta, T. Hyslop, L. Bubendorf, K. Alanen, T. Mirtti, and M.T. Nevalainen. 2010. Stat5 promotes metastatic behavior of human prostate cancer cells in vitro and in vivo. *Endocr. Relat. Cancer*. 17:481. doi:10.1677/ERC-09-0328.

Gual, P., V. Baron, V. Lequoy, and E. Van Obberghen. 1998. Interaction of Janus kinases JAK-1 and JAK-2 with the insulin receptor and the insulin-like growth factor-1 receptor. *Endocrinology*. 139:884–893. doi:10.1210/ENDO.139.3.5829.

Guevara-Aguirre, J., P. Balasubramanian, M. Guevara-Aguirre, M. Wei, F. Madia, C.-W. Cheng, D. Hwang, A. Martin-Montalvo, J. Saavedra, S. Ingles, R. de Cabo, P. Cohen, and V.D. Longo. 2011. Growth hormone receptor deficiency is associated with a major reduction in pro-aging signaling, cancer, and diabetes in humans. *Sci. Transl. Med.* 3:70ra13. doi:10.1126/scitranslmed.3001845.

Guha, M. 2013. Anticancer IGF1R classes take more knocks. *Nat. Rev. Drug Discov.* 12:250–250. doi:10.1038/nrd3992.

Guilliams, M., C.A. Dutertre, C.L. Scott, N. McGovern, D. Sichien, S. Chakarov, S. Van Gassen, J. Chen, M. Poidinger, S. De Prijck, S.J. Tavernier, I. Low, S.E. Irac, C.N. Mattar, H.R. Sumatoh, G.H.L. Low, T.J.K. Chung, D.K.H. Chan, K.K. Tan, T.L.K. Hon, E. Fossum, B. Bogen, M. Choolani, J.K.Y. Chan, A. Larbi, H. Luche, S. Henri, Y. Saeys, E.W. Newell, B.N. Lambrecht, B. Malissen, and F. Ginhoux. 2016. Unsupervised High-Dimensional Analysis Aligns Dendritic Cells across Tissues and Species. *Immunity*. 45:669–684. doi:10.1016/J.IMMUNI.2016.08.015.

Guo, T., L. Xu, X. Che, S. Zhang, C. Li, J. Wang, J. Gong, R. Ma, Y. Fan, K. Hou, H. Zhou, X. Hu, Y. Liu, and X. Qu. 2017. Formation of the IGF1R/CAV1/SRC tri-complex antagonizes TRAIL-induced apoptosis in gastric cancer cells. *Cell Biol. Int.* 41:749–760. doi:10.1002/CBIN.10775.

Guo, Y.-J., W.-W. Pan, S.-B. Liu, Z.-F. Shen, Y. Xu, and L.-L. Hu. 2020. ERK/MAPK signalling pathway and tumorigenesis. *Exp. Ther. Med.* 19:1997. doi:10.3892/ETM.2020.8454.

Guo, Z., X. Yang, F. Sun, R. Jiang, D.E. Linn, H. Chen, H. Chen, X. Kong, J. Melamed,

C.G. Tepper, H.J. Kung, A.M.H. Brodie, J. Edwards, and Y. Qiu. 2009. A novel androgen receptor splice variant is up-regulated during prostate cancer progression and promotes androgen depletion-resistant growth. *Cancer Res.* 69:2305–2313. doi:10.1158/0008-5472.CAN-08-3795.

H-F Zhang, X., X. Jin, S. Malladi, Y. Zou, Y.H. Wen, E. Brogi, M. Smid, J. Foekens, and J. Massagué. 2013. Selection of Bone Metastasis Seeds by Mesenchymal Signals in the Primary Tumor Stroma. doi:10.1016/j.cell.2013.07.036.

Haffner, M.C., G. Guner, D. Taheri, G.J. Netto, D.N. Palsgrove, Q. Zheng, L.B. Guedes, K. Kim, H. Tsai, D.M. Esopi, T.L. Lotan, R. Sharma, A.K. Meeker, A.M. Chinnaiyan, W.G. Nelson, S. Yegnasubramanian, J. Luo, R. Mehra, E.S. Antonarakis, C.G. Drake, and A.M. De Marzo. 2018. Comprehensive Evaluation of Programmed Death-Ligand 1 Expression in Primary and Metastatic Prostate Cancer. *Am. J. Pathol.* 188:1478–1485. doi:10.1016/J.AJPATH.2018.02.014.

Hähnel, P.S., S. Thaler, E. Antunes, C. Huber, M. Theobald, and M. Schuler. 2008. Targeting AKT Signaling Sensitizes Cancer to Cellular Immunotherapy. *Cancer Res.* 68:3899–3906. doi:10.1158/0008-5472.CAN-07-6286.

Hamdy, F.C., J.L. Donovan, J.A. Lane, M. Mason, C. Metcalfe, P. Holding, M. Davis, T.J. Peters, E.L. Turner, R.M. Martin, J. Oxley, M. Robinson, J. Staffurth, E. Walsh, P. Bollina, J. Catto, A. Doble, A. Doherty, D. Gillatt, R. Kockelbergh, H. Kynaston, A. Paul, P. Powell, S. Prescott, D.J. Rosario, E. Rowe, and D.E. Neal. 2016. 10-Year Outcomes after Monitoring, Surgery, or Radiotherapy for Localized Prostate Cancer. *N. Engl. J. Med.* 375:1415–1424. doi:10.1056/NEJMOA1606220.

Han, H., A.D. Jain, M.I. Truica, J. Izquierdo-Ferrer, J.F. Anker, B. Lysy, V. Sagar, Y. Luan, Z.R. Chalmers, K. Unno, H. Mok, R. Vatapalli, Y.A. Yoo, Y. Rodriguez, I. Kandela, J.B. Parker, D. Chakravarti, R.K. Mishra, G.E. Schiltz, and S.A. Abdulkadir. 2019. Small Molecule MYC Inhibitors Suppress Tumor Growth and Enhance Immunotherapy. *Cancer Cell*. 36:483. doi:10.1016/J.CCELL.2019.10.001.

Han, X.J., X.L. Ma, L. Yang, Y.Q. Wei, Y. Peng, and X.W. Wei. 2020. Progress in Neoantigen Targeted Cancer Immunotherapies. *Front. Cell Dev. Biol.* 8:728. doi:10.3389/FCELL.2020.00728/BIBTEX.

Hanahan, D. 2022. Hallmarks of Cancer: New Dimensions. *Cancer Discov.* 12:31–46.

doi:10.1158/2159-8290.CD-21-1059.

Hanahan, D., and R.A. Weinberg. 2000. The Hallmarks of Cancer. *Cell*. 100:57–70. doi:10.1016/S0092-8674(00)81683-9.

Hanahan, D., and R.A. Weinberg. 2011. Hallmarks of cancer: The next generation. *Cell*. 144:646–674. doi:10.1016/J.CELL.2011.02.013/ATTACHMENT/3F528E16-8B3C-4D8D-8DE5-43E0C98D8475/MMC1.PDF.

Hankinson, S.E., W.C. Willett, G.A. Colditz, D.J. Hunter, D.S. Michaud, B. Deroo, B. Rosner, F.E. Speizer, and M. Pollak. 1998. Circulating concentrations of insulin-like growth factor I and risk of breast cancer. *Lancet*. 351:1393–1396. doi:10.1016/S0140-6736(97)10384-1.

Hanna, R.N., C. Cekic, D. Sag, R. Tacke, G.D. Thomas, H. Nowyhed, E. Herrley, N. Rasquinha, S. McArdle, R. Wu, E. Peluso, D. Metzger, H. Ichinose, I. Shaked, G. Chodaczek, S.K. Biswas, and C.C. Hedrick. 2015. Patrolling monocytes control tumor metastasis to the lung. *Science*. 350:985–990. doi:10.1126/SCIENCE.AAC9407.

Hansen, A., C. Massard, P.A. Ott, N. Haas, J. Lopez, S. Ejadi, J. Wallmark, B. Keam, J.-P. Delord, R. Aggarwal, M. Gould, P. Qiu, S. Saraf, S. Keefe, and S.A. Piha-Paul. 2016. Pembrolizumab for patients with advanced prostate adenocarcinoma: Preliminary results from the KEYNOTE-028 study. *Ann. Oncol.* 27:vi247. doi:10.1093/ANNONC/MDW372.09.

Haque, A., J. Engel, S.A. Teichmann, and T. Lönnberg. 2017. A practical guide to single-cell RNA-sequencing for biomedical research and clinical applications. *Genome Med.* 9. doi:10.1186/S13073-017-0467-4.

Harding, S.M., J.L. Benci, J. Irianto, D.E. Discher, A.J. Minn, and R.A. Greenberg. 2017. Mitotic progression following DNA damage enables pattern recognition within micronuclei. *Nat. 2017 5487668*. 548:466–470. doi:10.1038/nature23470.

Haughey, C.M., D. Mukherjee, R.E. Steele, A. Popple, L. Dura-Perez, A. Pickard, M. Patel, S. Jain, P.B. Mullan, R. Williams, P. Oliveira, N.E. Buckley, J. Honeychurch, S.S. McDade, T. Illidge, I.G. Mills, and S.L. Eddie. 2020. Investigating Radiotherapy Response in a Novel Syngeneic Model of Prostate Cancer. *Cancers (Basel).* 12:1–20. doi:10.3390/CANCERS12102804.

Hay, N., and N. Sonenberg. 2004. Upstream and downstream of mTOR. *Genes Dev.* 18:1926–1945. doi:10.1101/GAD.1212704.

Heck, S., F. Lezoualc'h, S. Engert, and C. Behl. 1999. Insulin-like Growth Factor-1-mediated Neuroprotection against Oxidative Stress Is Associated with Activation of Nuclear Factor κB *. *J. Biol. Chem.* 274:9828–9835. doi:10.1074/JBC.274.14.9828.

Hellawell, G.O., G.D.H. Turner, D.R. Davies, R. Poulsom, S.F. Brewster, and V.M. Macaulay. 2002. Expression of the type 1 insulin-like growth factor receptor is up-regulated in primary prostate cancer and commonly persists in metastatic disease. *Cancer Res.* 62:2942–50.

Hennecke, J., and D.C. Wiley. 2001. T Cell Receptor–MHC Interactions up Close. *Cell*. 104:1–4. doi:10.1016/S0092-8674(01)00185-4.

Hickman, O.J., R.A. Smith, P. Dasgupta, S. Narayana Rao, S. Nayak, S. Sreenivasan, A. Vyakarnam, and C. Galustian. 2016. Expression of two WFDC1/ps20 isoforms in prostate stromal cells induces paracrine apoptosis through regulation of PTGS2/COX-2. *Br. J. Cancer 2016 11411*. 114:1235–1242. doi:10.1038/bjc.2016.91.

Himpe, E., and R. Kooijman. 2009. Insulin-like growth factor-I receptor signal transduction and the Janus Kinase/Signal Transducer and Activator of Transcription (JAK-STAT) pathway. *BioFactors*. 35:76–81. doi:10.1002/biof.20.

Hinz, M., P. Lemke, I. Anagnostopoulos, C. Hacker, D. Krappmann, S. Mathas, B. Dörken, M. Zenke, H. Stein, and C. Scheidereit. 2002. Nuclear factor kappaB-dependent gene expression profiling of Hodgkin's disease tumor cells, pathogenetic significance, and link to constitutive signal transducer and activator of transcription 5a activity. *J. Exp. Med.* 196:605–617. doi:10.1084/JEM.20020062.

Hirakawa, T., M. Yashiro, A. Murata, K. Hirata, K. Kimura, R. Amano, N. Yamada, B. Nakata, and K. Hirakawa. 2013. IGF-1 receptor and IGF binding protein-3 might predict prognosis of patients with resectable pancreatic cancer. *BMC Cancer*. 13:392. doi:10.1186/1471-2407-13-392.

Ho, S.C., S.M. Wu, P.H. Feng, W. Te Liu, K.Y. Chen, H.C. Chuang, Y.F. Chan, L.W. Kuo, and K.Y. Lee. 2017. Noncanonical NF-κB mediates the Suppressive Effect of Neutrophil Elastase on IL-8/CXCL8 by Inducing NKRF in Human Airway Smooth Muscle. *Sci. Reports 2017 71*. 7:1–11. doi:10.1038/srep44930.

Ho, S.S., W.Y. Zhang, N.Y. Tan, M. Khatoo, M.A. Suter, S. Tripathi, F.S. Cheung, W.K. Lim, P.H. Tan, J. Ngeow, and S. Gasser. 2016a. The DNA Structure-Specific Endonuclease MUS81 Mediates DNA Sensor STING-Dependent Host Rejection of Prostate Cancer Cells. *Immunity*. 44:1177–1189. doi:10.1016/j.immuni.2016.04.010.

Ho, S.S.W., W.Y.L. Zhang, N.Y. Jie, H. Tan, J. Ngeow, and S.G. Correspondence. 2016b. The DNA Structure-Specific Endonuclease MUS81 Mediates DNA Sensor STING-Dependent Host Rejection of Prostate Cancer Cells Highlights d Presence of cytosolic DNA in prostate cancer cells depends on Mus81 d Mus81 induces STING-dependent type I interferon expression d Immune rejection of prostate cancer cells relies on Mus81 and STING d Mus81 enhances innate and adaptive anti-cancer immune responses In Brief. *Immunity*. 44:1177–1189. doi:10.1016/j.immuni.2016.04.010.

Hoang, D.T., L. Gu, Z. Liao, F. Shen, P.G. Talati, M. Koptyra, S.H. Tan, E. Ellsworth, S. Gupta, H. Montie, A. Dagvadorj, S. Savolainen, B. Leiby, T. Mirtti, D.E. Merry, and M.T. Nevalainen. 2015. Inhibition of Stat5a/b enhances proteasomal degradation of androgen receptor liganded by antiandrogens in prostate cancer. *Mol. Cancer Ther.* 14:713–726. doi:10.1158/1535-7163.MCT-14-0819/85391/AM/INHIBITION-OF-STAT5A-B-ENHANCES-PROTEASOMAL.

Hoffman, W., F.G. Lakkis, and G. Chalasani. 2016. B Cells, Antibodies, and More. *Clin. J. Am. Soc. Nephrol.* 11:137. doi:10.2215/CJN.09430915.

Holly, J.M.P., K. Biernacka, and C.M. Perks. 2020. The role of insulin-like growth factors in the development of prostate cancer. *Expert Rev. Endocrinol. Metab.* 15:237–250. doi:10.1080/17446651.2020.1764844.

Holzenberger, M., J. Dupont, B. Ducos, P. Leneuve, A. Géloën, P.C. Even, P. Cervera, and Y. Le Bouc. 2003. IGF-1 receptor regulates lifespan and resistance to oxidative stress in mice. *Nature*. 421:182–187. doi:10.1038/NATURE01298.

Hompland, T., K.H. kon Hole, H.B. Ragnum, E.K. Aarnes, L. Vlatkovic, A. Kathrine Lie, S. Patzke, B. Brennhovd, T. Seierstad, and H. Lyng. 2018. Combined MR Imaging of Oxygen Consumption and Supply Reveals Tumor Hypoxia and Aggressiveness in Prostate Cancer Patients. *Cancer Res.* 78:4774–4785. doi:10.1158/0008-5472.CAN-17-3806.

Honegger, A., and R.E. Humbel. 1986. Insulin-like growth factors I and II in fetal and

adult bovine serum. Purification, primary structures, and immunological cross-reactivities. *Biol. Chem.* 261:569–575. doi:10.1016/S0021-9258(17)36130-6.

Hotte, S.J., and F. Saad. 2010. Current management of castrate-resistant prostate cancer. *Curr. Oncol.* 17:S72. doi:10.3747/CO.V17I0.718.

Hsieh, C.S., S.E. Macatonia, C.S. Tripp, S.F. Wolf, A. O'Garra, and K.M. Murphy. 1993. Development of TH1 CD4+ T cells through IL-12 produced by Listeria-induced macrophages. *Science*. 260:547–549. doi:10.1126/SCIENCE.8097338.

Hu, C.K., S. McCall, J. Madden, H. Huang, R. Clough, R.L. Jirtle, and M.S. Anscher. 2005. Loss of heterozygosity of M6P/IGF2R gene is an early event in the development of prostate cancer. *Prostate Cancer Prostatic Dis. 2006 91*. 9:62–67. doi:10.1038/sj.pcan.4500842.

Huang, C.T., M.C. Chang, Y.L. Chen, T.C. Chen, C.A. Chen, and W.F. Cheng. 2015. Insulin-like growth factors inhibit dendritic cell-mediated anti-tumor immunity through regulating ERK1/2 phosphorylation and p38 dephosphorylation. *Cancer Lett.* 359:117–126. doi:10.1016/J.CANLET.2015.01.007.

Huang, H., W. Zhou, R. Chen, B. Xiang, S. Zhou, and L. Lan. 2021. CXCL10 is a Tumor Microenvironment and Immune Infiltration Related Prognostic Biomarker in Pancreatic Adenocarcinoma. *Front. Mol. Biosci.* 8:23. doi:10.3389/FMOLB.2021.611508/BIBTEX.

Huang, Y.-F., M.-R. Shen, K.-F. Hsu, Y.-M. Cheng, and C.-Y. Chou. 2008. Clinical implications of insulin-like growth factor 1 system in early-stage cervical cancer. *Br. J. Cancer*. 99:1096–1102. doi:10.1038/sj.bjc.6604661.

Huggins, C. 1941. STUDIES ON PROSTATIC CANCER. *Arch. Surg.* 43:209. doi:10.1001/archsurg.1941.01210140043004.

Humar, M., I. Kern, G. Vlacic, V. Hadzic, and T. Cufer. 2017. Insulin-like Growth Factor 1 Receptor Expression in Advanced Non-small-cell Lung Cancer and its Impact on Overall Survival. *Radiol. Oncol.* 51:195–202. doi:10.1515/raon-2017-0020.

Humphrey, P.A. 2017. Histopathology of Prostate Cancer. *Cold Spring Harb. Perspect. Med.* 7. doi:10.1101/CSHPERSPECT.A030411.

Hussain, A.R., S.O. Ahmed, M. Ahmed, O.S. Khan, S. Al AbdulMohsen, L.C. Platanias, K.S. Al-Kuraya, and S. Uddin. 2012. Cross-Talk between NFkB and the PI3-

Kinase/AKT Pathway Can Be Targeted in Primary Effusion Lymphoma (PEL) Cell Lines for Efficient Apoptosis. *PLoS One*. 7. doi:10.1371/JOURNAL.PONE.0039945.

Ireland, L., A. Santos, M.S. Ahmed, C. Rainer, S.R. Nielsen, V. Quaranta, U. Weyer-Czernilofsky, D.D. Engle, P.A. Perez-Mancera, S.E. Coupland, A. Taktak, T. Bogenrieder, D.A. Tuveson, F. Campbell, M.C. Schmid, and A. Mielgo. 2016. Chemoresistance in Pancreatic Cancer Is Driven by Stroma-Derived Insulin-Like Growth Factors. *Cancer Res.* 76:6851–6863. doi:10.1158/0008-5472.CAN-16-1201.

Ishida, Y., Y. Agata, K. Shibahara, and T. Honjo. 1992. Induced expression of PD-1, a novel member of the immunoglobulin gene superfamily, upon programmed cell death. *EMBO J.* 11:3887. doi:10.1002/j.1460-2075.1992.tb05481.x.

James, N.D., M.R. Sydes, N.W. Clarke, M.D. Mason, D.P. Dearnaley, M.R. Spears, A.W.S. Ritchie, C.C. Parker, J.M. Russell, G. Attard, J. De Bono, W. Cross, R.J. Jones, G. Thalmann, C. Amos, D. Matheson, R. Millman, M. Alzouebi, S. Beesley, A.J. Birtle, S. Brock, R. Cathomas, P. Chakraborti, S. Chowdhury, A. Cook, T. Elliott, J. Gale, S. Gibbs, J.D. Graham, J. Hetherington, R. Hughes, R. Laing, F. McKinna, D.B. McLaren, J.M. O'Sullivan, O. Parikh, C. Peedell, A. Protheroe, A.J. Robinson, N. Srihari, R. Srinivasan, J. Staffurth, S. Sundar, S. Tolan, D. Tsang, J. Wagstaff, and M.K.B. Parmar. 2016. Addition of docetaxel, zoledronic acid, or both to first-line long-term hormone therapy in prostate cancer (STAMPEDE): survival results from an adaptive, multiarm, multistage, platform randomised controlled trial. *Lancet (London, England)*. 387:1163–1177. doi:10.1016/S0140-6736(15)01037-5.

Jansen, F.H., R.H.N. van Schaik, J. Kurstjens, W. Horninger, H. Klocker, J. Bektic, M.F. Wildhagen, M.J. Roobol, C.H. Bangma, and G. Bartsch. 2010. Prostate-Specific Antigen (PSA) Isoform p2PSA in Combination with Total PSA and Free PSA Improves Diagnostic Accuracy in Prostate Cancer Detection. *Eur. Urol.* 57:921–927. doi:10.1016/J.EURURO.2010.02.003.

Jean, S., and A.A. Kiger. 2014. Classes of phosphoinositide 3-kinases at a glance. *J. Cell Sci.* 127:923–928. doi:10.1242/JCS.093773/-/DC1.

Johannesson, B., S. Sattler, E. Semenova, S. Pastore, T.M. Kennedy-Lydon, R.D. Sampson, M.D. Schneider, N. Rosenthal, and D. Bilbao. 2014. Insulin-like growth factor-1 induces regulatory T cell-mediated suppression of allergic contact dermatitis

in mice. *DMM Dis. Model. Mech.* 7:977–985. doi:10.1242/dmm.015362.

Johnson, G.E. 2012. Mammalian cell HPRT gene mutation assay: test methods. *Methods Mol. Biol.* 817:55–67. doi:10.1007/978-1-61779-421-6_4.

Jones, J.I., and D.R. Clemmons. 1995. Insulin-like growth factors and their binding proteins: biological actions. *Endocr. Rev.* 16:3–34. doi:10.1210/EDRV-16-1-3.

Joung, S.M., Z.-Y. Park, S. Rani, O. Takeuchi, S. Akira, and J.Y. Lee. 2011. Akt Contributes to Activation of the TRIF-Dependent Signaling Pathways of TLRs by Interacting with TANK-Binding Kinase 1. *J. Immunol.* 186:499–507. doi:10.4049/JIMMUNOL.0903534.

Joung, Y.H., M.Y. Lee, E.J. Lim, M.S. Kim, T.S. Hwang, S.Y. Kim, S.K. Ye, J.D. Lee, T. Park, Y.S. Woo, I.M. Chung, and Y.M. Yang. 2007. Hypoxia activates the IGF-1 expression through STAT5b in human HepG2 cells. *Biochem. Biophys. Res. Commun.* 358:733–738. doi:10.1016/J.BBRC.2007.04.201.

Kang, S.-H., B. Keam, Y.-O. Ahn, H.-R. Park, M. Kim, T.M. Kim, D.-W. Kim, and D.S. Heo. 2019. Inhibition of MEK with trametinib enhances the efficacy of anti-PD-L1 inhibitor by regulating anti-tumor immunity in head and neck squamous cell carcinoma. *Oncoimmunology*. 8:e1515057. doi:10.1080/2162402X.2018.1515057.

Kantoff, P.W., C.S. Higano, N.D. Shore, E.R. Berger, E.J. Small, D.F. Penson, C.H. Redfern, A.C. Ferrari, R. Dreicer, R.B. Sims, Y. Xu, M.W. Frohlich, and P.F. Schellhammer. 2010. Sipuleucel-T Immunotherapy for Castration-Resistant Prostate Cancer. *N. Engl. J. Med.* 363:411–422. doi:10.1056/NEJMOA1001294/SUPPL_FILE/NEJMOA1001294_DISCLOSURES.PDF.

Kapellos, T.S., L. Bonaguro, I. Gemünd, N. Reusch, A. Saglam, E.R. Hinkley, and J.L. Schultze. 2019. Human monocyte subsets and phenotypes in major chronic inflammatory diseases. *Front. Immunol.* 10:2035. doi:10.3389/FIMMU.2019.02035/BIBTEX.

Kasprzak, A., W. Kwasniewski, A. Adamek, and A. Gozdzicka-Jozefiak. 2017. Insulin-like growth factor (IGF) axis in cancerogenesis. *Mutat. Res. Mutat. Res.* 772:78–104. doi:10.1016/J.MRREV.2016.08.007.

Katz, T.A., S.G. Liao, V.J. Palmieri, R.K. Dearth, T.N. Pathiraja, Z. Huo, P. Shaw, S.

Small, N.E. Davidson, D.G. Peters, G.C. Tseng, S. Oesterreich, and A. V. Lee. 2015. Targeted DNA Methylation Screen in the Mouse Mammary Genome Reveals a Parity-Induced Hypermethylation of Igf1r That Persists Long after Parturition. *Cancer Prev. Res. (Phila).* 8:1000–1009. doi:10.1158/1940-6207.CAPR-15-0178.

Kavran, J.M., J.M. McCabe, P.O. Byrne, M.K. Connacher, Z. Wang, A. Ramek, S. Sarabipour, Y. Shan, D.E. Shaw, K. Hristova, P.A. Cole, and D.J. Leahy. 2014. How IGF-1 activates its receptor. *Elife*. 3. doi:10.7554/ELIFE.03772.

Kawada, M., H. Inoue, T. Masuda, and D. Ikeda. 2006. Insulin-like Growth Factor I Secreted from Prostate Stromal Cells Mediates Tumor-Stromal Cell Interactions of Prostate Cancer. *Cancer Res.* 66:4419–4425. doi:10.1158/0008-5472.CAN-05-4239.

Key, T.J., P.N. Appleby, G.K. Reeves, A.W. Roddam, K.J. Helzlsouer, A.J. Alberg, D.E. Rollison, K. Overvad, R. Kaaks, D. Trichopoulos, F. Clavel-Chapelon, P. Vineis, M.D. Chirlaque, P.H.M. Peeters, S. Rinaldi, E. Riboli, N.E. Allen, D.S. Allen, I.S. Fentiman, J.M. Holly, L.J. Vatten, D. Gunnell, S. Tretli, H. Grønbæk, A. Tjønneland, R. Krajcik, J. Manjer, P. Lenner, G. Hallmans, L. Baglietto, D.R. English, G.G. Giles, G. Severi, H.A. Morris, S.E. Hankinson, E.S. Schernhammer, K. Koenig, A. Zeleniuch-Jacquotte, A.A. Arslan, P. Toniolo, R.E. Shore, V. Krogh, A. Micheli, F. Berrino, P. Muti, C. Schairer, R.G. Ziegler, C.D. Berg, C.A. McCarty, H.B. Bueno-de-Mesquita, J.A. Cauley, L.Y. Lui, S.R. Cummings, M.J. Gunter, T.E. Rohan, and H.D. Strickler. 2010. Insulin-like growth factor 1 (IGF1), IGF binding protein 3 (IGFBP3), and breast cancer risk: pooled individual data analysis of 17 prospective studies. *Lancet. Oncol.* 11:530–542. doi:10.1016/S1470-2045(10)70095-4.

Kfoury, Y., N. Baryawno, N. Severe, S. Mei, K. Gustafsson, T. Hirz, T. Brouse, E.W. Scadden, A.A. Igolkina, K. Kokkaliaris, B.D. Choi, N. Barkas, M.A. Randolph, J.H. Shin, P.J. Saylor, D.T. Scadden, D.B. Sykes, and P. V. Kharchenko. 2021. Human prostate cancer bone metastases have an actionable immunosuppressive microenvironment. *Cancer Cell*. 39:1464-1478.e8. doi:10.1016/J.CCELL.2021.09.005.

Khaleghpour, K., S. Pyronnet, A.-C. Gingras, and N. Sonenberg. 1999. Translational homeostasis: eukaryotic translation initiation factor 4E control of 4E-binding protein 1 and p70 S6 kinase activities. *Mol. Cell. Biol.* 19:4302–4310.

doi:10.1128/MCB.19.6.4302.

Kim, E.H., and M. Suresh. 2013. Role of PI3K/Akt signaling in memory CD8 T cell differentiation. *Front. Immunol.* 4:20. doi:10.3389/FIMMU.2013.00020/BIBTEX.

Kimura, A., and T. Kishimoto. 2010. IL-6: regulator of Treg/Th17 balance. *Eur. J. Immunol.* 40:1830–1835. doi:10.1002/EJI.201040391.

Kiniwa, Y., Y. Miyahara, H.Y. Wang, W. Peng, G. Peng, T.M. Wheeler, T.C. Thompson, L.J. Old, and R.F. Wang. 2007. CD8+ Foxp3+ regulatory T cells mediate immunosuppression in prostate cancer. *Clin. Cancer Res.* 13:6947–6958. doi:10.1158/1078-0432.CCR-07-0842.

Kisseleva, T., S. Bhattacharya, J. Braunstein, and C.W. Schindler. 2002. Signaling through the JAK/STAT pathway, recent advances and future challenges. *Gene*. 285:1–24. doi:10.1016/S0378-1119(02)00398-0.

Knuppel, A., G.K. Fensom, E.L. Watts, M.J. Gunter, N. Murphy, K. Papier, A. Perez-Cornago, J.A. Schmidt, K.S. Byrne, R.C. Travis, and T.J. Key. 2020. Circulating Insulin-like Growth Factor-I Concentrations and Risk of 30 Cancers: Prospective Analyses in UK Biobank. doi:10.1158/0008-5472.CAN-20-1281.

Kohli, K., V.G. Pillarisetty, and T.S. Kim. 2021. Key chemokines direct migration of immune cells in solid tumors. *Cancer Gene Ther.* doi:10.1038/S41417-021-00303-X.

Konkel, J.E., F. Frommer, M.D. Leech, H. Yagita, A. Waisman, and S.M. Anderton. 2010. PD-1 signalling in CD4(+) T cells restrains their clonal expansion to an immunogenic stimulus, but is not critically required for peptide-induced tolerance. *Immunology*. 130:92–102. doi:10.1111/J.1365-2567.2009.03216.X.

Kooijman, R., and A. Coppens. 2004. Insulin-like growth factor-I stimulates IL-10 production in human T cells. *J. Leukoc. Biol.* 76:862–867. doi:10.1189/jlb.0404248.

Kooijman, R., M. Willems, C.J. De Haas, G.T. Rijkers, A.L. Schuurmans, S.C. Van Buul-Offers, C.J. Heijnen, and B.J. Zegers. 1992. Expression of type I insulin-like growth factor receptors on human peripheral blood mononuclear cells. *Endocrinology*. 131:2244–2250. doi:10.1210/endo.131.5.1425423.

Kook, H., S.B. Seo, and R. Jain. 2017. EZ Switch from EZH2 to EZH1: Histone Methylation Opens a Window of Cardiac Regeneration. *Circ. Res.* 121:91–94. doi:10.1161/CIRCRESAHA.117.311351.

Koretzky, G.A. 2010. Multiple Roles of CD4 and CD8 in T Cell Activation. *J. Immunol.* 185:2643–2644. doi:10.4049/JIMMUNOL.1090076.

Kosalai, S.T., M.H.A. Morsy, N. Papakonstantinou, L. Mansouri, N. Stavroyianni, C. Kanduri, K. Stamatopoulos, R. Rosenquist, and M. Kanduri. 2019. EZH2 upregulates the PI3K/AKT pathway through IGF1R and MYC in clinically aggressive chronic lymphocytic leukaemia. *Epigenetics*. 14:1125–1140. doi:10.1080/15592294.2019.1633867/SUPPL_FILE/KEPI_A_1633867_SM4771.ZIP .

Kotsantis, P., L.M. Silva, S. Irmscher, R.M. Jones, L. Folkes, N. Gromak, and E. Petermann. 2016. Increased global transcription activity as a mechanism of replication stress in cancer. *Nat. Commun. 2016 71*. 7:1–13. doi:10.1038/ncomms13087.

Kuemmerle, J.F. 2000. Endogenous IGF-I regulates IGF binding protein production in human intestinal smooth muscle cells. *Am. J. Physiol. Gastrointest. Liver Physiol.* 278. doi:10.1152/AJPGI.2000.278.5.G710.

Kumagai, S., Y. Togashi, T. Kamada, E. Sugiyama, H. Nishinakamura, Y. Takeuchi, K. Vitaly, K. Itahashi, Y. Maeda, S. Matsui, T. Shibahara, Y. Yamashita, T. Irie, A. Tsuge, S. Fukuoka, A. Kawazoe, H. Udagawa, K. Kirita, K. Aokage, G. Ishii, T. Kuwata, K. Nakama, M. Kawazu, T. Ueno, N. Yamazaki, K. Goto, M. Tsuboi, H. Mano, T. Doi, K. Shitara, and H. Nishikawa. 2020. The PD-1 expression balance between effector and regulatory T cells predicts the clinical efficacy of PD-1 blockade therapies. *Nat. Immunol.* 21:1346–1358. doi:10.1038/S41590-020-0769-3.

Kumar, D., A.L. Abdulovic, J. Viberg, A.K. Nilsson, T.A. Kunkel, and A. Chabes. 2011. Mechanisms of mutagenesis in vivo due to imbalanced dNTP pools. *Nucleic Acids Res.* 39:1360–1371. doi:10.1093/nar/gkq829.

Kwon, E.D., C.G. Drake, H.I. Scher, K. Fizazi, A. Bossi, A.J. van den Eertwegh, M. Krainer, N. Houede, R. Santos, H. Mahammedi, S. Ng, M. Maio, F.A. Franke, S. Sundar, N. Agarwal, A.M. Bergman, T.E. Ciuleanu, E. Korbenfeld, L. Sengelov, S. Hansen, C. Logothetis, T.M. Beer, M.B. McHenry, P. Gagnier, D. Liu, W.R. Gerritsen, and C.A. Investigators. 2014a. Ipilimumab versus placebo after radiotherapy in patients with metastatic castration-resistant prostate cancer that had

progressed after docetaxel chemotherapy (CA184-043): a multicentre, randomised, double-blind, phase 3 trial. *Lancet Oncol.* 15:700–712. doi:10.1016/S1470-2045(14)70189-5.

Kwon, E.D., C.G. Drake, H.I. Scher, K. Fizazi, A. Bossi, A.J.M. Van den Eertwegh, M. Krainer, N. Houede, R. Santos, H. Mahammedi, S. Ng, M. Maio, F.A. Franke, S. Sundar, N. Agarwal, A.M. Bergman, T.E. Ciuleanu, E. Korbenfeld, L. Sengeløv, S. Hansen, C. Logothetis, T.M. Beer, M.B. McHenry, P. Gagnier, D. Liu, and W.R. Gerritsen. 2014b. Ipilimumab versus placebo after radiotherapy in patients with metastatic castration-resistant prostate cancer that had progressed after docetaxel chemotherapy (CA184-043): a multicentre, randomised, double-blind, phase 3 trial. *Lancet Oncol.* 15:700–712. doi:10.1016/S1470-2045(14)70189-5.

Laron, Z. 2001. Insulin-like growth factor 1 (IGF-1): a growth hormone. *Mol. Pathol.* 54:311–6.

Laron, Z., S. Ginsberg, P. Lilos, M. Arbiv, and N. Vaisman. 2006. Body composition in untreated adult patients with Laron syndrome (primary GH insensitivity). *Clin. Endocrinol. (Oxf).* 65:114–117. doi:10.1111/J.1365-2265.2006.02558.X.

Laron, Z., A. Pertzelan, and M. Karp. 1968. Pituitary dwarfism with high serum levels of growth hormone. *Isr. J. Med. Sci.* 4:883–894.

Lastwika, K.J., W. Wilson, Q.K. Li, J. Norris, H. Xu, S.R. Ghazarian, H. Kitagawa, S. Kawabata, J.M. Taube, S. Yao, L.N. Liu, J.J. Gills, and P.A. Dennis. 2016. Control of PD-L1 Expression by Oncogenic Activation of the AKT-mTOR Pathway in Non-Small Cell Lung Cancer. *Cancer Res.* 76:227–238. doi:10.1158/0008-5472.CAN-14-3362.

Law-Ping-Man, S., F. Toutain, F. Rieux-Laucat, C. Picard, S. Kammerer-Jacquet, A. Magérus-Chatinet, A. Dupuy, and H. Adamski. 2018. Chronic granulomatous skin lesions leading to a diagnosis of TAP1 deficiency syndrome. *Pediatr. Dermatol.* 35:e375–e377. doi:10.1111/PDE.13676.

Lawrence, T. 2009. The Nuclear Factor NF-κB Pathway in Inflammation. *Cold Spring Harb. Perspect. Biol.* 1. doi:10.1101/CSHPERSPECT.A001651.

Lazzeri, M., A. Haese, A. De La Taille, J. Palou Redorta, T. McNicholas, G. Lughezzani, V. Scattoni, V. Bini, M. Freschi, A. Sussman, B. Ghaleh, P. Le Corvoisier, J.

Alberola Bou, S. Esquena Fernández, M. Graefen, and G. Guazzoni. 2013. Serum Isoform [−2]proPSA Derivatives Significantly Improve Prediction of Prostate Cancer at Initial Biopsy in a Total PSA Range of 2–10 ng/ml: A Multicentric European Study. *Eur. Urol.* 63:986–994. doi:10.1016/J.EURURO.2013.01.011.

Leach, D.R., M.F. Krummel, and J.P. Allison. 1996. Enhancement of antitumor immunity by CTLA-4 blockade. *Science*. 271:1734–1736. doi:10.1126/SCIENCE.271.5256.1734.

Lee, C., L. Raffaghello, S. Brandhorst, F.M. Safdie, G. Bianchi, A. Martin-Montalvo, V. Pistoia, M. Wei, S. Hwang, A. Merlino, L. Emionite, R. De Cabo, and V.D. Longo. 2012. Fasting cycles retard growth of tumors and sensitize a range of cancer cell types to chemotherapy. *Sci. Transl. Med.* 4. doi:10.1126/SCITRANSLMED.3003293/SUPPL_FILE/4-124RA27_SM.PDF.

Lee, C., F.M. Safdie, L. Raffaghello, M. Wei, F. Madia, E. Parrella, D. Hwang, P. Cohen, G. Bianchi, and V.D. Longo. 2010. Reduced Levels of IGF-I Mediate Differential Protection of Normal and Cancer Cells in Response to Fasting and Improve Chemotherapeutic Index. *Cancer Res.* 70:1564–1572. doi:10.1158/0008-5472.CAN-09-3228.

Lee, C.G., T.E. Kim, S. Hong, J. Chu, J.E. Kang, H.G. Park, J.Y. Choi, K. Song, S.Y. Rha, S. Lee, J.S. Choi, S.M. Kim, H.M. Jeong, and Y.K. Shin. 2021. Antibody-Based Targeting of Interferon-Beta-1a Mutein in HER2-Positive Cancer Enhances Antitumor Effects Through Immune Responses and Direct Cell Killing. *Front. Pharmacol.* 11:2166. doi:10.3389/FPHAR.2020.608774/BIBTEX.

Lee, G.R. 2018. The Balance of Th17 versus Treg Cells in Autoimmunity. *Int. J. Mol. Sci.* 19. doi:10.3390/IJMS19030730.

Li, J., E. Choi, H. Yu, and X. chen Bai. 2019. Structural basis of the activation of type 1 insulin-like growth factor receptor. *Nat. Commun.* 10. doi:10.1038/S41467-019-12564-0.

Li, T., and Z.J. Chen. 2018. The cGAS-cGAMP-STI NG pathway connects DNA damage to inflammation, senescence, and cancer. *J. Exp. Med.* 215:1287–1299. doi:10.1084/jem.20180139.

Liang, M.-Q., F.-Q. Yu, and C. Chen. 2020. C-Myc regulates PD-L1 expression in

esophageal squamous cell carcinoma. *Am. J. Transl. Res.* 12:379.

Lieberman, J. 2003. The ABCs of granule-mediated cytotoxicity: new weapons in the arsenal. *Nat. Rev. Immunol. 2003 35*. 3:361–370. doi:10.1038/nri1083.

Lin, J.X., P. Li, D. Liu, H.T. Jin, J. He, M.A.U. Rasheed, Y. Rochman, L. Wang, K. Cui, C. Liu, B.L. Kelsall, R. Ahmed, and W.J. Leonard. 2012. Critical Role of STAT5 Transcription Factor Tetramerization for Cytokine Responses and Normal Immune Function. *Immunity*. 36:586–599. doi:10.1016/J.IMMUNI.2012.02.017.

Lin, Y., J. Xu, and H. Lan. 2019. Tumor-associated macrophages in tumor metastasis: biological roles and clinical therapeutic applications. *J. Hematol. Oncol. 2019 121*. 12:1–16. doi:10.1186/S13045-019-0760-3.

Lin, Y., L. Xu, H. Jin, Y. Zhong, J. Di, and Q. de Lin. 2009. CXCL12 enhances exogenous CD4+CD25+ T cell migration and prevents embryo loss in non-obese diabetic mice. *Fertil. Steril.* 91:2687–2696. doi:10.1016/J.FERTNSTERT.2008.01.109.

Ling, A., A. Löfgren-Burström, P. Larsson, X. Li, M.L. Wikberg, Å. Öberg, R. Stenling, S. Edin, and R. Palmqvist. 2017. TAP1 down-regulation elicits immune escape and poor prognosis in colorectal cancer. *Oncoimmunology*. 6. doi:10.1080/2162402X.2017.1356143.

Lipinski, R.J., C.H. Cook, D.H. Barnett, J.J. Gipp, R.E. Peterson, and W. Bushman. 2005. Sonic hedgehog signaling regulates the expression of insulin-like growth factor binding protein-6 during fetal prostate development. *Dev. Dyn.* 233:829–836. doi:10.1002/DVDY.20414.

Littman, D.R., and A.Y. Rudensky. 2010. Th17 and regulatory T cells in mediating and restraining inflammation. *Cell*. 140:845–858. doi:10.1016/J.CELL.2010.02.021.

Liu, J.P., J. Baker, A.S. Perkins, E.J. Robertson, and A. Efstratiadis. 1993. Mice carrying null mutations of the genes encoding insulin-like growth factor I (Igf-1) and type 1 IGF receptor (Igf1r). *Cell*. 75:59–72. doi:10.1016/S0092-8674(05)80084-4.

Liu, T., L. Zhang, D. Joo, and S.C. Sun. 2017a. NF-κB signaling in inflammation. *Signal Transduct. Target. Ther.* 2:17023. doi:10.1038/sigtrans.2017.23.

Liu, T., L. Zhang, D. Joo, and S.C. Sun. 2017b. NF-κB signaling in inflammation. *Signal Transduct. Target. Ther. 2017 21*. 2:1–9. doi:10.1038/sigtrans.2017.23.

Liu, X., T. Turbyville, A. Fritz, and L. Whitesell. 1998. Inhibition of insulin-like growth

factor I receptor expression in neuroblastoma cells induces the regression of established tumors in mice. *Cancer Res.* 58:5432–8.

Livak, K.J., and T.D. Schmittgen. 2001. Analysis of Relative Gene Expression Data Using Real-Time Quantitative PCR and the 2−ΔΔCT Method. *Methods*. 25:402–408. doi:10.1006/meth.2001.1262.

Lloret, M., P.C. Lara, E. Bordón, B. Pinar, A. Rey, O. Falcón, F. Molano, and M.A. Hernández. 2007. IGF-1R expression in localized cervical carcinoma patients treated by radiochemotherapy. *Gynecol. Oncol.* 106:8–11. doi:10.1016/J.YGYNO.2007.04.004.

Lochhead, P.A., M. Coghlan, S.Q.J. Rice, and C. Sutherland. 2001. Inhibition of GSK-3 selectively reduces glucose-6-phosphatase and phosphatase and phosphoenolypyruvate carboxykinase gene expression. *Diabetes*. 50:937–946. doi:10.2337/DIABETES.50.5.937.

Loeb, S., M.G. Sanda, D.L. Broyles, S.S. Shin, C.H. Bangma, J.T. Wei, A.W. Partin, G.G. Klee, K.M. Slawin, L.S. Marks, R.H.N. Van Schaik, D.W. Chan, L.J. Sokoll, A.B. Cruz, I.A. Mizrahi, and W.J. Catalona. 2015. The Prostate Health Index Selectively Identifies Clinically Significant Prostate Cancer. *J. Urol.* 193:1163–1169. doi:10.1016/J.JURO.2014.10.121.

Lopes, R.L., T.J. Borges, R.F. Zanin, and C. Bonorino. 2016. IL-10 is required for polarization of macrophages to M2-like phenotype by mycobacterial DnaK (heat shock protein 70). *Cytokine*. 85:123–129. doi:10.1016/j.cyto.2016.06.018.

Lu, C., J.D. Klement, M.L. Ibrahim, W. Xiao, P.S. Redd, A. Nayak-Kapoor, G. Zhou, and K. Liu. 2019. Type i interferon suppresses tumor growth through activating the STAT3-granzyme B pathway in tumor-infiltrating cytotoxic T lymphocytes. *J. Immunother. Cancer*. 7:1–11. doi:10.1186/S40425-019-0635-8/FIGURES/7.

Lu, M.C., C.L. Yu, H.C. Chen, H.C. Yu, H.B. Huang, and N.S. Lai. 2014. Increased miR-223 expression in T cells from patients with rheumatoid arthritis leads to decreased insulin-like growth factor-1-mediated interleukin-10 production. *Clin. Exp. Immunol.* 177:641–651. doi:10.1111/cei.12374.

Lu, X., J.W. Horner, E. Paul, X. Shang, P. Troncoso, P. Deng, S. Jiang, Q. Chang, D.J. Spring, P. Sharma, J.A. Zebala, D.Y. Maeda, Y.A. Wang, and R.A. Depinho. 2017.

Effective combinatorial immunotherapy for castration-resistant prostate cancer. *Nature*. 543:728–732. doi:10.1038/NATURE21676.

Ma, J., M.N. Pollak, E. Giovannucci, J.M. Chan, Y. Tao, C.H. Hennekens, and M.J. Stampfer. 1999. Prospective Study of Colorectal Cancer Risk in Men and Plasma Levels of Insulin-Like Growth Factor (IGF)-I and IGF-Binding Protein-3. *JNCI J. Natl. Cancer Inst.* 91:620–625. doi:10.1093/jnci/91.7.620.

Maddur, M.S., and J. Bayry. 2015. B cells drive Th2 responses by instructing human dendritic cell maturation. *Oncoimmunology*. 4. doi:10.1080/2162402X.2015.1005508.

Maio, M., S.L. Groenland, T. Bauer, D. Rischin, I. Gardeazabal, V. Moreno, J.M. Trigo Perez, M. Chisamore, J.S. Shaik, F. Rigat, C. Ellis, H. Chen, R. Gagnon, S. Scherer, D. Turner, S. Yadavilli, M. Ballas, A. Hoos, E. Angevin, S. Schuster, D. Akolkar, S. Patil, D. Patil, V. Datta, A. Srinivasan, R. Datar, M.M. Grzybowski, J. Pe ˛czkowicz-Szyszka, P. Wolska, P.S. Sta, M. Welzer, E. Nikolaev, A.M. Siwi Nska, R. Błaszczyk, B. Borek, M. Dzie, A. Gzik, J. Nowicka, J. Brzezi Nska, K. Je, J. Chrzanowski, A. Gołe, J. Olczak, K. Dzwonek, and P. Dobrza. 2019. Targeting ARG2 as a novel therapeutic approach for cancer. *Ann. Oncol.* 30:v793–v794. doi:10.1093/ANNONC/MDZ268.100.

Malaguarnera, R., and A. Belfiore. 2011. The insulin receptor: a new target for cancer therapy. *Front. Endocrinol. (Lausanne).* 2. doi:10.3389/FENDO.2011.00093.

Mangan, P.R., L.E. Harrington, D.B. O'Quinn, W.S. Helms, D.C. Bullard, C.O. Elson, R.D. Hatton, S.M. Wahl, T.R. Schoeb, and C.T. Weaver. 2006. Transforming growth factor-beta induces development of the T(H)17 lineage. *Nature*. 441:231–234. doi:10.1038/NATURE04754.

Manning, B.D., and L.C. Cantley. 2007. AKT/PKB signaling: navigating downstream. *Cell*. 129:1261–1274. doi:10.1016/J.CELL.2007.06.009.

Mantovani, A., C.A. Dinarello, M. Molgora, and C. Garlanda. 2019. Interleukin-1 and Related Cytokines in the Regulation of Inflammation and Immunity. *Immunity*. 50:778–795. doi:10.1016/J.IMMUNI.2019.03.012.

Marx, V. 2021. Method of the Year: spatially resolved transcriptomics. *Nat. Methods*. 18:9–14. doi:10.1038/S41592-020-01033-Y.

De Marzo, A.M., M.C. Haffner, T.L. Lotan, S. Yegnasubramanian, and W.G. Nelson.

2016. Premalignancy in Prostate Cancer: Rethinking What we Know. *Cancer Prev. Res. (Phila).* 9:648–656. doi:10.1158/1940-6207.CAPR-15-0431.

Massoner, P., M. Ladurner Rennau, I. Heidegger, A. Kloss-Brandstätter, M. Summerer, E. Reichhart, G. Schäfer, and H. Klocker. 2011. Expression of the IGF axis is decreased in local prostate cancer but enhanced after benign prostate epithelial differentiation and TGF-β treatment. *Am. J. Pathol.* 179:2905–19. doi:10.1016/j.ajpath.2011.08.026.

Mathieson, W., and G.A. Thomas. 2020. Why Formalin-fixed, Paraffin-embedded Biospecimens Must Be Used in Genomic Medicine: An Evidence-based Review and Conclusion. *J. Histochem. Cytochem.* 68:543. doi:10.1369/0022155420945050.

Matsuno, Y., Y. Atsumi, A. Shimizu, K. Katayama, H. Fujimori, M. Hyodo, Y. Minakawa, Y. Nakatsu, S. Kaneko, R. Hamamoto, T. Shimamura, S. Miyano, T. Tsuzuki, F. Hanaoka, and K. ichi Yoshioka. 2019. Replication stress triggers microsatellite destabilization and hypermutation leading to clonal expansion in vitro. *Nat. Commun. 2019 101*. 10:1–13. doi:10.1038/s41467-019-11760-2.

Matz-Soja, M., S. Aleithe, E. Marbach, J. Böttger, K. Arnold, W. Schmidt-Heck, J. Kratzsch, and R. Gebhardt. 2014. Hepatic Hedgehog signaling contributes to the regulation of IGF1 and IGFBP1 serum levels. *Cell Commun. Signal.* 12:11. doi:10.1186/1478-811X-12-11.

Meadows, S.A., F. Vega, A. Kashishian, D. Johnson, V. Diehl, L.L. Miller, A. Younes, and B.J. Lannutti. 2012. PI3Kδ inhibitor, GS-1101 (CAL-101), attenuates pathway signaling, induces apoptosis, and overcomes signals from the microenvironment in cellular models of Hodgkin lymphoma. *Blood*. 119:1897–1900. doi:10.1182/BLOOD-2011-10-386763.

Melnik, B.C. 2009. Role of FGFR2-signaling in the pathogenesis of acne. *Dermatoendocrinol.* 1:141. doi:10.4161/DERM.1.3.8474.

Melnik, B.C., S.M. John, and G. Schmitz. 2011. Over-stimulation of insulin/IGF-1 signaling by western diet may promote diseases of civilization: lessons learnt from laron syndrome. *Nutr. Metab. (Lond).* 8:41. doi:10.1186/1743-7075-8-41.

Meyts, P. De. 2016. The Insulin Receptor and Its Signal Transduction Network. *Endotext*.

De Meyts, P., and J. Whittaker. 2002. Structural biology of insulin and IGF1 receptors: implications for drug design. *Nat. Rev. Drug Discov.* 1:769–783.

doi:10.1038/NRD917.

Mildner, A., and S. Jung. 2014. Development and function of dendritic cell subsets. *Immunity*. 40:642–656. doi:10.1016/J.IMMUNI.2014.04.016.

Mills, C.D., K. Kincaid, J.M. Alt, M.J. Heilman, and A.M. Hill. 2000. M-1/M-2 macrophages and the Th1/Th2 paradigm. *J. Immunol.* 164:6166–6173. doi:10.4049/JIMMUNOL.164.12.6166.

Mills, J. V., E. Osher, G. Rieunier, I.G. Mills, and V.M. Macaulay. 2021. IGF-1R nuclear import and recruitment to chromatin involves both alpha and beta subunits. *Discov. Oncol.* 12:1–11. doi:10.1007/S12672-021-00407-8/FIGURES/4.

Milosevic, M., P. Warde, C. Meńard, P. Chung, A. Toi, A. Ishkanian, M. McLean, M. Pintilie, J. Sykes, M. Gospodarowicz, C. Catton, R.P. Hill, and R. Bristow. 2012. Tumor hypoxia predicts biochemical failure following radiotherapy for clinically localized prostate cancer. *Clin. Cancer Res.* 18:2108–2114. doi:10.1158/1078-0432.CCR-11-2711.

Mimae, T., K. Tsuta, T. Kondo, H. Nitta, T.M. Grogan, M. Okada, H. Asamura, and H. Tsuda. 2012. Protein expression and gene copy number changes of receptor tyrosine kinase in thymomas and thymic carcinomas. *Ann. Oncol.* 23:3129–3137. doi:10.1093/ANNONC/MDS147.

Mittendorf, E.A., A. V. Philips, F. Meric-Bernstam, N. Qiao, Y. Wu, S. Harrington, X. Su, Y. Wang, A.M. Gonzalez-Angulo, A. Akcakanat, A. Chawla, M. Curran, P. Hwu, P. Sharma, J.K. Litton, J.J. Molldrem, and G. Alatrash. 2014. PD-L1 Expression in Triple-Negative Breast Cancer. *Cancer Immunol. Res.* 2:361–370. doi:10.1158/2326-6066.CIR-13-0127.

Miyagawa, I., S. Nakayamada, K. Nakano, K. Yamagata, K. Sakata, K. Yamaoka, and Y. Tanaka. 2017. Induction of Regulatory T Cells and Its Regulation with Insulin-like Growth Factor/Insulin-like Growth Factor Binding Protein-4 by Human Mesenchymal Stem Cells. *J. Immunol.* 199:1616–1625. doi:10.4049/jimmunol.1600230.

Modolell, M., B.S. Choi, R.O. Ryan, M. Hancock, R.G. Titus, T. Abebe, A. Hailu, I. Müller, M.E. Rogers, C.R.M. Bangham, M. Munder, and P. Kropf. 2009. Local Suppression of T Cell Responses by Arginase-Induced L-Arginine Depletion in

Nonhealing Leishmaniasis. *PLoS Negl. Trop. Dis.* 3:480. doi:10.1371/JOURNAL.PNTD.0000480.

Mohrin, M., J. Liu, J. Zavala-Solorio, S. Bhargava, J. Maxwell Trumble, A. Brito, D. Hu, D. Brooks, G. Koukos, L. Alabdulaaly, J.S. Paw, K. Hake, G. Kolumam, M.L. Bouxsein, R. Baron, Y. Kutskova, and A. Freund. 2021. Inhibition of longevity regulator PAPP-A modulates tissue homeostasis via restraint of mesenchymal stromal cells. *Aging Cell*. 20. doi:10.1111/ACEL.13313.

Moins-Teisserenc, H., S.D. Gadola, M. Cella, P.R. Dunbar, A. Exley, N. Blake, C. Baycal, J. Lambert, P. Bigliardi, M. Willemsen, M. Jones, S. Buechner, M. Colonna, W.L. Gross, and V. Cerundolo. 1999. Association of a syndrome resembling Wegener's granulomatosis with low surface expression of HLA class-I molecules. *Lancet (London, England)*. 354:1598–1603. doi:10.1016/S0140-6736(99)04206-3.

Montgomery, R.B., E.A. Mostaghel, R. Vessella, D.L. Hess, T.F. Kalhorn, C.S. Higano, L.D. True, and P.S. Nelson. 2008. Maintenance of intratumoral androgens in metastatic prostate cancer: A mechanism for castration-resistant tumor growth. *Cancer Res.* 68:4447–4454. doi:10.1158/0008-5472.CAN-08-0249.

Moore, T.C., and T.M. Petro. 2013. IRF3 and ERK MAP-kinases control Nitric Oxide production from macrophages in response to poly-I:C. *FEBS Lett.* 587:3014. doi:10.1016/J.FEBSLET.2013.07.025.

Moretta, L., R. Biassoni, C. Bottino, C. Cantoni, D. Pende, M.C. Mingari, and A. Moretta. 2002. Human NK cells and their receptors. *Microbes Infect.* 4:1539–1544. doi:10.1016/S1286-4579(02)00037-0.

Morimoto, Y., T. Kishida, S. ichiro Kotani, K. Takayama, and O. Mazda. 2018. Interferon-β signal may up-regulate PD-L1 expression through IRF9-dependent and independent pathways in lung cancer cells. *Biochem. Biophys. Res. Commun.* 507:330–336. doi:10.1016/J.BBRC.2018.11.035.

Moschos, S.J., and C.S. Mantzoros. 2002. The role of the IGF system in cancer: from basic to clinical studies and clinical applications. *Oncology*. 63:317–332. doi:10.1159/000066230.

Moul, J.W. 2014. Utility of LHRH antagonists for advanced prostate cancer. *Can. J. Urol.* 21:22–27.

Mountzios, G., I. Kostopoulos, V. Kotoula, I. Sfakianaki, E. Fountzilas, K. Markou, I. Karasmanis, S. Leva, N. Angouridakis, K. Vlachtsis, A. Nikolaou, I. Konstantinidis, and G. Fountzilas. 2013. Insulin-Like Growth Factor 1 Receptor (IGF1R) Expression and Survival in Operable Squamous-Cell Laryngeal Cancer. *PLoS One*. 8:e54048. doi:10.1371/journal.pone.0054048.

Mukherjee, R., P. Kanti Barman, P. Kumar Thatoi, R. Tripathy, B. Kumar Das, and B. Ravindran. 2015. Non-Classical monocytes display inflammatory features: Validation in Sepsis and Systemic Lupus Erythematous. *Sci. Reports 2015 51*. 5:1–14. doi:10.1038/srep13886.

Murphy, L.O., J.P. MacKeigan, and J. Blenis. 2004. A network of immediate early gene products propagates subtle differences in mitogen-activated protein kinase signal amplitude and duration. *Mol. Cell. Biol.* 24:144–153. doi:10.1128/MCB.24.1.144-153.2004.

Murphy, L.O., S. Smith, R.H. Chen, D.C. Fingar, and J. Blenis. 2002. Molecular interpretation of ERK signal duration by immediate early gene products. *Nat. Cell Biol.* 4:556–564. doi:10.1038/NCB822.

Murphy, N., R. Carreras-Torres, M. Song, A.T. Chan, R.M. Martin, N. Papadimitriou, N. Dimou, K.K. Tsilidis, B. Banbury, K.E. Bradbury, J. Besevic, S. Rinaldi, E. Riboli, A.J. Cross, R.C. Travis, C. Agnoli, D. Albanes, S.I. Berndt, S. Bézieau, D.T. Bishop, H. Brenner, D.D. Buchanan, N.C. Onland-Moret, A. Burnett-Hartman, P.T. Campbell, G. Casey, S. Castellví-Bel, J. Chang-Claude, M.D. Chirlaque, A. de la Chapelle, D. English, J.C. Figueiredo, S.J. Gallinger, G.G. Giles, S.B. Gruber, A. Gsur, J. Hampe, H. Hampel, T.A. Harrison, M. Hoffmeister, L. Hsu, W.Y. Huang, J.R. Huyghe, M.A. Jenkins, T.O. Keku, T. Kühn, S.S. Kweon, L. Le Marchand, C.I. Li, L. Li, A. Lindblom, V. Martín, R.L. Milne, V. Moreno, P.A. Newcomb, K. Offit, S. Ogino, J. Ose, V. Perduca, A.I. Phipps, E.A. Platz, J.D. Potter, C. Qu, G. Rennert, L.C. Sakoda, C. Schafmayer, R.E. Schoen, M.L. Slattery, C.M. Tangen, C.M. Ulrich, F.J.B. van Duijnhoven, B. Van Guelpen, K. Visvanathan, P. Vodicka, L. Vodickova, V. Vymetalkova, H. Wang, E. White, A. Wolk, M.O. Woods, A.H. Wu, W. Zheng, U. Peters, and M.J. Gunter. 2020a. Circulating Levels of Insulin-like Growth Factor 1 and Insulin-like Growth Factor Binding Protein 3 Associate With Risk of Colorectal

Cancer Based on Serologic and Mendelian Randomization Analyses. *Gastroenterology*. 158:1300-1312.e20. doi:10.1053/J.GASTRO.2019.12.020.

Murphy, N., A. Knuppel, N. Papadimitriou, R.M. Martin, K.K. Tsilidis, K. Smith-Byrne, G. Fensom, A. Perez-Cornago, R.C. Travis, T.J. Key, and M.J. Gunter. 2020b. Insulin-like growth factor-1, insulin-like growth factor-binding protein-3, and breast cancer risk: observational and Mendelian randomization analyses with ~430 000 women. *Ann. Oncol. Off. J. Eur. Soc. Med. Oncol.* 31:641–649. doi:10.1016/J.ANNONC.2020.01.066.

Murray, P.J. 2017. Macrophage Polarization. *http://dx.doi.org/10.1146/annurev-physiol-022516-034339*. 79:541–566. doi:10.1146/ANNUREV-PHYSIOL-022516-034339.

Nackiewicz, D., M. Dan, M. Speck, S.Z. Chow, Y.C. Chen, J.A. Pospisilik, C.B. Verchere, and J.A. Ehses. 2020. Islet Macrophages Shift to a Reparative State following Pancreatic Beta-Cell Death and Are a Major Source of Islet Insulin-like Growth Factor-1. *iScience*. 23. doi:10.1016/J.ISCI.2019.100775.

Nagarsheth, N., M.S. Wicha, and W. Zou. 2017. Chemokines in the cancer microenvironment and their relevance in cancer immunotherapy. *Nat. Rev. Immunol.* 17:559. doi:10.1038/NRI.2017.49.

Nakagawa, M., and I. Kitabayashi. 2018. Oncogenic roles of enhancer of zeste homolog 1/2 in hematological malignancies. *Cancer Sci.* 109:2342. doi:10.1111/CAS.13655.

Ng, N., K. Purshouse, I.P. Foskolou, M.M. Olcina, and E.M. Hammond. 2018. Challenges to DNA replication in hypoxic conditions. *FEBS J.* 285:1563–1571. doi:10.1111/FEBS.14377.

Ng, T.H.S., G.J. Britton, E. V. Hill, J. Verhagen, B.R. Burton, and D.C. Wraith. 2013. Regulation of adaptive immunity; the role of interleukin-10. *Front. Immunol.* 4. doi:10.3389/fimmu.2013.00129.

Nicholson, K.M., and N.G. Anderson. 2002. The protein kinase B/Akt signalling pathway in human malignancy. *Cell. Signal.* 14:381–395. doi:10.1016/S0898-6568(01)00271-6.

Nicotera, T.M., D.P. Schuster, M. Bourhim, K. Chadha, G. Klaich, and D.A. Corral. 2009. Regulation of PSA secretion and survival signaling by calcium-independent phopholipase A(2)beta in prostate cancer cells. *Prostate*. 69:1270–1280.

doi:10.1002/PROS.20968.

Nordstrand, A., S.H. Bergström, E. Thysell, E. Bovinder-Ylitalo, U.H. Lerner, A. Widmark, A. Bergh, and P. Wikström. 2017a. Inhibition of the insulin-like growth factor-1 receptor potentiates acute effects of castration in a rat model for prostate cancer growth in bone. *Clin. Exp. Metastasis*. 34:261–271. doi:10.1007/s10585-017-9848-8.

Nordstrand, A., · Sofia, H. Bergström, E. Thysell, E. Bovinder-Ylitalo, · Ulf, H. Lerner, A. Widmark, A. Bergh, and · Pernilla Wikström. 2017b. Inhibition of the insulin-like growth factor-1 receptor potentiates acute effects of castration in a rat model for prostate cancer growth in bone. 34:261–271. doi:10.1007/s10585-017-9848-8.

Norris, J.L., and A.S. Baldwin. 1999. Oncogenic Ras Enhances NF-κB Transcriptional Activity through Raf-dependent and Raf-independent Mitogen-activated Protein Kinase Signaling Pathways *. *J. Biol. Chem.* 274:13841–13846. doi:10.1074/JBC.274.20.13841.

Numata, K., T. Oshima, K. Sakamaki, K. Yoshihara, T. Aoyama, T. Hayashi, T. Yamada, T. Sato, H. Cho, M. Shiozawa, T. Yoshikawa, Y. Rino, C. Kunisaki, M. Akaike, T. Imada, and M. Masuda. 2016. Clinical significance of IGF1R gene expression in patients with Stage II/III gastric cancer who receive curative surgery and adjuvant chemotherapy with S-1. *J. Cancer Res. Clin. Oncol.* 142:415–422. doi:10.1007/s00432-015-2039-6.

Nutt, S.L., P.D. Hodgkin, D.M. Tarlinton, and L.M. Corcoran. 2015. The generation of antibody-secreting plasma cells. *Nat. Rev. Immunol. 2015 153*. 15:160–171. doi:10.1038/nri3795.

O'Connor, R. 2003. Regulation of IGF-I Receptor Signaling in Tumor Cells. *Horm. Metab. Res.* 35:771–777. doi:10.1055/s-2004-814166.

O'Donnell, J.S., D. Massi, M.W.L. Teng, and M. Mandala. 2018a. PI3K-AKT-mTOR inhibition in cancer immunotherapy, redux. *Semin. Cancer Biol.* 48:91–103. doi:10.1016/J.SEMCANCER.2017.04.015.

O'Donnell, J.S., M.W.L. Teng, and M.J. Smyth. 2018b. Cancer immunoediting and resistance to T cell-based immunotherapy. *Nat. Rev. Clin. Oncol. 2018 163*. 16:151–167. doi:10.1038/s41571-018-0142-8.

O'Neill, B.T., K.Y. Lee, K. Klaus, S. Softic, M.T. Krumpoch, J. Fentz, K.I. Stanford, M.M. Robinson, W. Cai, A. Kleinridders, R.O. Pereira, M.F. Hirshman, E.D. Abel, D. Accili, L.J. Goodyear, K.S. Nair, and C.R. Kahn. 2016. Insulin and IGF-1 receptors regulate FoxO-mediated signaling in muscle proteostasis. *J. Clin. Invest.* 126:3433–46. doi:10.1172/JCI86522.

Olingy, C.E., H.Q. Dinh, and C.C. Hedrick. 2019. Monocyte heterogeneity and functions in cancer. *J. Leukoc. Biol.* 106:309–322. doi:10.1002/JLB.4RI0818-311R.

Opal, S.M., and V.A. DePalo. 2000. Anti-inflammatory cytokines. *Chest*. 117:1162–1172. doi:10.1378/CHEST.117.4.1162.

Ottoson, N.C., J.T. Pribila, A.S.H. Chan, and Y. Shimizu. 2001. Cutting edge: T cell migration regulated by CXCR4 chemokine receptor signaling to ZAP-70 tyrosine kinase. *J. Immunol.* 167:1857–1861. doi:10.4049/JIMMUNOL.167.4.1857.

Oyewole-Said, D., V. Konduri, J. Vazquez-Perez, S.A. Weldon, J.M. Levitt, and W.K. Decker. 2020. Beyond T-Cells: Functional Characterization of CTLA-4 Expression in Immune and Non-Immune Cell Types. *Front. Immunol.* 11:3168. doi:10.3389/FIMMU.2020.608024/BIBTEX.

Ozga, A.J., M.T. Chow, and A.D. Luster. 2021. Chemokines and the immune response to cancer. *Immunity*. 54:859–874. doi:10.1016/J.IMMUNI.2021.01.012.

Packham, S., D. Warsito, Y. Lin, S. Sadi, R. Karlsson, B. Sehat, and O. Larsson. 2014. Nuclear translocation of IGF-1R via p150Glued and an importin-β/RanBP2-dependent pathway in cancer cells. *Oncogene 2015 3417*. 34:2227–2238. doi:10.1038/onc.2014.165.

Pandini, G., F. Frasca, R. Mineo, L. Sciacca, R. Vigneri, and A. Belfiore. 2002. Insulin/insulin-like growth factor I hybrid receptors have different biological characteristics depending on the insulin receptor isoform involved. *J. Biol. Chem.* 277:39684–39695. doi:10.1074/JBC.M202766200.

Pandini, G., M. Genua, F. Frasca, R. Vigneri, and A. Belfiore. 2009. Sex Steroids Upregulate the IGF-1R in Prostate Cancer Cells through a Nongenotropic Pathway. *Ann. N. Y. Acad. Sci.* 1155:263–267. doi:10.1111/j.1749-6632.2009.04361.x.

Pandini, G., R. Mineo, F. Frasca, C.T. Roberts, M. Marcelli, R. Vigneri, and A. Belfiore. 2005. Androgens up-regulate the insulin-like growth factor-I receptor in prostate

cancer cells. *Cancer Res.* 65:1849–1857. doi:10.1158/0008-5472.CAN-04-1837.

Pandya, P.H., M.E. Murray, K.E. Pollok, and J.L. Renbarger. 2016. The Immune System in Cancer Pathogenesis: Potential Therapeutic Approaches. *J. Immunol. Res.* 2016. doi:10.1155/2016/4273943.

Parkes, E.E., S.M. Walker, L.E. Taggart, N. McCabe, L.A. Knight, R. Wilkinson, K.D. McCloskey, N.E. Buckley, K.I. Savage, M. Salto-Tellez, S. McQuaid, M.T. Harte, P.B. Mullan, D.P. Harkin, and R.D. Kennedy. 2017. Activation of STING-Dependent Innate Immune Signaling By S-Phase-Specific DNA Damage in Breast Cancer. *JNCI J. Natl. Cancer Inst.* 109. doi:10.1093/JNCI/DJW199.

Parmar, H., I. Edwards, R.H. Phillips, I. Allen, and S.I. Lightman. 1987. Orchiectomy versus Long-acting D-Trp-6-LHRH in Advanced Prostatic Cancer. *Br. J. Urol.* 59:248–254. doi:10.1111/j.1464-410X.1987.tb04616.x.

Patsoukis, N., D. Sari, and V.A. Boussiotis. 2012. PD-1 inhibits T cell proliferation by upregulating p27 and p15 and suppressing Cdc25A. *Cell Cycle*. 11:4305–4309. doi:10.4161/CC.22135.

Patsoukis, N., Q. Wang, L. Strauss, and V.A. Boussiotis. 2020. Revisiting the PD-1 pathway. *Sci. Adv.* 6. doi:10.1126/SCIADV.ABD2712/ASSET/8662045C-ECEA-4ECE-B989-814BF9AF17E2/ASSETS/GRAPHIC/ABD2712-F5.JPEG.

Paul, W.E., and R.A. Seder. 1994. Lymphocyte responses and cytokines. *Cell*. 76:241–251. doi:10.1016/0092-8674(94)90332-8.

Peiró, G., S. Benlloch, L. Sánchez-Tejada, E. Adrover, E. Lerma, F.M. Peiró, J. Sánchez-Payá, and F.I. Aranda. 2009. Low activation of Insulin-like Growth Factor 1-Receptor (IGF1R) is associated with local recurrence in early breast carcinoma. *Breast Cancer Res. Treat.* 117:433–441. doi:10.1007/S10549-008-0139-6.

Pennock, N.D., S. Jindal, W. Horton, D. Sun, J. Narasimhan, L. Carbone, S.S. Fei, R. Searles, C.A. Harrington, J. Burchard, S. Weinmann, P. Schedin, and Z. Xia. 2019. RNA-seq from archival FFPE breast cancer samples: Molecular pathway fidelity and novel discovery. *BMC Med. Genomics*. 12:1–18. doi:10.1186/S12920-019-0643-Z/TABLES/2.

Perez-Cornago, A., P.N. Appleby, T. Pischon, K.K. Tsilidis, A. Tjønneland, A. Olsen, K. Overvad, R. Kaaks, T. Kühn, H. Boeing, A. Steffen, A. Trichopoulou, P. Lagiou, M.

Kritikou, V. Krogh, D. Palli, C. Sacerdote, R. Tumino, H.B. Bueno-de-Mesquita, A. Agudo, N. Larrañaga, E. Molina-Portillo, A. Barricarte, M.-D. Chirlaque, J.R. Quirós, P. Stattin, C. Häggström, N. Wareham, K.-T. Khaw, J.A. Schmidt, M. Gunter, H. Freisling, D. Aune, H. Ward, E. Riboli, T.J. Key, and R.C. Travis. 2017. Tall height and obesity are associated with an increased risk of aggressive prostate cancer: results from the EPIC cohort study. *BMC Med.* 15:115. doi:10.1186/s12916-017-0876-7.

Pidugu, V.K., M.M. Wu, A.H. Yen, H.B. Pidugu, K.W. Chang, C.J. Liu, and T.C. Lee. 2019. IFIT1 and IFIT3 promote oral squamous cell carcinoma metastasis and contribute to the anti-tumor effect of gefitinib via enhancing p-EGFR recycling. *Oncogene*. 38:3232–3247. doi:10.1038/S41388-018-0662-9.

Pieper, K., B. Grimbacher, and H. Eibel. 2013. B-cell biology and development. *J. Allergy Clin. Immunol.* 131:959–971. doi:10.1016/J.JACI.2013.01.046.

Pierorazio, P.M., P.C. Walsh, A.W. Partin, and J.I. Epstein. 2013. Prognostic Gleason grade grouping: data based on the modified Gleason scoring system. *BJU Int.* 111:753–760. doi:10.1111/J.1464-410X.2012.11611.X.

Pires, B.R.B., R. Binato, G.M. Ferreira, R. Cecchini, C. Panis, and E. Abdelhay. 2018. NF-kappaB Regulates Redox Status in Breast Cancer Subtypes. *Genes (Basel).* 9. doi:10.3390/GENES9070320.

Pollak, M. 2008. Insulin and insulin-like growth factor signalling in neoplasia. *Nat. Rev. Cancer*. 8:915–928. doi:10.1038/nrc2536.

Pollak, M. 2012. The insulin and insulin-like growth factor receptor family in neoplasia: an update. *Nat. Rev. Cancer*. 12:159–169. doi:10.1038/NRC3215.

Pombo Antunes, A.R., I. Scheyltjens, F. Lodi, J. Messiaen, A. Antoranz, J. Duerinck, D. Kancheva, L. Martens, K. De Vlaminck, H. Van Hove, S.S. Kjølner Hansen, F.M. Bosisio, K. Van der Borght, S. De Vleeschouwer, R. Sciot, L. Bouwens, M. Verfaillie, N. Vandamme, R.E. Vandenbroucke, O. De Wever, Y. Saeys, M. Guilliams, C. Gysemans, B. Neyns, F. De Smet, D. Lambrechts, J.A. Van Ginderachter, and K. Movahedi. 2021. Single-cell profiling of myeloid cells in glioblastoma across species and disease stage reveals macrophage competition and specialization. *Nat. Neurosci. 2021 244*. 24:595–610. doi:10.1038/s41593-020-00789-y.

Powderly, J.D., S. Jang, J. Lohr, A.I. Spira, G.C. Bohac, and M. Sharma. 2020. Preliminary dose escalation results from a phase I/II, first-in-human study of MGC018 (anti-B7-H3 antibody-drug conjugate) in patients with advanced solid tumors. *https://doi.org/10.1200/JCO.2020.38.15_suppl.3071*. 38:3071–3071. doi:10.1200/JCO.2020.38.15_SUPPL.3071.

Del Prete, A., F. Sozio, I. Barbazza, V. Salvi, L. Tiberio, M. Laffranchi, A. Gismondi, D. Bosisio, T. Schioppa, and S. Sozzani. 2020. Functional Role of Dendritic Cell Subsets in Cancer Progression and Clinical Implications. *Int. J. Mol. Sci.* 21. doi:10.3390/IJMS21113930.

Pulverer, B.J., J.M. Kyriakis, J. Avruch, E. Nikolakaki, and J.R. Woodgett. 1991. Phosphorylation of c-jun mediated by MAP kinases. *Nat. 1991 3536345*. 353:670–674. doi:10.1038/353670a0.

Purshouse, K., and A.S. Protheroe. 2019. Abiraterone acetate in combination with prednisone in the treatment of metastatic hormone-sensitive prostate cancer: clinical evidence and experience. *Ther. Adv. Urol.* 11. doi:10.1177/1756287218820804.

Qin, H., L. Wang, T. Feng, C.O. Elson, S.A. Niyongere, S.J. Lee, S.L. Reynolds, C.T. Weaver, K. Roarty, R. Serra, E.N. Benveniste, and Y. Cong. 2009. TGF-β Promotes Th17 Cell Development through Inhibition of SOCS3. *J. Immunol.* 183:97–105. doi:10.4049/JIMMUNOL.0801986.

Quail, D.F., R.L. Bowman, L. Akkari, M.L. Quick, A.J. Schuhmacher, J.T. Huse, E.C. Holland, J.C. Sutton, and J.A. Joyce. 2016. The tumor microenvironment underlies acquired resistance to CSF-1R inhibition in gliomas. *Science*. 352. doi:10.1126/SCIENCE.AAD3018.

Quintar, A., S. McArdle, D. Wolf, A. Marki, E. Ehinger, M. Vassallo, J. Miller, Z. Mikulski, K. Ley, and K. Buscher. 2017. Endothelial Protective Monocyte Patrolling in Large Arteries Intensified by Western Diet and Atherosclerosis. *Circ. Res.* 120:1789–1799. doi:10.1161/CIRCRESAHA.117.310739.

Rajapaksha, H., and B.E. Forbes. 2015. Ligand-Binding Affinity at the Insulin Receptor Isoform-A and Subsequent IR-A Tyrosine Phosphorylation Kinetics are Important Determinants of Mitogenic Biological Outcomes. *Front. Endocrinol. (Lausanne).* 6:107. doi:10.3389/fendo.2015.00107.

Rajaram, S., D.J. Baylink, and S. Mohan. 1997. Insulin-Like Growth Factor-Binding Proteins in Serum and Other Biological Fluids: Regulation and Functions. *Endocr. Rev.* 18:801–831. doi:10.1210/EDRV.18.6.0321.

Ramalingam, P., M.G. Poulos, E. Lazzari, M.C. Gutkin, D. Lopez, C.C. Kloss, M.J. Crowley, L. Katsnelson, A.G. Freire, M.B. Greenblatt, C.Y. Park, and J.M. Butler. 2020. Chronic activation of endothelial MAPK disrupts hematopoiesis via NFKB dependent inflammatory stress reversible by SCGF. *Nat. Commun. 2020 111*. 11:1–20. doi:10.1038/s41467-020-14478-8.

Rao, S.R., N.K. Alham, E. Upton, S. McIntyre, R. Bryant, L. Cerundolo, E. Bowes, S. Jones, M. Browne, I. Mills, A. Lamb, I. Tomlinson, D. Wedge, L. Browning, K. Sirinukunwattana, C. Palles, F. Hamdy, J. Rittscher, and C. Verrill. 2019. Detailed molecular and immune marker profiling of archival prostate cancer samples reveals an inverse association between TMPRSS2:ERG fusion status and immune cell infiltration. *under Rev.*

Rao, S.R., N.K. Alham, E. Upton, S. McIntyre, R.J. Bryant, L. Cerundolo, E. Bowes, S. Jones, M. Browne, I. Mills, A. Lamb, I. Tomlinson, D. Wedge, L. Browning, K. Sirinukunwattana, C. Palles, F.C. Hamdy, J. Rittscher, and C. Verrill. 2020. Detailed Molecular and Immune Marker Profiling of Archival Prostate Cancer Samples Reveals an Inverse Association between TMPRSS2:ERG Fusion Status and Immune Cell Infiltration. *J Mol Diagn*. 22:652–669. doi:10.1016/j.jmoldx.2020.02.012.

Rawlings, J.S., K.M. Rosler, and D.A. Harrison. 2004. The JAK/STAT signaling pathway. *J. Cell Sci.* 117:1281–1283. doi:10.1242/JCS.00963.

Rayes, R.F., S. Milette, M.C. Fernandez, B. Ham, N. Wang, F. Bourdeau, S. Perrino, S. Yakar, and P. Brodt. 2018. Loss of neutrophil polarization in colon carcinoma liver metastases of mice with an inducible, liver-specific IGF-I deficiency. *Oncotarget*. 9:15691–15704. doi:10.18632/oncotarget.24593.

Reisländer, T., E.P. Lombardi, F.J. Groelly, A. Miar, M. Porru, S. Di Vito, B. Wright, H. Lockstone, A. Biroccio, A. Harris, A. Londoño-Vallejo, and M. Tarsounas. 2019. BRCA2 abrogation triggers innate immune responses potentiated by treatment with PARP inhibitors. *Nat. Commun. 2019 101*. 10:1–13. doi:10.1038/s41467-019-11048-5.

Resnicoff, M., C. Sell, M. Rubini, D. Coppola, D. Ambrose, R. Baserga, and R. Rubin. 1994. Rat Glioblastoma Cells Expressing an Antisense RNA to the Insulin-like Growth Factor-1 (IGF-1) Receptor Are Nontumorigenic and Induce Regression of Wild-Type Tumors. *Cancer Res.* 54:2218–2222.

Rieunier, G., X. Wu, L.E. Harris, J. V Mills, A. Nandakumar, L. Colling, E. Seraia, S.B. Hatch, D. V Ebner, L.K. Folkes, U. Weyer-Czernilofsky, T. Bogenrieder, A.J. Ryan, and V.M. Macaulay. 2021. Targeting IGF perturbs global replication through ribonucleotide reductase dysfunction. *Cancer Res*. doi:10.1158/0008-5472.CAN-20-2860.

Rinaldi, S., R. Cleveland, T. Norat, C. Biessy, S. Rohrmann, J. Linseisen, H. Boeing, T. Pischon, S. Panico, C. Agnoli, D. Palli, R. Tumino, P. Vineis, P.H.M. Peeters, C.H. Van Gils, B.H. Bueno-de-Mesquita, A. Vrieling, N.E. Allen, A. Roddam, S. Bingham, K.T. Khaw, J. Manjer, S. Borgquist, V. Dumeaux, I.T. Gram, E. Lund, A. Trichopoulou, G. Makrygiannis, V. Benetou, E. Molina, I.D. Suárez, A.B. Gurrea, C.A. Gonzalez, M.J. Tormo, J.M. Altzibar, A. Olsen, A. Tjonneland, H. Grønbæk, K. Overvad, F. Clavel-Chapelon, M.C. Boutron-Ruault, S. Morois, N. Slimani, P. Boffetta, M. Jenab, E. Riboli, and R. Kaaks. 2010. Serum levels of IGF-I, IGFBP-3 and colorectal cancer risk: results from the EPIC cohort, plus a meta-analysis of prospective studies. *Int. J. cancer*. 126:1702–1715. doi:10.1002/IJC.24927.

Rinderknecht, E., and R.E. Humbel. 1978. The amino acid sequence of human insulin-like growth factor I and its structural homology with proinsulin. *J. Biol. Chem.* 253:2769–2776. doi:10.1016/S0021-9258(17)40889-1.

Rizq, O., N. Mimura, M. Oshima, A. Saraya, S. Koide, Y. Kato, K. Aoyama, Y. Nakajima-Takagi, C. Wang, T. Chiba, A. Ma, J. Jin, T. Iseki, C. Nakaseko, and A. Iwama. 2017. Dual Inhibition of EZH2 and EZH1 Sensitizes PRC2-Dependent Tumors to Proteasome Inhibition. *Clin. Cancer Res.* 23:4817–4830. doi:10.1158/1078-0432.CCR-16-2735.

Robinson, A., C.Z. Han, C.K. Glass, and J.W. Pollard. 2021. Feature Review Monocyte Regulation in Homeostasis and Malignancy. *Trends Immunol.* 42:104–119. doi:10.1016/j.it.2020.12.001.

Roddam, A.W., N.E. Allen, P. Appleby, T.J. Key, L. Ferrucci, H.B. Carter, E.J. Metter, C.

Chen, N.S. Weiss, A. Fitzpatrick, A.W. Hsing, J. V Lacey, K. Helzlsouer, S. Rinaldi, E. Riboli, R. Kaaks, J.A.M.J.L. Janssen, M.F. Wildhagen, F.H. Schröder, E.A. Platz, M. Pollak, E. Giovannucci, C. Schaefer, C.P. Quesenberry, J.H. Vogelman, G. Severi, D.R. English, G.G. Giles, P. Stattin, G. Hallmans, M. Johansson, J.M. Chan, P. Gann, S.E. Oliver, J.M. Holly, J. Donovan, F. Meyer, I. Bairati, and P. Galan. 2008. Insulin-like growth factors, their binding proteins, and prostate cancer risk: analysis of individual patient data from 12 prospective studies. *Ann. Intern. Med.* 149:461–71, W83-8.

Rodrigues, D.N., P. Rescigno, D. Liu, W. Yuan, S. Carreira, M.B. Lambros, G. Seed, J. Mateo, R. Riisnaes, S. Mullane, C. Margolis, D. Miao, S. Miranda, D. Dolling, M. Clarke, C. Bertan, M. Crespo, G. Boysen, A. Ferreira, A. Sharp, I. Figueiredo, D. Keliher, S. Aldubayan, K.P. Burke, S. Sumanasuriya, M.S. Fontes, D. Bianchini, Z. Zafeiriou, L.S.T. Mendes, K. Mouw, M.T. Schweizer, C.C. Pritchard, S. Salipante, M.E. Taplin, H. Beltran, M.A. Rubin, M. Cieslik, D. Robinson, E. Heath, N. Schultz, J. Armenia, W. Abida, H. Scher, C. Lord, A. D'Andrea, C.L. Sawyers, A.M. Chinnaiyan, A. Alimonti, P.S. Nelson, C.G. Drake, E.M. Van Allen, and J.S. De Bono. 2018. Immunogenomic analyses associate immunological alterations with mismatch repair defects in prostate cancer. *J. Clin. Invest.* 128:4441–4453. doi:10.1172/JCI121924.

Romanelli, R.J., A.P. LeBeau, C.G. Fulmer, D.A. Lazzarino, A. Hochberg, and T.L. Wood. 2007. Insulin-like growth factor type-I receptor internalization and recycling mediate the sustained phosphorylation of Akt. *J. Biol. Chem.* 282:22513–22524. doi:10.1074/JBC.M704309200.

Rudd, C.E., A. Taylor, and H. Schneider. 2009. CD28 and CTLA-4 coreceptor expression and signal transduction. *Immunol. Rev.* 229:12–26. doi:10.1111/J.1600-065X.2009.00770.X.

Runcie, K.D., and M.C. Dallos. 2021. Prostate Cancer Immunotherapy—Finally in From the Cold? *Curr. Oncol. Reports 2021 238*. 23:1–13. doi:10.1007/S11912-021-01084-0.

Ruytinx, P., P. Proost, J. Van Damme, and S. Struyf. 2018. Chemokine-induced macrophage polarization in inflammatory conditions. *Front. Immunol.* 9:1930.

doi:10.3389/FIMMU.2018.01930/BIBTEX.

Sachdev, D., and D. Yee. 2007. Disrupting insulin-like growth factor signaling as a potential cancer therapy. *Mol. Cancer Ther.* 6:1–12. doi:10.1158/1535-7163.MCT-06-0080.

Saha, R.N., M. Jana, and K. Pahan. 2007. MAPK p38 Regulates Transcriptional Activity of NF-κB in Primary Human Astrocytes via Acetylation of p65. *J. Immunol.* 179:7101. doi:10.4049/JIMMUNOL.179.10.7101.

Sakellariou, C., O. Elhage, E. Papaevangelou, G. Giustarini, A.M. Esteves, D. Smolarek, R.A. Smith, P. Dasgupta, and C. Galustian. 2020. Prostate cancer cells enhance interleukin-15-mediated expansion of NK cells. *BJU Int.* 125:89–102. doi:10.1111/BJU.14893.

Salminen, A., and K. Kaarniranta. 2010. Insulin/IGF-1 paradox of aging: Regulation via AKT/IKK/NF-κB signaling. *Cell. Signal.* 22:573–577. doi:10.1016/j.cellsig.2009.10.006.

Salminen, A., K. Kaarniranta, and A. Kauppinen. 2021. Insulin/IGF-1 signaling promotes immunosuppression via the STAT3 pathway: impact on the aging process and age-related diseases. *Inflamm. Res.* 70:1043–1061. doi:10.1007/s00011-021-01498-3.

Sandhu, S., C.M. Moore, E. Chiong, H. Beltran, R.G. Bristow, and S.G. Williams. 2021. Prostate cancer. *Lancet (London, England)*. 398:1075–1090. doi:10.1016/S0140-6736(21)00950-8.

Sarbassov, D.D., D.A. Guertin, S.M. Ali, and D.M. Sabatini. 2005. Phosphorylation and regulation of Akt/PKB by the rictor-mTOR complex. *Science*. 307:1098–1101. doi:10.1126/SCIENCE.1106148.

Sarfstein, R., M. Pasmanik-Chor, A. Yeheskel, L. Edry, N. Shomron, N. Warman, E. Wertheimer, S. Maor, L. Shochat, and H. Werner. 2012. Insulin-like growth factor-I receptor (IGF-IR) translocates to nucleus and autoregulates IGF-IR gene expression in breast cancer cells. *J. Biol. Chem.* 287:2766–76. doi:10.1074/jbc.M111.281782.

Sato, H., A. Niimi, T. Yasuhara, T.B.M. Permata, Y. Hagiwara, M. Isono, E. Nuryadi, R. Sekine, T. Oike, S. Kakoti, Y. Yoshimoto, K.D. Held, Y. Suzuki, K. Kono, K. Miyagawa, T. Nakano, and A. Shibata. 2017. DNA double-strand break repair pathway regulates PD-L1 expression in cancer cells. *Nat. Commun.* 8.

doi:10.1038/s41467-017-01883-9.

Sayeed, A., N. Alam, M. Trerotola, and L.R. Languino. 2012. Insulin-like growth factor 1 stimulation of androgen receptor activity requires β 1A integrins. *J. Cell. Physiol.* 227:751–758. doi:10.1002/jcp.22784.

Schillaci, R., M.G. Brocardo, A. Galeano, and A. Roldán. 1998. Downregulation of Insulin-like Growth Factor-1 Receptor (IGF-1R) Expression in Human T Lymphocyte Activation. *Cell. Immunol.* 183:157–161. doi:10.1006/CIMM.1997.1237.

Schillaci, R., M. Salatino, J. Cassataro, C.J. Proietti, G.H. Giambartolomei, M.A. Rivas, R.P. Carnevale, E.H. Charreau, and P. V Elizalde. 2006. Immunization with murine breast cancer cells treated with antisense oligodeoxynucleotides to type I insulin-like growth factor receptor induced an antitumoral effect mediated by a CD8+ response involving Fas/Fas ligand cytotoxic pathway. *J. Immunol.* 176:3426–37.

Schmid, P., M.P. Sablin, J. Bergh, S.A. Im, Y.S. Lu, N. Martínez, P. Neven, K.S. Lee, S. Morales, J.A. Pérez-Fidalgo, D. Adamson, A. Gonçalves, A. Prat, G. Jerusalem, L. Schlieker, R.M. Espadero, T. Bogenrieder, D.C.L. Huang, J. Crown, and J. Cortés. 2021. A phase Ib/II study of xentuzumab, an IGF-neutralising antibody, combined with exemestane and everolimus in hormone receptor-positive, HER2-negative locally advanced/metastatic breast cancer. *Breast Cancer Res.* 23. doi:10.1186/S13058-020-01382-8.

Schreiber, R.D., L.J. Old, and M.J. Smyth. 2011. Cancer immunoediting: Integrating immunity's roles in cancer suppression and promotion. *Science (80-.).* 331:1565–1570. doi:10.1126/SCIENCE.1203486/SUPPL_FILE/1565.MP3.

Schroeder, A., O. Mueller, S. Stocker, R. Salowsky, M. Leiber, M. Gassmann, S. Lightfoot, W. Menzel, M. Granzow, and T. Ragg. 2006. The RIN: An RNA integrity number for assigning integrity values to RNA measurements. *BMC Mol. Biol.* 7:1–14. doi:10.1186/1471-2199-7-3/FIGURES/8.

Schulze-Osthoff, K., D. Ferrari, K. Riehemann, and S. Wesselborg. 1997. Regulation of NF-kappa B activation by MAP kinase cascades. *Immunobiology*. 198:35–49. doi:10.1016/S0171-2985(97)80025-3.

Schumacher, T.N., and R.D. Schreiber. 2015. Neoantigens in cancer immunotherapy.

Science (80-.). 348:69–74. doi:10.1126/SCIENCE.AAA4971/ASSET/9BC707C7-9B25-479A-8F2D-54AE27164ADA/ASSETS/GRAPHIC/348_69_F4.JPEG.

Sciacca, L., R. Le Moli, and R. Vigneri. 2012. Insulin analogs and cancer. *Front. Endocrinol. (Lausanne).* 3:21. doi:10.3389/FENDO.2012.00021/BIBTEX.

Sciacca, L., M. Prisco, A. Wu, A. Belfiore, R. Vigneri, and R. Baserga. 2003. Signaling Differences from the A and B Isoforms of the Insulin Receptor (IR) in 32D Cells in the Presence or Absence of IR Substrate-1. *Endocrinology*. 144:2650–2658. doi:10.1210/EN.2002-0136.

Seder, R.A., R. Gazzinelli, A. Sher, and W.E. Paul. 1993. Interleukin 12 acts directly on CD4+ T cells to enhance priming for interferon gamma production and diminishes interleukin 4 inhibition of such priming. *Proc. Natl. Acad. Sci. U. S. A.* 90:10188–10192. doi:10.1073/PNAS.90.21.10188.

Sehat, B., A. Tofigh, Y. Lin, E. Trocme, U. Liljedahl, J. Lagergren, and O. Larsson. 2010. SUMOylation Mediates the Nuclear Translocation and Signaling of the IGF-1 Receptor. *Sci. Signal.* 3:ra10–ra10. doi:10.1126/scisignal.2000628.

Sell, C., G. Dumenil, C. Deveaud, M. Miura, D. Coppola, T. DeAngelis, R. Rubin, A. Efstratiadis, and R. Baserga. 1994. Effect of a null mutation of the insulin-like growth factor I receptor gene on growth and transformation of mouse embryo fibroblasts. *Mol. Cell. Biol.* 14:3604–12.

Selman, C., S. Lingard, A.I. Choudhury, R.L. Batterham, M. Claret, M. Clements, F. Ramadani, K. Okkenhaug, E. Schuster, E. Blanc, M.D. Piper, H. Al-Qassab, J.R. Speakman, D. Carmignac, I.C.A. Robinson, J.M. Thornton, D. Gems, L. Partridge, and D.J. Withers. 2008. Evidence for lifespan extension and delayed age-related biomarkers in insulin receptor substrate 1 null mice. *FASEB J.* 22:807–818. doi:10.1096/FJ.07-9261COM.

Selman, C., L. Partridge, and D.J. Withers. 2011. Replication of extended lifespan phenotype in mice with deletion of insulin receptor substrate 1. *PLoS One*. 6. doi:10.1371/JOURNAL.PONE.0016144.

Servant, R., M. Garioni, T. Vlajnic, M. Blind, H. Pueschel, D.C. Müller, T. Zellweger, A.J. Templeton, A. Garofoli, S. Maletti, S. Piscuoglio, M.A. Rubin, H. Seifert, C.A. Rentsch, L. Bubendorf, and C. Le Magnen. 2021. Prostate cancer patient-derived

organoids: detailed outcome from a prospective cohort of 81 clinical specimens. *J. Pathol.* 254:543–555. doi:10.1002/PATH.5698.

Shah, O.J., and T. Hunter. 2006. Turnover of the active fraction of IRS1 involves raptor-mTOR- and S6K1-dependent serine phosphorylation in cell culture models of tuberous sclerosis. *Mol. Cell. Biol.* 26:6425–34. doi:10.1128/MCB.01254-05.

Shahaf, G., S. Zisman-Rozen, D. Benhamou, D. Melamed, and R. Mehr. 2016. B cell development in the bone marrow is regulated by homeostatic feedback exerted by mature B cells. *Front. Immunol.* 7:77. doi:10.3389/FIMMU.2016.00077/BIBTEX.

Shanskii, Y.D., N.S. Sergeeva, I.K. Sviridova, M.S. Kirakozov, V.A. Kirsanova, S.A. Akhmedova, A.I. Antokhin, and V.I. Chissov. 2013. Human platelet lysate as a promising growth-stimulating additive for culturing of stem cells and other cell types. *Bull. Exp. Biol. Med.* 156:146–151. doi:10.1007/S10517-013-2298-7.

Sharma, P., R.K. Pachynski, V. Narayan, Y. Hu, G.C. Han, K.F. Correspondence, A. Flé, G. Gravis, M.D. Galsky, H. Mahammedi, A. Patnaik, S.K. Subudhi, M. Ciprotti, B. Simsek, A. Saci, and K. Fizazi. 2020. Nivolumab Plus Ipilimumab for Metastatic Castration-Resistant Prostate Cancer: Preliminary Analysis of Patients in the CheckMate 650 Trial. *Cancer Cell*. 38:489–499. doi:10.1016/j.ccell.2020.08.007.

Shen, X., L. Zhang, J. Li, Y. Li, Y. Wang, and Z.X. Xu. 2019. Recent Findings in the Regulation of Programmed Death Ligand 1 Expression. *Front Immunol*. 10:1337. doi:10.3389/fimmu.2019.01337.

Shevah, O., and Z. Laron. 2007. Patients with congenital deficiency of IGF-I seem protected from the development of malignancies: A preliminary report. *Growth Horm. IGF Res.* 17:54–57. doi:10.1016/J.GHIR.2006.10.007.

Shi, Y., J. Chen, C.M. Karner, and F. Long. 2015. Hedgehog signaling activates a positive feedback mechanism involving insulin-like growth factors to induce osteoblast differentiation. *Proc. Natl. Acad. Sci. U. S. A.* 112:4678–4683. doi:10.1073/PNAS.1502301112/-/DCSUPPLEMENTAL.

Shweiki, D., A. Itin, D. Soffer, and E. Keshet. 1992. Vascular endothelial growth factor induced by hypoxia may mediate hypoxia-initiated angiogenesis. *Nat. 1992 3596398*. 359:843–845. doi:10.1038/359843a0.

Sichani, M.M., F.S. Yazdi, N.A. Moghaddam, A. Chehrei, M. Kabiri, A. Naeimi, and D.

Taheri. 2010. Prognostic value of insulin- like growth factor-I receptor expression in renal cell carcinoma. *Saudi J. Kidney Dis. Transpl.* 21:69–74.

Siech, C., J. Rutz, S. Maxeiner, T. Grein, M. Sonnenburg, I. Tsaur, F.K.H. Chun, and R.A. Blaheta. 2022. Insulin-like Growth Factor-1 Influences Prostate Cancer Cell Growth and Invasion through an Integrin α3, α5, αV, and β1 Dependent Mechanism. *Cancers (Basel).* 14. doi:10.3390/CANCERS14020363.

de Silva, H.C., M.Z. Lin, L. Phillips, J.L. Martin, and R.C. Baxter. 2019. IGFBP-3 interacts with NONO and SFPQ in PARP-dependent DNA damage repair in triple-negative breast cancer. *Cell. Mol. Life Sci.* 76:2015–2030. doi:10.1007/S00018-019-03033-4.

Simanshu, D.K., D. V. Nissley, and F. McCormick. 2017. RAS Proteins and Their Regulators in Human Disease. *Cell*. 170:17–33. doi:10.1016/J.CELL.2017.06.009.

Simon, S., and N. Labarriere. 2018. PD-1 expression on tumor-specific T cells: Friend or foe for immunotherapy? *Oncoimmunology*. 7. doi:10.1080/2162402X.2017.1364828.

Simpson, A., W. Petnga, V.M. Macaulay, U. Weyer-Czernilofsky, and T. Bogenrieder. 2017. Insulin-Like Growth Factor (IGF) Pathway Targeting in Cancer: Role of the IGF Axis and Opportunities for Future Combination Studies. *Target. Oncol.* 12:571–597. doi:10.1007/s11523-017-0514-5.

Simpson, A.D., Y.W.J. Soo, G. Rieunier, T. Aleksic, O. Ansorge, C. Jones, and V.M. Macaulay. 2020. Type 1 IGF receptor associates with adverse outcome and cellular radioresistance in paediatric high-grade glioma. *Br. J. Cancer*. 122:624. doi:10.1038/S41416-019-0677-1.

Sinha, P., C. Okoro, D. Foell, H.H. Freeze, S. Ostrand-Rosenberg, and G. Srikrishna. 2008. Proinflammatory S100 Proteins Regulate the Accumulation of Myeloid-Derived Suppressor Cells. *J. Immunol.* 181:4666–4675. doi:10.4049/JIMMUNOL.181.7.4666.

Slaaby, R., L. Schäffer, I. Lautrup-Larsen, A.S. Andersen, A.C. Shaw, I.S. Mathiasen, and J. Brandt. 2006. Hybrid Receptors Formed by Insulin Receptor (IR) and Insulin-like Growth Factor I Receptor (IGF-IR) Have Low Insulin and High IGF-1 Affinity Irrespective of the IR Splice Variant. *J. Biol. Chem.* 281:25869–25874. doi:10.1074/jbc.M605189200.

Smittenaar, C.R., K.A. Petersen, K. Stewart, and N. Moitt. 2016. Cancer incidence and mortality projections in the UK until 2035. *Br. J. Cancer*. 115:1147–1155. doi:10.1038/bjc.2016.304.

Sobell, H.M. 1985. Actinomycin and DNA transcription. *Proc. Natl. Acad. Sci.* 82:5328–5331. doi:10.1073/PNAS.82.16.5328.

Solomon-Zemler, R., Y. Pozniak, T. Geiger, and H. Werner. 2019. Identification of nucleolar protein NOM1 as a novel nuclear IGF1R-interacting protein. *Mol. Genet. Metab.* 126:259–265. doi:10.1016/J.YMGME.2019.01.002.

Somasundaram, R., G. Zhang, M. Fukunaga-Kalabis, M. Perego, C. Krepler, X. Xu, C. Wagner, D. Hristova, J. Zhang, T. Tian, Z. Wei, Q. Liu, K. Garg, J. Griss, R. Hards, M. Maurer, C. Hafner, M. Mayerhöfer, G. Karanikas, A. Jalili, V. Bauer-Pohl, F. Weihsengruber, K. Rappersberger, J. Koller, R. Lang, C. Hudgens, G. Chen, M. Tetzlaff, L. Wu, D.T. Frederick, R.A. Scolyer, G. V. Long, M. Damle, C. Ellingsworth, L. Grinman, H. Choi, B.J. Gavin, M. Dunagin, A. Raj, N. Scholler, L. Gross, M. Beqiri, K. Bennett, I. Watson, H. Schaider, M.A. Davies, J. Wargo, B.J. Czerniecki, L. Schuchter, D. Herlyn, K. Flaherty, M. Herlyn, and S.N. Wagner. 2017. Tumor-associated B-cells induce tumor heterogeneity and therapy resistance. *Nat. Commun.* 8. doi:10.1038/S41467-017-00452-4.

Somri-Gannam, L., S. Meisel-Sharon, S. Hantisteanu, G. Groisman, O. Limonad, M. Hallak, and I. Bruchim. 2020. IGF1R Axis Inhibition Restores Dendritic Cell Antitumor Response in Ovarian Cancer. *Transl. Oncol.* 13:100790. doi:10.1016/J.TRANON.2020.100790.

Song, H., H.N.W. Weinstein, P. Allegakoen, M.H. Wadsworth, J. Xie, H. Yang, E.A. Castro, K.L. Lu, B.A. Stohr, F.Y. Feng, P.R. Carroll, B. Wang, M.R. Cooperberg, A.K. Shalek, and F.W. Huang. 2022. Single-cell analysis of human primary prostate cancer reveals the heterogeneity of tumor-associated epithelial cell states. *Nat. Commun. 2022 131*. 13:1–20. doi:10.1038/s41467-021-27322-4.

De Souza, A.P., V.L.C. Vale, M.D.C. Silva, I.B.D.O. Araújo, S.C. Trindade, L.F. De Moura-Costa, G.C. Rodrigues, T.S. Sales, H.A. Dos Santos, P.C. De Carvalho-Filho, M.G. De Oliveira-Neto, R.E. Schaer, and R. Meyer. 2014. MAPK involvement in cytokine production in response to Corynebacterium pseudotuberculosis infection.

BMC Microbiol. 14:1–9. doi:10.1186/S12866-014-0230-6/FIGURES/8.

Spadaro, O., C.D. Camell, L. Bosurgi, K.Y. Nguyen, Y.H. Youm, C. V. Rothlin, and V.D. Dixit. 2017. IGF1 Shapes Macrophage Activation in Response to Immunometabolic Challenge. *Cell Rep.* 19:225–234. doi:10.1016/J.CELREP.2017.03.046.

Stabile, A., F. Giganti, A.B. Rosenkrantz, S.S. Taneja, G. Villeirs, I.S. Gill, C. Allen, M. Emberton, C.M. Moore, and V. Kasivisvanathan. 2020. Multiparametric MRI for prostate cancer diagnosis: current status and future directions. *Nat. Rev. Urol.* 17:41–61. doi:10.1038/S41585-019-0212-4.

Steuerman, R., O. Shevah, and Z. Laron. 2011. Congenital IGF1 deficiency tends to confer protection against post-natal development of malignancies. *Eur. J. Endocrinol.* 164:485–489. doi:10.1530/EJE-10-0859.

Stovsky, M., E.A. Klein, A. Chait, K. Manickam, A.J. Stephenson, M. Wagner, M. Dineen, Y. Lotan, A. Partin, J. Baniel, A. Kestranek, P. Gawande, and B. Zaslavsky. 2019. Clinical Validation of IsoPSA^{TM}, a Single Parameter, Structure Based Assay for Improved Detection of High Grade Prostate Cancer. *J. Urol.* 201:1115–1120. doi:10.1097/JU.0000000000000185.

Stuart, T., and R. Satija. 2019. Integrative single-cell analysis. *Nat. Rev. Genet. 2019 205*. 20:257–272. doi:10.1038/s41576-019-0093-7.

Stutvoet, T.S., A. Kol, E.G.E. de Vries, M. de Bruyn, R.S.N. Fehrmann, A.G.T. Terwisscha van Scheltinga, and S. de Jong. 2019. MAPK pathway activity plays a key role in PD-L1 expression of lung adenocarcinoma cells. *J. Pathol.* 249:52–64. doi:10.1002/PATH.5280.

Su, C., W. Wang, and C. Wang. 2018. IGF-1-induced MMP-11 expression promotes the proliferation and invasion of gastric cancer cells through the JAK1/STAT3 signaling pathway. *Oncol. Lett.* 15:7000. doi:10.3892/OL.2018.8234.

Subramanian, A., P. Tamayo, V.K. Mootha, S. Mukherjee, B.L. Ebert, M.A. Gillette, A. Paulovich, S.L. Pomeroy, T.R. Golub, E.S. Lander, and J.P. Mesirov. 2005. Gene set enrichment analysis: A knowledge-based approach for interpreting genome-wide expression profiles. *Proc. Natl. Acad. Sci.* 102:15545–15550. doi:10.1073/PNAS.0506580102.

Suen, J.L., T.T. Wu, Y.H. Li, C.L. Lee, F.C. Kuo, P.S. Yan, C.F. Wu, M. Tran, C.J. Wang,

C.H. Hung, M.T. Wu, M.W.Y. Chan, and S.K. Huang. 2020. Environmental Factor-Mediated Transgenerational Inheritance of Igf2r Hypomethylation and Pulmonary Allergic Response via Targeting Dendritic Cells. *Front. Immunol.* 11:3391. doi:10.3389/FIMMU.2020.603831/BIBTEX.

Sun, J., G. Dotti, L.E. Huye, A.E. Foster, B. Savoldo, M.M. Gramatges, D.M. Spencer, and C.M. Rooney. 2010. T Cells Expressing Constitutively Active Akt Resist Multiple Tumor-associated Inhibitory Mechanisms. *Mol. Ther.* 18:2006. doi:10.1038/MT.2010.185.

Swain, S.L., K.K. McKinstry, and T.M. Strutt. 2012. Expanding roles for CD4+ T cells in immunity to viruses. *Nat. Rev. Immunol. 2012 122*. 12:136–148. doi:10.1038/nri3152.

Takahashi, T., K. Fukuda, J. Pan, H. Kodama, M. Sano, S. Makino, T. Kato, T. Manabe, and S. Ogawa. 1999. Characterization of Insulin-Like Growth Factor-1–Induced Activation of the JAK/STAT Pathway in Rat Cardiomyocytes. *Circ. Res.* 85:884–891. doi:10.1161/01.RES.85.10.884.

Tan, G.H., G. Nason, K. Ajib, D.T.S. Woon, J. Herrera-Caceres, O. Alhunaidi, and N. Perlis. 2019. Smarter screening for prostate cancer. *World J. Urol.* 37:991–999. doi:10.1007/s00345-019-02719-5.

Tannock, I.F., R. de Wit, W.R. Berry, J. Horti, A. Pluzanska, K.N. Chi, S. Oudard, C. Théodore, N.D. James, I. Turesson, M.A. Rosenthal, and M.A. Eisenberger. 2004. Docetaxel plus prednisone or mitoxantrone plus prednisone for advanced prostate cancer. *N. Engl. J. Med.* 351:1502–1512. doi:10.1056/NEJMOA040720.

Tarn, C., L. Rink, E. Merkel, D. Flieder, H. Pathak, D. Koumbi, J.R. Testa, B. Eisenberg, M. Von Mehren, and A.K. Godwin. 2008. Insulin-like growth factor 1 receptor is a potential therapeutic target for gastrointestinal stromal tumors. *Proc. Natl. Acad. Sci.* 105:8387–8392. doi:10.1073/PNAS.0803383105.

Tay, R.E., E.K. Richardson, and H.C. Toh. 2020. Revisiting the role of CD4+ T cells in cancer immunotherapy—new insights into old paradigms. *Cancer Gene Ther. 2020 281*. 28:5–17. doi:10.1038/s41417-020-0183-x.

Taylor, B.S., N. Schultz, H. Hieronymus, C. Sander, C.L. Sawyers, and W.L. Gerald. 2015. Integrative Genomic Profiling of Advanced Prostate Cancer. *Cell*. 161:1215–28.

Teisserenc, H., W. Schmitt, N. Blake, R. Dunbar, S. Gadola, W.L. Gross, A. Exley, and V. Cerundolo. 1997. A case of primary immunodeficiency due to a defect of the major histocompatibility gene complex class I processing and presentation pathway. *Immunol. Lett.* 57:183–187. doi:10.1016/S0165-2478(97)00072-2.

Teo, M.Y., D.E. Rathkopf, and P. Kantoff. 2019. Treatment of Advanced Prostate Cancer. *Annu. Rev. Med.* 70:479–499. doi:10.1146/annurev-med-051517-011947.

Tesmer, L.A., S.K. Lundy, S. Sarkar, and D.A. Fox. 2008. Th17 cells in human disease. *Immunol. Rev.* 223:87. doi:10.1111/J.1600-065X.2008.00628.X.

Thomas, G.D., R.N. Hanna, N.T. Vasudevan, A.A. Hamers, C.E. Romanoski, S. McArdle, K.D. Ross, A. Blatchley, D. Yoakum, B.A. Hamilton, Z. Mikulski, M.K. Jain, C.K. Glass, and C.C. Hedrick. 2016. Deleting an Nr4a1 Super-Enhancer Subdomain Ablates Ly6C low Monocytes while Preserving Macrophage Gene Function. *Immunity*. 45:975–987. doi:10.1016/J.IMMUNI.2016.10.011.

Tian, X., A. Zhang, C. Qiu, W. Wang, Y. Yang, C. Qiu, A. Liu, L. Zhu, S. Yuan, H. Hu, W. Wang, Q. Wei, X. Zhang, and J. Xu. 2015. The Upregulation of LAG-3 on T Cells Defines a Subpopulation with Functional Exhaustion and Correlates with Disease Progression in HIV-Infected Subjects. *J. Immunol.* 194:3873–3882. doi:10.4049/JIMMUNOL.1402176/-/DCSUPPLEMENTAL.

Tonkin, J., L. Temmerman, R.D. Sampson, E. Gallego-Colon, L. Barberi, D. Bilbao, M.D. Schneider, A. Musarò, and N. Rosenthal. 2015. Monocyte/Macrophage-derived IGF-1 Orchestrates Murine Skeletal Muscle Regeneration and Modulates Autocrine Polarization. *Mol. Ther.* 23:1189–1200. doi:10.1038/MT.2015.66.

Topalian, S.L., F.S. Hodi, J.R. Brahmer, S.N. Gettinger, D.C. Smith, D.F. McDermott, J.D. Powderly, R.D. Carvajal, J.A. Sosman, M.B. Atkins, P.D. Leming, D.R. Spigel, S.J. Antonia, L. Horn, C.G. Drake, D.M. Pardoll, L. Chen, W.H. Sharfman, R.A. Anders, J.M. Taube, T.L. McMiller, H. Xu, A.J. Korman, M. Jure-Kunkel, S. Agrawal, D. McDonald, G.D. Kollia, A. Gupta, J.M. Wigginton, and M. Sznol. 2012. Safety, Activity, and Immune Correlates of Anti–PD-1 Antibody in Cancer. *N. Engl. J. Med.* 366:2443–2454. doi:10.1056/NEJMOA1200690/SUPPL_FILE/NEJMOA1200690_DISCLOSURES.PDF.

Topham, N.J., and E.W. Hewitt. 2009. Natural killer cell cytotoxicity: how do they pull the trigger? *Immunology*. 128:7. doi:10.1111/J.1365-2567.2009.03123.X.

Townsend, A., C. Öhlén, J. Bastin, H.G. Ljunggren, L. Foster, and K. Kärre. 1989. Association of class I major histocompatibility heavy and light chains induced by viral peptides. *Nat. 1989 3406233*. 340:443–448. doi:10.1038/340443a0.

Townsend, A.R.M., J. Rothbard, F.M. Gotch, G. Bahadur, D. Wraith, and A.J. McMichael. 1986. The epitopes of influenza nucleoprotein recognized by cytotoxic T lymphocytes can be defined with short synthetic peptides. *Cell*. 44:959–968. doi:10.1016/0092-8674(86)90019-X.

Tran, C., S. Ouk, N.J. Clegg, Y. Chen, P.A. Watson, V. Arora, J. Wongvipat, P.M. Smith-Jones, D. Yoo, A. Kwon, T. Wasielewska, D. Welsbie, C.D. Chen, C.S. Higano, T.M. Beer, D.T. Hung, H.I. Scher, M.E. Jung, and C.L. Sawyers. 2009. Development of a second-generation antiandrogen for treatment of advanced prostate cancer. *Science*. 324:787–790. doi:10.1126/SCIENCE.1168175.

Travis, R.C., P.N. Appleby, R.M. Martin, J.M.P. Holly, D. Albanes, A. Black, H.B.A. Bueno-de-Mesquita, J.M. Chan, C. Chen, M.-D. Chirlaque, M.B. Cook, M. Deschasaux, J.L. Donovan, L. Ferrucci, P. Galan, G.G. Giles, E.L. Giovannucci, M.J. Gunter, L.A. Habel, F.C. Hamdy, K.J. Helzlsouer, S. Hercberg, R.N. Hoover, J.A.M.J.L. Janssen, R. Kaaks, T. Kubo, L. Le Marchand, E.J. Metter, K. Mikami, J.K. Morris, D.E. Neal, M.L. Neuhouser, K. Ozasa, D. Palli, E.A. Platz, M. Pollak, A.J. Price, M.J. Roobol, C. Schaefer, J.M. Schenk, G. Severi, M.J. Stampfer, P. Stattin, A. Tamakoshi, C.M. Tangen, M. Touvier, N.J. Wald, N.S. Weiss, R.G. Ziegler, T.J. Key, and N.E. Allen. 2016. A Meta-analysis of Individual Participant Data Reveals an Association between Circulating Levels of IGF-I and Prostate Cancer Risk. *Cancer Res.* 76:2288–2300. doi:10.1158/0008-5472.CAN-15-1551.

Trojan, J., H.T. Duc, L.C. Upegui-Gonzalez, F. Hor, Y. Guo, D. Anthony, and J. Ilan. 1996. Presence of MHC-I and B-7 molecules in rat and human glioma cells expressing antisense IGF-I mRNA. *Neurosci. Lett.* 212:9–12. doi:10.1016/0304-3940(96)12770-1.

Trojan, J., T.R. Johnson, S.D. Rudin, J. Ilan, M.L. Tykocinski, and J. Ilan. 1993. Treatment and prevention of rat glioblastoma by immunogenic C6 cells expressing

antisense insulin-like growth factor I RNA. *Science*. 259:94–7.

Tuong, Z.K., K.W. Loudon, B. Berry, N. Richoz, J. Jones, X. Tan, Q. Nguyen, A. George, S. Hori, S. Field, A.G. Lynch, K. Kania, P. Coupland, A. Babbage, R. Grenfell, T. Barrett, A.Y. Warren, V. Gnanapragasam, C. Massie, and M.R. Clatworthy. 2021. Resolving the immune landscape of human prostate at a single-cell level in health and cancer. *Cell Rep.* 37:110132. doi:10.1016/J.CELREP.2021.110132/ATTACHMENT/63268A2E-BCD0-4486-81FF-1D28E2D69ACA/MMC3.XLSX.

Turner, B.C., B.G. Haffty, L. Narayanan, J. Yuan, P.A. Havre, A.A. Gumbs, L. Kaplan, J.-L. Burgaud, D. Carter, R. Baserga, and P.M. Glazer. 1997. Insulin-like Growth Factor-I Receptor Overexpression Mediates Cellular Radioresistance and Local Breast Cancer Recurrence after Lumpectomy and Radiation. *Cancer Res.* 57.

Turner, M.D., B. Nedjai, T. Hurst, and D.J. Pennington. 2014. Cytokines and chemokines: At the crossroads of cell signalling and inflammatory disease. *Biochim. Biophys. Acta - Mol. Cell Res.* 1843:2563–2582. doi:10.1016/J.BBAMCR.2014.05.014.

Turney, B.W., G.D.H. Turner, S.F. Brewster, and V.M. Macaulay. 2011. Serial analysis of resected prostate cancer suggests up-regulation of type 1 IGF receptor with disease progression. *BJU Int.* 107:1488–1499. doi:10.1111/j.1464-410X.2010.09556.x.

Ullrich, A., A. Gray, A.W. Tam, T. Yang-Feng, M. Tsubokawa, C. Collins, W. Henzel, T. Le Bon, S. Kathuria, and E. Chen. 1986. Insulin-like growth factor I receptor primary structure: comparison with insulin receptor suggests structural determinants that define functional specificity. *EMBO J.* 5:2503. doi:10.1002/j.1460-2075.1986.tb04528.x.

Unger, C., N. Kramer, D. Unterleuthner, M. Scherzer, A. Burian, A. Rudisch, M. Stadler, M. Schlederer, D. Lenhardt, A. Riedl, S. Walter, A. Wernitznig, L. Kenner, M. Hengstschläger, J. Schüler, W. Sommergruber, and H. Dolznig. 2017. Stromal-derived IGF2 promotes colon cancer progression via paracrine and autocrine mechanisms. *Oncogene*. 36:5341–5355. doi:10.1038/ONC.2017.116.

Vafa, O., M. Wade, S. Kern, M. Beeche, T.K. Pandita, G.M. Hampton, and G.M. Wahl. 2002. c-Myc can induce DNA damage, increase reactive oxygen species, and mitigate p53 function: a mechanism for oncogene-induced genetic instability. *Mol. Cell*.

9:1031–1044. doi:10.1016/S1097-2765(02)00520-8.

Vanhaesebroeck, B., and D.R. Alessi. 2000. The PI3K–PDK1 connection: more than just a road to PKB. *Biochem. J.* 346:561–576. doi:10.1042/BJ3460561.

Veldhoen, M., R.J. Hocking, C.J. Atkins, R.M. Locksley, and B. Stockinger. 2006. TGFbeta in the context of an inflammatory cytokine milieu supports de novo differentiation of IL-17-producing T cells. *Immunity*. 24:179–189. doi:10.1016/J.IMMUNI.2006.01.001.

Vella, V., A. Milluzzo, N.M. Scalisi, P. Vigneri, and L. Sciacca. 2018. Insulin Receptor Isoforms in Cancer. *Int. J. Mol. Sci.* 19. doi:10.3390/IJMS19113615.

Verdeil, G., T. Lawrence, A.M. Schmitt-Verhulst, and N. Auphan-Anezin. 2019. Targeting STAT3 and STAT5 in Tumor-Associated Immune Cells to Improve Immunotherapy. *Cancers (Basel).* 11. doi:10.3390/CANCERS11121832.

Vernieri, C., G. Fuca, F. Ligorio, V. Huber, A. Vingiani, F. Iannelli, A. Raimondi, D. Rinchai, G. Frige, A. Belfiore, L. Lalli, C. Chiodoni, V. Cancila, F. Zanardi, A. Ajazi, S. Cortellino, V. Vallacchi, P. Squarcina, A. Cova, S. Pesce, P. Frati, R. Mall, P.A. Corsetto, A.M. Rizzo, C. Ferraris, S. Folli, M.C. Garassino, G. Capri, G. Bianchi, M.P. Colombo, S. Minucci, M. Foiani, V.D. Longo, G. Apolone, V. Torri, G. Pruneri, D. Bedognetti, L. Rivoltini, and F. de Braud. 2021. Fasting-mimicking diet is safe and reshapes metabolism and antitumor immunity in cancer patients. *Cancer Discov.* candisc.0030.2021. doi:10.1158/2159-8290.CD-21-0030.

Vernieri, C., G. Fucà, F. Ligorio, V. Huber, A. Vingiani, F. Iannelli, A. Raimondi, D. Rinchai, G. Frigè, A. Belfiore, L. Lalli, C. Chiodoni, V. Cancila, F. Zanardi, A. Ajazi, S. Cortellino, V. Vallacchi, P. Squarcina, A. Cova, S. Pesce, P. Frati, R. Mall, P.A. Corsetto, A.M. Rizzo, C. Ferraris, S. Folli, M.C. Garassino, G. Capri, G. Bianchi, M.P. Colombo, S. Minucci, M. Foiani, V.D. Longo, G. Apolone, V. Torri, G. Pruneri, D. Bedognetti, L. Rivoltini, and F. de Braud. 2022. Fasting-Mimicking Diet Is Safe and Reshapes Metabolism and Antitumor Immunity in Patients with Cancer. *Cancer Discov.* 12:90–107. doi:10.1158/2159-8290.CD-21-0030.

Vesely, M.D., M.H. Kershaw, R.D. Schreiber, and M.J. Smyth. 2011. Natural Innate and Adaptive Immunity to Cancer. *http://dx.doi.org/10.1146/annurev-immunol-031210-101324*. 29:235–271. doi:10.1146/ANNUREV-IMMUNOL-031210-101324.

Vilgelm, A.E., and A. Richmond. 2019. Chemokins modulate immune surveillance in tumorignesis, metastatsis, and response to immunotherapy. *Front. Immunol.* 10:333. doi:10.3389/FIMMU.2019.00333/BIBTEX.

Visakorpi, T., E. Hyytinen, P. Koivisto, M. Tanner, R. Keinänen, C. Palmberg, A. Palotie, T. Tammela, J. Isola, and O.P. Kallioniemi. 1995. In vivo amplification of the androgen receptor gene and progression of human prostate cancer. *Nat. Genet.* 9:401–406. doi:10.1038/ng0495-401.

Vitkin, N., S. Nersesian, D.R. Siemens, and M. Koti. 2019. The Tumor Immune Contexture of Prostate Cancer. *Front Immunol*. 10:603. doi:10.3389/fimmu.2019.00603.

Vivanco, I., and C.L. Sawyers. 2002. The phosphatidylinositol 3-Kinase–AKT pathway in human cancer. *Nat. Rev. Cancer 2002 27*. 2:489–501. doi:10.1038/nrc839.

Van Vugt, M.A.T.M., and E.E. Parkes. 2021. When breaks get hot: inflammatory signaling in BRCA1/2-mutant cancers. doi:10.1016/j.trecan.2021.12.003.

Waldhauer, I., and A. Steinle. 2008. NK cells and cancer immunosurveillance. *Oncogene*. 27:5932–5943. doi:10.1038/ONC.2008.267.

Walker, J.A., and A.N.J. McKenzie. 2017. TH2 cell development and function. *Nat. Rev. Immunol. 2017 182*. 18:121–133. doi:10.1038/nri.2017.118.

Wang, C., S. Li, Y. Wang, Y. An, K. Shen, X. Wang, W. Luan, F. Ma, L. Ni, H. Zhou, M. Liu, and L. Yu. 2020a. Targeting IRS-1/mPGES-1/NOX2 to inhibit the inflammatory response caused by insulin-like growth factor-I-induced activation of NF-κB and NLRP3 in cancer cells. *Vet. Comp. Oncol.* doi:10.1111/vco.12596.

Wang, F., J. Flanagan, N. Su, L.C. Wang, S. Bui, A. Nielson, X. Wu, H.T. Vo, X.J. Ma, and Y. Luo. 2012. RNAscope: A Novel in Situ RNA Analysis Platform for Formalin-Fixed, Paraffin-Embedded Tissues. *J. Mol. Diagn.* 14:22. doi:10.1016/J.JMOLDX.2011.08.002.

Wang, H., S. Hu, X. Chen, H. Shi, C. Chen, L. Sun, and Z.J. Chen. 2017. cGAS is essential for the antitumor effect of immune checkpoint blockade. *Proc. Natl. Acad. Sci. U. S. A.* 114:1637–1642. doi:10.1073/PNAS.1621363114/-/DCSUPPLEMENTAL.

Wang, X., L. Lin, B. Lan, Y. Wang, L. Du, X. Chen, Q. Li, K. Liu, M. Hu, Y. Xue, A.I.

Roberts, C. Shao, G. Melino, Y. Shi, Y. Wang, Y. Shi, and Y. Wang. 2020b. IGF2R-initiated proton rechanneling dictates an anti-inflammatory property in macrophages. *Sci. Adv.* 6. doi:10.1126/SCIADV.ABB7389.

Wang, Y.J., Q. Shi, P. Sun, Q. Zhou, M. Darowish, T.F. Li, Y.F. Dong, W.W. Lu, and J.C.Y. Leong. 2006. Insulin-like growth factor-1 treatment prevents anti-Fas antibody-induced apoptosis in endplate chondrocytes. *Spine (Phila. Pa. 1976).* 31:736–741. doi:10.1097/01.BRS.0000208128.49912.64.

Waraky, A., Y. Lin, D. Warsito, F. Haglund, E. Aleem, O. Larsson, and X.F. Wang. 2017. Nuclear insulin-like growth factor 1 receptor phosphorylates proliferating cell nuclear antigen and rescues stalled replication forks after DNA damage. *J. Biol. Chem.* 292:18227–18239. doi:10.1074/JBC.M117.781492/ATTACHMENT/60836E09-A09B-4CB1-9370-86DDA183778C/MMC1.ZIP.

Warsito, D., S. Sjöström, S. Andersson, O. Larsson, and B. Sehat. 2012. Nuclear IGF1R is a transcriptional co-activator of LEF1/TCF. *EMBO Rep.* 13:244–250. doi:10.1038/EMBOR.2011.251.

Warzecha, Z., A. Dembinski, P. Ceranowicz, S.J. Konturek, R. Tomaszewska, J. Stachura, and P.C. Konturek. 2003. IGF-1 stimulates production of interleukin-10 and inhibits development of caerulein-induced pancreatitis. *J. Physiol. Pharmacol.* 54:575–90.

Watkinson, F., S.K. Nayar, A. Rani, C.A. Sakellariou, O. Elhage, E. Papaevangelou, P. Dasgupta, and C. Galustian. 2020. IL-15 Upregulates Telomerase Expression and Potently Increases Proliferative Capacity of NK, NKT-Like, and CD8 T Cells. *Front. Immunol.* 11:594620. doi:10.3389/FIMMU.2020.594620/FULL.

Watson, P.A., K. Ellwood-Yen, J.C. King, J. Wongvipat, M.M. Lebeau, and C.L. Sawyers. 2005a. Context-dependent hormone-refractory progression revealed through characterization of a novel murine prostate cancer cell line. *Cancer Res*. 65:11565–11571. doi:10.1158/0008-5472.CAN-05-3441.

Watson, P.A., K. Ellwood-Yen, J.C. King, J. Wongvipat, M.M. LeBeau, and C.L. Sawyers. 2005b. Context-dependent hormone-refractory progression revealed through characterization of a novel murine prostate cancer cell line. *Cancer Res.* 65:11565–11571. doi:10.1158/0008-5472.CAN-05-3441.

Watts, E.L., G.K. Fensom, K. Smith Byrne, A. Perez-Cornago, N.E. Allen, A. Knuppel,

M.J. Gunter, M. V. Holmes, R.M. Martin, N. Murphy, K.K. Tsilidis, B.B. Yeap, T.J. Key, and R.C. Travis. 2021. Circulating insulin-like growth factor-I, total and free testosterone concentrations and prostate cancer risk in 200 000 men in UK Biobank. *Int. J. cancer*. 148:2274–2288. doi:10.1002/IJC.33416.

Watts, E.L., G.K. Fensom, K. Smith Byrne, A. Perez-Cornago, N.E. Allen, A. Knuppel, M.J. Gunter, M. V Holmes, R.M. Martin, N. Murphy, K.K. Tsilidis, B.B. Yeap, T.J. Key, and R.C. Travis. 2020. Circulating insulin-like growth factor-I, total and free testosterone concentrations and prostate cancer risk in 200 000 men in UK Biobank. *Int J Cancer*. doi:10.1002/ijc.33416.

Wickremasinghe, M.I., L.H. Thomas, C.M. O'Kane, J. Uddin, and J.S. Friedland. 2004. Transcriptional mechanisms regulating alveolar epithelial cell-specific CCL5 secretion in pulmonary tuberculosis. *J. Biol. Chem.* 279:27199–27210. doi:10.1074/JBC.M403107200.

Williams, A., C.A. Peh, and T. Elliott. 2002. The cell biology of MHC class I antigen presentation. *Tissue Antigens*. 59:3–17. doi:10.1034/J.1399-0039.2002.590103.X.

Williams, C., D. Rezgui, S.N. Prince, O.J. Zaccheo, E.J. Foulstone, B.E. Forbes, R.S. Norton, J. Crosby, A.B. Hassan, and M.P. Crump. 2007. Structural Insights into the Interaction of Insulin-like Growth Factor 2 with IGF2R Domain 11. *Structure*. 15:1065–1078. doi:10.1016/J.STR.2007.07.007.

Wright, A.S., L.N. Thomas, R.C. Douglas, C.B. Lazier, and R.S. Rittmaster. 1996. Relative potency of testosterone and dihydrotestosterone in preventing atrophy and apoptosis in the prostate of the castrated rat. *J. Clin. Invest.* 98:2558. doi:10.1172/JCI119074.

Wu, H., T. Sun, and R.U.I. Bi. 2019. Inhibition of insulin-like growth factor 1 signaling synergistically enhances the tumor suppressive role of triptolide in triple-negative breast cancer cells. *Oncol. Lett.* 18:822–829. doi:10.3892/OL.2019.10356/HTML.

Wu, J., and E. Yu. 2014. Insulin-like growth factor receptor-1 (IGF-IR) as a target for prostate cancer therapy. *Cancer Metastasis Rev.* 33:607–17. doi:10.1007/s10555-013-9482-0.

Wu, J.D., K. Haugk, L. Woodke, P. Nelson, I. Coleman, and S.R. Plymate. 2006. Interaction of IGF signaling and the androgen receptor in prostate cancer progression.

J. Cell. Biochem. 99:392–401. doi:10.1002/jcb.20929.

Wu, S.Y., F. Xing, S. Sharma, K. Wu, A. Tyagi, Y. Liu, D. Zhao, R.P. Deshpande, Y. Shiozawa, T. Ahmed, W. Zhang, M. Chan, J. Ruiz, T.W. Lycan, A. Dothard, and K. Watabe. 2020. Nicotine promotes brain metastasis by polarizing microglia and suppressing innate immune function. *J. Exp. Med.* 217. doi:10.1084/JEM.20191131.

Wu, X.Y., Z.F. Wu, Q.H. Cao, C. Chen, Z.W. Chen, Z. Xu, W.S. Li, F.K. Liu, X.Q. Yao, and G. Li. 2014. Insulin-like growth factor receptor-1 overexpression is associated with poor response of rectal cancers to radiotherapy. *World J. Gastroenterol.* 20:16268–16274. doi:10.3748/wjg.v20.i43.16268.

Xia, H., J. Wang, X. Guo, Z. Lv, J. Liu, Q. Yan, M. Liu, and J. Wang. 2021. Identification of a Hypoxia-Related Gene Signature for Predicting Systemic Metastasis in Prostate Cancer. *Front. Cell Dev. Biol.* 9:2839. doi:10.3389/FCELL.2021.696364/BIBTEX.

Xiong, D., Y. Wang, A.K. Singavi, A.C. Mackinnon, B. George, and M. You. 2018. Immunogenomic Landscape Contributes to Hyperprogressive Disease after Anti-PD-1 Immunotherapy for Cancer. *iScience*. 9:258–277. doi:10.1016/j.isci.2018.10.021.

Xu, L., X. Qu, X. Hu, Z. Zhu, C. Li, E. Li, Y. Ma, N. Song, and Y. Liu. 2013. Lipid raft-regulated IGF-1R activation antagonizes TRAIL-induced apoptosis in gastric cancer cells. *FEBS Lett.* 587:3815–3823. doi:10.1016/J.FEBSLET.2013.10.007.

Xu, W.W., B. Li, X.Y. Guan, S.K. Chung, Y. Wang, Y.L. Yip, S.Y.K. Law, K.T. Chan, N.P.Y. Lee, K.W. Chan, L.Y. Xu, E.M. Li, S.W. Tsao, Q.Y. He, and A.L.M. Cheung. 2017. Cancer cell-secreted IGF2 instigates fibroblasts and bone marrow-derived vascular progenitor cells to promote cancer progression. *Nat. Commun.* 8. doi:10.1038/NCOMMS14399.

Xu, Y., G.K.W. Kong, J.G. Menting, M.B. Margetts, C.A. Delaine, L.M. Jenkin, V. V. Kiselyov, P. De Meyts, B.E. Forbes, and M.C. Lawrence. 2018. How ligand binds to the type 1 insulin-like growth factor receptor. *Nat. Commun.* 9. doi:10.1038/S41467-018-03219-7.

Xuan, N.T., N.H. Hoang, V.P. Nhung, N.T. Duong, N.H. Ha, and N. Van Hai. 2017. Regulation of dendritic cell function by insulin/IGF-1/PI3K/Akt signaling through klotho expression. *J. Recept. Signal Transduct.* 37:297–303. doi:10.1080/10799893.2016.1247862.

Xue, L., L. Chiang, C. Kang, and A. Winoto. 2008. The role of the PI3K-AKT kinase pathway in T cell development beyond the β checkpoint. *Eur. J. Immunol.* 38:3200. doi:10.1002/EJI.200838614.

Yadav, A., A. Kalita, S. Dhillon, and K. Banerjee. 2005. JAK/STAT3 pathway is involved in survival of neurons in response to insulin-like growth factor and negatively regulated by suppressor of cytokine signaling-3. *J. Biol. Chem.* 280:31830–31840. doi:10.1074/JBC.M501316200.

Yanase, T., and W. Fan. 2009. Chapter 23 Modification of Androgen Receptor Function by Igf-1 Signaling. *In* Vitamins and hormones. 649–666.

Yang, L., Q. Liu, X. Zhang, X. Liu, B. Zhou, J. Chen, D. Huang, J. Li, H. Li, F. Chen, J. Liu, Y. Xing, X. Chen, S. Su, and E. Song. 2020. DNA of neutrophil extracellular traps promotes cancer metastasis via CCDC25. *Nature*. 583:133–138. doi:10.1038/S41586-020-2394-6.

Ye, P., and J. D'Ercole. 1998. Insulin-like growth factor I (IGF-I) regulates IGF binding protein-5 gene expression in the brain. *Endocrinology*. 139:65–71. doi:10.1210/ENDO.139.1.5676.

Yee, D. 2012. Insulin-like growth factor receptor inhibitors: baby or the bathwater? *J. Natl. Cancer Inst.* 104:975–981. doi:10.1093/JNCI/DJS258.

Yeo, C.D., Y.A. Kim, H.Y. Lee, J.W. Kim, S.H. Lee, S.J. Kim, S.S. Kwon, Y.H. Kim, and S.C. Kim. 2017. Inhibiting IGF-1R attenuates cell proliferation and VEGF production in IGF-1R over-expressing EGFR mutant non-small cell lung cancer cells. *Exp. Lung Res.* 43:29–37. doi:10.1080/01902148.2017.1282994.

Yokokawa, J., V. Cereda, C. Remondo, J.L. Gulley, P.M. Arlen, J. Schlom, and K.Y. Tsang. 2008. Enhanced functionality of CD4+CD25(high)FoxP3+ regulatory T cells in the peripheral blood of patients with prostate cancer. *Clin. Cancer Res.* 14:1032–1040. doi:10.1158/1078-0432.CCR-07-2056.

Yu, S., S. Xia, D. Yang, K. Wang, S. Yeh, Z. Gao, and C. Chang. 2013. Androgen receptor in human prostate cancer-associated fibroblasts promotes prostate cancer epithelial cell growth and invasion. *Med. Oncol. 2013 303*. 30:1–7. doi:10.1007/S12032-013-0674-9.

Yuan, J., Z. Yin, K. Tao, G. Wang, and J. Gao. 2018. Function of insulin-like growth

factor 1 receptor in cancer resistance to chemotherapy. *Oncol. Lett.* 15:41–47. doi:10.3892/ol.2017.7276.

Zhang, B., M. Li, L. Chen, K. Yang, Y. Shan, L. Zhu, S. Sun, L. Li, and C. Wang. 2009. The TAK1-JNK cascade is required for IRF3 function in the innate immune response. *Cell Res. 2009 194*. 19:412–428. doi:10.1038/cr.2009.8.

Zhang, C., L. Hao, L. Wang, Y. Xiao, H. Ge, Z. Zhu, Y. Luo, Y. Zhang, and Y. Zhang. 2010. Elevated IGFIR expression regulating VEGF and VEGF-C predicts lymph node metastasis in human colorectal cancer. *BMC Cancer*. 10. doi:10.1186/1471-2407-10-184.

Zhang, J., Z. Gao, J. Yin, M.J. Quon, and J. Ye. 2008. S6K directly phosphorylates IRS-1 on Ser-270 to promote insulin resistance in response to TNF-(alpha) signaling through IKK2. *J. Biol. Chem.* 283:35375–82. doi:10.1074/jbc.M806480200.

Zhang, L., Z. Li, K.M. Skrzypczynska, Q. Fang, W. Zhang, S.A. O'Brien, Y. He, L. Wang, Q. Zhang, A. Kim, R. Gao, J. Orf, T. Wang, D. Sawant, J. Kang, D. Bhatt, D. Lu, C.M. Li, A.S. Rapaport, K. Perez, Y. Ye, S. Wang, X. Hu, X. Ren, W. Ouyang, Z. Shen, J.G. Egen, Z. Zhang, and X. Yu. 2020. Single-Cell Analyses Inform Mechanisms of Myeloid-Targeted Therapies in Colon Cancer. *Cell*. 181:442-459.e29. doi:10.1016/J.CELL.2020.03.048.

Zhang, L., M. Zhang, L. Wang, J. Li, T. Yang, Q. Shao, X. Liang, M. Ma, N. Zhang, M. Jing, R. Song, and J. Fan. 2021a. Identification of CCL4 as an Immune-Related Prognostic Biomarker Associated With Tumor Proliferation and the Tumor Microenvironment in Clear Cell Renal Cell Carcinoma. *Front. Oncol.* 11:4964. doi:10.3389/FONC.2021.694664/BIBTEX.

Zhang, Z., M. Lu, Y. Qin, W. Gao, L. Tao, W. Su, and J. Zhong. 2021b. Neoantigen: A New Breakthrough in Tumor Immunotherapy. *Front. Immunol.* 12. doi:10.3389/FIMMU.2021.672356.

Zhao, D., K. Bakirtzi, Y. Zhan, H. Zeng, H.W. Koon, and C. Pothoulakis. 2011. Insulin-like growth factor-1 receptor transactivation modulates the inflammatory and proliferative responses of neurotensin in human colonic epithelial cells. *J. Biol. Chem.* 286:6092–6099. doi:10.1074/jbc.M110.192534.

Zhao, F., B. Hoechst, A. Duffy, J. Gamrekelashvili, S. Fioravanti, M.P. Manns, T.F.

Greten, and F. Korangy. 2012. S100A9 a new marker for monocytic human myeloid-derived suppressor cells. *Immunology*. 136:176. doi:10.1111/J.1365-2567.2012.03566.X.

Zhao, Y.I., M. Mehta, A. Walton, K. Talsania, Y. Levin, J. Shetty, E.M. Gillanders, B. Tran, and D. Mercatante CarrickID. 2019. Robustness of RNA sequencing on older formalin-fixed paraffin-embedded tissue from high-grade ovarian serous adenocarcinomas. *PLoS One*. 14:e0216050. doi:10.1371/JOURNAL.PONE.0216050.

Zhao, Z., N. Zhang, A. Li, B. Zhou, Y. Chen, S. Chen, M. Huang, F. Wu, and L. Zhang. 2020. Insulin-like growth factor-1 receptor induces immunosuppression in lung cancer by upregulating B7-H4 expression through the MEK/ERK signaling pathway. *Cancer Lett.* 485:14–26. doi:10.1016/J.CANLET.2020.04.013.

Zheng, X., H. Baker, W.S. Hancock, F. Fawaz, M. McCaman, and E. Pungor. 2006. Proteomic analysis for the assessment of different lots of fetal bovine serum as a raw material for cell culture. Part IV. Application of proteomics to the manufacture of biological drugs. *Biotechnol. Prog.* 22:1294–1300. doi:10.1021/BP060121O.

Zhou, J., Z. Tang, S. Gao, C. Li, Y. Feng, and X. Zhou. 2020. Tumor-Associated Macrophages: Recent Insights and Therapies. *Front. Oncol.* 10:188. doi:10.3389/FONC.2020.00188/BIBTEX.

Zhu, P., D. Martinvalet, D. Chowdhury, D. Zhang, A. Schlesinger, and J. Lieberman. 2009. The cytotoxic T lymphocyte protease granzyme A cleaves and inactivates poly(adenosine 5'-diphosphate-ribose) polymerase-1. *Blood*. 114:1205–1216. doi:10.1182/BLOOD-2008-12-195768.

Zhu, Y., X. An, X. Zhang, Y. Qiao, T. Zheng, and X. Li. 2019. STING: a master regulator in the cancer-immunity cycle. *Mol. Cancer 2019 181*. 18:1–15. doi:10.1186/S12943-019-1087-Y.

Zimmermann, H.W., S. Seidler, J. Nattermann, N. Gassler, C. Hellerbrand, A. Zernecke, J.J.W. Tischendorf, T. Luedde, R. Weiskirchen, C. Trautwein, and F. Tacke. 2010. Functional Contribution of Elevated Circulating and Hepatic Non-Classical CD14+CD16+ Monocytes to Inflammation and Human Liver Fibrosis. *PLoS One*. 5:e11049. doi:10.1371/JOURNAL.PONE.0011049.

Zlotnik, A., and O. Yoshie. 2012. The Chemokine Superfamily Revisited. *Immunity*.

36:705–716. doi:10.1016/J.IMMUNI.2012.05.008.

Zong, C.S., J. Chan, D.E. Levy, C. Horvath, H.B. Sadowski, and L.H. Wang. 2000. Mechanism of STAT3 activation by insulin-like growth factor I receptor. *J. Biol. Chem.* 275:15099–15105. doi:10.1074/JBC.M000089200.

Zou, J., M. Zhuang, X. Yu, N. Li, R. Mao, Z. Wang, J. Wang, X. Wang, H. Zhou, L. Zhang, and Y. Shi. 2018. MYC inhibition increases PD-L1 expression induced by IFN-γ in hepatocellular carcinoma cells. *Mol. Immunol.* 101:203–209. doi:10.1016/J.MOLIMM.2018.07.006.